NEW INSIGHTS INTO THE FORMATION AND MODIFICATION OF CARBONATE-BEARING MINERALS AND METHANE GAS IN GEOLOGICAL SYSTEMS USING MULTIPLY SUBSTITUTED ISOTOPOLOGUES

Thesis by
Daniel Aaron Stolper

In Partial Fulfillment of the Requirements for the Degree
of
Doctor of Philosophy

CALIFORNIA INSTITUTE OF TECHNOLOGY
Pasadena, California
2014
(Defended May 13, 2014)

ACKNOWLEDGEMENTS

Acknowledging all of the people who have been instrumental in bringing me to this point in my life is simply impossible. Those of you not mentioned, you know who you are and I deeply appreciate all of your support and advice. First and foremost I need to thank the love of my life, Leslie — the past two and a half years have been the best of my life, and I could never have gotten here without you. I love you very much. Mom and Dad, your support and advice have kept me grounded and fed throughout much of graduate school. My only regret on graduating is that I will not be able to stop by unannounced and see the two of you (and Shelby and Murphy) whenever I please. Jennifer and Jon, I could not ask for a more supportive and kind sister and brother-in-law. John Eiler and John Grotzinger, I cannot describe how much I have learned from you both intellectually and personally. I have never met more patient and inspiring people. I owe much of my understanding of how science and scientific discourse should take place to the Saturday lunches at Shakers that I went to with my dad as a boy. The GPS faculty (Sam Epstein, Lee Silver, Dave Stevenson, Joe Kirschvink, Brian Wernicke, Dianne Newman, Mark Simons, and others) who regularly attended treated me as an equal in their vigorous debates, and I learned more from those lunches about how to be a member of a scientific community than anywhere else. Finally, I would like to thank my graduate class, Megan, Joel, Erika, Paul, Alison, and Jeff — it is impossible to imagine going through graduate school without you.

ABSTRACT

This thesis describes the use of multiply-substituted stable isotopologues of carbonate minerals and methane gas to better understand how these environmentally significant minerals and gases form and are modified throughout their geological histories. Stable isotopes have a long tradition in earth science as a tool for providing quantitative constraints on how molecules, in or on the earth, formed in both the present and past. Nearly all studies, until recently, have only measured the bulk concentrations of stable isotopes in a phase or species. However, the abundance of various isotopologues within a phase, for example the concentration of isotopologues with multiple rare isotopes (multiply substituted or 'clumped' isotopologues) also carries potentially useful information. Specifically, the abundances of clumped isotopologues in an equilibrated system are a function of temperature and thus knowledge of their abundances can be used to calculate a sample's formation temperature. In this thesis, measurements of clumped isotopologues are made on both carbonate-bearing minerals and methane gas in order to better constrain the environmental and geological histories of various samples.

Clumped-isotope-based measurements of ancient carbonate-bearing minerals, including apatites, have opened up paleotemperature reconstructions to a variety of systems and time periods. However, a critical issue when using clumped-isotope based measurements to reconstruct ancient mineral formation temperatures is whether the samples being measured have faithfully recorded their original internal isotopic distributions. These original distributions can be altered, for example, by diffusion of atoms in the mineral lattice or through diagenetic reactions. Understanding these processes quantitatively is critical for the use of clumped isotopes to reconstruct past temperatures, quantify diagenesis, and calculate time-temperature burial histories of carbonate minerals. In order to help orient this part of the thesis, Chapter 2 provides a broad overview and history of clumped-isotope based measurements in carbonate minerals.

In Chapter 3, the effects of elevated temperatures on a sample's clumped-isotope composition are probed in both natural and experimental apatites (which contain structural carbonate groups) and calcites. A quantitative model is created that is calibrated by the experiments and consistent with the natural samples. The model allows for calculations of the change in a sample's clumped isotope abundances as a function of any time-temperature history.

In Chapter 4, the effects of diagenesis on the stable isotopic compositions of apatites are explored on samples from a variety of sedimentary phosphorite deposits. Clumped isotope temperatures and bulk isotopic measurements from carbonate and phosphate groups are compared for all samples. These results demonstrate that samples have experienced isotopic exchange of

oxygen atoms in both the carbonate and phosphate groups. A kinetic model is developed that allows for the calculation of the amount of diagenesis each sample has experienced and yields insight into the physical and chemical processes of diagenesis.

The thesis then switches gear and turns its attention to clumped isotope measurements of methane. Methane is critical greenhouse gas, energy resource, and microbial metabolic product and substrate. Despite its importance both environmentally and economically, much about methane's formational mechanisms and the relative sources of methane to various environments remains poorly constrained. In order to add new constraints to our understanding of the formation of methane in nature, I describe the development and application of methane clumped isotope measurements to environmental deposits of methane. To help orient the reader, a brief overview of the formation of methane in both high and low temperature settings is given in Chapter 5.

In Chapter 6, a method for the measurement of methane clumped isotopologues via mass spectrometry is described. This chapter demonstrates that the measurement is precise and accurate. Additionally, the measurement is calibrated experimentally such that measurements of methane clumped isotope abundances can be converted into equivalent formational temperatures. This study represents the first time that methane clumped isotope abundances have been measured at useful precisions.

In Chapter 7, the methane clumped isotope method is applied to natural samples from a variety of settings. These settings include thermogenic gases formed and reservoired in shales, migrated thermogenic gases, biogenic gases, mixed biogenic and thermogenic gas deposits, and experimentally generated gases. In all cases, calculated clumped isotope temperatures make geological sense as formation temperatures or mixtures of high and low temperature gases. Based on these observations, we propose that the clumped isotope temperature of an unmixed gas represents its formation temperature — this was neither an obvious nor expected result and has important implications for how methane forms in nature. Additionally, these results demonstrate that methane-clumped isotope compositions provided valuable additional constraints to studying natural methane deposits.

TABLE OF CONTENTS

Chapter I

An introduction

1. Introduction

This thesis describes two distinct projects designed to provide new insights into how, and under what environmental conditions, (1) carbonate-bearing minerals and (2) methane gas form and are altered within the earth's crust. These projects, though distinct in detail, are unified by approach: both use multiply substituted isotopologues in order to provide new constraints on the geological histories and basic chemistry and physics of these environmentally important compounds. Multiply substituted isotopologues, or, more colloquially and as will be used in this thesis, 'clumped' isotopologues or isotopes are isotopologues with two or more rare, heavy isotopes — examples include D_2, $^{15}N_2$, $^{13}CH_3D$, and $^{13}C^{16}O^{18}O$. Clumped isotopologues are of interest because, *at equilibrium*, their abundances are a function of temperature (Eiler, 2007; Eiler, 2011; Eiler, 2013; Schauble et al., 2006; Urey and Rittenberg, 1933; Wang et al., 2004). As a result, a measurement that constrains their abundances allows, in some situations, for the calculation and reconstruction of the sample's formation or alteration (e.g., recrystallization) temperature and for kinetic and equilibrium processes to be identified and quantified. Consequently, clumped isotopologues can provide critical constraints on the types of environments where minerals and gases form or are altered and the mechanisms by which these processes occur.

In this thesis, clumped isotopologues are used to study two different phases: carbonate-bearing minerals and methane gas. The thesis is thus split into two parts: (1)

Kinetics of clumped isotopes in carbonate-bearing minerals in both high and low temperature settings. And (2) *The development and application of clumped isotopes to the study of methane formation at both high and low temperatures.*

The goal of part (1), most broadly, is to understand better the meaning of clumped-isotope-based temperatures of carbonate-bearing minerals in the context of both sedimentary diagenesis and high-temperature thermal histories. The first study (Chapter 3) uses experiments, measurements of natural samples, and models to understand how high-temperature processes can alter and set, through the diffusion of carbon and oxygen atoms in both calcites and apatites, clumped-isotope-based temperatures. A quantitative understanding of these processes and their effects on the clumped isotope composition of samples is needed to use carbonate clumped isotopes to study metamorphic processes, reconstruct thermal histories of crustal rocks, and understand the conditions required for samples to preserve their original clumped-isotope compositions. The second study in part (1), Chapter 4, uses clumped isotopes to gain quantitative insight into the diagenesis of sedimentary apatites. This study employs both bulk oxygen isotopes in carbonate groups and phosphate groups in apatites and the clumped isotope composition of the carbonate groups in the apatites to identify which samples have likely been diagenetically modified, the amount of diagenesis, and the environmental conditions during both formation and alteration. This work represents a well-constrained case study in how to interpret and quantify the effects of diagenesis using carbonate clumped isotopes and allows for new physical and chemical insights to be gained into how diagenesis proceeds in apatites.

In part (2) of the thesis a new method for measuring clumped isotopologues of methane is presented (Chapter 6) including a theoretical basis for and mechanics and calibration of the measurement. Then, in Chapter 7, methane clumped isotope values are measured in a variety of systems including experimentally generated methane, thermogenic natural gas deposits and biogenic gas deposits. These measurements are used to elucidate the basic mechanisms and environments of methane formation and the geological history of the samples.

For clarity, a brief introduction will precede each of these parts of the thesis (Chapters 2 and 5) with a background review for each part. However, because all chapters of this thesis employ measurements of clumped isotopologues, I first present a short review of their theory and history.

2. Stable isotopes background

Isotopic substitutions are of interest to the earth sciences because they have measureable effects on the chemical and physical properties of molecules including (but not limited to) diffusivities, vapor pressures (Herzfeld and Teller, 1938), reaction rates (Bigeleisen and Wolfsberg, 1958), and equilibrium constants (Urey, 1947). Generally, for physical processes, isotopic substitutions alter the physical parameter of interest due to a change in mass — e.g., the relative velocities (or diffusivities) of gases in a vacuum follow Graham's law, which is entirely a function of mass. The changes in the chemical properties of a molecule due to isotopic substitutions dominantly arise instead from changes in a molecule's chemical energy. This change in energy on isotopic substitution causes isotopes to partition into different phases at different concentrations. For example,

at equilibrium, there is a higher concentration of ^{18}O relative to ^{16}O in a carbonate mineral as compared to water.

Generally, the history of stable isotope geochemistry is marked by two landmark papers, Urey (1947) and Bigeleisen and Mayer (1947). These studies outline the basic theory needed to calculate the expected distribution of isotopes between two phases at equilibrium at a given temperature. Most importantly, Urey (1947) recognized and suggested that differences in the isotopic abundance of ^{18}O and ^{16}O in carbonates vs. in water could be used for paleotemperature reconstructions. This proposed application essentially launched the field of stable isotope geochemistry by taking an understood chemical phenomenon — the effect of isotopes on heterogeneous phase equilibrium constants — and justifying its capacity to solve important geological problems.

Interestingly, before such key discoveries were made, Urey and Rittenberg (1933) theoretically demonstrated that isotopic effects were noticeable *within a single phase* (homogenous-phase equilibrium): specifically they showed that the partitioning of hydrogen and deuterium amongst H_2, HD, and D_2 is not random as classical thermodynamics would predict. This internal exchange reaction can be written as follows:

$$H_2 + D_2 \leftrightarrow 2HD. \quad (1)$$

In this example, D_2 is the clumped isotopologue. The classical equilibrium constant for this reaction is 4. In contrast, Urey and Rittenberg (1933) predicted and Gould et al. (1934) measured an equilibrium constant of 3.3 at room temperature for this reaction. This indicates that the molecules on the left side of the reaction in Equation (1) are favored (and thus higher in concentration) as compared to that expected for a random

distribution. As a result, this system has an excess of D_2, the clumped isotopologue, at room temperature as compared to the random distribution of isotopes. Consequently, despite the seemingly relatively recent entry of isotopic clumping (Eiler and Schauble, 2004) into the field of geochemistry, it is in fact the first stable isotope-based technique used to both experimentally and theoretically probe the temperature dependence of reactions at chemical and isotopic equilibrium.

I now explore why, at equilibrium, clumped isotopes are in excess as compared to what would be expected for a random distribution of isotopes. To explain this and gain intuition into why clumping occurs, I will use the example presented above in Equation (1) in which hydrogen and deuterium are exchanged between H_2, HD, and D_2. Classical thermodynamics, which ignores the quantization of energy, will always predict that for an equilibrated system at any temperature, the isotopes of hydrogen will be randomly distributed amongst all isotopologues (Bigeleisen and Mayer, 1947). Quantum mechanics is required to explain, specifically, why clumping occurs in an equilibrated system, and more broadly why, at equilibrium, isotopes do not distribute randomly among different phases (Bigeleisen and Mayer, 1947). The core reason that clumping occurs can be understood through a simplified view of zero-point energies and the differences in these energies for different isotopologues.

All molecules have a zero-point energy, the minimum vibrational energy of a molecular bond, even at a temperature of absolute zero. For a molecule modeled as a harmonic oscillator, the zero-point energy is $\frac{1}{2}\hbar\omega$ where $\hbar$ is Plank's constant (reduced) and ω is the angular oscillation frequency of the bond. Because the molecule is harmonic, $\omega=\sqrt{(k/\mu)}$, where k is the force constant and μ is the reduced mass of the oscillator. For a

two-body spring, $\mu=(m_1 \times m_2)/(m_1 + m_2)$, where m is the mass of one of the atoms in the bond. A basic premise used in most simple representations of quantum mechanical systems is that the electronic energy of isotopologues is identical (a statement of the Born-Oppenheimer approximation) meaning that k is the same for all isotopologues.

The zero-point energy change of going from two HD molecules to one H_2 and D_2 molecule is

$$\Delta E = \frac{1}{2}\hbar\sqrt{k}\left(\frac{1}{\sqrt{\mu_{H2}}} + \frac{1}{\sqrt{\mu_{D2}}} - \frac{2}{\sqrt{\mu_{HD}}}\right), \quad (2)$$

where $\mu_{H2} = 1/2$, $\mu_{D2} = 2/3$, and $\mu_{HD} = 1$. These values give: $\Delta E = \frac{1}{2}\hbar\sqrt{k}(-.04)$. Thus, converting 2HD to H_2 and D_2 causes the overall energy of the system to drop (Figure 1). The actual value of the energy change in this analysis does not signify — what is important is that the energy is lowered by turning two singly substituted species into one clumped and one unsubstituted species (ΔE is negative) and, as a result, systems tend to become enriched in clumped isotopologues as compared to what would be expected for a random distribution of isotopes. This favoring of clumped molecules, as mentioned above, is generally observed, though it is not universal — for example asymmetric molecules like N_2O (N-N-O) can actually prefer to be 'anti-clumped' such that the concentration of some clumped isotopologues is lower than that expected for a random distribution (Wang et al., 2004). This simple model does not explain, however, the temperature dependence of clumping.

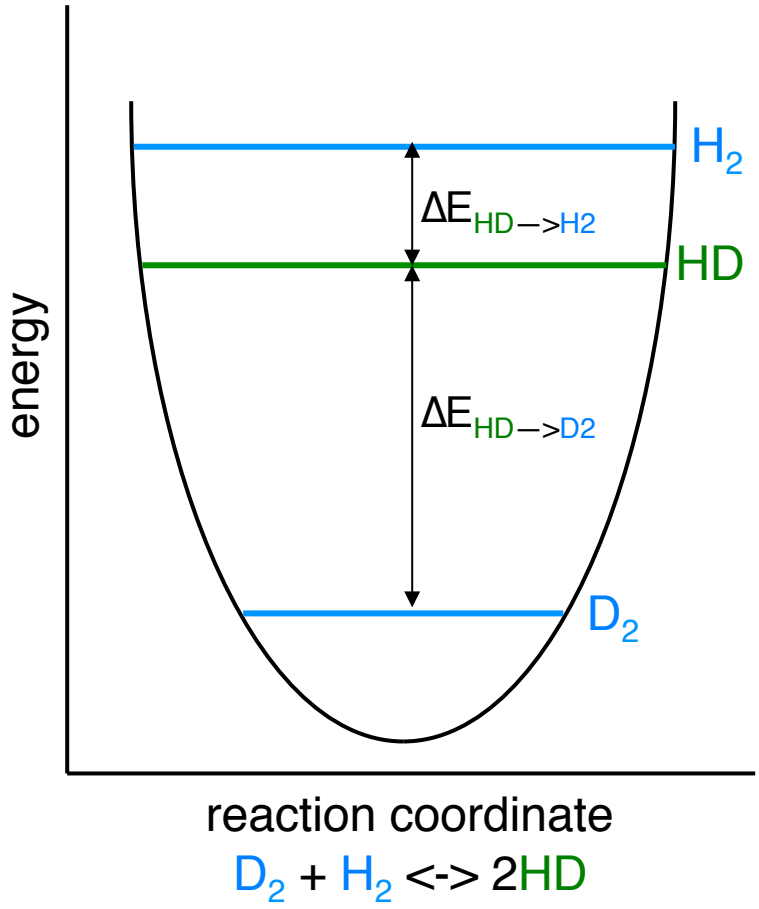

Figure 1. Exaggerated cartoon of the potential energy surface for a hydrogen molecule under the approximation that it is a harmonic oscillator. In this approximation, the potential energy surface is a parabola. The zero-point energies of the vibrational energy levels are given for H_2, HD, and D_2. D_2 has the lowest zero-point energy, followed by HD, and then H_2. As can be seen, the drop in energy of going from HD to D_2 is larger (in absolute value) than the rise in energy of going from HD to H_2.

Classical thermodynamics sheds light on this temperature dependence. The Gibbs free energy (G) of a system can be written as a function of enthalpy (H), entropy (S), and temperature (T):

$$\Delta G^\circ = \Delta H^\circ - T\Delta S^\circ. \quad (3)$$

The free energy of a system can be minimized at a given T and pressure either via a minimization of the enthalpy or maximization of the entropy. The enthalpy can be thought of as the energy of the bonds and the entropy as the state of ordering. The highest configurational entropy obtainable in the system occurs for a random isotopic

distribution. The minimum enthalpy of the system occurs when all the isotopes are partitioned into H_2 and D_2 molecules. As can be seen in Equation (3), the contribution of entropy to the minimization of the free energy of the system becomes increasingly more important as temperature increases. Thus at higher temperatures one favors the maximization of disorder (higher entropy) over the energy drop obtained by having more doubly substituted molecules (lower enthalpy) as compared to the random distribution (Figure 2). At lower temperatures, on the other hand, the entropy becomes less important to the overall minimization of the free energy of the system, and the energy drop associated with lowering the enthalpy (by having more clumped isotopologues) becomes increasingly important. Thus clumping occurs in isotopically equilibrated systems due to energetic differences between the various isotopologues in the system such that the energy drop associated with changing a singly substituted isotopologue into a clumped isotopologue is generally larger (in absolute value) than the energy rise associated with changing a singly substituted species into an unsubstituted species. The temperature dependence of the reaction then represents the energetic competition between the system's desire to maximize its entropy while at the same time minimizing its enthalpy.

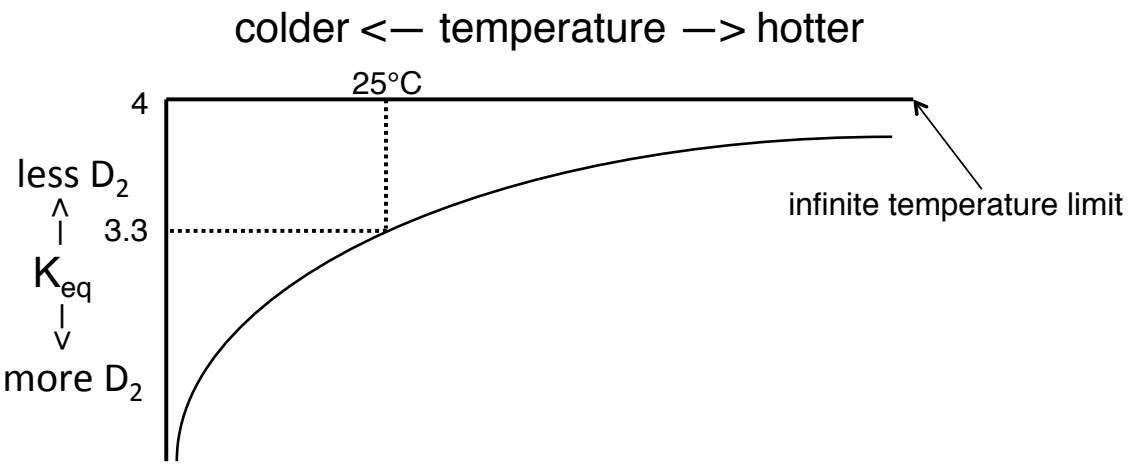

Figure 2. Cartoon of the dependence of the equilibrium constant (K_{eq}) for the reaction $H_2 + D_2$ <—> 2HD. At infinite temperatures, the equilibrium constant approaches the classical value of 4, which corresponds to a random distribution of isotopes amongst all isotopologues. At all finite temperatures, the equilibrium constant is smaller than 4, which indicates a higher abundance of clumped isotopologues, specifically D_2, than would be expected for a random distribution of isotopes.

3. Why clumped isotopes?

It is worthwhile to think through why, and the conditions under which, clumped isotopes can provide new information to help solve and inform problems in earth science such as paleothermometry. A way to frame this question is to follow an old Jewish custom that occurs on Passover every year. That is to ask, "How is this night different from all other nights?" We can instead ask for this thesis, "How are clumped isotopes different from all other isotopes?" We begin to answer by noting that most isotopically grounded paleothermometers are based on heterogeneous phase equilibrium reactions, while clumped isotope paleothermometry is based on homogeneous phase equilibrium reactions. This difference in type of reaction creates both the benefits and complexities associated with the use of clumped isotopes in geochemistry.

The classic, and best-understood heterogeneous-phase isotope geothermometer is the carbonate-water oxygen isotope thermometer (Epstein et al., 1953; McCrea, 1950;

Urey, 1947). As will be discussed in the next section, this thermometer is based on the preference of ^{18}O, relative to ^{16}O, to concentrate into carbonate minerals as compared to in water, with the size of this preference a function of temperature. In order to calculate a meaningful temperature using this technique, the oxygen isotope composition of both the carbonate and water must be known. This requires that the isotopic composition of both of these phases (carbonate and water) be measureable or at least can be estimated, which is often quite challenging and controversial for historical problems (Jaffrés et al., 2007; Kasting et al., 2006; Lécuyer and Allemand, 1999; Muehlenbachs, 1986; Veizer et al., 1999). This is true for any heterogeneous phase geothermometer: one must know the isotopic composition of two phases to estimate a formation temperature.

Clumped isotope geothermometry, on the other hand, is based on reactions that occur within a single phase. For example, in the example given above in Equation (1), the exchange reaction only occurs within hydrogen gas. If the system is at equilibrium, knowledge of the abundances of the three isotopologues of hydrogen gas is all that is necessary to calculate the temperature of the system. Importantly, the reaction need not actually occur as written — for example the hydrogen gas could exchange with another phase or species in the system, and that phase/species may be necessary, and thus act as a catalyst for hydrogen exchange to proceed among the different hydrogen gas isotopologues. However, at equilibrium, regardless of the mechanism of isotope exchange, the abundance of H_2, D_2, and HD uniquely constrain the temperature of isotopic equilibration.

This analysis demonstrates two critical features of clumped isotopes: (1) Only the measurement, and thus preservation in the rock record, of a single phase is needed for

formation temperature determinations. However, at the same time, any alteration to the chemical bonds in the sample via, for example, diffusion of atoms within or recrystallization of a mineral or re-equilibration of a gas will alter the measured clumped isotope compositions, but not necessarily the bulk average isotopic composition. The first part of this thesis is devoted to understanding the meaning of temperatures reconstructed using carbonate clumped isotopes in past minerals in which clumped isotopic compositions have been disturbed post mineral formation. (2) Even if the sample has not isotopically equilibrated, a temperature can still be calculated. Thus clumped isotopes provide a built-in reference frame for the exploration of the reaction dynamics of various phases in nature. If calculated temperatures exceed realistic expectations (e.g., the reconstructed formation temperatures of minerals exceed that of the sun), then the clumped isotope compositions immediately yield insight into the fact that the isotopic composition of the material is set by a kinetic process as opposed to an equilibrium process. This built-in reference frame of equilibrium will play a key role in the exploration and understanding of the meaning of methane clumped isotope composition in the second part of the thesis.

4. References

Bigeleisen, J., Mayer, M.G., 1947. Calculation of equilibrium constants for isotopic exchange reactions. *The Journal of Chemical Physics* 15, 261.

Bigeleisen, J., Wolfsberg, M., 1958. Theoretical and experimental aspects of isotope effects in chemical kinetics. *Advances in Chemical Physics*, 15-76.

Eiler, J.M., 2007. "Clumped-isotope" geochemistry - The study of naturally-occurring, multiply-substituted isotopologues. *Earth and Planetary Science Letters* 262, 309-327.

Eiler, J.M., 2011. Paleoclimate reconstruction using carbonate clumped isotope thermometry. *Quaternary Science Reviews* 30, 3575-3588.

Eiler, J.M., 2013. The isotopic anatomies of molecules and minerals. *Annual Review of Earth and Planetary Sciences* 41, 411-441.

Eiler, J.M., Schauble, E., 2004. $^{18}O^{13}C^{16}O$ in Earth's atmosphere. *Geochimica et Cosmochimica Acta* 68, 4767-4777.

Epstein, S., Buchsbaum, R., Lowenstam, H.A., Urey, H.C., 1953. Revised carbonate-water isotopic temperature scale. *Geological Society of America Bulletin* 64, 1315-1325.

Gould, A.J., Bleakney, W., Taylor, H.S., 1934. The inter-relations of hydrogen and deuterium molecules. *The Journal of Chemical Physics* 2, 362.

Herzfeld, K.F., Teller, E., 1938. The vapor pressure of isotopes. *Physical Review* 54, 912.

Jaffrés, J.B.D., Shields, G.A., Wallmann, K., 2007. The oxygen isotope evolution of seawater: A critical review of a long-standing controversy and an improved

geological water cycle model for the past 3.4 billion years. *Earth-Science Reviews* 83, 83-122.

Kasting, J.F., Howard, M.T., Wallmann, K., Veizer, J., Shields, G., Jaffrés, J., 2006. Paleoclimates, ocean depth, and the oxygen isotopic composition of seawater. *Earth and Planetary Science Letters* 252, 82-93.

Lécuyer, C., Allemand, P., 1999. Modelling of the oxygen isotope evolution of seawater: Implications for the climate interpretation of the $\delta^{18}O$ of marine sediments. *Geochimica et Cosmochimica Acta* 63, 351-361.

McCrea, J.M., 1950. On the isotopic chemistry of carbonates and a paleotemperature Scale. *Journal of Chemical Physics* 18, 849-857.

Muehlenbachs, K., 1986. Alteration of the oceanic crust and the ^{18}O history of seawater. *Reviews in Mineralogy and Geochemistry* 16, 425-444.

Schauble, E.A., Ghosh, P., Eiler, J.M., 2006. Preferential formation of ^{13}C-^{18}O bonds in carbonate minerals, estimated using first-principles lattice dynamics. *Geochimica et Cosmochimica Acta* 70, 2510-2529.

Urey, H.C., 1947. The thermodynamic properties of isotopic substances. *Journal of the Chemical Society*, 562-581.

Urey, H.C., Rittenberg, D., 1933. Some thermodynamic properties of the H^1H^1, H^2H^2 molecules and compounds containing the H^2 atom. *The Journal of Chemical Physics* 1, 137.

Veizer, J., Ala, D., Azmy, K., Bruckschen, P., Buhl, D., Bruhn, F., Carden, G.A., Diener, A., Ebneth, S., Godderis, Y., 1999. $^{87}Sr/^{86}Sr$, $\delta^{13}C$ and $\delta^{18}O$ evolution of Phanerozoic seawater. *Chemical Geology* 161, 59-88.

Wang, Z., Schauble, E.A., Eiler, J.M., 2004. Equilibrium thermodynamics of multiply substituted isotopologues of molecular gases. *Geochimica et Cosmochimica Acta* 68, 4779-4797.

Chapter II

Kinetics of clumped isotopes in carbonate-bearing minerals in both high and low temperature settings

1. An introduction to carbonate clumped isotopes

Understanding the past thermal history of earth's surface and shallow crust is a major goal of the earth sciences. Surface temperature reflects climate state of the earth and play a key role in regulating the habitability for life, the mineral assemblages present in the shallow crust, and the generation of economically important oil and gas reserves. Due to the importance of temperature in Earth's history, many methods have been established to reconstruct past temperatures. These include observations of qualitative geological structures such as pillow basalts and sedimentary features that require liquid water, and thus sub-boiling and above-freezing temperatures (e.g., Nutman et al., 1997) or the presence of certain organisms such as cold cold-blooded animals (e.g., Tarduno et al., 1998); geochemical and geobiological parameters based on the structure of organic matter (e.g., Brassell et al., 1986), partitioning of metals in minerals (e.g., Rosenthal et al., 1997), and the isotopic composition of minerals (Epstein et al., 1953; Kim and O'Neil, 1997; McCrea, 1950; Urey, 1947); and, for higher temperature/pressure processes, the entire field of metamorphic petrology.

One of the first proposed applications of stable isotopes to geological problems was for the determination of oceanic paleotemperatures using the partitioning of oxygen isotopes between water and coexisting carbonate minerals (Urey, 1947). Given this thermometer's importance historically and its utility as a foil to carbonate clumped isotope paleothermometry, I explain its theoretical basis in detail here. This thermometer

is based on heterogeneous isotope exchange reactions between water and carbonate isotopologues. For example, for the following isotope exchange reaction between carbonate oxygen in calcite or aragonite with oxygen in water:

$$\frac{1}{3}C^{16}O_3 + H_2^{18}O \leftrightarrow \frac{1}{3}C^{18}O_3 + H_2^{16}O, \quad (1)$$

the right side of the reaction is favored compared to the left such that ^{18}O is more concentrated in the carbonate groups than in water. This can be quantified with the equilibrium constant for this reaction:

$$K_{eq} = \frac{\left[H_2^{16}O\right] \text{ x } \left[C^{18}O_3\right]^{1/3}}{\left[H_2^{18}O\right] \text{ x } \left[C^{16}O_3\right]^{1/3}}, \quad (2)$$

where brackets denote concentrations and K_{eq} is the equilibrium constant. If we assume the isotopes are at a random distribution in the phases (which is not strictly true — see below), the equilibrium constant can be well approximated by the following equation:

$$K_{eq} \cong \frac{\left(\frac{^{18}O}{^{16}O}\right)_{CO3}}{\left(\frac{^{18}O}{^{16}O}\right)_{H2O}}, \quad (3)$$

where the $^{18}O/^{16}O$ ratio represents the concentration of ^{18}O vs. ^{16}O in the phase. Because the equilibrium constant for this reaction is a function of temperature as demonstrated both theoretically (Urey, 1947) and empirically (Epstein et al., 1953; Kim and O'Neil, 1997; McCrea, 1950), measurements of the $^{18}O/^{16}O$ ratio in a carbonate-bearing mineral and in water can be used to constrain the formation temperature of the mineral, if it was formed in isotope equilibrium with the water. For this reaction, at lower temperatures, ^{18}O is more concentrated into calcite than at higher temperatures.

The need to measure two phases in order to calculate a mineral's formation temperature is a critical feature of this thermometer that greatly limits its applicability to historical problems: although carbonates are widely present in the sedimentary rock record, few examples of the water from which they precipitated are available. Geochemists have worked around this problem by estimating the isotopic composition of the coexisting water (e.g., Jaffrés et al., 2007; Zachos et al., 2001), but such estimates are subject to considerable uncertainty (e.g., they require knowledge of the amount of ice on the Earth), and they become more problematic the further back in time one goes. Indeed, estimates of the isotopic composition of water in the past is one of the more controversial subjects in earth history (Jaffrés et al., 2007; Kasting et al., 2006; Lécuyer and Allemand, 1999; Muehlenbachs, 1986; Veizer et al., 1999). This, combined with questions over the isotopic integrity of ancient carbonates (Degens and Epstein, 1962; Killingley, 1983; Land, 1995; Schrag et al., 1995; Veizer et al., 1997; Veizer et al., 1986), has made it challenging to ascertain the precise meaning of the oxygen isotope composition of ancient carbonates. The general observation of ancient carbonates is that in the past, on average, the isotopic composition of carbonates becomes less enriched (i.e. lower) in $^{18}O/^{16}O$ ratios, quantified with δ (Footnote 1) notation (Jaffrés et al., 2007; Veizer et al., 1999; Veizer et al., 1997; Veizer et al., 1986). At its most basic level, this trend can be interpreted via three end-member scenarios: (1) There has been a secular decrease in surface temperatures with time to the present, with the $\delta^{18}O$ values of the oceans held constant (Karhu and Epstein, 1986; Knauth and Epstein, 1976; though note that these

[1] $\delta=(R_{sample}/R_{standard}-1)*1000$ where $R=[^{13}C]/[^{12}C]$ for carbon isotopes and $[^{18}O]/[^{16}O]$ or $[^{17}O]/[^{16}O]$ for oxygen isotopes. For carbon isotopes samples are referenced to VPDB and VSMOW for oxgyen isotopes. We assume that ^{17}R and ^{18}R are related following a mass law of 0.5164 (Affek and Eiler, 2006).

66 studies and their conclusions are based on the oxygen isotopic composition silica and
67 phosphate groups in apatites). This is because at higher temperatures the difference in
68 $\delta^{18}O$ between water and carbonates diminishes. (2) There has been a secular increase in
69 the isotopic composition of waters to the present with the temperature of the earth's
70 surface remaining roughly the same (Jaffrés et al., 2007; Kasting et al., 2006; Veizer et
71 al., 1999; Veizer et al., 1997; Veizer et al., 1986). And (3) the carbonates have been
72 compromised by diagenesis and thus do not faithfully record their original formational
73 environment (Land, 1995).

74 Differentiating between these possibilities is challenging and requires, at the very
75 least, an independent measurement of the formation temperature of these ancient
76 carbonates. A relatively new technique that quantifies the abundances of carbonate
77 clumped isotopologues has proven to be a major breakthrough in beginning to unravel
78 these contentious issues and probe new ground (Eiler, 2007; Eiler, 2011; Eiler, 2013;
79 Eiler and Schauble, 2004; Ghosh et al., 2006). The dominant clumped isotopologue in
80 carbonates on the earth is $^{13}C^{16}O_2{}^{18}O$, which controls the clumped isotope measurements
81 described below. To explain how this technique works, I write an equilibrium reaction
82 involving exchange of oxygen isotopes with this isotopologue and some of the other
83 major isotopologues of carbonates:

84 $$^{12}C^{16}O_3 + {}^{13}C^{16}O_2{}^{18}O \leftrightarrow {}^{13}C^{16}O_3 + {}^{12}C^{16}O_2{}^{18}O\,. \quad (4)$$

85 The equilibrium constant for this reaction,

86 $$K_{eq} = \frac{\left[{}^{13}C^{16}O_3\right] \text{ x } \left[{}^{12}C^{16}O_2{}^{18}O\right]}{\left[{}^{12}C^{16}O_3\right] \text{ x } \left[{}^{13}C^{16}O_2{}^{18}O\right]}, \quad (5)$$

is a function of temperature such that the left side of the reaction, which includes the clumped isotopologue, is favored compared to the right side at all finite temperatures (Schauble et al., 2006). Consequently, despite the assumption built into all $\delta^{18}O$ measurements of carbonate minerals that isotopes are randomly distributed amongst all isotopologues, the distribution is not random — this effect though measureable (as described below) is too subtle to affect $\delta^{18}O$ and $\delta^{13}C$ values of carbonates within commonly reported errors. Thus constraints on the composition of these four isotopologues would allow for the calculation of the formation temperature of the carbonate (assuming the carbonate isotopologues are formed in internal isotopic equilibrium) *without any need for the knowledge of the isotopic composition of the water in which the carbonate formed or other minerals with which it equilibrated*. Thus, this technique eliminates one of the more problematic issues associated with the interpretation of ancient carbonate $\delta^{18}O$ values — the isotopic composition of the water in which the carbonate grew. It does not, as will be discussed below, eliminate issues of diagenesis and it faces other challenges that conventional isotopic analyses of carbonates do not.

In practice, no techniques currently exist that can measure intact carbonate isotopologue abundances at useful precisions. Instead, the most common technique for the measurement of carbonate isotopic compositions is to 'digest' the carbonate in phosphoric acid and generate CO_2, which is then measured on a mass spectrometer (McCrea, 1950). In order to measure the multiply substituted isotopologues released from the carbonate minerals, the mass 47 isotopologue of CO_2 is measured. It includes three species: $^{13}C^{16}O^{18}O$, $^{13}C^{17}O_2$, and $^{12}C^{17}O^{18}O$. These species, along with the mass 44, 45, and 46 CO_2 isotopologues are measured through mass spectrometry (Eiler and Schauble,

2004; Huntington et al., 2009). The amount of mass 47 isotopologues present vs. that expected for a random isotopic distribution is represented with the symbol Δ_{47} where

$$\Delta_{47} = 1000 \times \left(\frac{^{47}R}{^{47}R^{*}} - 1 \right) \quad (6)$$

and ^{47}R represents the relative concentration of mass 47 CO_2 isotopologues vs. mass 44 CO_2 isotopologues ($^{47}R = [^{47}CO_2]/[^{44}CO_2]$) and the * indicates the concentration of isotopologues expected for a random distribution of isotopes (Wang et al., 2004).

It has been both theoretically (Eagle et al., 2010; Guo et al., 2009; Schauble et al., 2006) and empirically demonstrated that Δ_{47} values of carbonates are functions of temperature for minerals that are precipitated in equilibrium both for synthetic (Ghosh et al., 2006; Zaarur et al., 2013) and biogenic carbonates (Came et al., 2007; Eagle et al., 2010; Ghosh et al., 2007; Tripati et al., 2010). Thus Δ_{47} values can be used for accurate and precise temperature measurements. Indeed, Δ_{47}-based temperatures have now been demonstrated to have achievable precisions (±1 standard error, s.e.) better than ± 0.5°C (Tripati et al., 2014).

Δ_{47} values have mostly been interpreted in the context of formation/re-equilibration temperatures. However, it is important to recognize that the measured quantity in a sample is its Δ_{47} value, which, from a physical point of view, only gives information on the relative amounts of multiply substituted isotopologues in the sample. Only under certain special conditions does this value relate to a formation/equilibration temperature. Specifically, in order for a Δ_{47} value to have a direct, thermal meaning, the carbonate being measured must have (1) formed (or recrystallized/re-equilibrated) in internal isotopic equilibrium and (2) preserved that original equilibrium isotopic state up

until being measured in the lab. These requirements are also necessary for classical oxygen isotope based paleothermometry (except that external equilibrium between a carbonate and another phase must be established for the classic methods as opposed to internal equilibrium), though with slightly different caveats as will be discussed.

Formation in isotopic equilibrium for ancient minerals can only ever be assumed — however, the demonstration that Δ_{47} values for many modern types of carbonates reflect accurate formation temperatures indicates this assumption is grounded. Understanding the preservation of the isotopic integrity of ancient carbonates, on the other hand, is a challenging and controversial issue (Degens and Epstein, 1962; Killingley, 1983; Land, 1995; Schrag et al., 1992, 1995; Veizer et al., 1999; Veizer et al., 1997; Veizer et al., 1986). However, there is an important difference in directly translating the debates on the preservation of $\delta^{18}O$ values in samples to the framework of Δ_{47} values (Figure 1). For example, only 'open-system' modification of carbonate minerals can modify $\delta^{18}O$ values — this would include recrystallization of carbonate in a water buffered solution at a different temperature or water isotopic composition as compared to the original formational environment. Additionally, high temperature open-system diffusion in which oxygen atoms from other mineral phases penetrate into and leave the carbonate lattice can also result in changes in $\delta^{18}O$ values. Critically, in these examples, $\delta^{18}O$ values are compromised due to open-system isotope exchange between the mineral and its surrounding environment. Both of these styles of alteration were recognized early on as potential issues by Urey et al. (1951). If this occurs, the $\delta^{18}O$ value *and* Δ_{47} values will be altered to reflect either partially or wholly the new environmental conditions. Although in such a system the isotopic composition of the minerals would no

longer reflect the original formational environments, these modified isotopic values would still capture an important aspect of the carbonate's history in the rock record including diagenesis and metamorphism. Thus open system exchange of oxygen isotopes of a carbonate crystal lattice, though often viewed negatively due to its effect on paleotemperature reconstructions, yields important information on mass transfer reactions in sediments and the crust and thermal histories post deposition. However, in order to study any of these processes, a quantitative understanding of their effect on the isotopic composition of the samples of interest must be understood.

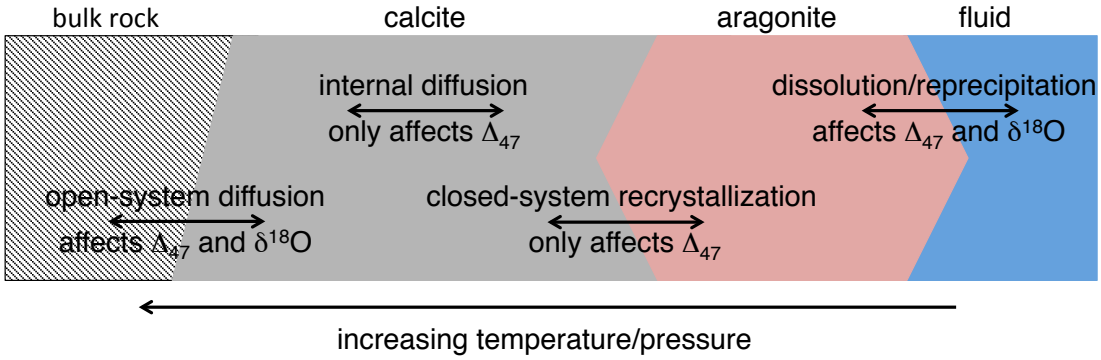

Figure 1: Cartoon representation of various diffusional and diagenetic pathways that can cause $\delta^{18}O$ and/or Δ_{47} values to change.

Significantly, Δ_{47} values can be altered during diffusion and diagenetic transformations even in the absence of changes in $\delta^{18}O$ values. For example, closed-system recrystallization of aragonite to calcite in which no mass transfer reactions occur would preserve the mineral's original $\delta^{18}O$ value (Urey et al., 1951). However, during this process, C-O bonds would be broken and reformed and thus Δ_{47} values, which track (mostly) the distributions of ^{13}C-^{18}O bonds, would be altered. Additionally, internal diffusion of carbon or oxygen in a mineral lattice would not alter $\delta^{18}O$ values, but this diffusion would result in bonds breaking and forming and thus alter Δ_{47} values (Passey

and Henkes, 2012). Again, in order to use Δ_{47} values to interpret ancient formation temperatures of rocks that have experienced any heating and perhaps diagenesis during burial (i.e. all ancient rocks) and use Δ_{47} values to quantify and reconstruct diagenetic reactions and thermal histories, the effects of these processes on Δ_{47} values must be understood.

Some work has already been done on understanding the effects of these processes on clumped isotope-based measurements of carbonates. For high temperature processes such as diffusion, this previous work includes the observations of Ghosh et al. (2006) and Ferry et al. (2011) that in natural, slowly cooled marbles, Δ_{47} values yield temperatures of ~200 °C for calcite and ~300 °C for dolomite. These are not formation temperatures because the rocks were metamorphosed and recrystallized at higher temperatures. Instead these represent 'closure' temperatures (Dodson, 1973). A closure temperature is the measured temperature (based on the parameter of interest; e.g., Δ_{47} values) at which, for the case of Δ_{47} values, internal and external isotopic exchange processes in the mineral lattice cease and Δ_{47} values are 'locked' into the mineral. Closure temperatures are not universal, depending on, for example, the cooling rate of the system. The concept of closure is explained in detail in Chapter 3, but these temperatures give a rough idea of the kinds of environmental temperatures required for the internal diffusion of carbon and oxygen to occur and Δ_{47} values to begin to change. These observations are additionally supported by the work of Dennis and Schrag (2010) on slowly cooled igneous carbonate minerals (carbonatites), which also indicate Δ_{47} closure temperatures in calcites of between ~150-250 °C (though with some exceptions). One quantitative, experimentally-grounded model of diffusion in the context of Δ_{47} values was derived by Passey and

Henkes (2012) for calcite. This model is based on laboratory heating experiments of calcites as a function of time and temperature. In these experiments, non-first order kinetics were observed in the experimental products, with a rapid change in Δ_{47} at the start of heating, followed by slower changes. In order to quantify the kinetics of these experiments, the initial, rapid kinetics of the data were discarded as an artifact due to defect annealment of the crystals at the start of the experiment and only the slower kinetics modeled.

In Chapter 3 of this thesis I follow up on these natural observations and experiments of high-temperature processes and their effects on Δ_{47} values by adding new constraints with measurements of igneous apatites and calcites from carbonatites, laboratory heating experiments of apatites and calcites, and a new model framework to quantify both the experimental data and measurements of natural samples. A model framework is created that is capable, in a physically justifiable way, of capturing the non-first order kinetics of the experimental data, which has so far been lacking. With this model, I additionally comment on the general capacity of calcite and apatite minerals to preserve their original clumped temperatures in the context of commonly encountered burial histories.

Diagenesis is another key process that must be understood quantitatively to correctly interpret the meaning of Δ_{47} values for ancient rocks. In nearly all studies of ancient carbonates that use Δ_{47} values, the effects of diagenesis are grappled with in various manners including petrographic examinations, trace element measurements, and/or comparison of Δ_{47} values of various phases such as cements vs. fossils or comparison of Δ_{47}-based temperatures to other paleothermometers (e.g., Came et al.,

2007; Dennis et al., 2013; Finnegan et al., 2011; Keating-Bitonti et al., 2011; Price and Passey, 2013; Snell et al., 2013; VanDeVelde et al., 2013). However, as noted in Came et al. (2007) the lack of diagenesis in a sample can never be proven and as discussed in Finnegan et al. (2011) there may be and perhaps always is a small amount of diagenetic alteration in samples, even those that pass all typical 'quality of preservation' criteria. This is due, in part, to the large mass (8 mg of calcite) needed for each measurement. One approach that has been taken, due to this subtle, often unknown amount of diagenesis in each sample, is to take the lowest measured temperature from any given geological section interrogated as a best estimate for the upper-limit environmental temperature for that time period (Finnegan et al., 2011). Such approaches of taking the lowest observed temperature from a geological section have been used in previous isotopic studies as well (e.g., Karhu and Epstein, 1986).

Additionally, beyond just calcite and aragonite, apatites (specifically structurally bound carbonate groups in apatites) are now being used for clumped isotope-based temperature reconstructions (Eagle et al., 2010; Eagle et al., 2011). Apatites are thought to undergo diagenesis differently from carbonate minerals like calcite and aragonite (Longinelli et al., 2003; Shemesh et al., 1983; Shemesh et al., 1988), generally being thought to be more resistant to diagenesis. This, however, often refers to phosphate groups in the apatite instead of the carbonate groups (Kohn and Cerling, 2002; Shemesh et al., 1983; Shemesh et al., 1988). Because these minerals are not measured as frequently as carbonate minerals for paleoclimate reconstructions, there are fewer established ways to assess diagenetic alteration (Shemesh et al., 1983) for either bulk isotopes and especially Δ_{47} values.

Diagenesis is sometimes seen as an 'issue' to be avoided in sample selection because it has the potential to alter a sample's formational chemical or isotopic properties. However, diagenesis itself reflects the history of a sample post formation, how the sample interacts with its burial environment and becomes a rock, and its post-depositional thermal history. Thus, understanding diagenesis not only increases our capacity to identify its presence and avoid it for paleoclimate reconstructions, but adds insight into sedimentary reactions (Fantle et al., 2010). For clumped isotopes, although diagenesis can often be demonstrated by, for example, measured temperatures well in excess of reasonable surface temperatures (Came et al., 2007; Eagle et al., 2011; Finnegan et al., 2011; Snell et al., 2013; VanDeVelde et al., 2013), only a few studies have used clumped isotopes to explicitly study diagenesis (Dale et al., 2014; Ferry et al., 2011; Huntington et al., 2011), and none with a focus on carbonate groups in apatites. Additionally, these studies often treat diagenesis as a binary issue — for example a sample is either pristine or altered and the degree of alteration not always of interest.

In Chapter 3 of this thesis, the issue of recrystallization and diagenesis is addressed in the context of Δ_{47} values. To do this, apatite minerals, which contain structural carbonate suitable for isotopic measurements (Eagle et al., 2010; Eagle et al., 2011; Kolodny and Kaplan, 1970; Shemesh et al., 1983; Silverman et al., 1952), from phosphorite deposits ranging in age from modern to 265 million years old, were measured for Δ_{47} values and $\delta^{18}O$ values. These samples were selected as they were previously measured for phosphate apatite $\delta^{18}O$ values (Shemesh et al., 1983; Shemesh et al., 1988) and are suspected of undergoing poorly constrained amounts diagenesis that result in systematic relationships between the oxygen isotopic composition of the

phosphate and carbonate groups, but for unknown reasons. Using the clumped isotope temperatures in combination with the oxygen isotope compositions of the carbonate and phosphate groups, a diagenetic model is generated that allows for the quantification of how much diagenesis each sample has experienced and the environments in which that diagenesis occurred. This model is then interpreted in the context of the physical environment in which diagenesis takes place and a conceptual model is put forward to explain the insights gained from the modeling effort.

2. References

Brassell, S., Eglinton, G., Marlowe, I., Pflaumann, U., Sarnthein, M., 1986. Molecular stratigraphy: A new tool for climatic assessment. *Nature* 320, 129-133.

Came, R.E., Eiler, J.M., Veizer, J., Azmy, K., Brand, U., Weidman, C.R., 2007. Coupling of surface temperatures and atmospheric CO_2 concentrations during the Palaeozoic era. *Nature* 449, 198-201.

Dale, A., John, C.M., Mozley, P.S., Smalley, P., Muggeridge, A.H., 2014. Time-capsule concretions: Unlocking burial diagenetic processes in the Mancos Shale using carbonate clumped isotopes. *Earth and Planetary Science Letters* 394, 30-37.

Degens, E.T., Epstein, S., 1962. Relationship between O^{18}/O^{16} ratios in coexisting carbonates, cherts, and diatomites: geological notes. *AAPG Bulletin* 46, 534-542.

Dennis, K., Cochran, J., Landman, N., Schrag, D., 2013. The climate of the Late Cretaceous: New insights from the application of the carbonate clumped isotope thermometer to Western Interior Seaway macrofossil. *Earth and Planetary Science Letters* 362, 51-65.

Dennis, K.J., Schrag, D.P., 2010. Clumped isotope thermometry of carbonatites as an indicator of diagenetic alteration. *Geochimica et Cosmochimica Acta* 74, 4110-4122.

Dodson, M.H., 1973. Closure temperature in cooling geochronological and petrological systems. *Contributions to Mineralogy and Petrology* 40, 259-274.

Eagle, R.A., Schauble, E.A., Tripati, A.K., Tütken, T., Hulbert, R.C., Eiler, J.M., 2010. Body temperatures of modern and extinct vertebrates from ^{13}C-^{18}O bond abundances in bioapatite. *Proceedings of the National Academy of Sciences* 107, 10377.

296 Eagle, R.A., Tütken, T., Martin, T.S., Tripati, A.K., Fricke, H.C., Connely, M., Cifelli,
297 R.L., Eiler, J.M., 2011. Dinosaur body temperatures determined from isotopic (^{13}C-
298 ^{18}O) ordering in fossil biominerals. *Science* 333, 443.
299 Eiler, J.M., 2007. "Clumped-isotope" geochemistry - The study of naturally-occurring,
300 multiply-substituted isotopologues. *Earth and Planetary Science Letters* 262, 309-
301 327.
302 Eiler, J.M., 2011. Paleoclimate reconstruction using carbonate clumped isotope
303 thermometry. *Quaternary Science Reviews* 30, 3575-3588.
304 Eiler, J.M., 2013. The isotopic anatomies of molecules and minerals. *Annual Review of*
305 *Earth and Planetary Sciences* 41, 411-441.
306 Eiler, J.M., Schauble, E., 2004. ^{18}O^{13}C^{16}O in Earth's atmosphere. *Geochimica et*
307 *Cosmochimica Acta* 68, 4767-4777.
308 Epstein, S., Buchsbaum, R., Lowenstam, H.A., Urey, H.C., 1953. Revised carbonate-
309 water isotopic temperature scale. *Geological Society of America Bulletin* 64, 1315-
310 1325.
311 Fantle, M., Maher, K., DePaolo, D., 2010. Isotopic approaches for quantifying the rates
312 of marine burial diagenesis. *Reviews of Geophysics* 48.
313 Ferry, J.M., Passey, B.H., Vasconcelos, C., Eiler, J.M., 2011. Formation of dolomite at
314 40–80° C in the Latemar carbonate buildup, Dolomites, Italy, from clumped isotope
315 thermometry. *Geology* 39, 571-574.
316 Finnegan, S., Bergmann, K., Eiler, J.M., Jones, D.S., Fike, D.A., Eisenman, I., Hughes,
317 N.C., Tripati, A.K., Fischer, W.W., 2011. The magnitude and duration of Late
318 Ordovician-Early Silurian glaciation. *Science* 331, 903.

Ghosh, P., Adkins, J., Affek, H., Balta, B., Guo, W., Schauble, E.A., Schrag, D., Eiler, J.M., 2006. ^{13}C-^{18}O bonds in carbonate minerals: A new kind of paleothermometer. *Geochimica et Cosmochimica Acta* 70, 1439-1456.

Ghosh, P., Eiler, J., Campana, S.E., Feeney, R.F., 2007. Calibration of the carbonate 'clumped isotope' paleothermometer for otoliths. *Geochimica et cosmochimica acta* 71, 2736-2744.

Guo, W., Mosenfelder, J.L., Goddard, W.A., Eiler, J.M., 2009. Isotopic fractionations associated with phosphoric acid digestion of carbonate minerals: Insights from first-principles theoretical modeling and clumped isotope measurements. *Geochimica Et Cosmochimica Acta* 73, 7203-7225.

Huntington, K., Eiler, J., Affek, H., Guo, W., Bonifacie, M., Yeung, L., Thiagarajan, N., Passey, B., Tripati, A., Daëron, M., 2009. Methods and limitations of 'clumped' CO_2 isotope (Δ_{47}) analysis by gas-source isotope ratio mass spectrometry. *Journal of Mass Spectrometry* 44, 1318-1329.

Huntington, K.W., Budd, D.A., Wernicke, B.P., Eiler, J.M., 2011. Use of clumped-isotope thermometry to constrain the crystallization temperature of diagenetic calcite. *Journal of Sedimentary Research* 81, 656-669.

Jaffrés, J.B.D., Shields, G.A., Wallmann, K., 2007. The oxygen isotope evolution of seawater: A critical review of a long-standing controversy and an improved geological water cycle model for the past 3.4 billion years. *Earth-Science Reviews* 83, 83-122.

Karhu, J., Epstein, S., 1986. The implication of the oxygen isotope records in coexisting cherts and phosphates. *Geochimica et Cosmochimica Acta* 50, 1745-1756.

342 Kasting, J.F., Howard, M.T., Wallmann, K., Veizer, J., Shields, G., Jaffrés, J., 2006.
343 Paleoclimates, ocean depth, and the oxygen isotopic composition of seawater. *Earth*
344 *and Planetary Science Letters* 252, 82-93.
345 Keating-Bitonti, C.R., Ivany, L.C., Affek, H.P., Douglas, P., Samson, S.D., 2011. Warm,
346 not super-hot, temperatures in the early Eocene subtropics. *Geology* 39, 771-774.
347 Killingley, J.S., 1983. Effects of diagenetic recrystallization on $^{18}O/^{16}O$ values of deep-sea
348 sediments. *Nature* 301, 594-597.
349 Kim, S.T., O'Neil, J.R., 1997. Equilibrium and nonequilibrium oxygen isotope effects in
350 synthetic carbonates. *Geochimica et Cosmochimica Acta* 61, 3461-3475.
351 Knauth, L.P., Epstein, S., 1976. Hydrogen and oxygen isotope ratios in nodular and
352 bedded cherts. *Geochimica et Cosmochimica Acta* 40, 1095-1108.
353 Kohn, M.J., Cerling, T.E., 2002. *Stable isotope compositions of biological apatite*, in:
354 Kohn, M.J., Rakovan, J.M., Huges, J.M. (Eds.), *Phosphates—Geochemical,*
355 *Geobiological, and Materials Importance*. Mineralogical Society of America,
356 Washington, DC, pp. 455-488.
357 Kolodny, Y., Kaplan, I., 1970. Carbon and oxygen isotopes in apatite CO_2 and co-
358 existing calcite from sedimentary phosphorite. *Journal of Sedimentary Research* 40,
359 954-959.
360 Land, L.S., 1995. Comment on "Oxygen and carbon isotopic composition of Ordovician
361 brachiopods: Implications for coeval seawater" by H. Qing and J. Veizer. *Geochimica*
362 *et Cosmochimica Acta* 59, 2843-2844.

363 Lécuyer, C., Allemand, P., 1999. Modelling of the oxygen isotope evolution of seawater:
364 Implications for the climate interpretation of the $\delta^{18}O$ of marine sediments.
365 *Geochimica et Cosmochimica Acta* 63, 351-361.
366 Longinelli, A., Wierzbowski, H., Di Matteo, A., 2003. $\delta^{18}O(PO_4^{3-})$ and $\delta^{18}O(CO_3^{2-})$ from
367 belemnite guards from Eastern Europe: Implications for palaeoceanographic
368 reconstructions and for the preservation of pristine isotopic values. *Earth and*
369 *Planetary Science Letters* 209, 337-350.
370 McCrea, J.M., 1950. On the isotopic chemistry of carbonates and a paleotemperature
371 Scale. *Journal of Chemical Physics* 18, 849-857.
372 Muehlenbachs, K., 1986. Alteration of the oceanic crust and the ^{18}O history of seawater.
373 *Reviews in Mineralogy and Geochemistry* 16, 425-444.
374 Nutman, A.P., Mojzsis, S.J., Friend, C.R., 1997. Recognition of ≥ 3850 Ma water-lain
375 sediments in West Greenland and their significance for the early Archaean Earth.
376 *Geochimica et Cosmochimica Acta* 61, 2475-2484.
377 Passey, B., Henkes, G., 2012. Carbonate clumped isotope bond reordering and
378 geospeedometry. *Earth and Planetary Science Letters* 351-352, 223-236.
379 Price, G.D., Passey, B.H., 2013. Dynamic polar climates in a greenhouse world:
380 Evidence from clumped isotope thermometry of Early Cretaceous belemnites.
381 *Geology* 41, 923-926.
382 Rosenthal, Y., Boyle, E.A., Slowey, N., 1997. Temperature control on the incorporation
383 of magnesium, strontium, fluorine, and cadmium into benthic foraminiferal shells
384 from Little Bahama Bank: Prospects for thermocline paleoceanography. *Geochimica*
385 *et Cosmochimica Acta* 61, 3633-3643.

386 Schauble, E.A., Ghosh, P., Eiler, J.M., 2006. Preferential formation of ^{13}C-^{18}O bonds in
387 carbonate minerals, estimated using first-principles lattice dynamics. *Geochimica et*
388 *Cosmochimica Acta* 70, 2510-2529.
389 Schrag, D.P., DePaolo, D.J., Richter, F.M., 1992. Oxygen isotope exchange in a two-
390 layer model of oceanic crust. *Earth and Planetary Science Letters* 111, 305-317.
391 Schrag, D.P., DePaolo, D.J., Richter, F.M., 1995. Reconstructing past sea surface
392 temperatures: Correcting for diagenesis of bulk marine carbonate. *Geochimica et*
393 *Cosmochimica Acta* 59, 2265-2278.
394 Shemesh, A., Kolodny, Y., Luz, B., 1983. Oxygen isotope variations in phosphate of
395 biogenic apatites, II. Phosphorite rocks. *Earth and Planetary Science Letters* 64, 405-
396 416.
397 Shemesh, A., Kolodny, Y., Luz, B., 1988. Isotope geochemistry of oxygen and carbon in
398 phosphate and carbonate of phosphorite francolite. *Geochimica et Cosmochimica*
399 *Acta* 52, 2565-2572.
400 Silverman, S.R., Fuyat, R.K., Weiser, J.D., 1952. Quantitative determination of calcite
401 associated with carbonate-bearing Apatites. *American Mineralogist* 37, 211-222.
402 Snell, K.E., Thrasher, B.L., Eiler, J.M., Koch, P.L., Sloan, L.C., Tabor, N.J., 2013. Hot
403 summers in the Bighorn Basin during the early Paleogene. *Geology* 41, 55-58.
404 Tarduno, J., Brinkman, D., Renne, P., Cottrell, R., Scher, H., Castillo, P., 1998. Evidence
405 for extreme climatic warmth from Late Cretaceous Arctic vertebrates. *Science* 282,
406 2241-2243.

407 Tripati, A.K., Eagle, R.A., Thiagarajan, N., Gagnon, A.C., Bauch, H., Halloran, P.R.,
408 Eiler, J.M., 2010. $^{13}C^{18}O$ isotope signatures and 'clumped isotope' thermometry in
409 foraminifera and coccoliths. *Geochimica et Cosmochimica Acta* 74, 5697-5717.
410 Tripati, A.K., Sahany, S., Pittman, D., Eagle, R.A., Neelin, J.D., Mitchell, J.L., Beaufort,
411 L., 2014. Modern and glacial tropical snowlines controlled by sea surface temperature
412 and atmospheric mixing. *Nature Geoscience* 7, 205-209.
413 Urey, H.C., 1947. The thermodynamic properties of isotopic substances. *Journal of the*
414 *Chemical Society*, 562-581.
415 Urey, H.C., Lowenstam, H.A., Epstein, S., McKinney, C.R., 1951. Measurement of
416 paleotemperatures and temperatures of the Upper Cretaceous of England, Denmark,
417 and the southeastern United States. *Geological Society of America Bulletin* 62, 399-
418 416.
419 VanDeVelde, J.H., Bowen, G.J., Passey, B.H., Bowen, B.B., 2013. Climatic and
420 diagenetic signals in the stable isotope geochemistry of dolomitic paleosols spanning
421 the Paleocene–Eocene boundary. *Geochimica et Cosmochimica Acta* 109, 254-267.
422 Veizer, J., Ala, D., Azmy, K., Bruckschen, P., Buhl, D., Bruhn, F., Carden, G.A., Diener,
423 A., Ebneth, S., Godderis, Y., 1999. $^{87}Sr/^{86}Sr$, $\delta^{13}C$ and $\delta^{18}O$ evolution of Phanerozoic
424 seawater. *Chemical Geology* 161, 59-88.
425 Veizer, J., Bruckschen, P., Pawellek, F., Diener, A., Podlaha, O.G., Carden, G.A., Jasper,
426 T., Korte, C., Strauss, H., Azmy, K., 1997. Oxygen isotope evolution of Phanerozoic
427 seawater. *Palaeogeography, Palaeoclimatology, Palaeoecology* 132, 159-172.

428 Veizer, J., Fritz, P., Jones, B., 1986. Geochemistry of brachiopods: Oxygen and carbon
429 isotopic records of Paleozoic oceans. *Geochimica et Cosmochimica Acta* 50, 1679-
430 1696.
431 Wang, Z., Schauble, E.A., Eiler, J.M., 2004. Equilibrium thermodynamics of multiply
432 substituted isotopologues of molecular gases. *Geochimica et Cosmochimica Acta* 68,
433 4779-4797.
434 Zaarur, S., Affek, H.P., Brandon, M.T., 2013. A revised calibration of the clumped
435 isotope thermometer. *Earth and Planetary Science Letters* 382, 47-57.
436 Zachos, J., Pagani, M., Sloan, L., Thomas, E., Billups, K., 2001. Trends, rhythms, and
437 aberrations in global climate 65 Ma to present. *Science* 292, 686-693.
438
439

Chapter III

The kinetics of clumped isotopes in inorganic calcites and apatites in natural and experimental samples

DA Stolper[a] and JM Eiler[a]

[a]*Division of Geological and Planetary Sciences, California Institute of Technology, Pasadena, CA 91125, USA*

Accepted to *The American Journal of Science*

Abstract: Carbonate clumped isotope geothermometry is a tool used to reconstruct formation or (re)equilibration temperatures of carbonate-bearing minerals, including carbonate groups substituted into apatite. It is based on the preference for isotopologues with multiple heavy isotopes (for example, $^{13}C^{16}O_2{}^{18}O^{2-}$ groups) to be more abundant at equilibrium than would be expected if all isotopes were randomly distributed amongst all carbonate groups. Because this preference is only a function of temperature, excesses of multiply substituted species can be used to calculate formation temperatures without knowledge of the isotopic composition of water from which the mineral precipitated or other phases with which it may have equilibrated. However, the measured temperature could be modified after mineral growth if exchange of isotopes among carbonate groups has occurred by solid-state diffusion. Because diffusion is a thermally activated process, its rate depends on temperature and increases in magnitude at higher temperatures. Thus solid-state diffusion could lead to effective re-equilibration at high temperatures, overprinting the original temperatures recorded during mineral growth. We measured clumped isotope temperatures in carbonate bearing minerals (including apatites) from several carbonatites to constrain the kinetics of diffusion-controlled resetting. We observe that in carbonatites, carbonate minerals (where calcite is the dominant constituent) and apatite clumped isotope temperatures decrease with increasing intrusion depth, and that apatites record lower closure temperatures than carbonate minerals from the same carbonatite intrusion. We additionally conducted heating experiments at different temperatures to derive the temperature dependence for the rate constants that describe the alteration of clumped isotope temperatures with time in calcites and apatites. We find that calcites exhibit complex, non-first-order kinetics. To quantify these results, we constructed a model that incorporates both diffusion of isotopes through the crystal lattice and isotope exchange between adjacent carbonate groups. We tested this model through comparison to samples with known cooling histories and find that the model is able to reasonably capture observed closure temperatures of calcites with geologically reasonable cooling rates. A similar model for apatite overpredicts the closure temperatures found in natural samples; we hypothesize that this discrepancy is the result of annealment of radiation damage in our experiments, which lowers the diffusivity of carbonate groups compared to damaged natural samples. Finally, we ran models to understand how heating can alter the recorded clumped isotope temperature. Our model predicts that samples are capable of quickly altering their recorded clumped isotope

temperatures by up to 2°C if held at 60°C for 100 million years and up to 40°C if held at 120°C. A second, slower change occurs above 120°C after 100 million years taking the apparent temperature measured by clumped isotope thermometry up to the true ambient temperature. This result implies that old (hundreds of millions of years) samples that have only experienced mild thermal histories could exhibit small (order 10°C) changes in their clumped isotope temperatures. We compared this heating model to clumped isotope measurements from paleosol samples from the Siwalik Basin in Nepal, which were buried up to 5 km and then rapidly uplifted to the surface and often do not give reasonable surface temperatures. The modeled temperatures agree with measured temperatures of these samples as a function of maximum burial depth.

1. Introduction

The carbonate 'clumped isotope' thermometer (Ghosh et al., 2006) provides a method for measuring formation temperatures of carbonate minerals formed at equilibrium, including carbonate groups in apatite (Eagle et al., 2010). This temperature proxy is based on the thermodynamic preference for carbonate groups with multiple heavy isotopes, which we term 'clumped' isotopologues (for example, $^{13}C^{16}O_2{}^{18}O^{2-}$), to be measurably enriched compared to a random ordering of isotopes among all carbonate groups (Schauble et al., 2006). For example, for the following homogenous exchange reaction,

$$Ca^{12}C^{16}O_3 + Ca^{13}C^{16}O_2{}^{18}O \leftrightarrow Ca^{12}C^{16}O_2{}^{18}O + Ca^{13}C^{16}O_3, \quad (1)$$

the left side of this reaction is slightly favored (<0.1%) over the right side when compared to a random distribution of isotopes. This preference for heavier isotopes to "clump" together is temperature dependent and increases in magnitude with decreasing temperatures. The equilibrium constant for Equation (1) has been studied experimentally by measuring the relative abundances of isotopologues of CO_2 (dominantly $^{12}C^{16}O_2$, $^{13}C^{16}O_2$, $^{12}C^{16}O^{18}O$, and $^{13}C^{16}O^{18}O$) produced by the phosphoric acid digestion of carbonate minerals.

The carbonate clumped isotope thermometer is distinct from many other low-temperature (<~300°C) isotopic geothermometers because it constrains temperature independently of the isotopic composition of water from which a carbonate-bearing mineral grew. Conventional stable isotope thermometry for low-temperature systems, in contrast, is generally based on the difference in oxygen isotope composition between water and carbonate-bearing minerals (Epstein et al., 1953; McCrea, 1950; Urey, 1947).

Because this latter approach requires equilibrium between two phases, for example, water and calcite, temperature can only be solved for if the isotopic composition of both phases is known. Although carbonate-bearing minerals are available throughout much of the geological record, surface water samples are not. It is possible to work around this problem by estimating the isotopic composition of the coexisting water (for example, Zachos et al., 2001), but such estimates are subject to uncertainties (for example, they require knowledge of the amount of ice on the Earth), and become more problematic the further back in time one goes (Jaffrés et al., 2007). In carbonate clumped isotope thermometry, only a single phase is required (that is, the isotopic composition of ancient water is no longer needed), potentially opening up to paleothermometry the large number of ancient rocks that contain carbonate-bearing minerals (for example, Came et al., 2007; Finnegan et al., 2011).

Though the study of clumped isotopes offers great promise to many geological problems, an outstanding issue is understanding how well minerals retain their original clumped isotope signature. Isotopic clumping in carbonates is susceptible to resetting from recrystallization, open-system diffusion-limited exchange (that is, where the crystal lattice undergoes mass transfer reactions with the outside environment), and reordering through closed-system atomic migration through the crystal lattice. In this respect, the carbonate clumped isotope thermometer most resembles petrologic geothermometers based on homogenous-phase order-disorder reactions, such as the ordering of iron and magnesium on the M1 and M2 sites in orthopyroxenes (Zhang, 2008). If any of these processes has occurred in a sample, the temperature measured through the clumped isotope thermometer will not reflect the original formation temperature of the mineral.

Additionally, closed-system reordering or diffusion-limited open-system exchange may also interfere with use of this proxy to study recrystallization during diagenesis or metamorphism. On the other hand, if this process were well understood it might provide a new tool for studying the thermal histories of shallow crustal rocks. Interpretations of measured temperatures require a quantitative knowledge of the kinetics of recrystallization, diffusion-limited exchange, and closed-system reordering. We focus here on understanding the kinetics of closed-system reordering.

The kinetics of clumped isotopes in carbonates was addressed by Dennis and Schrag (2010) through the measurement of apparent temperatures recorded by carbonate minerals in carbonatites. It was suggested that these measured temperatures reflect the closure temperature of the carbonate clumped isotope thermometer, which can be broadly understood as the temperature below which internal reordering by closed-system atomic migration becomes so slow that Equation (1) ceases to proceed in either the forward or backward direction. Dennis and Schrag (2010) found that carbonate minerals from carbonatites generally record clumped isotope temperatures between ~100°C and 280°C — lower than the magmatic temperatures of carbonatites. This result is consistent with previous and subsequent findings that calcitic marbles generally record temperatures between 150-200°C (below peak metamorphic temperatures; Bonifacie et al., 2013; Ghosh et al., 2006). These results give a general guide to the closure temperatures of calcite with respect to Equation (1). However, it is not obvious whether these temperatures reflect the kinetics of internal reordering alone or might also be influenced by recrystallization or diffusion-limited open-system isotopic exchange. More generally, without quantitative knowledge of the actual reaction kinetics as a function of

temperature, it is difficult to predict the temperatures and, equally importantly, the time durations necessary to measurably modify the recorded clumped isotope temperature. Additionally, it isn't clear whether the closure temperatures of different carbonate bearing phases are the same or different, though dolomitic marbles appear to record higher closure temperatures than calcitic marbles (Bonifacie et al., 2013; Ferry et al., 2011) .

Most studies of the carbonate clumped isotope thermometer thus far have focused on calcite, aragonite, and dolomite. However, an additional mineral of interest to paleoclimate, paleobiology, and petrology that is amenable to clumped isotope analyses is apatite (Eagle et al., 2010; Eagle et al., 2011). Apatites can be used for clumped isotope measurements as they can contain carbonate groups in their mineral structure, which can be analyzed for their clumped isotope composition via acid-digestion release of CO_2. Carbonate in apatite substitutes for either phosphate groups or F, Cl and OH groups (McClellan, 1980; Silverman et al., 1952). Apatites are useful for reconstructions of temperatures for both paleoclimate and paleobiology as many organisms make their skeletons or teeth out of apatite. Additionally, apatite is a common constituent in igneous, metamorphic and sedimentary rocks. Apatites are believed to undergo diagenesis differently from carbonate minerals, and therefore may provide a useful point of comparison to deconvolve post-depositional changes to clumped isotope signatures. Specifically, it is generally thought that apatites are more resistant to isotopic exchange with diagenetic fluids, as compared to calcite and aragonite (Longinelli et al., 2003). However there is evidence that this resistance to diagenesis may only be true of the oxygen groups of phosphate (PO_4^{3-}) in apatite and not of the carbonate groups (Shemesh et al., 1988), though in the presence of microorganisms even phosphate-bound oxygen

atoms in bioapatite can be measurably exchanged with water at 28°C on laboratory time scales (Zazzo et al., 2004). A potentially useful check on paleotemperature reconstructions is the comparison of temperatures derived via clumped isotope analyses from carbonate groups in both apatites and carbonate minerals from the same lithological unit. There currently exists no estimate for the closure temperature of carbonate groups in apatites for clumped isotope measurements — this information is needed to put such a comparison into context. Fossil dinosaur teeth yield maximum temperatures of ~80-100°C, which must be the result of either diagenesis or closed-system reordering as these temperatures are too hot for animal survival (Eagle et al., 2011). Though it is not known whether diagenesis or diffusion caused these high temperatures, they imply closure temperatures are at least ~80-100°C in apatite or higher.

In order to better constrain the kinetics of formation and destruction of multiply substituted carbonate groups in both calcite and apatite, we measured clumped isotope temperatures of igneous calcite and apatite samples from the same intrusion from three carbonatite bodies. Additionally we performed heating experiments on natural optical calcite from Mexico and carbonate-bearing apatite from the Siilinjarvi carbonatite (Finland). We fit the experimental results to a model of isotopic re-equilibration resulting from the migration of carbon and oxygen through the mineral. We used this model to extrapolate the experimental measurements to lower temperature in order to explore how our model predicts the closure temperature of carbonate-bearing minerals with well known cooling histories. Finally, we modeled hypothetical time-temperature heating paths to better understand the responses of clumped isotope temperatures to thermal perturbations and compared our model to measured paleosol samples from the Siwalik

basin that experienced a simple, well-constrained thermal history. Passey and Henkes (2012) conducted similar experiments on calcite, and found results consistent with those we present here, though they present a different interpretation of the atomistic mechanisms responsible for the kinetics of isotopic ordering in calcite. This difference results in divergent predictions for changes in clumped isotope temperature with heating and cooling.

2. Theory and nomenclature

Here we briefly review the theory and nomenclature of carbonate clumped isotope thermometry used in this paper. This material is presented in greater detail in Eiler (2007, 2011) and references therein. The critical feature of clumped isotope geothermometry is that the left side of Equation (1) (which has $^{13}C^{16}O_2{}^{18}O^{2-}$) is thermodynamically favored over the right side, resulting in an excess of multiply substituted isotopologues compared to a random (stochastic) distribution at any finite temperature. The favoring of the left side of Equation (1) occurs as the reaction has a non-zero enthalpy of reaction — the left side of Equation (1) has a lower enthalpy than the right side. Quantum mechanically, this energy difference is largely due to the lower total zero-point energy of the left side of Equation (1) compared to the right side. The temperature dependence of the reaction is the result of the additional energetic contribution of configurational entropy to the total energy of the system. The configurational entropy is maximized (thus minimizing the total energy) when the distribution of isotopes among all possible isotopologues is random. Because entropy increases in relative importance as a component of free energy

(as compared to enthalpy) as temperature increases, the equilibrium constant for equation (1) increasingly favors a random distribution of isotopes as temperature increases.

We do not probe Equation (1) directly in current clumped isotope measurements. Instead, we measure the distribution of isotopes among isotopologues of CO_2 released from carbonate minerals via a phosphoric acid digestion (Ghosh et al., 2006). The amount of multiply substituted CO_2 at mass 47 (a combination of $^{13}C^{16}O^{18}O$, $^{12}C^{17}O^{18}O$, and $^{13}C^{17}O_2$) released from carbonates relative to the expected random distribution of atoms is largely controlled (~97%) by the equilibrium constant for Equation (1), and thus is proportional to temperature in carbonates that form in equilibrium (Ghosh et al., 2006; Guo et al., 2009).

We represent the degree of isotopic ordering (that is, the relative enrichment in clumped isotopologues) in CO_2 extracted from carbonate ions via Δ_{47} where

$$\Delta_{47} = \left(\frac{^{47}R}{^{47}R^*} - 1\right)*1000 - \left(\frac{^{46}R}{^{46}R^*} - 1\right)*1000 - \left(\frac{^{45}R}{^{45}R^*} - 1\right)*1000 . \quad (2)$$

Here, $^{i}R=[^{i}CO_2]/[^{44}CO_2]$ and the superscript * denotes a system with a random distribution of isotopes amongst all isotopologues. If one compares this equation to a similar expression for the following reaction,

$$^{12}C^{16}O_2 + {}^{13}C^{16}O^{18}O \leftrightarrow {}^{12}C^{16}O^{18}O + {}^{13}C^{16}O_2, \quad (3)$$

the equilibrium constant versus the equilibrium constant for a random distribution is approximately

$$-1000\ln\left(\frac{K}{K^*}\right) = \left(\frac{^{13}C^{18}O^{16}O R}{^{13}C^{18}O^{16}O R^*} - 1\right)*1000 - \left(\frac{^{13}C^{16}O_2 R}{^{13}C^{16}O_2 R^*} - 1\right)*1000 - \left(\frac{^{12}C^{18}O^{16}O R}{^{12}C^{18}O^{16}O R^*} - 1\right)*1000 \quad (4)$$

as described in Wang et al. (2004) where K is the equilibrium constant for Equation (3). Equation (4) purposefully bears a resemblance to Equation (2). The key difference

between the two is that our measurement, as discussed above, does not differentiate between internal isobars of CO_2 at a mass of 47 amu. However, 97% of CO_2 molecules with a mass of 47 amu are $^{13}C^{16}O^{18}O$ — thus one would expect that values determined in Equation (2) to strongly follow those of Equation (4). This temperature dependence has been demonstrated multiple times both experimentally and on natural samples with known formation temperatures (Eiler, 2011).

3. Experimental methods

~8 mg (±2) of calcite and 100-500 mg of apatite were used for each sample analysis. Samples, if not already powdered (as in the case of standards used), were hand crushed (dry) with an agate mortar and pestle. CO_2 was extracted on one of two custom made (and nearly identical) automatic vacuum lines attached directly to a Thermo MAT 253 mass spectrometer at Caltech following Passey et al. (2010). $\delta^{13}C$ and $\delta^{18}O$ (Footnote 1) values were measured by comparison of samples to a gas with known isotopic composition using an ion correction algorithm in the Isodat software program (Huntington et al., 2009) and standardized to VPDB for carbon isotope measurements and VSMOW for oxygen isotope measurements.

Δ_{47} values were standardized by comparison of samples with gases of independently known bulk isotopic composition and with gases that had been heated to achieve a near random distribution of isotopes following Huntington et al. (2009) and reported in the 'Ghosh' (or Caltech intralab) reference frame (Dennis et al., 2011; Ghosh et al., 2006). We provide a conversion to the absolute reference frame by following

[1] ${}^{i}\delta=1000*({}^{i}R_{sample}/{}^{i}R_{std}-1)$; $^{13}R=[^{13}C]/[^{12}C]$ $^{18}R=[^{18}O]/[^{16}O]$; the standard (std) is VPDB for carbon isotope measurements and VSMOW for oxygen isotope measurements.

Dennis et al. (2011) and using standards run in the lab with both known Ghosh and absolute reference frame values. We analyze and perform all models using data in the Ghosh reference frame because data points used in the Δ_{47} vs. temperature calibration here were universally produced in the Ghosh reference frame at Caltech. Some of these data points are published (Ghosh et al., 2006; Guo et al., 2009), and have been converted to the absolute reference frame (Dennis et al., 2011), but the dolomite calibration (see below), which ranges from 25-350°C and represents a key temperature interval for high temperature processes, has only been presented in abstract form (Bonifacie et al., 2011) in the Ghosh reference frame. Thus, in order to convert our Δ_{47} values into temperatures in what we believe to be the most self-consistent manner, we keep all data in the Ghosh reference frame.

For some analytical sessions the reference frame of measured states of ordering for the heated gases changed slowly with time (for example, Passey et al., 2010). Measurements of secondary carbonate standards during these sessions demonstrated that an accurate standardization could be accomplished by normalizing data to heated gases analyzed close in time to carbonate samples (generally within a 2-4 day window bracketing the time of sample analysis). Precision and accuracy were determined by measuring a Carrara marble standard multiple times within each measurement session. The average value in the Ghosh reference frame obtained over the course of 2 years of measurements was 0.360 ± 0.014‰ (1 standard deviation; σ), as compared to the long-term average of 0.352‰.

Calcite heating experiments were conducted on an optical grade calcite (see below) more depleted in both carbon and oxygen isotopes ($^{47}\delta$=-34‰; Footnote 2) than our secondary standards or commonly analyzed heated gases ($^{47}\delta$~-5 to 28‰). In order to standardize the Δ_{47} values of these optical calcites to the heated gas reference frame, additional heated gases more depleted in bulk isotopic composition than the optical calcites were run ($^{47}\delta$~-50‰) to ensure that we were always comparing unknown samples to an interpolated heated gas line. We noticed that although the external reproducibility of Δ_{47} measurements of optical calcites was normal over the coarse of a session (1σ=0.014‰), precision deteriorated between sessions. To improve external precision between analytical sessions, we performed corrections to the heated optical calcite Δ_{47} values using the unheated optical calcite Δ_{47} values (effectively treating the unheated optical calcite as a secondary standard as in Dennis et al., 2011). In all sessions an unheated optical calcite sample was run daily each day heated samples were run (for 33 total measurements of the unheated optical calcite sample). The difference of a given session's average unheated optical calcite Δ_{47} value from the global average across all sessions was added to all optical calcite samples for that session. For example, if a session's unheated optical calcite average was higher in Δ_{47} by +0.01‰ than the global average, 0.01‰ was subtracted from all heated optical calcites for that session. Six of the seven sessions had corrections of less than 0.024‰, less than 2σ of our general reproducibility (1$\sigma\approx$0.014 ‰). One session required a larger correction of 0.037‰. Similar types of correction have been applied previously, generally due to subtle changes in the heated gas reference frame (for example, Passey et al., 2010). We emphasize this

[2] $^{47}\delta=1000*(^{47}R_{sample}/^{47}R_{std}-1)$; $^{47}R=[^{47}CO_2]/[^{44}CO_2]$; the standard (std) is our working gas.

was only done for the optical calcites, and we infer it was necessary only due to the especially low δ_{47} value of CO_2 evolved from that material.

We applied a different kind of empirical correction to the Δ_{47} value of one heated apatite measurement (500°C, 5.5 hours). This sample was run in a different session from the other apatite samples heated to 500°C. An unheated sample from Siilinjarvi run directly before this sample was 0.077‰ lower than the average Δ_{47} value measured for unheated Siilinjarvi apatites. We corrected this single apatite sample by adding 0.077‰ to its Δ_{47} value. This correction places the 500°C, 5.5 hour apatite sample very near a point interpolated between the samples heated for longer and shorter times. Thus, while this correction is large, it appears to have been successfully accounted for. In any event, this data point does not drive any first-order interpretations in this study and so could be ignored.

Heating experiments were conducted in a rapid-quench furnace set-up with a René 41 metal cold-seal bomb (Blank et al., 1993). Samples were run between 500-650 bars pressurized with argon gas. Bombs were pre-heated to the temperature of interest with the sample held below room temperature in the quenching portion of the bomb. Once the temperature stabilized (though temperatures did sometimes drift by <5°C, usually down over the course of some experiments) samples were introduced into the hot spot of the bomb by being 'levitated' on a magnetic pedestal. They were heated for a specific time period, which varied for each experiment, and then quenched by dropping the magnet, immediately causing the sample to drop into the cold portion of the bomb where cooling occurred within 2-3 seconds (Ihinger, 1991).

Temperatures in the cold-seal bombs were measured with a type K thermocouple (chromel-alumel) inserted into a drilled hole near the top the bomb (where the hole does not penetrate the pressurized interior). We calibrated this outside temperature by measuring an internal temperature gradient along the top three inches of the cold-seal (done open to air). We report for all experiments the temperature 0.5 inches from the top of the cold-seal (which is the midpoint of our larger capsules) based on a quadratic extrapolation between all measured points (0, 1, 2, and 3 inches). These extrapolations are all within 5°C of the measured external temperature. We estimate our error as the maximum temperature difference between 0.5 inches and 0 and 1 inches, which is ±12°C.

Two different sample types were heated: For calcite heating experiments an optical calcite from Mexico of unknown origin was used and samples were chipped from the crystal along cleavage planes. For apatite heating experiments, apatite crystals from a sample from Siilinjarvi (see below) were chipped from a large apatite crystal. For all heating experiments large (mm size or greater) grains were used. Samples were contained in platinum capsules open to the argon atmosphere. Before loading samples, platinum capsules were pre-cleaned in 0.5 M (or greater) HCl for an hour, sonicated in acetone for 5 minutes, then heated at 1000°C for ten minutes in a 1 atm furnace.

Cleaning experiments were conducted in 0.1 M acetic acid at a pH of 4.5 on crushed apatite samples from Siilinjarvi and Oka following Eagle et al. (2010). ~1 gram of sample was immersed in the acetic acid for 4 or 24 hours, shaken occasionally, then washed three times with deionized H_2O and dried overnight between 70-90°C.

4. Results and discussion

4.1 Carbonatites

Carbonatites are igneous rocks containing greater than 50 modal percent carbonate minerals (Mitchell, 2005). These rocks crystallize from melts at high (~650°C) temperatures (Wyllie and Tuttle, 1960). Carbonatites preserved in the geological record are generally intrusive and, consequently, cooled over geologic time scales. As recognized by Dennis and Schrag (2010), these geologically slow cooling histories make carbonatites potential systems for constraining the closure temperature of the carbonate clumped isotope thermometer in carbonate minerals and apatites. Here, we define the 'closure temperature' as the empirically observed temperature recorded by the carbonate clumped isotope thermometer in a sample that started at a high temperature (operationally, greater than ~350 ˚C) and has since cooled. It reflects both the cooling rate of the sample and the temperature-dependent kinetics of isotopic exchange for a system as it cools (fig. 1; Dodson, 1973).

Closure temperatures can be considered to reflect the temperature below which atomic diffusion and isotopic exchange within a mineral slows to the point that the reaction of interest halts. For an equilibrium-based reaction (as opposed to the production of radiogenic daughter products), it represents the thermodynamic state of the system at which the rates of forward and backward reactions become negligible. The closure temperature is not a unique value (it depends on the cooling path) and could vary from sample to sample. Importantly, samples from carbonatites may not reflect a true closure temperature as defined above. For example, if samples have recrystallized during cooling or later metasomatism or experienced later heating the temperature measured could, in

part or whole, reflect these more recent events and would instead be termed an apparent temperature, which is any measured temperature that does not represent a closure or formation temperature.

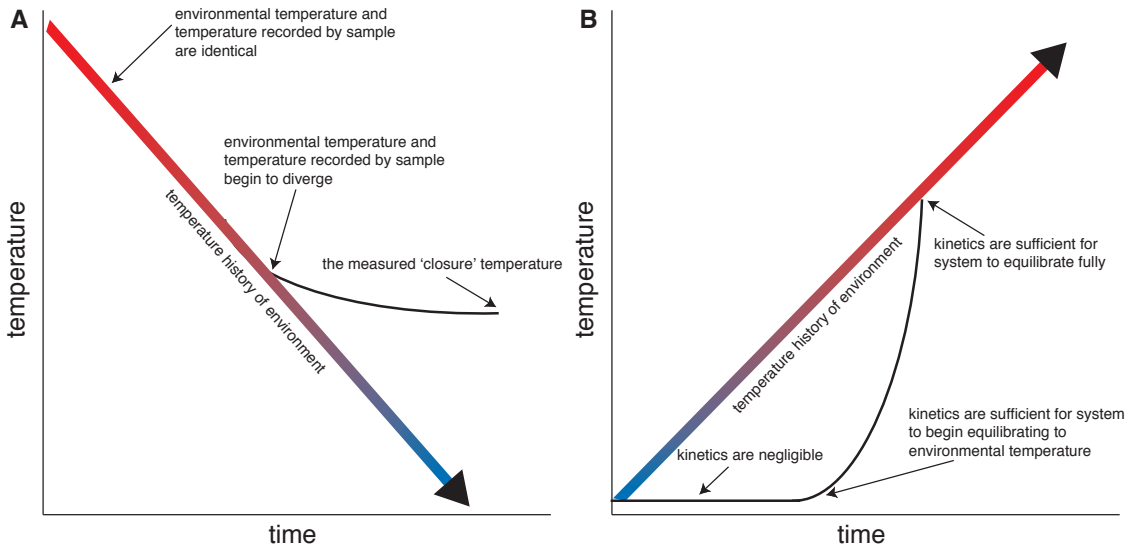

Figure 1. A) A schematic representation of the temperature recorded by the clumped isotope thermometer vs. the actual environmental temperature for a system originally starting at high temperature and cooling. At the start of the history both the environmental and recorded clumped temperature are identical. At a lower temperature the kinetics of exchange and diffusion slow sufficiently causing the recorded clumped isotope temperature to lock in, which is termed the closure temperature. B) A schematic representation of the temperature recorded by the clumped isotope thermometer vs. the actual environmental temperature for a system originally starting at low temperature and heating. As the environment initially rises in temperature, the recorded clumped temperature does not change. Only until the environment reaches a threshold temperature does the clumped isotope temperature being to change. At first the kinetics are not sufficient to catch up to the environmental temperature, which occurs at a higher temperature (or after a sufficient amount of time).

We measured stable isotope compositions (including clumped isotope compositions) of carbonates and cogenetic apatites from three intrusive calcitic carbonatites: Kovdor (Russia, 370 Ma), Oka (Canada, 160 Ma), Siilinjarvi (Finland, 2600 Ma), where Ma signifies millions of years from the present. No samples are from associated fenites. The Oka and Siilinjarvi samples and apatites from Kovdor examined here are the same as those in the study of Nadeau et al. (1999); the Kovdor carbonate

samples were provided by Keith Bell (Carleton University). Although all samples come from calcitic carbonatites (Kapustin, 1986; Nadeau et al., 1999), calcite samples can contain trace dolomite, siderite, or magnesite (for example, Haynes et al., 2002). Thus, following Nadeau et al. (1999) and Dennis and Schrag (2010), we refer to these samples (excluding apatite samples), in the most general sense, as carbonates. Results for the average of all measurements for samples are presented in Table 1. The first-order result of these measurements is that carbonate groups in apatites record higher Δ_{47} values than coexisting carbonates in all cases. Δ_{47} values are most easily interpreted by conversion to clumped isotope temperatures. We now discuss the assumptions and calibrations used to convert these Δ_{47} values to temperatures from both the carbonate and apatite samples.

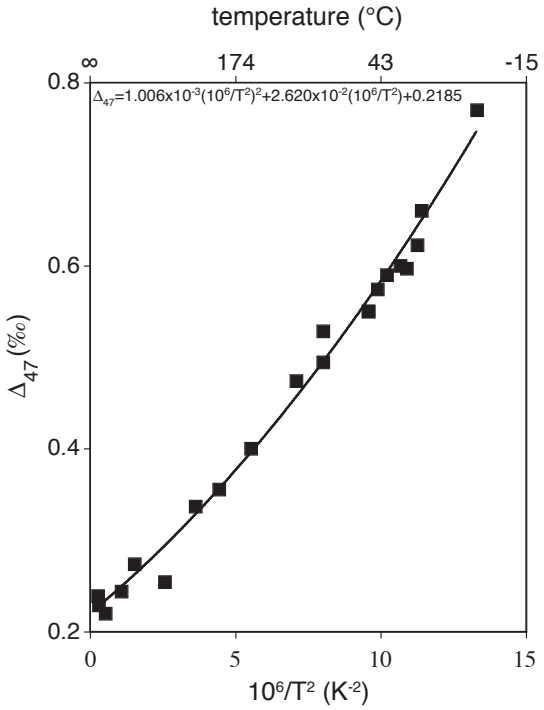

Figure 2: Data used for the temperature vs. Δ_{47} calibration. All Δ_{47} values are presented in the Ghosh reference frame. Data include experimental measurements on dolomites from Bonifacie et al. (2011) and calcites from Ghosh et al. (2006), Guo et al. (2009) and the work presented here. These temperatures range from 1-1650°C.

Δ_{47} values are converted to temperatures by assuming that all carbonate minerals (including apatites) share an identical Δ_{47} vs. temperature relationship. To make this conversion, we use experimental data from synthetic calcites precipitated from 1-50°C (Ghosh et al., 2006), synthetic dolomites precipitated from 25-350°C (Bonifacie et al., 2011), calcites internally re-equilibrated in the high temperature cold-seal apparatus experiments described above from 500-700°C, and calcites recrystallized from 1100-1650°C in piston cylinder experiments (Ghosh et al., 2006; Guo et al., 2009). All data points used to make this calibration are presented in Figure 2 in the Ghosh reference frame.

The assumption that calcites and dolomites share an identical temperature vs. Δ_{47} relationship is supported by both the theoretical study of Schauble et al. (2006) that predicts the cation and crystal structure of the carbonate containing mineral has a negligible (and unmeasurable beyond error) effect on clumping in calcite vs. dolomite and the overlap of experimental calcite and dolomite clumped isotope calibrations (Bonifacie et al., 2011; Ghosh et al., 2006). The assumption that calcite and apatite have identical temperature vs. Δ_{47} relationships is supported by theoretical models at all temperatures and by experiments at low temperatures (24-37°C; Eagle et al., 2010). High temperature experiments described below from 500-700°C also support this assumption. Although there is no theoretical prediction regarding the differences in acid digestion fractionation between calcite and carbonate groups in apatite for clumped isotope measurements, the experimental results of Eagle et al. (2010) suggest that any such differences are smaller than the error of the measurement.

With these assumptions in mind, the Δ_{47} values yield apparent clumped isotope temperatures for the carbonatite samples of ~125-190°C for carbonates and ~60-130°C for apatites (Table 1 and Fig. 3). For Siilinjarvi, two different apatite samples were measured giving 83 ± 4 and 62 ± 2°C (where the error is 2 standard errors; s.e.). We do not know the cause of this difference but it implies some heterogeneity within the carbonatite. The carbonate mineral temperatures are similar to those observed for slowly cooled calcitic marbles (150-200°C; Bonifacie et al., 2013; Ghosh et al., 2006) as well as other carbonatites (~100-280°C; Dennis and Schrag, 2010). Broadly, these results imply that carbonate groups in apatite have a lower closure temperature than in carbonate minerals.

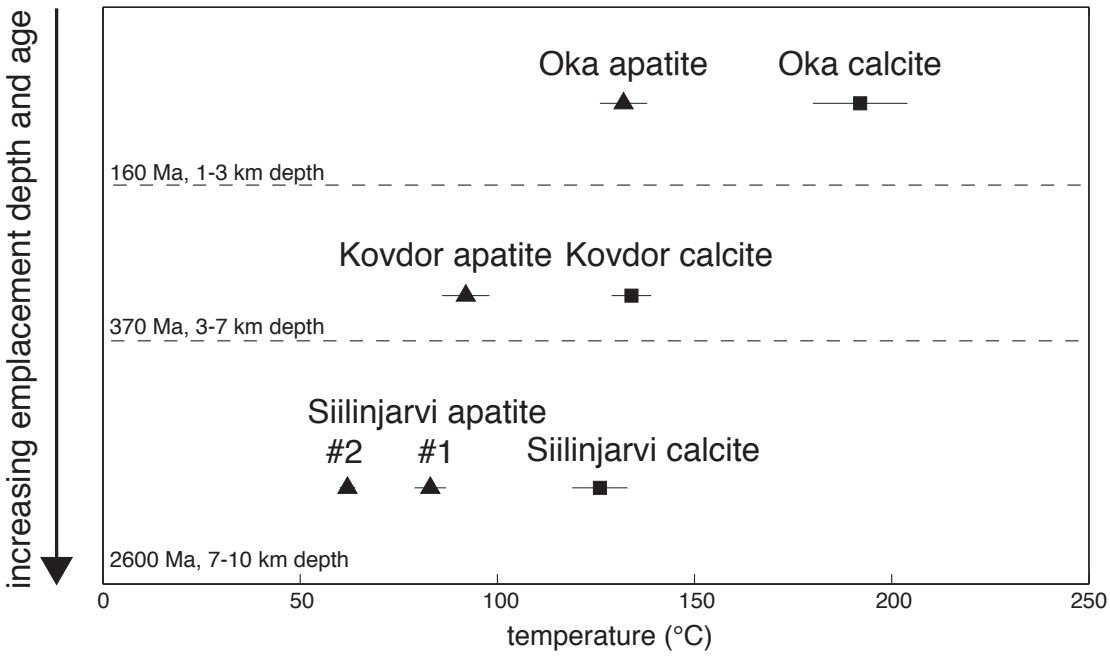

Figure 3. Clumped isotope temperatures from calcites and apatites from carbonatites. Emplacement depths are from Kapustin (1986). Error bars are 2 standard errors. Ma signifies millions of years ago. Apatites give lower temperatures than calcites in all cases implying they have a lower closure temperature.

It is possible that our results for carbonate groups in apatite reflect contamination by other carbonate-bearing minerals. We measured up to 500 mg of apatite, releasing an

amount of CO_2 equivalent to that released from ~8 mg of calcite. Consequently, even a fraction of a percent of calcite contamination in our apatite samples could influence our results. We explored this issue by cleaning apatite samples in acetic acid prior to stable isotope analysis (see experimental methods). Acetic acid dissolves so-called labile carbonate groups, calcite, and dolomite, but is not believed to attack structural carbonate groups in apatites (Eagle et al., 2010; Koch et al., 1997; Kohn and Cerling, 2002). Apatites from Siilinjarvi were treated for 4 and 24 hours and those from Oka for 4 hours. In no cases did we observe a statistically significant shift in Δ_{47} between treated and untreated apatite samples (Table 2). We conclude that trace contamination from calcite and other forms of labile carbonate groups does not contribute in a statistically significant way to our measured Δ_{47} values. Consequently, throughout the rest of this paper, we do not differentiate between acetic acid-treated and untreated apatite samples.

Igneous crystallization temperatures are demonstrably not recorded by clumped isotope compositions because crystallization of carbonatite melts occur at temperatures around 650°C (Wyllie and Tuttle, 1960), while all measured temperatures are less than 200°C. This indicates that the clumped isotope temperatures recorded by both the apatites and calcites in carbonatites record and reflect post-formational processes. A relevant question is whether or not the carbonate clumped isotope compositions of carbonate-bearing minerals in carbonatites reflect diffusion-controlled 'closure' of the magmatic phases or sub-solidus recrystallization during original cooling or later metamorphism/diagenesis.

Sub-solidus recrystallization of carbonate minerals in carbonatites occurs commonly and often rapidly after crystallization (Zhabin, 1971) and is well documented

to have occurred in samples from Siilinjarvi (Tichomirowa et al., 2006). Consequently, sub-solidus recrystallization of carbonates likely occurred in all of our samples. This recrystallization is important to consider because it presumably causes the clumped isotope composition of carbonate minerals to record the recrystallization temperature (as long as equilibrium is reached) and masks the history of prior cooling and internal, diffusion-controlled isotopic exchange. However, much of this recrystallization occurs at elevated temperatures close to the time of original crystallization (Zhabin, 1971). Thus it is possible that this recrystallization occurs above the nominal clumped isotope closure temperature of the carbonate and allows for diffusion-controlled internal isotopic exchange to continue during further cooling. If so, it has no impact on the final clumped isotope temperature recorded by a slowly cooled carbonatite.

Several observations lead us to conclude that the measured temperatures largely or entirely reflect diffusion-limited closure temperatures as opposed to recrystallization temperatures during original cooling or later possible diagenesis/metamorphism. First, apatites are thought to be more resistant to recrystallization in carbonatites than carbonate minerals (Zhabin, 1971), yet we find apatites yield consistently lower clumped temperatures than co-genetic carbonates (Table 1 and Fig. 3). This is consistent with measured temperatures being diffusionally controlled closure temperatures and implies that apatites have a lower clumped isotope closure temperature than carbonates.

Second, the carbonate minerals in our samples show no obvious signs of later diagenesis in their carbon and oxygen isotope ratios. All carbonate mineral oxygen isotope compositions fall within the field defined by Taylor et al. (1967) for ‘primary’ carbonatites (~6-8.75 ‰ relative to VSMOW). Taylor et al., (1967) additionally defined a

pristine carbon isotope field between -5 to -8 ‰. Siilinjarvi and Kovdor ($\delta^{13}C$ = -3.65 and -4.02‰, respectively) differ from this field, but plausibly for reasons unrelated to diagenesis. For example, Siilinjarvi's higher carbon isotope ratio compared to the field of Taylor et al. (1967) was argued by Tichomirowa et al. (2006) to be the result of magmatic fractionations during differentiation of the parent melt of the carbonatite. No such explanation has been offered for Kovdor's elevated carbon isotope ratio. However, oxygen isotopes tend to be more reliable indicators of sub-solidus exchange in carbonates than carbon isotopes, and so we find Kovdor's 'pristine' oxygen isotope composition to be a sufficient argument for its lack of significant diagenesis.

Third, the oxygen isotope fractionation between co-existing carbonates and apatite also provides a constraint on whether the samples we have examined underwent sub-solidus isotopic exchange through recrystallization or other processes. We interpret these data using the calibration of the apatite-calcite oxygen fractionation factor of Fortier and Lüttge (1995), which can be interpolated between 350°C and 800°C. Oxygen isotope compositions of apatites have been measured for Siilinjarvi (Tichomirowa et al., 2006) and Oka (Conway and Taylor Jr, 1969), but not Kovdor, so we restrict our discussion here to just these first two locations. As a note, oxygen isotope data for apatite from these references were measured on bulk crystals and thus include oxygen from PO_4^{3-}, OH^-, and CO_3^{2-} groups as was done for the calibration of the carbonate-apatite fractionation we use (Fortier and Lüttge, 1995). This approach can lead to systematic errors due to differences in chemical composition between the apatites used in the calibration and the apatites examined here, though igneous apatites with large amounts of OH are rare (most are fluoroapatites followed by chloroapatites). Regardless, applying these fractionation

factors yields apatite-calcite oxygen isotope temperatures between ~300°C and 900°C (Table 3). These temperatures are consistent with the bulk isotopes of the apatite and calcite being set by high temperature processes. The comparatively lower temperatures recorded by the clumped isotope thermometer can be interpreted as a result of continuing internal isotopic redistribution (that is, by intracrystalline diffusion) after apatite and calcite ceased intercrystalline exchange.

Fourth and finally, the differences in carbonate clumped isotope temperatures between the intrusions examined here are consistent (at least in direction) with the expected effects of diffusion-limited closure of the intramineralic isotopic distributions. Oka gives the highest temperatures, Kovdor is intermediate and Siilinjarvi is the lowest in temperature for each phase. Importantly, this ranking applies to both calcite and apatite. These temperature trends correlate to emplacement depths: Oka is estimated to have been emplaced the shallowest (1-3 km), Kovdor is intermediate (3-7 km) and Siilinjarvi is the deepest (7-10 km) (Kapustin, 1986). More deeply intruded magmas are generally expected to cool more slowly as compared to more shallowly emplaced intrusions because of higher ambient temperatures at the depth of emplacement. Because diffusion-limited closure temperatures generally decrease with decreasing cooling rate, we should expect Oka to have cooled the fastest and record the highest apparent temperatures, for Kovdor to have cooled more slowly and record a lower temperature, and for Siilinjarvi to have cooled slowest and preserve the lowest apparent temperatures. This prediction is met by the measured temperatures. The temperature vs. emplacement depth trends are also reflected in the bulk oxygen apatite-calcite temperatures, where Oka gives a higher

temperature than Siilinjarvi, further supporting the inference that the isotopes of the apatites and carbonate minerals have not been significantly disturbed since cooling.

We thus conclude that the clumped isotope temperatures recorded in carbonatite carbonate minerals and apatites measured here most likely reflect diffusion controlled closure temperatures and not crystallization or recrystallization temperatures. The clumped isotope temperatures recorded in the carbonate minerals from calcitic carbonatites are similar to those from slowly cooled calcites in marbles discussed above (Bonifacie et al., 2013; Dennis and Schrag, 2010; Ghosh et al., 2006), indicating that calcites have clumped isotope closure temperatures that range from ~120-200°C. Apatites, in contrast, record lower closure temperatures from 60-130°C.

4.2 Heating experiments

Clumped isotope measurements from originally high-temperature natural samples provide an important window into processes like solid-state diffusion that occur over geologic timescales. However, the thermal histories of natural samples are rarely known precisely, and may include multiple episodes of heating, cooling and reaction (or other complexities), limiting their use in making quantitative predictions. Laboratory heating experiments, on the other hand, allow for controlled changes in clumped isotope values and thus quantitative evaluations of the kinetic rate constants of interest. The disadvantage of laboratory experiments is that, in general, they must be performed at temperatures higher than observed in natural environments in order to generate measurable changes on laboratory timescales. Such a strategy inevitably requires extrapolation to lower temperatures, which may or may not be justified.

We conducted a series of heating experiments on optical calcites from Mexico (these crystals were obtained from the Caltech mineral research collection, but their source within Mexico is unknown) and on apatites from the Siilinjarvi complex. Details of the experimental apparatus and procedures can be found in the experimental methods section. The experimental results can be found in Table 4 for calcites and Table 5 for apatites. For apatites, each experimental run product could only be analyzed once as the platinum capsule could at most contain 250 mg of sample (the minimum amount needed for an isotopic measurement of Siilinjarvi apatite). Experimental run products of optical calcites, on the other hand, could be analyzed in replicate. For the experiment in which apatite was heated for 5.5 hours at 536°C and all experiments in which apatite was heated to 692°C, two different 250 mg aliquots of sample were subjected to experimental heating and then combined and measured as a single sample. The measurement of unheated Siilinjarvi apatite (that is, the initial time point in the plots and tables) is the average of two measurements on Siilinjarvi samples taken from the same batch of apatites used for the experiments. Note that apatites from Siilinjarvi vary in starting Δ_{47} (Table 1), and so the products of heating experiments must be compared with the initial composition of these two sub-samples of the starting materials rather than other Siilinjarvi samples.

Our first heating experiments yielded results at odds with the rest of our observations: optical calcites were heated at 536 ˚C for 1 hour, 24 hours, and 72 hours, and yielded run products with Δ_{47} values of 0.545, 0.356 and 0.402 ‰ respectively. These results lack the evidence for rapid changes in Δ_{47} during the first hour of heating seen in later experiments. Additionally, this is the only case in which a relatively long

heating experiment results in a significantly higher Δ_{47} than shorter heating experiments at the same temperature. We noticed nothing unusual about either the experimental procedures or the measurements of run products for these experiments, but suspect that an unnoticed error or irregularity in procedure occurred in this first attempt. For this reason, and because of the peculiar nature of the resulting data, we do not consider these experiments in our general interpretation described below.

Some general observations can be made about the heating experiments in both calcites and apatites. Δ_{47} values of calcite samples heated at 209°C for 7 days and 323°C for 6 days and apatite samples heated at 430°C from 1 hour to 1 day do not change, beyond measurement error, from their initial Δ_{47} values. In all other experiments, Δ_{47} values decrease monotonically with time. Also, importantly, rates increase with increasing temperatures — the 430°C calcite experiments show the slowest change in clumped isotope composition, never reaching a stable value, while the 692°C calcite experiments stabilize in minutes. The 536°C calcite experiments stabilize in clumped isotope composition over the course of hours. This is the expected relationship for reaction rates, which generally follow Arrhenian rate laws (see below), and increase with increasing temperature. An interesting observation of the 430°C data is that the data has a distinctively 'kinked' shape to its evolution in Δ_{47} with time as opposed to a smooth decrease in Δ_{47} with time. These kinks are also observed in some of the experiments of Passey and Henkes (2012) on both optical grade calcites and natural, void-filling spar cements from temperatures ranging from 385-475°C. We will return to the importance of these kinked features when models are constructed to quantify these experiments below.

Our 430°C experiment does not reach a constant value of Δ_{47}, implying that internal isotopic equilibrium was never reached. The 536°C and 692°C calcite and apatites, on the other hand do reach constant values of Δ_{47}, within the error of measurements, at the end of each experiment. We interpret the constant Δ_{47} values reached at the end of the 536°C and 692°C experiments for both apatites and calcites to represent equilibrium Δ_{47} values at those temperatures. The final Δ_{47} value (in the Ghosh reference frame) for the 536°C calcite experiments (using the final three time points) is 0.274 ± .013‰ (2 s.e.) and 0.244 ± .008‰ (2 s.e.) for the 692°C calcite experiments (using the final five time points). In comparison, the final values in the apatite experiments are 0.271 ± .025‰ (2σ) at 536 ˚C (using the final time point) and 0.252 ± .016‰ (2 s.e.) at 692 ˚C (using the final four time points). Significantly, within error, apatites and calcites equilibrated to high temperature have the same clumped isotope values. This result is consistent with the model predictions of Eagle et al. (2010), and supports our assumption that, at equilibrium, carbonate groups in calcite and apatite have the same clumped isotope composition.

The 536°C and 692°C equilibrium Δ_{47} values calculated above are consistent with previous experimental calibrations of the carbonate clumped isotope thermometer at high temperature (Fig. 2), with values between the >1100°C piston cylinder experiments (Ghosh et al., 2006; Guo et al., 2009) and 25-350°C dolomite experiments (Bonifacie et al., 2011) (Fig. 2). However, the 350°C dolomite sample is between our 536 and 692°C points; we have no obvious explanation of this apparent discrepancy except that this dolomite point is offset from the general trend with or without our data by 0.03‰ (~2

times the general internal error of the measurement). Regardless, we consider these experiments to give equilibrium Δ_{47} values and use them in our calibration (Fig. 2).

5. Modeling the experimental data

A kinetic model is required to understand and quantify the experimental heating results of the previous section. Any model presented should incorporate both the observed increase in overall reaction rate with temperature and, ideally, be able to fit the kinked features observed in our 430°C calcite experiment and those of Passey and Henkes (2012), which indicate a divergence from simple, first-order kinetics. First-order kinetics would predict shapes that exponentially decay towards the final, equilibrium value. The evidence for such 'kinks' in time series data are only visually obvious in our data for calcite at 430°C. However, we find it compelling that similar phenomena were observed by Passey and Henkes (2012), and therefore we attempt to provide a complete model that explains these kinks rather than treating them as an aberration. We present two separate models that attempt to quantitatively explain these data. Both models can explain the increase in rate with temperature, but the first, simpler model, fails to model the 'kinks', while the second, more complex model does. We present the first, simpler model despite its failure to fully fit our experimental results because the discussion illustrates the essential features of the kinetics of changes in the clumped isotope compositions of carbonates during heating before the introduction of the more complex model. We apply this more complex model first to the calcite experiments and then to the apatite experiments.

5.1 First-order kinetic model

Changes to Δ_{47} values of our experimental run products are likely controlled by both exchange reactions (that is, the rate of swapping isotopes among different carbonate groups) and by the rate of diffusion of those different isotopes in the crystal lattice. Modeling of diffusion in our experiments is challenging as there is no length scale inherent to the measurement. In general, diffusivities are measured either by introducing a tracer on a surface or via exchange between phases (Cherniak et al., 2010). This kind of information is not generated by our experiments. To deal with this, our 'simple,' first-order kinetic model implicitly assumes that isotopic diffusion in solid carbonates occurs sufficiently rapidly such that it is not the rate-limiting step. The exclusion of diffusion in this model ultimately leads to its failure. Nevertheless, continuing with this simple analysis, the chemical kinetics of exchange of isotopes between already adjacent carbonate groups controls the reaction rate according to the following equation:

$$^{12}C^{16}O_3^{2-} + {}^{13}C^{16}O_2\,{}^{18}O^{2-} \leftrightarrow {}^{12}C^{16}O_2\,{}^{18}O^{2-} + {}^{13}C^{16}O_3^{2-} \quad (5)$$

The excess of $^{13}C^{16}O_2{}^{18}O^{2-}$ relative to a random distribution of isotopes that should be present when this reaction reaches equilibrium can be described by a Δ_{63} value with a form similar to that of Equation (2). We make a further approximation at this point: though there are multiple carbonate species that contribute to the Δ_{47} value ($^{12}C^{17}O^{18}O_2{}^{2-}$, $^{12}C^{17}O_2{}^{18}O^{2-}$, $^{12}C^{16}O^{17}O^{18}O^{2-}$, $^{13}C^{16}O_2{}^{18}O^{2-}$, $^{13}C^{16}O^{17}O_2{}^{2-}$, $^{13}C^{17}O_2{}^{18}O^{2-}$, $^{13}C^{17}O_3{}^{2-}$, $^{13}C^{16}O^{17}O^{18}O^{2-}$, $^{13}C^{16}O^{18}O_2{}^{2-}$) the $^{13}C^{16}O_2{}^{18}O^{2-}$ group represents ~93.5% of the total signal. Inclusion of all the species would introduce more free variables than we are currently able to constrain. As such we proceed here, and in the model following, to assume that the Δ_{47} value is controlled by Equation (5). Additionally, we assume that the

Δ_{63} of a sample is directly related to the Δ_{47} of CO_2 extracted from that carbonate by acid digestion, through the expression: $\Delta_{47} = \Delta_{63} + 0.218$ ($\pm$ 0.020, 2σ) ‰, which is the extrapolated intercept in Figure 2. Guo et al. (2009) present an argument that this offset could be a subtle function of Δ_{63} rather than a constant; however, no published experimental evidence supports this more complex treatment of the acid digestion fractionation so we will proceed with a constant offset — if, in future, a more complex function is found to be more accurate it can be incorporated into the models presented here.

We first assume that Equation (5) is elementary (reacts as written and not through unspecified intermediates). Additionally we write all reactions in terms of a reaction progress parameter, ξ (Zhang, 2008), which tracks change in the number of $^{13}C^{16}O_2{}^{18}O^{2-}$ molecules with time. At the start of each experiment ξ is zero as no reactions have occurred. Using ξ we write

$$\frac{d\xi}{dt} = k_f[{}^{12}C^{16}O_3{}^{2-}][{}^{13}C^{16}O_2{}^{18}O^{2-}] - k_b[{}^{12}C^{16}O_2{}^{18}O^{2-}][{}^{13}C^{16}O_3{}^{2-}]. \qquad (6)$$

The k_f and k_b are the forward and reverse reaction constants respectively. [x] represents the concentrations of the species normalized such that the total of all carbonate isotopologues is equal to one. At equilibrium, by definition, the forward and reverse reaction rates balance:

$$k_f[{}^{12}C^{16}O_3{}^{2-}]_{eq}[{}^{13}C^{16}O_2{}^{18}O^{2-}]_{eq} = k_b[{}^{12}C^{16}O_2{}^{18}O^{2-}]_{eq}[{}^{13}C^{16}O_3{}^{2-}]_{eq}, \qquad (7)$$

where the $[x]_{eq}$ represents the concentration of a given isotopologue at equilibrium. We can rewrite this reaction in terms of the equilibrium constant:

$$\frac{k_f}{k_b}=\frac{[^{12}C^{16}O_2{}^{18}O^{2-}]_{eq}[^{13}C^{16}O_3{}^{2-}]_{eq}}{[^{12}C^{16}O_3{}^{2-}]_{eq}[^{13}C^{16}O_2{}^{18}O^{2-}]_{eq}}=K_{eq}, \quad (8a)$$

where K_{eq} is the equilibrium constant for Equation (8). As K_{eq} (which is a function of temperature) is known from experiments conducted between 1-1650°C (Fig. 2) we can eliminate k_b from the equation by writing the following:

$$k_b=\frac{k_f}{K_{eq}}, \quad (8b)$$

Additionally, by writing our reactions in terms of a progress parameter, we can rewrite equation (6) in terms of ξ and the initial concentrations of the isotopologues:

$$\begin{aligned}\frac{d\xi}{dt}=&k_f([^{12}C^{16}O_3{}^{2-}]_0-\xi)([^{13}C^{16}O_2{}^{18}O^{2-}]_0-\xi)\\&-\frac{k_f}{K}([^{12}C^{16}O_2{}^{18}O^{2-}]_0+\xi)([^{13}C^{16}O_3{}^{2-}]_0+\xi)\end{aligned}, \quad (9)$$

where $[x]_0$ represents the initial normalized concentration of an isotopologue. This equation has only one unknown, k_f, and can be solved numerically in a straightforward manner (see below). With a knowledge of ξ(t) we can find the concentrations of all species of interest ($[x]_t=[x]_0 \pm \xi(t)$, which in turn allows for a calculation of Δ_{63}. Given known bulk isotopic compositions and Δ_{47} values of our experimental run products, we can calculate the normalized concentrations of all the isotopic species in Equation (9) following Huntington et al. (2009). ξ at a given time point is $[^{13}C^{16}O_2{}^{18}O^{2-}]_0$-$[^{13}C^{16}O_2{}^{18}O^{2-}]_t$. Finally the equilibrium constant at a given temperature is derived from the data of Figure 2 via the relation: $-1000\ln(K_{eq}) = \Delta_{63}$ (Wang et al., 2004).

An examination of the data in Table 4 shows that after heating the optical calcites have a tight distribution of $\delta^{18}O$ (all around 10 ± .2‰ [2 s.d.] relative to SMOW), which is similar to the external precision of the measurement (0.16-0.2‰; 2 s.d.). $\delta^{13}C$ values

have a larger range (-28.9 to -32‰) that is an order of magnitude larger than the external precision of the measurement (0.05-0.08‰; 2 s.d.). There is no correlation between $\delta^{13}C$ and temperature or duration of heating, and the range is similar to that for the optical calcites prior to heating (-29.6 to -32.1‰). We conclude that the $\delta^{13}C$ of the optical calcite sub-samples varies due to heterogeneities in the starting material, perhaps from carbon isotope variations in its growth environment. This range in $\delta^{13}C$ values is sampled at the scale of our sample preparations and retained after heating. Regardless, this isotopic variability has an impact on the modeling as an increase or decrease in the overall bulk $\delta^{13}C$ changes the overall concentration of $^{13}C^{16}O^{18}O^{2-}$ for identical Δ_{63} values. As we fit our model to overall concentrations and then convert to Δ_{47}, differences in bulk isotopic distribution due to heterogeneities in the optical calcite result in each experiment having a different initial concentration of $^{13}C^{16}O_2{}^{18}O^{2-}$. To deal with this, we simplify the problem by using the average the $\delta^{13}C$ and $\delta^{18}O$ of our unheated optical calcite as the starting and ending bulk isotopic composition for all experiments. However, it may be important to explicitly consider the role of changes to bulk isotopic composition with time when studying problems where isotopic clumping reactions are occurring simultaneous with significant changes in $\delta^{18}O$ and $\delta^{13}C$ values. We consider our simplification, which ignores the subtle isotopic heterogeneity in the unheated optical calcite starting material, to be acceptable as there is no evidence of changes in bulk isotopic composition of the samples with either temperature or time.

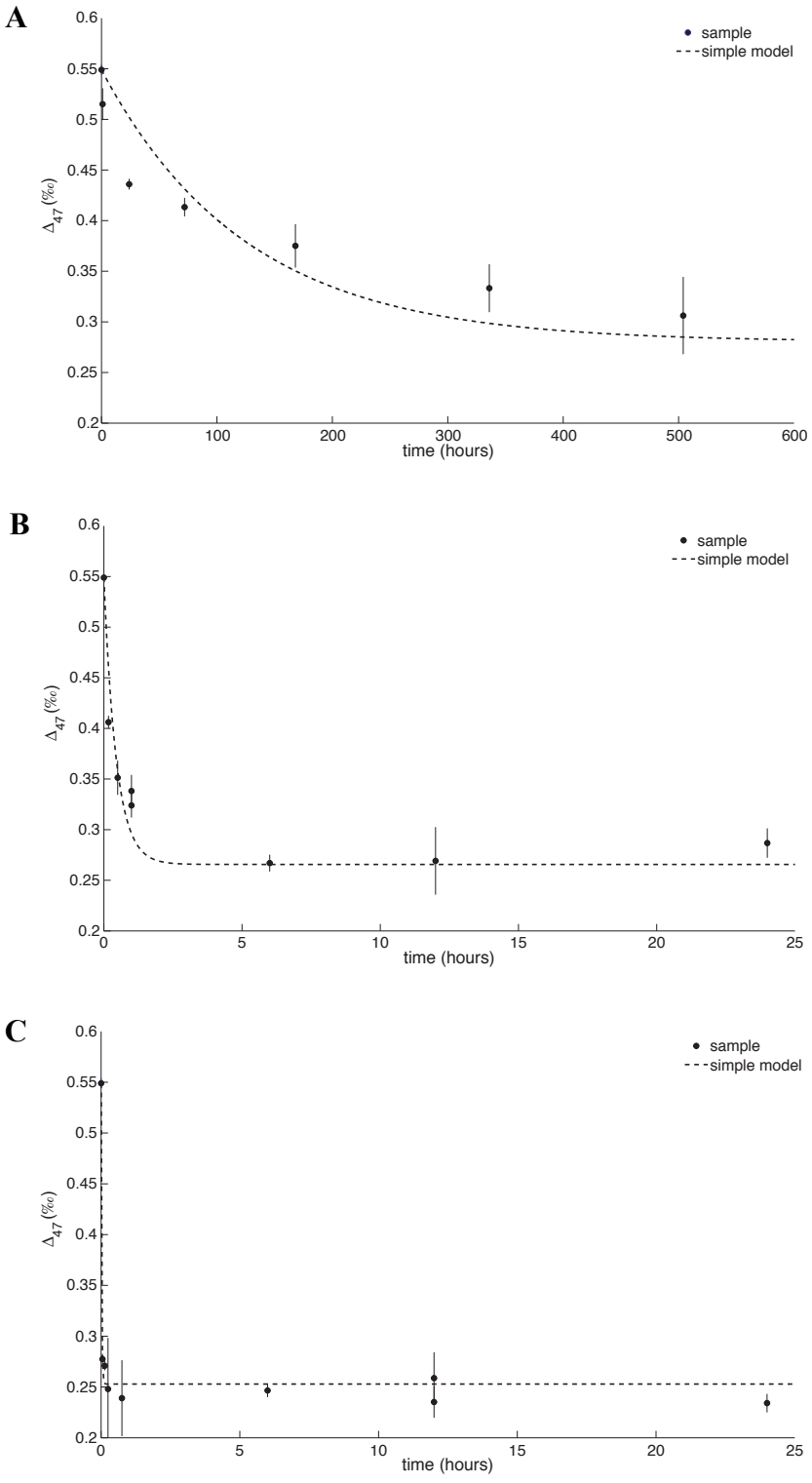

Figure 4. Simple, first-order model as applied to calcite data from calcite heating experiments performed in this lab. a) 430°C data; b) 536°C data; c) 692°C data. All Δ_{47} values are presented in the Ghosh reference frame. Error bars are 2 standard errors. This simple model is unable to fit the 430°C data as the model requires an exponentially decaying functional form.

All data (that is, Δ_{47} vs. time at each temperature) are fit as functions of k_f using the trust-region nonlinear least squares fitting algorithm of Matlab. Robust fitting is used with the bisquare option. A fit of the data with this model is presented in Figure 4a for the 430°C experiments, 4b for the 536°C calcite experiments, and 4c for the 692°C calcite experiments. The fit is robust for the 692°C data (r^2=0.98) and the 536°C data (r^2= 0.90). However, the fit poorly replicates the data for the 430°C fit (r^2=0.84). Though the correlation coefficients of all experiments are similar, a visual inspection of the fit through the 430°C experiment demonstrates that it is a poor fit: it is incapable of capturing the rapid movement at the start of the experiment and overshoots the data at the tail end of the experiment. Consequently, the simple model described above is incapable of representing the non-first-order ('kinked') behavior of the 430°C calcite heating experiments. This behavior, though only obviously visible at one experimental temperature (430°C) in this study, is apparent in many of the experiments of Passey and Henkes (2012), where the reaction speed at the very start of the experiments is faster than first-order kinetics would predict given the rate of change of Δ_{47} in the later portion of experiments. Consequently, we consider this 'kinked' shape to be a robust result and in the next section we develop a more sophisticated model with the express purpose of fitting our 430°C experiment.

5.2 Paired (reaction-diffusion) kinetic model

In this section we develop a model that can fit the non-first-order behavior of the 430°C experiment shown here as well as those from Passey and Henkes (2012). Passey and Henkes (2012) proposed that these rapid kinetics at the start of the reaction are driven by defects that allow for rapid migration of atoms/groups in the crystal lattice, enhancing

the initial reaction rates. In this interpretation, these 'rapid' defects are annealed out of the calcite early in the course of the experiment, causing reaction rates to slow down and generating the kink in the time series. This is a plausible explanation because previous studies have shown that annealment of calcites can change their diffusivity for oxygen presumably through an alteration of structural defects (Anderson, 1969; Farver, 1994; Kronenberg et al., 1984). As a result of this interpretation, Passey and Henkes (2012) do not use these initial, rapid data points in their quantitative modeling and only model the later, slower kinetics. Here, we take an alternative approach that describes the non-first-order behavior of clumped isotope kinetics through an atomistic mechanism that is both physically justifiable and capable of mathematically fitting the kinks in our data. However, we will present a hypothesis below that incorporates the presence or absence of radiation damage to understand the difference in kinetics between natural and heated apatites, which is similar to the defect-based hypothesis presented by Passey and Henkes (2012).

Our approach is motivated by the observation that the fast initial reaction rates are present (and appear more or less similar in form) in multiple samples of calcites, with a range of heating temperatures and durations studied in two different labs. This can only be true if the factors controlling the rapid kinetics seen early in heating experiments are universal (or at least common). Previous experiments on oxygen self-diffusion in calcites suggest this is unlikely if the factors controlling reaction rate are driven entirely by extrinsic defects of some kind: Farver (1994), for example, noticed that one of two samples investigated showed no dependence of oxygen self-diffusivities on annealment while another sample changed oxygen diffusivity as a function of annealment time.

Indeed, this latter sample actually increased in oxygen diffusivity from 600°C to 550°C which was thought to be related to more rapid diffusion of oxygen via defects at 550°C as compared to an annealed crystal at 600°C. This would predict that defects could cause increased rates at lower temperatures, which is not consistent with either our study of clumped isotope kinetics or with Passey and Henkes (2012).

To account for the non-first-order kinetics, we constructed a more physically complex reaction model. Our model explains the non-first-order kinetics as a natural consequence of the combined kinetics of diffusion and reaction in the carbonate lattice. We describe these combined kinetics by modifying the model of Zhang et al. (1995), which was used to model the non-first-order kinetics of the reaction: $H_2O + O <—> 2OH$, where 'O' is an oxygen bound to the silicate lattice.

This model explicitly accounts for the neighbors that surround any chemical species (such as the carbonate ion group) participating in a reaction. The dominant carbonate isotopologue in calcite is $^{12}C^{16}O_3^{2-}$ (~98 %). The probability that a carbonate group neighbors at least one unsubstituted carbonate is $1\text{-}0.02^6$. Consequently, a doubly substituted carbonate group like $^{13}C^{16}O_2{}^{18}O^{2-}$ can be approximated to always have one or more neighboring $^{12}C^{16}O_3^{2-}$ with which it can react and form two singly substituted species. As such the forward reaction rate of Equation (5) is never limited by solid-state diffusion of isotopes through the solid lattice — the two reaction partners can be approximated to be always present together.

In contrast, isotopic exchange between the singly substituted carbonate ions $^{13}C^{16}O_3^{2-}$ and $^{12}C^{16}O_2{}^{18}O^{2-}$ can be rate-limited by solid-state diffusion. These isotopologues are each of order 1% of all carbonate species. Thus, the chance that a

$^{13}C^{16}O_3^{2-}$ and $^{12}C^{16}O_2{}^{18}O^{2-}$ neighbor each other for a random distribution of groups is of order 5% in a calcite crystal. Consequently, approximately 95% of $^{13}C^{16}O_3^{2-}$ and $^{12}C^{16}O_2{}^{18}O^{2-}$ groups in the sample cannot immediately react to form a clumped species. Instead they can only react to form a clumped species if and when they are adjacent in the lattice.

In this model, we only account for the reaction of $^{13}C^{16}O_2{}^{18}O^{2-}$ with $^{12}C^{16}O_3^{2-}$, considering it to be the only reaction of importance in destroying $^{13}C^{16}O_2{}^{18}O^{2-}$ species. This is an approximation as reactions with isotopically substituted species are also possible, though they need not necessarily result in a net los of $^{13}C^{16}O_2{}^{18}O^{2}$. For example, exchange of $^{13}C^{16}O_2{}^{18}O^{2-}$ with $^{13}C^{16}O_3^{2-}$ (the dominant substituted group) can only result in another $^{13}C^{16}O_2{}^{18}O^{2-}$. Exchange with a $^{12}C^{16}O_2{}^{18}O^{2-}$ or $^{12}C^{17}O^{16}O_2^{2-}$ (the next most abundant substituted groups), on the other hand, could generate another multiply substituted species that we are not explicitly modeling due to their low abundance. However, these two species account for ~0.7% of carbonate groups (or ~4 percent of configurations; see below) in the sample and thus are not a common bonding partner. Additionally, given that errors in rate constants and diffusivities are generally larger than 4% relative, we do not include a correction term for the exchange of $^{13}C^{16}O_2{}^{18}O^{2-}$ with other species.

5.2.1 Model structure. — We begin by considering the following reactions:

$$\begin{aligned} {}^{12}C^{16}O_3^{2-} + {}^{13}C^{16}O_2{}^{18}O^{2-} &\leftrightarrow \text{pair} \\ \text{pair} &\leftrightarrow {}^{12}C^{16}O_{3,\text{single}}^{2-} + {}^{13}C^{16}O_2{}^{18}O_{\text{single}}^{2-}, \end{aligned} \tag{10}$$

where a pair signifies $^{13}C^{16}O_3^{2-}$ and $^{12}C^{16}O_2{}^{18}O^{2-}$ residing next to each other and 'single' signifies a singly substituted species that does not reside next to another singly substituted species in the crystal lattice, which we term a 'singleton'. In this formulation,

the pairs represent an intermediary through which clumped species interact with the majority of singly isotopically substituted species. We note that pairs include all situations where there are two or more singly substituted species next to each other including triplets, quadruplets, et cetera (Zhang et al., 1995). Pairs can be formed or destroyed either by diffusion or by reaction. An equation describing the kinetics of the top line of Equation (10), which assumes the reaction proceeds in an elementary fashion is:

$$\frac{d\xi}{dt} = k_f([^{12}C^{16}O_3^{2-}]_0)([^{13}C^{16}O_2{}^{18}O^{2-}]_0 - \xi) - k_b[\text{pair}]_t \,. \tag{11}$$

Additionally the concentration of pairs changes as a function of time according to:

$$\begin{aligned}\frac{dpair}{dt} = {} & k_f([^{12}C^{16}O_3{}^{2-}]_0)([^{13}C^{16}O_2{}^{18}O^{2-}]_0 - \xi) - k_b[\text{pair}]_t \\ & + k_{dif-single}[^{12}C^{16}O_2{}^{18}O^{2-}]_{single,0}[^{13}C^{16}O_3{}^{2-}]_{single,0} - k_{dif-pair}[\text{pair}].\end{aligned} \tag{12}$$

In Equation (12) the terms led by the reaction coefficients k_f and k_b represent an isotopic exchange reaction and the final two terms led by $k_{dif\text{-}single}$ and $k_{dif\text{-}pair}$ represent the process of diffusion (Zhang et al., 1995). We have assumed here that the concentrations of $^{12}C^{16}O_3{}^{2-}$ and the singletons vary so little that they can be treated as constants. Although Equation (12) has four kinetic parameters, they are not all independent. At equilibrium, by definition, $d\xi/dt=0$. As such we can write,

$$k_f[^{12}C^{16}O_3^{2-}]_{eq}[^{13}C^{16}O_2{}^{18}O^{2-}]_{eq} = k_b[\text{pair}]_{eq}. \tag{13}$$

The concentrations of $^{12}C^{16}O_3{}^{2-}$ and $^{13}C^{16}O_2{}^{18}O^{2-}$ at equilibrium are obtained by calculating the expected Δ_{63} at the temperature of the experiment and inverting for the bulk concentrations of the species (as done previously).

To find the concentration of pairs at equilibrium we initially assume that the solid carbonate solution is ideal, that is, at equilibrium the carbonate groups will be randomly distributed. Below we discuss the failure of this assumption and the need to modify it. We find the number of pairs at equilibrium as follows: we calculate the expected total amount of any given singly substituted carbonate group as was done for the simple model above. If an individual carbonate group is coordinated such that there are z carbonate groups surrounding it, the number of singleton $^{13}C^{16}O_3^{2-}$ groups is:

$$[^{13}C^{16}O_3^{2-}]_{single} = [^{13}C^{16}O_3^{2-}]_{total}(1-[^{12}C^{16}O_2{}^{18}O^{2-}]_{total})^z, \quad (14a)$$

and $^{12}C^{16}O_2{}^{18}O^{-2}$ groups is:

$$[^{12}C^{16}O_2{}^{18}O^{2-}]_{single} = [^{12}C^{16}O_2{}^{18}O^{2-}]_{total}(1-[^{13}C^{16}O_3^{2-}]_{total})^z. \quad (14b)$$

Equations (14a and b) represent the probability of finding a singleton given a random distribution of isotopologues in the mineral. We ignore pairing of other clumped species for the reaction. The concentration of paired species at equilibrium is:

$$[\text{pair}] = [^{12}C^{16}O_2{}^{18}O^{2-}]_{total} - [^{12}C^{16}O_2{}^{18}O^{2-}]_{total}(1-[^{13}C^{16}O_3^{2-}]_{total})^z \quad (15a)$$

or

$$[\text{pair}] = [^{13}C^{16}O_3^{2-}]_{total} - [^{13}C^{16}O_3^{2-}]_{total}(1-[^{12}C^{16}O_2{}^{18}O^{2-}]_{total})^z. \quad (15b)$$

The concentration of pairs at equilibrium should be independent of whether we choose Equation (15a) or (15b). However, as the pairs include situations with two or more singly substituted species next to each other (see above), Equations (15a and b) end up differing by ~1% relative. We average the values of the pairs calculated from Equations (15a and b) to find the equilibrium pair distribution. We found that the choice of using Equation (15a), (15b), or an average of the two had no noticeable effect on the results. We now write:

$$k_f \frac{[^{12}C^{16}O_3{}^{2-}]_{eq}[^{13}C^{16}O_2{}^{18}O^{2-}]_{eq}}{[pair]_{eq}} = k_b . \quad (16)$$

This allows for the elimination of one free parameter. Another can be eliminated through the requirement of equilibrium for Equation (12). At equilibrium Equation (13) holds and the pair concentration is constant. Thus dpair/dt=0 and

$$k_{dif-single}[^{12}C^{16}O_2{}^{18}O^{2-}]_{single,eq}[^{13}C^{16}O_3{}^{2-}]_{single,eq} = k_{dif-pair}[pair]_{eq} , \quad (17a)$$

which, if we use our equation for the singletons from above, we can rewrite as

$$k_{dif-pair} = k_{dif-single} \frac{[^{12}C^{16}O_2{}^{18}O^{2-}]_{eq}(1-[^{13}C^{16}O_3{}^{2-}]_{eq})^z[^{13}C^{16}O_3{}^{2-}]_{eq}(1-[^{12}C^{16}O_2{}^{18}O^{2-}]_{eq})^z}{[pair]_{eq}} . \quad (17b)$$

Now there are only two free parameters, one for exchange and one for diffusion.

5.2.2 Model intuition. — Before examining how this 'paired' model can be fit to the experimental results, it is worthwhile to first develop some qualitative insight into how this model works and why it may be capable of fitting the kinks observed in the experiments from this study and from Passey and Henkes (2012). The paired model requires that clumped species must first convert to pairs of singly substituted species before finally forming the more common singletons (and vice versa). In this way pairs act as an intermediary between clumped and singly substituted species in the following reaction scheme: clumped species <—> pair <—> singletons. If the concentration of pairs remains constant throughout a reaction (that is, dpair/dt=0), then they have no effect on the kinetics as any change in the clumped species will have to, for mass balance considerations, be immediately compensated for by the singletons. In this end member scenario, the first-order model of the previous section will be reproduced and no kinks will be observed. If, on the other hand, the concentration of pairs evolves with time, then

it can act to modify the kinetics of clumped isotope exchange. Specifically, if diffusion is slow compared to local exchange between clumped species and pairs, the population of pairs will increase or decrease in size (depending on whether clumped species are, in net, forming or being destroyed) faster than diffusion can form or destroy them. In this scenario, the pairs can act as a buffer to changes in the clumped isotope concentrations. For example, during heating, as clumped species dissociate to pairs, if diffusion cannot split pairs sufficiently quickly, the pair concentration will build to an excess until it is sufficiently out of equilibrium such that its back reaction to clumped species balances the splitting of clumped isotope species to pairs. This would slow and eventually halt the decline in clumped species. As diffusion proceeds and breaks excess pairs apart to singletons, clumped species could then continue to react and drop in abundance. The results of our 430°C experiment can be understood as the product of this dynamic relationship among singletons, pairs and clumps: the initial fast reaction could occur because there are not enough pairs to buffer the system at the start. Once the pairs are able to buffer the splitting of clumped species, the kinetics become controlled by the slower diffusional splitting of pairs to singletons as seen in latter part of the experiment. Thus, all of the clumped isotope experiments showing non-first-order behavior, both here and in Passey and Henkes (2012) can be understood if early in these experiments the initial population of pairs is first driven to a dynamic steady state with the clumped species, after which further reaction requires the slower process of separation of pairs by solid state diffusion.

This model, however, explicitly does not include certain physical parameters that are thought to influence the kinetics of diffusion in calcites and apatites. Specifically,

defects, water fugacity, and pressure are all hypothesized or documented to influence diffusion. At an even more basic level, it is important to consider what species or atoms are actually diffusing in calcites and apatites. The paired model presented here involves two distinct carbonate groups in the lattice interacting and diffusing. This may be an acceptable model for carbon in carbonates, which has been hypothesized to diffuse in carbonate groups (Anderson, 1969; Haul and Stein, 1955). Additionally, Labotka et al. (2004) showed that oxygen and carbon have similar diffusivities at low (0.1 mPa) pressures, which they interpreted as evidence for C and O diffusing together in a carbonate group. This indicates that our formulation of diffusion is consistent with some observations.

However, oxygen self-diffusion in calcite has a complex dependence on water fugacity (Farver, 1994; Kronenberg et al., 1984), presence of defects (Anderson, 1969; Farver, 1994; Kronenberg et al., 1984), pressure (Labotka et al., 2000; Labotka et al., 2004), and possibly trace metal content (Farver, 1994; Kronenberg et al., 1984) and can be decoupled in these circumstances from carbon diffusion. All of these physical parameters are worth exploring and understanding in quantitative detail in order to have a complete model of clumped isotope kinetics in carbonate minerals. However, such a complete description of the kinetics of clumped isotopes is not currently possible. Thus we neglect these many complexities and proceed with the more modest goal of fitting our experimental data with the paired model as fully as possible in order gain insight into both our experiments and the behavior of clumped-isotope kinetics on geologically relevant time scales As will be shown, the paired model is able to fully fit all of our experimental data as well as the experiments of Passey and Henkes (2012). Additionally,

the model predicts behaviors that are consistent with geologically relevant observations despite simplifying many of the suspected complexities demonstrating that it is a useful description of carbonate clumped isotope kinetics.

5.2.2 Paired model fitting. — We solve for rate constants, k_f and $k_{dif\text{-}single}$ through a minimization of the solutions of Equations (11) and (12) versus the data using the trust-region nonlinear least squares fitting algorithm of Matlab. Robust fitting is used with the bisquare option. This minimization requires a solution to Equations (11) and (12), coupled differential equations, which we integrate for every trial with Matlab's ordinary differential equation solver ODE45. Additionally we must initialize ξ and the number of pairs in the system. ξ is initially set to zero. The correct choice for the initial number of pairs in the system is not obvious, but is important because the concentration of pairs relative to the final equilibrium value at any given point in time is a critical parameter in the model. We explored how to initialize the pair concentration by generating models in which the initial and final value pair concentrations were either identical or different.

We found that initializing the pair concentration to be the same as the proscribed final, randomly distributed pair concentration resulted in a poor fit for the 430°C calcite experiments and was essentially identical to the fits produced without the inclusion of the pairs as a discrete group (first-order model section). This demonstrates that differences in the rates of diffusion versus clumped isotope-pair exchange are insufficient on their own to develop large enough temporary excesses or deficits in the concentration of pairs compared to the final value. In contrast, we observed that model runs where the pairs were initialized with a different concentration than their final, prescribed value did generate kinks. We found that the best fits for the 430°C occurred if the system was

initialized with either a slight deficit of pairs (1% lower) or a enrichment of pairs (0.015% higher) relative to the final value. The final value did not need to be the random distribution of pairs — instead only the relative difference between the initial and final number of pairs appears to matter. The need to have a non-random initial distribution of pairs was also required in the modeling of Zhang et al. (1995) on which our model is based. In the case of this previous study no thermodynamic justification for an initial non-random distribution of pairs was given, but was justified as the result of prior thermal histories. Here we hypothesize that excesses or deficits in 'pairs' are not a model artifact but instead arise from a thermodynamic driving force related to the distribution of pairs within a carbonate mineral.

Specifically, we hypothesize that pairs are enriched relative to that expected for a random distribution of pairs through the lattice due to a drop in enthalpy of the system when singly substituted carbonates are found as pairs as opposed to isolated as singletons. Thermodynamically, this requires a non-zero enthalpy of mixing for carbonate groups in the mineral lattice. Although pairs, as we define them, do not involve bonds between two heavy isotopes (which would lower the energy of the system; Schauble et al., 2006; Wang et al., 2004), they still involve a close association of those heavy isotopes. Such associations can be thought of as solid-state versions of clumped isotope species that lack immediately adjacent heavy isotopes, such as $^{12}C^{18}O_2$, where the ^{18}Os are on opposite sides of an isotopically normal carbon. These 'secondary' clumped species have excesses that are smaller in size, but otherwise generally similar to other clumped isotope equilibria (for example, Wang et al., 2004). For example, at equilibrium, $^{12}C^{18}O_2$ is half as enriched as $^{13}C^{16}O^{18}O$ at a given temperature and bulk isotopic composition. Such

thermodynamically driven excesses in pairs will be temperature dependent with a stronger favoring of pairs at lower temperatures and be controlled by equilibrium constants of the form, $K_{pair}=[pair_{actual}]/[pair_{random}]$, where $pair_{actual}$ is the actual concentration of pairs in the system while $pair_{random}$ is the concentration of pairs calculated as if all carbonate groups were randomly distributed throughout the lattice (see Equations 14a and b). $\ln(K_{pair})$ will be approximately linearly proportional to 1/T such that at infinite temperatures, due to entropy, the pairs will be at the random distribution. This requires that samples formed at low temperatures will have an excess of pairs compared to a system at a higher temperature and vice versa.

No theoretical model for the distribution or size of this hypothesized excess of pairs currently exists. Thus to calibrate the temperature dependence of K_{pair} we assume that $\ln(K_{pair})$ is linearly proportional 1/T. We find the intercept of this line by assuming that pairs are randomly distributed at infinite temperatures, giving an intercept of zero. We find the slope of this line by assuming our unheated optical calcite formed at its measured clumped isotope temperature of 55°C and at equilibrium has a 0.015% excess of pairs compared to equilibrium at 430°C, which was the excess we found provided a good fit the 430°C experimental data. We do not use 1% deficit of pairs (which yields equally good fits) as our model requires samples precipitated at low temperatures to have an initial excess of pairs when heated to higher temperatures. This results in the following equation for $\ln(K_{pair})$:

$$\ln(K_{pair})=\frac{0.00992}{T}, \tag{18}$$

where T is in Kelvin. When fitting our experimental data, we use the clumped isotope temperature of the unheated calcite (55°C) to find the initial number of pairs and the

experimental heating temperature to find the final number of pairs. This treatment of pairs is clearly a hypothesis anchored to an empirical finding of our model fits. However, it is potentially testable in several ways: One could create a lattice model that calculates the expected pair excesses as a function of temperature. Additionally, our model predicts that the kinetics of cooling should be distinct from that of heating (that is, because during cooling there would be a deficit of pairs initially rather than an excess). If sufficient quantities of samples could be heated to very high temperatures without decrepitation (as in a piston cylinder) and then reheated to 430°C for different time periods, we expect one would observe a kinetic behavior different to that seen here.

We incorporated Equation (18) into our model to find the initial and final pair concentrations and fit the model to the 430, 536, and 692°C calcite data. The 430 and 536°C calcite data were straightforward to fit using the methods outlined above due to the large spread in Δ_{47} over the course of the experiments (Fig. 5a and b; Table 6). The 692°C experiment, on the other hand, is 90% equilibrated within 3 minutes (Fig. 5c). Because of this, there are few points available to define the curvature. We found that, unlike the 430 and 536°C cases, different initial guesses for the values of k_f and $k_{dif\text{-}single}$, which are needed to initialize the fitting routine, resulted in different (though generally similar) final answers with indistinguishable goodness of fits — all final fits had r^2 values of ~0.97. This implies that there exist multiple values of k_f and $k_{dif\text{-}single}$ for the 692°C data that can produce equally robust fits. In order to choose which of these fitted parameters at 692°C to use in later modeling, we also required that the fits be consistent with the experimental observations that 6 day heats at 323°C and 7 day heats at 209°C do not generate changes in Δ_{47} (within the error of the measurement). In order to test this, we

combined all potential 692°C fitted parameters with those from the 430 and 536°C fits to create Arrhenian-based models for the temperature dependence of rate constants (see section 5.2.4 below) and calculated kinetic parameters for diffusion and exchange at 209 and 323°C. We then used these parameters to calculate the change in Δ_{47} at 209°C after 7 days, and 323°C after 6 days. We found that only one of the 692°C fits yielded k_f and $k_{dif\text{-}single}$ values consistent with no change in Δ_{47} for 7 day 209°C heats and 6 day 323°C heats. We selected this as our 'best' 692°C fit and used its parameters for all subsequent calculations.

The atomistic reaction/diffusion model we present is able to fit our dataset without ad hoc rejection of data or presumptions regarding the behaviors of defects; in particular, the explicit inclusion of pairs of singly substituted species provides a physical mechanism for non-first-order behavior observed in all experiments. However, a significant question is whether this model is applicable to other samples, or if clumped isotope kinetics vary depending on the starting material.

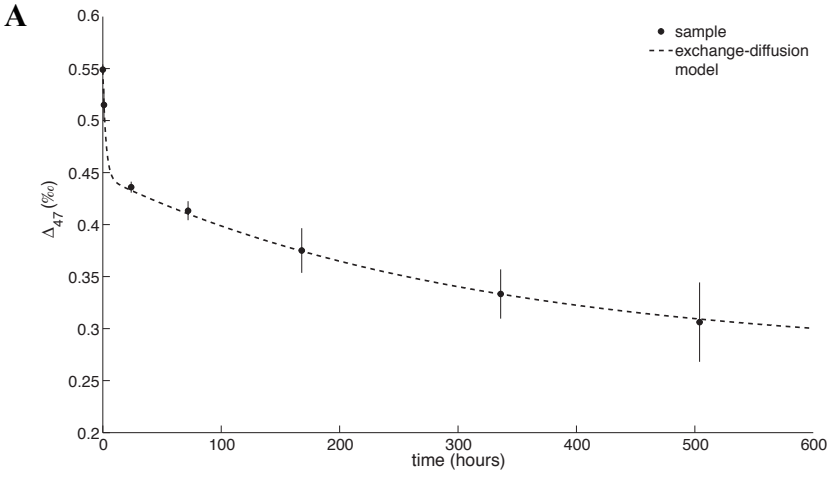

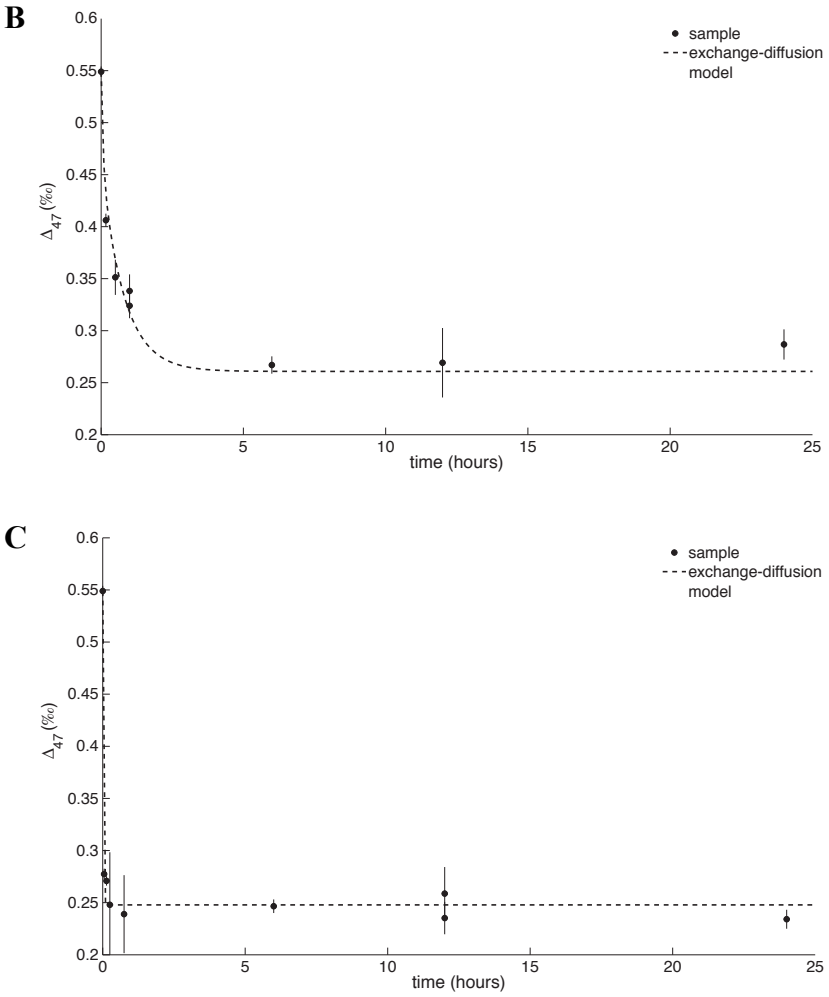

Figure 5. Exchange-diffusion model as applied to data from calcite heating experiments performed in this lab. a) 430°C data; b) 536°C data; c) 692°C data. All Δ_{47} values are presented in the Ghosh reference frame. Error bars are 2 standard errors.

Importantly, these fits were made using the same pair excess model as for our measurements. Fits are shown in Figure 6 and kinetic parameters in Table 9. We compare the kinetic parameters derived from our model from the data of Passey and Henkes (2012) to the data presented here in the next section. Our model is able to fit the data of Passey and Henkes (2012) in all cases and captures the rapid kinetics in the beginning of experiments. Given that their optical calcite is from a distinct source to ours, we consider it unlikely that both samples would happen to have a similar defect structure. A more straightforward conclusion is that the model we present here accurately describes the

atomistic basis for the non-first-order behavior of clumped isotope re-equilibration, and can be extrapolated beyond our specific sample. However, this is a hypothesis that needs to be tested with experiments on additional samples.

To evaluate this, we fit our model to the data of Passey and Henkes (2012). We only took the data from their experiments on optical calcites as their spar calcite appears to be heterogeneous in trace element content on the micron scale and thus may be a mixture of multiple carbonate precipitation events. Additionally, we did not fit data from their 385°C experiments because they only capture the initial, fast kinetics and thus cannot be used to constrain the diffusional rate parameter. All data was used in the 'Ghosh' reference frame as opposed to the Dennis et al. (2011) reference frame in order to be consistent with our measurements and the Δ_{47} calibration we are using, all of which are presented in the Ghosh reference frame. Before fitting their experiments, we compared their final, time-invariant values to those predicted by our high-temperature calibration (Fig. 2; Table 8). We found that their time-invariant (presumably equilibrated) values are on average 0.011‰ (± .005, 2 s.e.) higher than those predicted by our temperature calibration; this is a small multiple of analytical error and likely reflects subtle differences between the Caltech and Johns Hopkins intralab reference frames (in principle this should be correctable using the absolute reference frame of Dennis et al., 2011, though much of the data presented here was produced before the development of that method). As such, we subtracted 0.011‰ from the data of Passey and Henkes (2012) before fitting with our diffusion/reaction model. Additionally, one single point was not fitted from the Passey and Henkes (2012) 450°C experimental series (the data point from

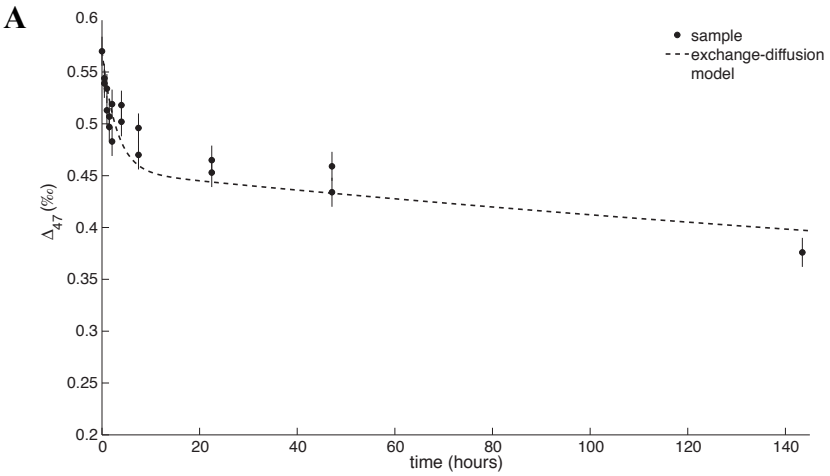
A
sample
exchange-diffusion model
Δ_{47} (‰)
time (hours)
0.6
0.55
0.5
0.45
0.4
0.35
0.3
0.25
0.2
0
20
40
60
80
100
120
140

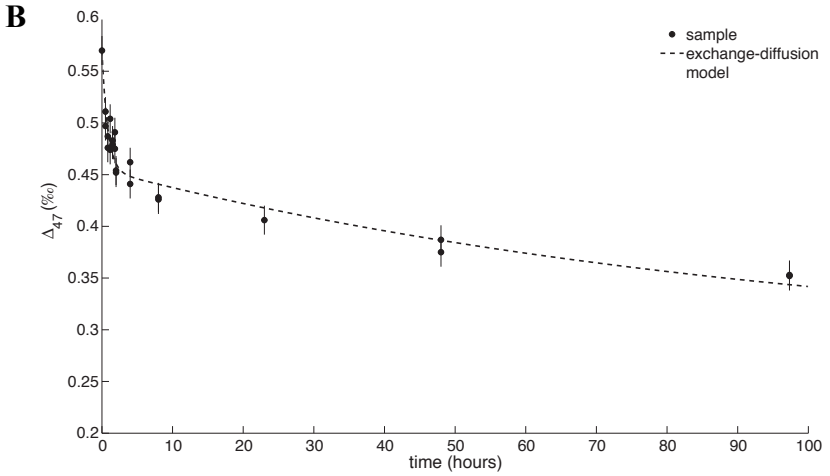
B
sample
exchange-diffusion model
Δ_{47} (‰)
time (hours)
0.6
0.55
0.5
0.45
0.4
0.35
0.3
0.25
0.2
0
10
20
30
40
50
60
70
80
90
100

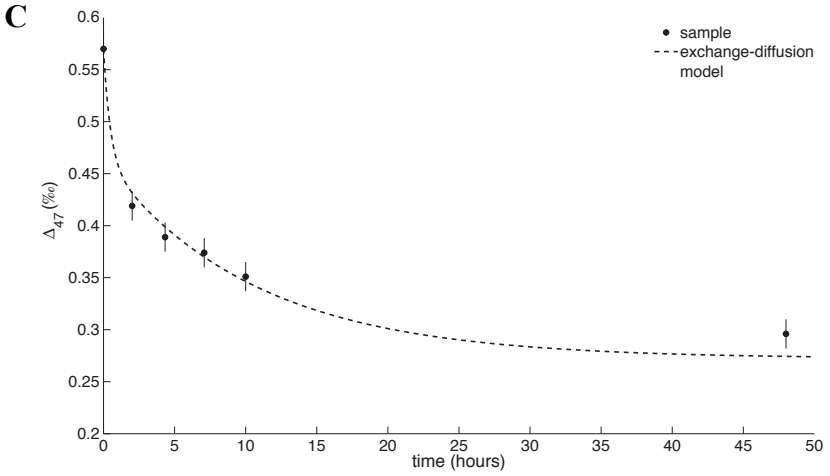
C
sample
exchange-diffusion model
Δ_{47} (‰)
time (hours)
0.6
0.55
0.5
0.45
0.4
0.35
0.3
0.25
0.2
0
5
10
15
20
25
30
35
40
45
50

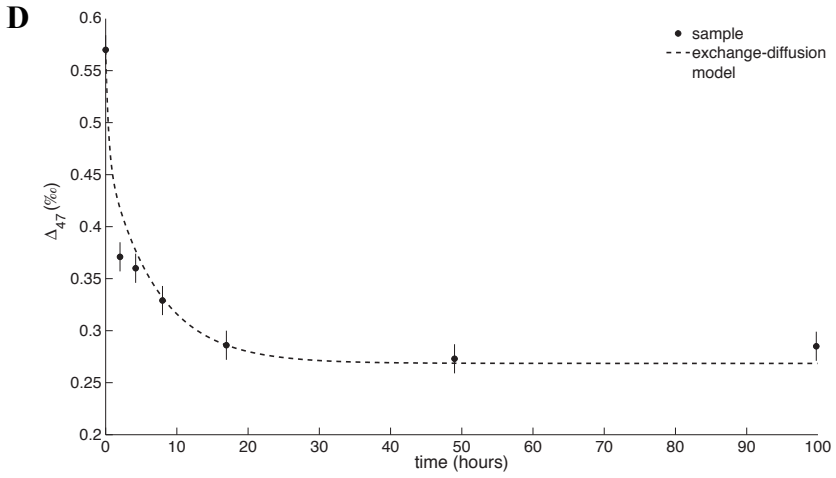

Figure 6. Exchange-diffusion model as applied to data from calcite heating experiments performed by Passey and Henkes (2012). a) 405°C data; b) 425°C data; c) 450°C data; 475°C data. All Δ_{47} values are presented in the Ghosh reference frame.

24 hours) as it caused coefficients to have high error (errors greater than 30 times the value of the rate constant).

5.2.3 Extension of the model to apatite. — We additionally performed heating experiments on apatite samples from Siilinjarvi at 430, 536, and 692°C (Fig. 7). No change in Δ_{47} values occur for the 430°C heat over a 24 hour period. The 536°C and 692°C, on the other hand, monotonically decrease in Δ_{47} values within 1 day. A critical question is whether apatites show non-first-order behavior. The 536°C experiment, which is where there is a chance of observing this behavior, does not have enough early time points to tell if there is a rapid change at the start of the experiment. Thus we cannot currently tell if apatites show non-first-order kinetics or not. To understand this will require additional experiments at temperatures between 400 and 500°C over month long timescales.

A question is how to model the exchange of isotopes of carbonate groups in the apatite lattice. For example, the paired model explicitly accounts for the groups surrounding individual carbonate groups, which is straightforward to formalize in the

case of calcite. However, carbonate groups in phosphates are defects and likely surrounded by phosphate groups rather than adjacent carbonate groups. It is unclear to us how to parameterize the geometric elements of our model (that is, the parameter, z, that describes the number of adjacent exchangeable groups) so that it can be extended to apatite. Here, we simplify the problem by adopting the same parameters as our calcite model; this is likely incorrect but lets us compare the experimental data for apatite and calcite in a self-consistent way. If future experiments demonstrate that apatites have definitively distinct kinetics from calcites (for example, are first-order) then an apatite-specific model will need to be constructed

We only modeled the 536 and 692°C data (Fig. 7b and c; Table 7) as there is no change in Δ_{47} for the 430°C experiments beyond the error of the measurements. To fit the 692°C data for the apatite, which has similar issues to the calcite data at the same temperature, we varied our guesses and chose the best fit. To check the robustness of our fits, we extrapolated the data to 430°C and ensured that the fit is in agreement with the experimental data (fig. 7a).

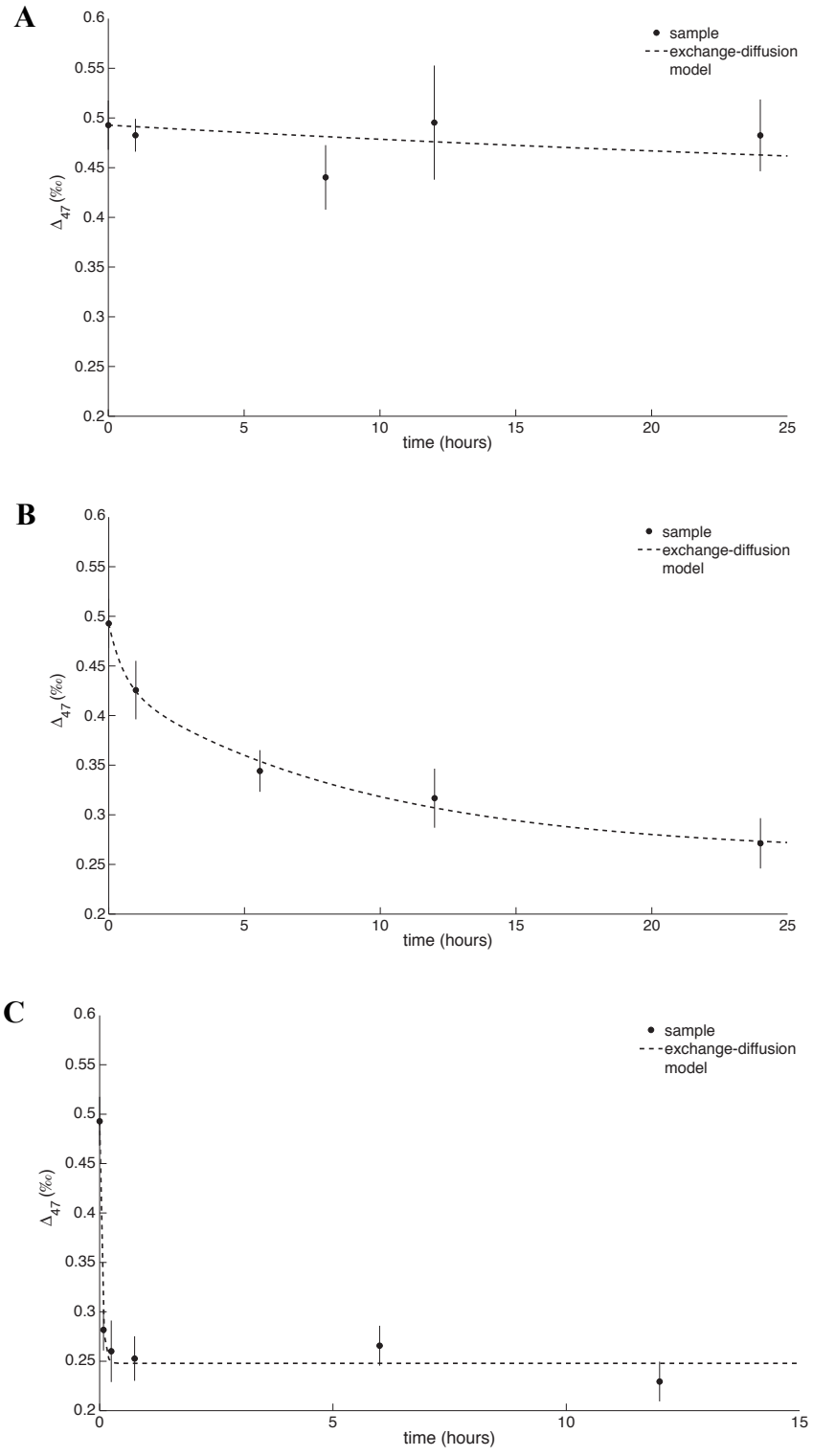

Figure 7. Exchange-diffusion model as applied to apatite data from apatite heating experiments.
a) Extrapolation of diffusion and exchange parameters derived from the 536 and 692°C as applied to the 430°C data; b 536°C data; c) 692°C data. All Δ_{47} values are presented in the Ghosh reference frame.

Our model is able to fit the experimental data from 536°C and 692°C. Additionally and importantly, the model parameters, when used to extrapolate the parameters to 430°C, fit the data within the error of the measurements. Thus, even though only two experiments are available for fitting, those fits are consistent with the lower temperature data. Interestingly, these data show slower kinetics at 430 and 536°C in apatites than in calcites. This is the opposite of what is predicted by the data from apatites and calcites from carbonatites where apatites always have lower clumped isotope temperatures than cogenetic calcites. This observation predicts that apatites should have *faster* kinetics than calcites at a given temperature. Thus the experimental results of the apatites, regardless of the model used, are inconsistent to zeroth order with observations from nature. We address this below by attributing this difference to the presence of radiation damage in natural samples that increases diffusion in the lattice, but is annealed away in the experiments, slowing down diffusion and the resultant exchange of isotopes.

6. Models of clumped isotope temperatures during heating and cooling

The purpose of the above experiments and model fits is to use them as a calibration for a general kinetic model of clumped isotopes in carbonates. Such a model allows for calculations of the change in Δ_{47} for any given time-temperature path of a sample. These models must be consistent with both the experimental results from above and the range of closure temperatures observed in carbonatites and marbles with externally estimated thermal histories.

6.1 Extrapolation of kinetic properties to other temperatures

In order to make model calculations at temperatures other than those constrained by experiments, we require a relationship between temperature and rate constant. Generally, rate constants are assumed to be Arrhenian: that is, ln(k) is linearly dependent on 1/T (where T is temperature). However, the equilibrium constant for all clumped species is pseudo-linear with $1/T^2$, as opposed to 1/T, at temperatures relevant to our experiments and most geological environments (Schauble et al., 2006; Wang et al., 2004). The logarithm of the ratio of the rate constants for both the diffusion and equilibrium constants are approximately linearly proportional to the equilibrium constant, and thus should vary linearly more strongly with $1/T^2$, not 1/T. Such a relationship can be accomplished either by (1) assuming that the kinetic terms vary with a strong 1/T and weak $1/T^2$ dependence, and are thus nearly Arrhenian. The 1/T dependence would then cancel out when the rate constants are ratioed leaving behind the $1/T^2$ dependence or (2) that the logarithm of the rate constants vary nearly linearly with $1/T^2$ and are not Arrhenian. As most models of diffusion and reaction kinetics use rate constants that follow a 1/T dependence, we will adopt that convention here.

The linear fits for ln(k) vs. 1/T are given in Figure 8 and include both the experiments generated in this study and those from Passey and Henkes (2012). The fits to our data and that from Passey and Henkes (2012) appear to form a single trend rather than forming two distinct groupings of data. This is significant as it supports the use of a single, unifying model for the kinetics of clumped isotopes in calcites that is independent of starting material and thus generalizable to any homogeneous sample. Inclusion of their data causes the slope of the fit to be slightly shallower than suggested by our data alone,

and would predict changes in Δ_{47} at 323°C over laboratory time scales that are not observed in our experiments. If, instead, our data are used alone to define the temperature dependence of these rate constants, we predict changes in Δ_{47} over laboratory time scales that are within error of zero (consistent with our 323 ˚C experiments). Despite this, we include both our data and that of Passey and Henkes (2012) for our model. If it is found that the model systematically overpredicts changes in Δ_{47} at low temperatures, then the model can be altered just to use our data. The relationships for calcite with 2σ errors are:

$$\ln(k_{f;calcite}) = \frac{-18200\ (\pm 3700)}{T} + 25.5\ (\pm 4.9),\ (r^2 = 0.97), \tag{19}$$

$$\ln(k_{dif\text{-}single;calcite}) = \frac{-23200\ (\pm 5900)}{T} + 30.5\ (\pm 8),\ (r^2 = 0.96). \tag{20}$$

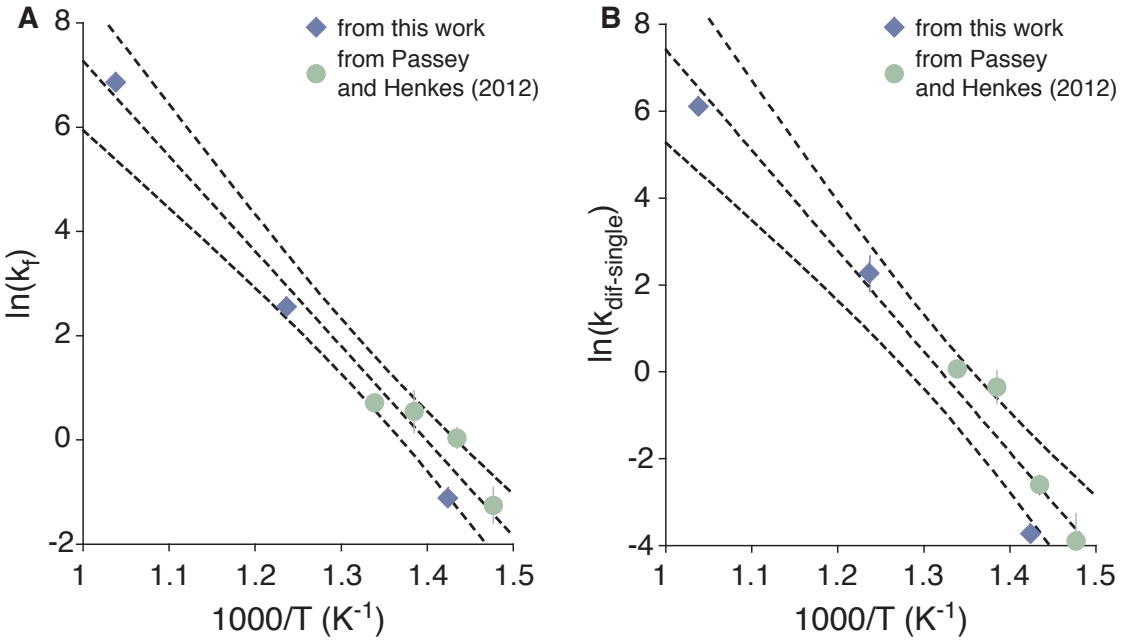

Fig. 8: 1/T extrapolation of rate constants from calcite data. Error bars are 2 standard errors. This includes data from experiments performed at Caltech and by Passey and Henkes (2012). The error envelope represents a 95% confidence interval. a) Forward exchange rate constants (k_f); b) Diffusion rate constants for singletons ($k_{dif\text{-}single}$).

Note that all rate constants are given with units of hour^{-1}. The slopes of these lines yield activation energies of 151 (±31, 2σ) and 193 (± 49, 2σ) kJ/mole for exchange and diffusion in calcites respectively. Activation energies of self-diffusion of oxygen in calcites have been estimated for dry experiments to be between 240 to 276 kJ/mol by Labotka et al. (2004) depending on the pressure, 381 kJ/mol by Anderson (1969), and 173 kJ/mole by Farver (1994). Activation energies for the diffusion of carbon are estimated to vary from 166 kJ/mol to 291 kJ/mol by Labotka et al. (2004), 364 kJ/mol by Kronenberg et al. (1984), and 71 to 368 kJ/mol by Anderson (1969). Thus our measurement is in the range for reported self-diffusivities of carbon and oxygen in calcites.

We performed similar extrapolations for the phosphate dataset using the 530 and 692°C experiments. The equations are:

$$\ln(k_{f;apatite}) = \frac{-23730}{T} + 29.7, \quad (21)$$

$$\ln(k_{dif\text{-}single;apatite}) = \frac{-26100}{T} + 32. \quad (22)$$

No correlation coefficient or errors are given as they are all two point fits. Extrapolating these equations to 430°C gives a change in Δ_{47} within the error of the measurements (fig. 7a) demonstrating that the extrapolations are at least consistent with the lower temperature data despite being based only on the two higher temperature experiments. The activation energies are 197 and 217 kJ/mole for exchange and diffusion. The only study on oxygen diffusion in apatites yielded an activation energy of 205 kJ/mole (Farver and Giletti, 1989).

6.2 Modeling and interpretation of closure temperatures during cooling

We used Equations (19) and (20) to model the closure temperature recorded by calcite for a variety of modeled cooling histories. Because previous studies have established commonly observed ranges of temperatures for slowly uplifted metamorphic rocks and carbonatites (~120°C-200°C; Bonifacie et al., 2013; Bonifacie et al., 2011; Dennis and Schrag, 2010; Ghosh et al., 2006), we have some basis for deciding whether the predictions of these models are reasonable. For these models, we began with a bulk stable isotope composition identical to the optical calcite used. We then subjected the sample to a modeled temperature history that first includes initial heating to 350°C for 10,000 years to ensure pairs and singletons were fully equilibrated at high temperatures. After this, we calculated the consequences of cooling the samples down to 0°C at linear rates ranging from 10,000°C to 1°C per million years (fig. 9).

Our model predicts rapidly cooled samples (10,000-1000°C/myr) will have closure temperatures between 205 and 180°C and more slowly cooled samples (100-1°C/myr) between 160-120°C. Our results for calcites from carbonatites (~190°C to 125°C) resemble the range predicted from the model. In particular, the Oka body was externally estimated to have cooled around 1000°C per million years based on oxygen isotope thermometry of multiple minerals (Haynes et al., 2002) and its clumped isotope temperature for calcite of 192 ±14 ˚C is within error of the predicted clumped isotope temperature of 181°C for the 1000°C/myr cooling rate. However, some carbonatites record temperatures of ~250°C and can go as high as 416°C (Dennis and Schrag, 2010). These results suggest either exceptionally rapid cooling rates for these materials, such that under some circumstances the reaction rates that control reordering of carbonate

clumped isotope temperatures may be slower than we found in our experiments, or that these samples represent some disequilibrium phenomenon. Additionally, the mineralogy of the carbonatites could be of importance as dolomites and calcites likely have distinct kinetics (Bonifacie et al., 2011; Eiler, 2011).

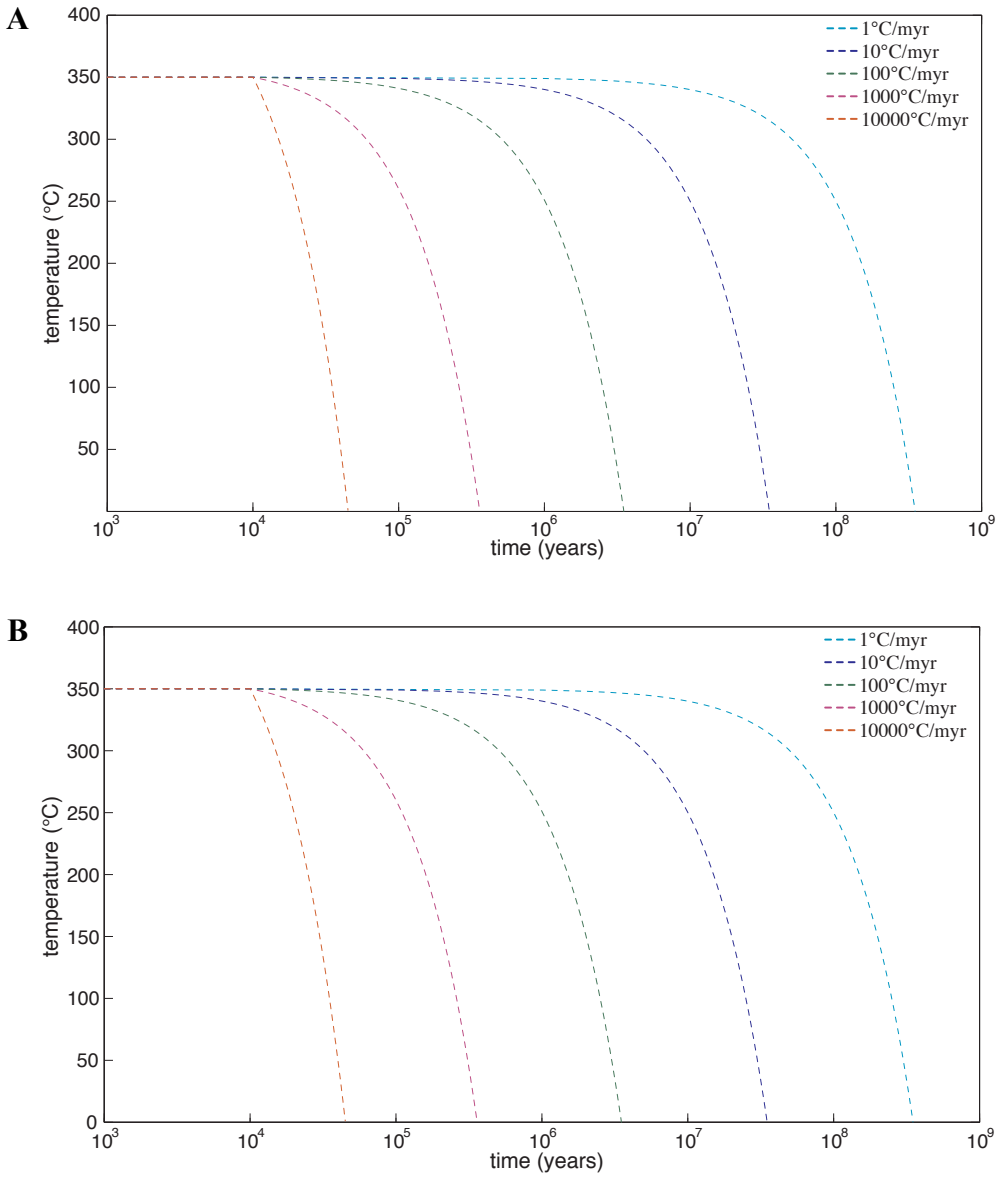

Fig. 9: Closure temperatures derived from modeled parameters. Dashed lines are the environmental temperature while solid points are the recorded clumped isotope temperatures. a) Calcites; b) Apatites.

We routinely measure a Carrara marble as an internal standard which has a long term average clumped isotope temperature of 206°C. The Carrara marble is predicted to

have cooled between 10 to 100°C per million years (myr) below 250°C via fission track and U/Th-He apatite and zircon thermochronology (Balestrieri et al., 2003). Our models predict closure temperatures for 10 and 100°C per million years as 136°C and 157°C degrees respectively. Calcite in marbles generally preserves apparent temperatures from 150 to 200°C (Bonifacie et al., 2011; Eiler, 2011) and have cooling rates between 1-100°C/myr. Consequently, the model predicts kinetics that are faster than observed for marbles. Note that the Oka carbonatite is thought to have cooled at least an order of magnitude faster than the Carrara marble sample, but the Oka sample has a lower measured clumped isotope temperature than the Carrara marble. Thus, no simple model will ever be able to reconcile the clumped isotope temperatures of both of these samples with the given cooling histories.

Nevertheless, our model predictions of reaction rates bound the range of apparent temperatures observed in most natural marbles and carbonatites (Dennis and Schrag, 2010) with reasonable modeled geological cooling rates. We consider it likely that some of the disagreements between model and observation stem from the simple assumptions of our models (that is, linear cooling rates; simple, single-phase cooling histories; no recrystallization during cooling). Greater complexity must be present in some of the studied samples. For this reason, we are generally encouraged by this comparison, as it suggests that rates observed in the laboratory are at least generally consistent with observations of natural samples. An additional test of our model and kinetic parameters could be accomplished through the measurement of a suite of related samples with well-constrained and simple thermal histories, such as carbonates near small igneous intrusions.

Comparison of model predictions with natural samples in the case of apatite yields a different result. Figure 9 presents the predicted closure temperatures of carbonate clumped isotope compositions of apatites for various cooling rates. In all cases we considered, apatites are predicted to have higher closure temperatures as compared to identically cooled calcites. This is in complete disagreement with natural samples. We suggest two possible explanations for this behavior:

(1) The model may not capture the kinetics of how carbonate groups exchange isotopes in apatites. Our model of carbonate exchange and diffusion in apatites could be missing key physical parameters such as the local exchange of oxygen between PO_4^{3-} and CO_3^{2-} groups. A way in which a model could account for both the experimental data (which suggest apatite is more refractory than calcite at temperatures greater than 400 ˚C) and the natural observations (which suggest apatite has a lower closure temperature than calcite) would be if the rate constants for exchange and/or diffusion apatites are strongly non-Arrhenian. Specifically, the kinetics would have to remain at relatively fast rates at temperatures just below our experimental range and then decrease quickly. Effectively this requires that the activation energy for one or both of the proposed exchanged steps decreases markedly just below ~400 ˚C. This is possible, but strikes us as less plausible than an alternative we propose below.

(2) All apatite samples that were heated as part of this study likely contained radiation damage (that is, fission tracks) that were annealed within the first few minutes of our heating experiments; fission track studies demonstrate that fission tracks are fully annealed away in apatites within 20 minutes at 400°C (Green et al., 1986). We hypothesize that these defects enhance reaction/diffusion rates in radiation-damaged

natural apatites, and their removal by annealing in our experiments decreases these rates, yielding slower kinetics of reordering than actually occurs in natural, fission-track rich apatite. Effectively, we suggest the hypothesis of Passey and Henkes (2012), while not part of our model for clumped isotope reordering of calcite, plays an important role in reordering in apatite, in which observable structural damage is created in samples and routinely documented.

The effect of annealing on measured diffusivities in apatites has been observed for a variety of different chemical species. For example, Cherniak et al. (1991) attempted to quantify lead diffusion in apatites and zircons via surface tracer implantation. This implantation generates lattice damage in the surface of a mineral. They noted that diffusivities of lead obtained using this method as compared to others that do not generate damage were similar in apatites but different in zircons — specifically the experiments that generate surface damage caused higher measured diffusivities in zircons but not in the apatites. Because the apatites anneal at lower temperatures than zircons, Cherniak et al. (1991) interpreted apatite's apparent indifference to the damaging implantation of lead as the result of apatite's ability to rapidly anneal radiation damage on laboratory timescales at the temperatures of these experiments. Zircon, on the other hand, could not anneal the damage resulting in rapid diffusion of lead in the surface compared to experiments that introduced lead without damaging the lattice.

By analogy to these experiments, we propose that natural apatites possess radiation damage that increases their rate of reordering of carbonate clumped isotope temperatures at low temperatures (<250°C) near the nominally predicted and measured closure temperatures in apatite and calcite. In our experiments at higher temperature

(>400°C) this damage was quickly annealed away, reducing the diffusivity of carbonate groups or oxygen in the apatite lattice. If correct, this suggests that the closure temperature of the carbonate clumped isotope thermometer in apatite could be sensitive to uranium and thorium content, age and/or thermal history. More studies on apatites will be needed to explore this hypothesis. For example, igneous apatites with high and low amounts of uranium and thorium and known thermal histories could be compared to see if increased potential for damage changes the closure temperature.

6.3 Modeling and Interpretation of Apparent Temperatures During Heating

We also modeled the changes in carbonate clumped isotope temperature that should accompany heating a sample that starts near Earth surface temperatures on geological timescale, as would occur in a subsiding sedimentary basin. We did this by initializing calcites and apatites with a clumped isotope composition equivalent to equilibrium at 25°C (Δ_{47} value of 0.641 in the Ghosh reference frame), initial overabundance of pairs derived from Equation (18), and bulk isotopic compositions equal to the average values for our optical calcite starting material. We then calculated the consequences of heating each sample instantaneously to a constant temperature for one hundred million years. Results of these calculations for calcite are presented in Figure 10. Our model predicts that measurable changes in the clumped isotope temperature do not occur below 40°C and that subtle changes (<2°C), less than the 1σ error of the measurement, occur following heating to 60°C after 100 million years. Full equilibration is not reached until the sample reaches ~160°C in this time frame.

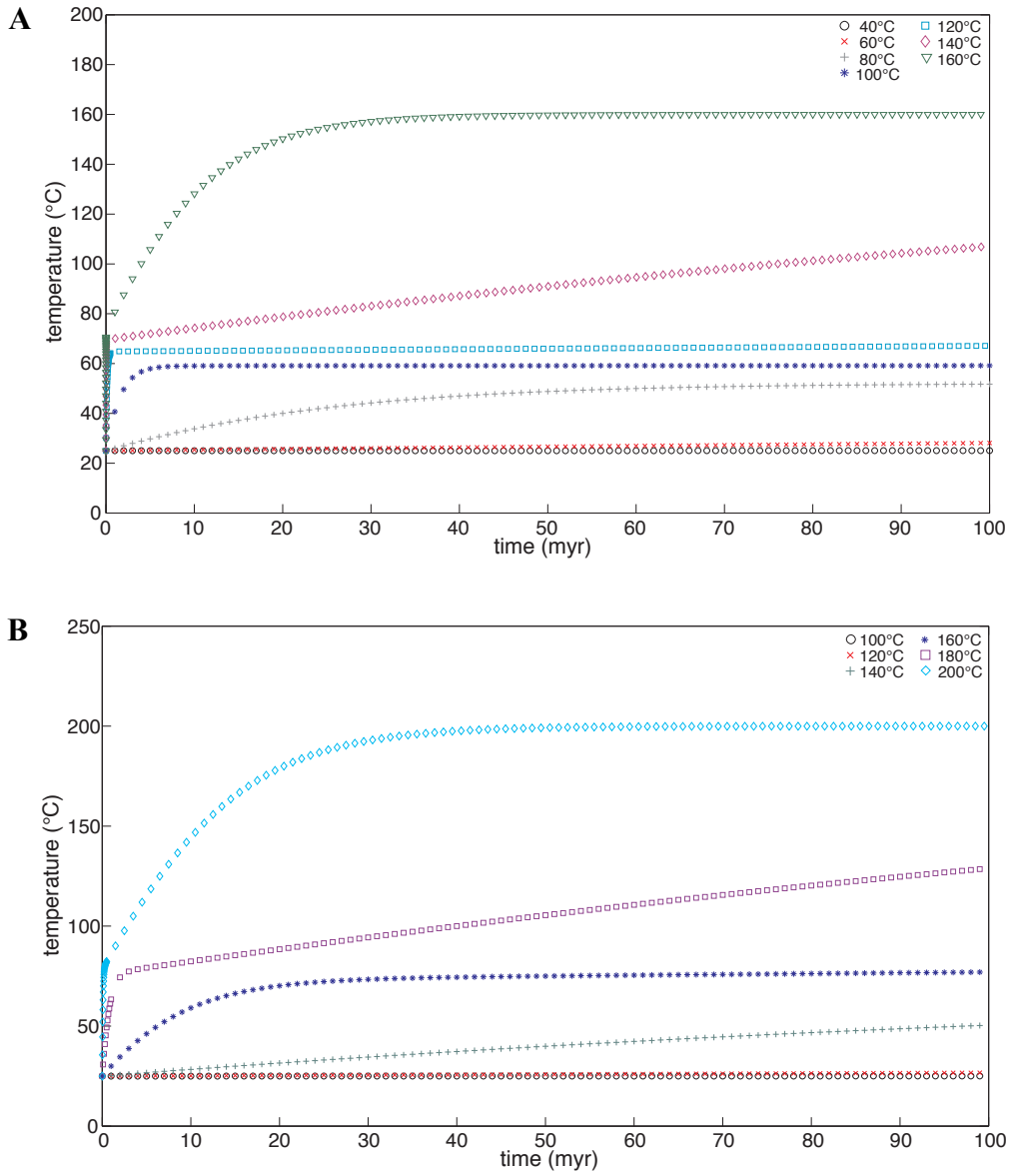

Figure 10. Change in Δ_{47}-derived temperatures from samples with originally low clumped isotope temperatures due to heating. Temperatures represent the recorded clumped isotope temperature after a heat soak for a given amount of time. a) Calcites; b) Apatites.

Of interest is that the predicted temperature changes occur in two distinct steps: increases in physical temperatures to below 120°C after 100 million years partially alter the clumped temperature recorded within a few tens of millions of years but then cease changing, reaching a steady state value below the actual ambient temperature. If the temperature is increased above 120°C, an initial rapid increase in clumped isotope

temperature occurs, followed by a slower increase until the ambient, environmental temperature is reached (Fig. 10). This two-stage change in clumped isotope temperature is the result of the explicit inclusion of pairs as a distinct population of isotopic species in the model, which act to buffer the creation and destruction of clumped species. During heating, clumped species initially react until a sufficient number of pairs are generated such that the reaction of clumps to pairs and pairs to clumps is balanced. If diffusion is sufficiently slow, such that the pairs do not diffuse apart appreciably, the pairs will stabilize above their equilibrium value and back react such that the clumped isotopes will be stabilized themselves at concentration above their equilibrium value (and thus give a lower clumped isotope temperature than the environmental temperature). Only when diffusion is sufficiently fast (occurring above ~120-140°C) can pairs diffuse apart into the background population of 'singletons', allowing more clumped species to react.

The apatites are predicted to have the same behavior as the calcites, but the stage of initial partial equilibration does not begin until higher temperatures (120°C; Fig. 10). Note that this prediction of our model is based on experimental data, which we infer is more refractory than many natural apatites due to annealing of radiation damage.

The model above predicts something potentially important regarding the nature of the clumped isotope record of ancient carbonates: we suggest that the relatively rapid kinetics of reaction between 'clumps' and 'pairs', combined with the relatively slow diffusive splitting of pairs at low temperatures, means that sedimentary carbonates exposed to moderate burial temperatures (~80-100 ˚C) can undergo small increases in recorded temperature (of order 10°C), which then stabilize for long periods of time. It is not until high burial temperatures (above ~120-140°C) that clumped isotope temperatures

approach the ambient temperature over geological timescales. This effect, if it really occurs in natural carbonates, could be a key systematic error in the interpretation of carbonate clumped isotope data for ancient, deeply buried platform limestone sequences, particularly those with maximum burial temperatures in the range ~60-100 ˚C, where conventional signs of burial metamorphism are subtle but temperatures are high enough to permit partial resetting. Such effects may be difficult to diagnose unless detailed thermal histories of the rocks are known. A potential way to understand these effects is to make measurements on phosphates and calcites from the same bed of rocks precipitated in similar conditions (for example, inarticulate vs. articulate brachiopods). Though the kinetics of exchange in phosphates are complex, it is clear they behave differently from calcites in natural rocks. As such, one could measure both and, if they give the same temperature, have increased confidence that that temperature represents a primary signal. Similar principles may apply to other pairs of phases (for example, calcite with aragonite or dolomite).

Though experiments from both this study and Passey and Henkes (2012) demonstrate that on heating, clumped isotope temperatures initially increase rapidly followed by a slower increase, a critical question is whether the initial rapid 'jump' in measured temperature occurs in samples from natural systems heated at geologically relevant rates. To explore this, we compared our model to a clumped isotope study of paleosols from the Siwalik Group in Nepal that experienced a simple, well constrained thermal history (Quade et al., 2012). In this study, all samples are from paleosols that formed within a few meters of the Earth's surface (and thus have a limited range of initial temperatures), were buried between 0 and 5 km within ~10-12 million years, and were

then rapidly uplifted to the surface. The samples from Quade et al. (2012) were interpreted to have never experienced burial temperatures above ~120°C and, based on petrographic arguments, never have recrystallized. However, these samples yield temperatures too hot (by ~10-30°C) to be interpreted as surface formation temperatures. Additionally, samples buried more deeply (>~2km) appear to give higher temperatures than more shallowly (<~2km) buried samples (Fig. 11).

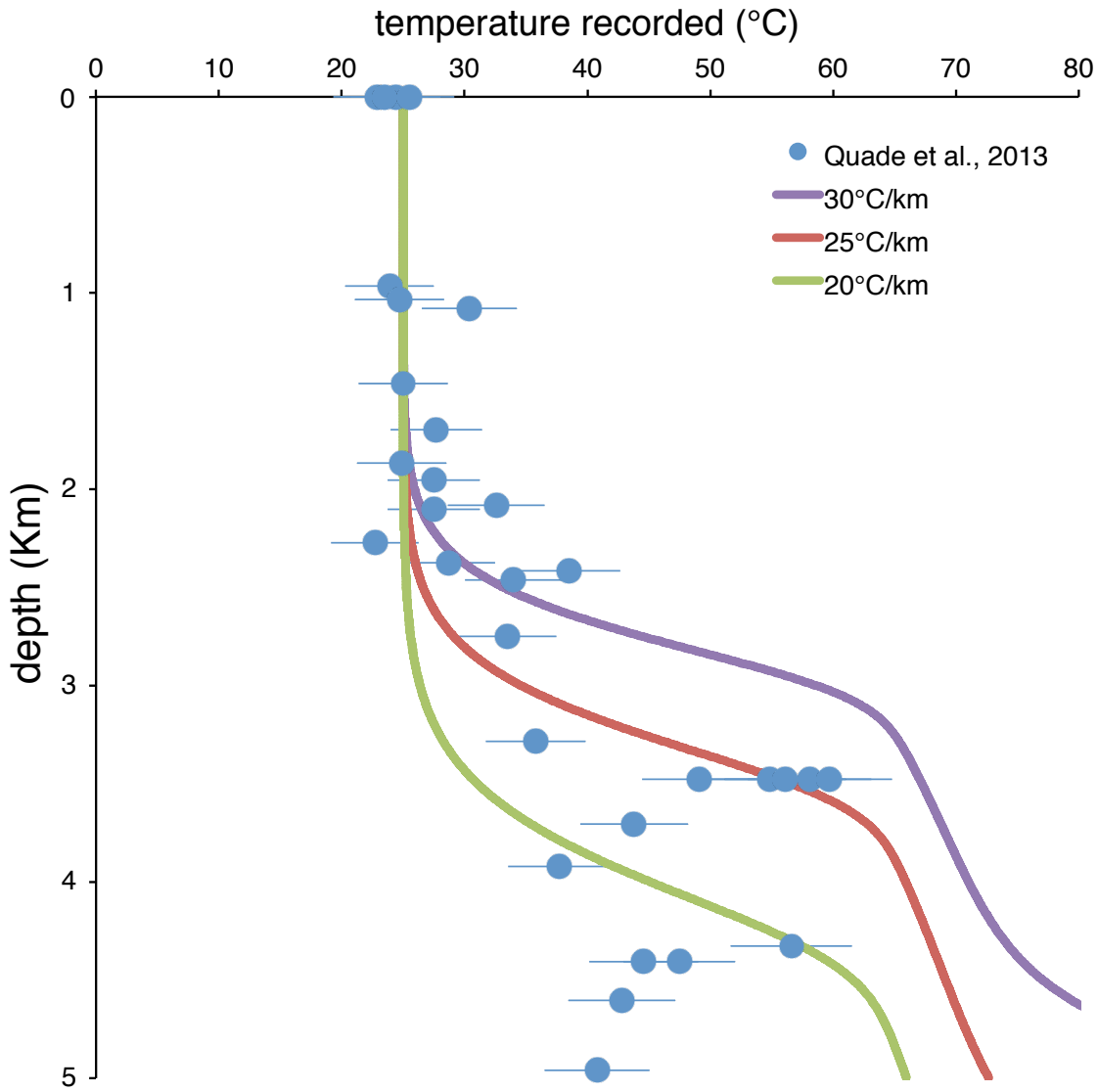

Fig. 11: Exchange-diffusion model applied to paleosol data from the Siwalik Basin, Nepal (Quade et al., 2012). Samples are assumed to have been buried to depths between 0 and 10 km at a rate of 0.5 km/million years. These burial histories are converted to thermal histories by assuming a 20, 25, or 30°C/km geotherm.

To explore whether these 'high' temperatures could be explained by our model, we assume a simple burial history in which the paleosol samples form at the surface of the Earth at 25°C (the average clumped isotope temperature of modern paleosols from the study area), with a concentration of pairs calculated from Equation (18). Samples are then assumed to have been buried between 0 and 5 km (the maximum burial depth) with a linear burial rate with time where the oldest, deepest samples are assumed to be 10 million years old. Samples are finally returned to the surface (still at 25°C) instantaneously, via faulting. We converted these burial histories into thermal histories by assuming geotherms of 20, 25, and 30°C/km, which are the published geotherms for the Siwalik Basin (Khan and Raza, 1986) and modeled the expected change in temperature of the samples vs. maximum burial depth (Fig. 11).

The modeled clumped isotope temperatures match the form of the observed clumped isotope temperatures with no change in temperature for the first 2 km, followed by a rapid shift in temperature between 2-4 km (burial temperatures of ~65-145°C depending on the geotherm), followed by a stabilization in temperature after 4 km in depth for the 20 and 25°C geotherms. The 30°C geotherm appears to strongly overpredict the maximum measured temperatures, but the 20 and 25°C do not. Maximum observed temperatures are ~60°C and modeled maximums are between 65 and 70°C for the 20 and 25°C geotherms. Critically, the model appears to be consistent with a real system with a known and simple burial history demonstrating that it can be used to model thermal histories and generate reasonable results. Furthermore, this test is consistent with rapid 'jumps' in clumped isotope temperatures of ~10-20°C during burial at ~80-100°C being a real phenomenon. This indicates that the 'pairs' mechanism we use to explain laboratory

experiments does capture the kinetics of clumped isotope reordering in natural carbonates at moderate temperatures.

We note, though, that all the models presented above should be approached with some caution because their predictions are based on extrapolation of experimental data to low tempratures, and the kinetic consequences of a hypothesized population of slow-diffusing 'pairs' in carbonates. Specifically, it is important to realize that changing our proposed model of pairs (that is, their temperature dependent abundance) would significantly alter the predicted kinetics of isotopic reordering, in some cases even allowing for 'overshoots' of apparent temperature on heating (where rapid heating causes the measured clumped isotope temperatures recorded to be temporarily higher that the physical environmental temperature during equilibration). Certain initial overabundances of pairs can also cause heating to actually lower the recorded temperature (as the extra pairs back react more than the clumped species split). It is unclear if such kinetics occur in natural samples. Furthermore, the complexity of diffusion in calcites and apatites (for example, the dependence on water, pressure, trace element content, and defects) must also be kept in mind.

Despite these caveats, we reemphasize that the models describe the non-first-order kinetics of our experiments and those of Passey and Henkes (2012), predict closure temperatures during cooling that bracket the ranges of clumped isotope temperatures observed in natural igneous and metamorphic calcites, and provide a reasonable fit to real samples that have undergone burial and exhumation. Thus, we believe the model behaviors we demonstrate are a useful guide to understanding how changes in physical temperature affects recorded carbonate clumped isotope temperatures in calcites and

apatites. A key insight to be taken away from the model is that heating of samples does not lead to simple kinetics. Rather, small (order 10°C) but rapid increases of the temperature recorded by samples initially precipitated or recrystallized at near-surface temperatures may occur.

7. Conclusions

We made measurements and conducted experiments aimed at understanding the kinetics of clumped isotopes in calcites and apatites. Measurements of natural carbonate minerals and carbonate groups in natural apatites yield closure temperatures in apatites lower than in co-occurring carbonate minerals, where closure temperature correlates to emplacement depth. Closure temperatures range from 60-130°C in apatites and 125-190°C for carbonate minerals (dominantly made of calcite). To better understand these results, we performed heating experiments on calcite and apatite minerals between 200 and 700°C. These experiments demonstrate that calcites exhibit complex, non-first-order kinetics and that apatites react more slowly in experiments than calcites, the opposite of what was observed in nature. Whether apatites also display non-first-order kinetics is unclear and will have to be explored through more experiments. To explain the results of our experiments, we developed a model that incorporates both reaction and diffusion in mineral lattices. This model allows for non-first-order kinetics and describes the features present in our data and similar results from previous related work. Extrapolation of the data is consistent with natural, slowly cooled carbonate minerals both from carbonatites and (less precisely) marbles. Observations from naturally occurring apatites and from experiments are in disagreement, which may be related to annealment of radiation

damage when natural apatites are exposed to high temperatures in our experiments. Our model predicts that on heating samples will not necessarily increase the clumped isotope temperature monotonically. Rather, at lower temperatures (~80°C), a small change in recorded temperature could occur and then stabilize. Not until higher temperatures (~>120°C) does a sample change its recorded temperature significantly throughout its burial history. This model is in agreement with the observed changes in clumped isotope temperature of paleosols from the Siwalik Group, Nepal which experienced a simple thermal history with burial temperatures up to ~150°C. This work has implications for our interpretation of samples that give warm temperatures for past environments, as well as for understanding cooling and heating paths for metamorphic systems.

.

8. Tables

Table 1. Age, isotopic values, and clumped isotope temperatures of all carbonatite samples. Errors are 2 standard errors. $\delta^{13}C$ values are standardized to VPDB, $\delta^{18}O$ to VSMOW, and Δ_{47} to the 'Ghosh' reference frame or 'absolute' (Abs) reference frame (Dennis et al., 2011; Ghosh et al., 2006).

Sample	Age (Ma)	$\delta^{13}C$ (‰)	$\delta^{18}O$ (‰)	$\Delta_{47,Ghosh}$ (‰)	$\Delta_{47,Abs}$ (‰)	°C	n
Oka Calcite	160	-5.28 ± .01	7.32 ± .11	0.361 ± .009	0.411 ± .01	192 ± 12	5
Oka Apatite	160	-5.31 ±. 02	8.17 ± .11	0.415 ± .007	0.468 ± .007	132 ± 6	15
Kovdor Calcite	370	-4.02 ± .01	7.42 ± .02	0.413 ± .006	0.466 ± .006	134 ± 5	8
Kovdor Apatite	370	-3.27 ± .01	10.98 ± .08	0.471 ± .011	0.527 ± .012	92 ± 6	4
Siilinjarvi Calcite	2600	-3.65 ± .003	8.29 ± .03	0.423 ± .009	0.476 ± .01	126 ± 7	11
Siilinjarvi Apatite #1	2600	-3.62 ± .01	10.74 ± .12	0.488 ± .008	0.545 ± .008	83 ± 4	17
Siilinjarvi Apatite #2	2600	-3.624 ± .02	10.53 ± .08	0.532 ± .005	0.592 ± .005	62 ± 2	2

Table 2. Cleaning experiment of Siilinjarvi and Oka apatites using acetic acid (see experimental methods section). All errors are 2 standard errors.

Sample	$\Delta_{47,Ghosh}$ (‰), not cleaned	$\Delta_{47,Ghosh}$ (‰), 4 hours	$\Delta_{47,Ghosh}$ (‰), 24 hours
Siilinjarvi apatite #1	0.490 ± .009 (n=11)	0.489 ± .017 (n=5;)	-
Oka apatite #1	0.428 ± .011 (n=11)	0.399 ± .022 (n=4;)	.412 ± .007 (n=5;)

Table 3. Comparison of clumped isotope temperatures with apatite-carbonate oxygen isotope temperatures using the calibration of Fortier and Lüttge (1995). Interphase temperatures are found using the difference between $\delta^{18}O$ values for carbonates and apatites. Temperatures for calcites are derived by using the carbonate $\delta^{18}O$ vs. the bulk apatite $\delta^{18}O$ value. Temperatures for apatites are derived using the $\delta^{18}O$ value of the internal carbonate groups vs. the bulk apatite $\delta^{18}O$ value. Bulk oxygen isotope data for apatites come from Conway and Taylor Jr (1969) for Oka. For Siilinjarvi, we took the average of all bulk apatite samples from Tichomirowa et al. (2006). We include, for comparison, temperatures derived from the clumped isotope measurements from Table 1. $\delta^{18}O$ values are all referenced to VSMOW.

sample	$\delta^{18}O_{carb}$ (‰)	$\delta^{18}O_{bulk}$ (‰)	T (°C, interphase $\alpha_{apatite\text{-}calcite}$)	T (°C, clump)
Siilinjarvi calcite	8.29	4.9	524	126
Siilinjarvi apatite #1	10.74	4.9	326	83
Siilinjarvi apatite #2	10.53	4.9	337	62
Oka calcite	7.32	5.6	885	192
Oka apatite	8.17	5.6	653	132

Table 4: Bulk and clumped isotope data and temperatures from heating experiments on calcites. All errors are 2 standard errors. $\delta^{13}C$ values are standardized to VPDB, $\delta^{18}O$ to VSMOW, and Δ_{47} to the 'Ghosh' reference frame or 'absolute' (Abs) reference frame (Dennis et al., 2011; Ghosh et al., 2006).

Time (hr)	T (°C)	$\delta^{13}C$ (‰)	$\delta^{18}O$ (‰)	$\Delta_{47,Ghosh}$ (‰)	$\Delta_{47,Abs}$ (‰)	n
0	-	-30.81 ± .30	10.01 ± .03	0.549 ± .005	0.610 ± .005	3
						3
168	209	-31.76 ± .004	9.98 ± .006	0.566 ± .012	0.628 ± .013	1
144	323	-31.08 ± .004	10.00 ± .005	0.560 ± .027	0.622 ± .029	1
1	430	-29.17 ± 0.12	10.05 ± .07	0.515 ± .016	0.574 ± .017	2
24	430	-29.78 ± .04	9.99 ± .04	0.436 ± .005	0.490 ± .005	3
72	430	-29.61 ± .12	10.047 ± .002	0.413 ± .009	0.466 ± .010	3
168	430	-31.59 ± .24	9.96 ± .03	0.375 ± .021	0.425 ± .022	3
336	430	-30.71 ± .07	10.06 ± .06	0.333 ± .024	0.381 ± .025	3
504	430	-29.85 ± .09	10.02 ± .003	0.306 ± .038	0.352 ± .04	3
0.167	536	-32.00 ± .01	10.05 ± .01	0.406 ± .006	0.458 ± .006	2
0.5	536	-31.31 ± .03	10.02 ± .07	0.351 ± .017	0.400 ± .018	4
1	536	-31.30 ± .09	10.10 ± .01	0.338 ± .016	0.386 ± .017	3
1	536	-31.75 ± .2	10.06 ± .04	0.324 ± .012	0.371 ± .013	6
6	536	-31.19 ± .08	10.04 ± .05	0.267 ± .008	0.311 ± .008	4
12	536	-31.18 ± .17	10.08 ± .03	0.269 ± .033	0.313 ± .035	4
24	536	-31.20 ± .13	10.06 ± .01	0.287 ± .014	0.332 ± .015	4
0.05	692	-30.95 ± .02	10.09 ± 0	0.277 ± .005	0.312 ± .005	2
0.133	692	-30.87 ± .16	10.10 ± 0	0.271 ± .004	0.315 ± .004	2
0.25	692	-28.93 ± .04	10.08 ± .38	0.248 ± .050	0.290 ± .053	2
0.75	692	-30.06 ± .31	10.06 ± .04	0.239 ± .037	0.281 ± .039	3
6	692	-30.09 ± .05	10.10 ± .10	0.247 ± .007	0.289 ± .007	2
12	692	-29.10 ± .02	10.138 ± .001	0.235 ± .016	0.277 ± .017	2
12	692	-31.20 ± .15	9.99 ± .05	0.259 ± .025	0.302 ± .027	5
24	692	-29.61 ± .06	10.16 ± .11	0.234 ± .009	0.276 ± 0.010	2

Table 5: Bulk and clumped isotope data and temperatures from heating experiments on apatites from Siilinjarvi. All errors are 2 standard errors. $\delta^{13}C$ values are standardized to VPDB, $\delta^{18}O$ to VSMOW, and Δ_{47} to the 'Ghosh' reference frame or 'absolute' (Abs) reference frame (Dennis et al., 2011; Ghosh et al., 2006).

Time (hr)	T (°C)	$\delta^{13}C$ (‰)	$\delta^{18}O$ (‰)	$\Delta_{47,Ghosh}$ (‰)	$\Delta_{47,Abs}$ (‰)	n
0	-	-3.63 ± .03	11.185 ± .96	0.493 ± .025	0.493 ± .027	2
1	430	-3.59 ± .005	10.68 ±.01	0.483 ± .016	0.483 ± .017	1
8	430	-3.62 ±.007	10.17 ± .02	0.440 ± .032	0.440 ± .034	1
12	430	-3.69 ± .004	11.15 ±.01	0.495 ± .057	0.495 ± .061	1
24	430	-3.64 ± .005	10.70 ± .01	0.482 ± .036	0.482 ± .038	1
1	536	-3.67 ± .006	10.58 ± .01	0.426 ± .029	0.426 ± .031	1
5.5	536	-3.68 ± .006	10.69 ± .01	0.344 ± .021	0.344 ± .022	1
12	536	-3.72 ± .006	10.13 ± .01	0.317 ± .030	0.317 ± .032	1
24	536	-3.65 ± .005	10.66 ± .01	0.271 ± .025	0.271 ± .027	1
0.0833	692	-3.599 ± .005	10.575 ± .01	0.282 ± .021	0.282 ± .022	1
0.25	692	-3.758 ± .005	10.763 ± .01	0.260 ± .031	0.260 ± .033	1
0.75	692	-3.743 ± .005	10.688 ± .01	0.253 ± .023	0.253 ± .024	1
6	692	-3.949 ± .006	10.456 ± .01	0.266 ± .020	0.266 ± .021	1
12	692	-4.003 ± .01	10.140 ± .01	0.229 ± .020	0.229 ± .021	1

Table 6: Rate constants derived from modeling of calcite heating experiments. Errors represent 95% confidence intervals.

Temperature (°C)	k_f ($hour^{-1}$)	$k_{dif\text{-}single}$ ($hour^{-1}$)
430	0.333 ± 0.080	0.0246 ± 0.0016
536	13.1 ± 2.0	9.88 ± 5.29
692	972 ± 72	461 ± 61

Table 7: Rates derived from modeling of apatite heating experiments. Errors represent 95% confidence intervals.

Temperature (°C)	k_f ($hour^{-1}$)	$k_{dif\text{-}single}$($hour^{-1}$)
536	1.53 ± 1.62	0.843 ± 0.306
692	169 ± 40	149 ± 19

Table 8: Comparison of experimental equilibrium Δ_{47} (‰) values measured by Passey and Henkes (2012) versus those predicted by our temperature calibration (fig. 2). The average deviation is +0.011 ‰, which use to correct all other data. Additionally all samples are in the 'Ghosh' reference frame. The error given is one standard error of the mean deviation.

T (°C)	Passey and Henkes (2012) Δ_{47} (‰)	predicted Δ_{47} (‰)	difference (‰)
800	0.259	0.242	0.017
700	0.253	0.247	0.006
650	0.256	0.250	0.005
600	0.266	0.254	0.011
560	0.273	0.258	0.015
		average difference	0.011
		1 standard error	0.0025

Table 9: Rates derived from modeling of calcite heating experiments using data from Passey and Henkes (2012). Errors represent 95% confidence intervals.

Temperature (°C)	k_f ($hour^{-1}$)	$k_{dif\text{-}single}$ ($hour^{-1}$)
405	0.294 ± 0.126	0.0211 ± 0.0191
425	1.07 ± 0.26	0.0766 ± 0.0193
450	1.78 ± .91	0.728 ± 0.350
475	2.10 ± 0.16	1.10 ± 0.13

9. References

Anderson, T.F., 1969. Self-diffusion of carbon and oxygen in calcite by isotope exchange with carbon dioxide. *Journal of Geophysical Research* 74, 3918-3932.

Balestrieri, M., Bernet, M., Brandon, M.T., Picotti, V., Reiners, P., Zattin, M., 2003. Pliocene and Pleistocene exhumation and uplift of two key areas of the Northern Apennines. *Quaternary International* 101, 67-73.

Blank, J., Stolper, E., Carroll, M., 1993. Solubilities of carbon dioxide and water in rhyolitic melt at 850 C and 750 bars. *Earth and Planetary Science Letters* 119, 27-36.

Bonifacie, M., Calmels, D., Eiler, J., 2013. Clumped isotope thermometry of marbles as an indicator of the closure temperatures of calcite and dolomite with respect to solid-state reordering of C–O bonds. *Mineralogical Magazine* 77, 735.

Bonifacie, M., Ferry, J.M., Horita, J., Vasconcelos, C., Passey, B., Eiler, J.M., 2011. Calibration and applications of the dolomite clumped isotope thermometer to high temperatures. *Mineralogical Magazine* 75, 551.

Came, R.E., Eiler, J.M., Veizer, J., Azmy, K., Brand, U., Weidman, C.R., 2007. Coupling of surface temperatures and atmospheric CO_2 concentrations during the Palaeozoic era. *Nature* 449, 198-201.

Cherniak, D., Lanford, W., Ryerson, F., 1991. Lead diffusion in apatite and zircon using ion implantation and Rutherford backscattering techniques. *Geochimica Et Cosmochimica Acta* 55, 1663-1673.

Cherniak, D.J., Hervig, R., Koepke, J., Zhang, Y., Zhao, D., 2010. *Analytical methods in diffusion studies*, in: Zhang, Y., Cherniak, D.J. (Eds.), Diffusion in Minerals and Melts. Mineralogical Society of America, Chantilly, Virginia, pp. 107-170.

Conway, C.M., Taylor Jr, H.P., 1969. O^{18}/O^{16} and C^{13}/C^{12} ratios of coexisting minerals in the Oka and Magnet Cove carbonatite bodies. *The Journal of Geology*, 618-626.

Dennis, K.J., Affek, H.P., Passey, B.H., Schrag, D.P., Eiler, J.M., 2011. Defining an absolute reference frame for 'clumped' isotope studies of CO_2. *Geochimica et Cosmochimica Acta* 75, 7117-7131.

Dennis, K.J., Schrag, D.P., 2010. Clumped isotope thermometry of carbonatites as an indicator of diagenetic alteration. *Geochimica et Cosmochimica Acta* 74, 4110-4122.

Dodson, M.H., 1973. Closure temperature in cooling geochronological and petrological systems. *Contributions to Mineralogy and Petrology* 40, 259-274.

Eagle, R.A., Schauble, E.A., Tripati, A.K., Tütken, T., Hulbert, R.C., Eiler, J.M., 2010. Body temperatures of modern and extinct vertebrates from ^{13}C-^{18}O bond abundances in bioapatite. *Proceedings of the National Academy of Sciences* 107, 10377.

Eagle, R.A., Tütken, T., Martin, T.S., Tripati, A.K., Fricke, H.C., Connely, M., Cifelli, R.L., Eiler, J.M., 2011. Dinosaur body temperatures determined from isotopic (^{13}C-^{18}O) ordering in fossil biominerals. *Science* 333, 443.

Eiler, J.M., 2007. "Clumped-isotope" geochemistry—The study of naturally-occurring, multiply-substituted isotopologues. *Earth and Planetary Science Letters* 262, 309-327.

Eiler, J.M., 2011. Paleoclimate reconstruction using carbonate clumped isotope thermometry. *Quaternary Science Reviews* 30, 3575-3588.

Epstein, S., Buchsbaum, R., Lowenstam, H.A., Urey, H.C., 1953. Revised carbonate-water isotopic temperature scale. *Geological Society of America Bulletin* 64, 1315-1325.

Farver, J.R., 1994. Oxygen self-diffusion in calcite: Dependence on temperature and water fugacity. *Earth and Planetary Science Letters* 121, 575-587.

Farver, J.R., Giletti, B.J., 1989. Oxygen and strontium diffusion kinetics in apatite and potential applications to thermal history determinations. *Geochimica Et Cosmochimica Acta* 53, 1621-1631.

Ferry, J.M., Passey, B.H., Vasconcelos, C., Eiler, J.M., 2011. Formation of dolomite at 40–80° C in the Latemar carbonate buildup, Dolomites, Italy, from clumped isotope thermometry. *Geology* 39, 571-574.

Finnegan, S., Bergmann, K., Eiler, J.M., Jones, D.S., Fike, D.A., Eisenman, I., Hughes, N.C., Tripati, A.K., Fischer, W.W., 2011. The magnitude and duration of Late Ordovician-Early Silurian glaciation. *Science* 331, 903.

Fortier, S.M., Lüttge, A., 1995. An experimental calibration of the temperature dependence of oxygen isotope fractionation between apatite and calcite at high temperatures (350-800°C). *Chemical Geology* 125, 281-290.

Ghosh, P., Adkins, J., Affek, H., Balta, B., Guo, W., Schauble, E.A., Schrag, D., Eiler, J.M., 2006. ^{13}C-^{18}O bonds in carbonate minerals: A new kind of paleothermometer. *Geochimica et Cosmochimica Acta* 70, 1439-1456.

Green, P., Duddy, I., Gleadow, A., Tingate, P., Laslett, G., 1986. Thermal annealing of fission tracks in apatite: 1. A qualitative description. *Chemical Geology: Isotope Geoscience section* 59, 237-253.

Guo, W., Mosenfelder, J.L., Goddard, W.A., Eiler, J.M., 2009. Isotopic fractionations associated with phosphoric acid digestion of carbonate minerals: Insights from first-

principles theoretical modeling and clumped isotope measurements. *Geochimica Et Cosmochimica Acta* 73, 7203-7225.

Haul, R., Stein, L., 1955. Diffusion in calcite crystals on the basis of isotopic exchange with carbon dioxide. *Trans. Faraday Soc.* 51, 1280-1290.

Haynes, E.A., Moecher, D.P., Spicuzza, M.J., 2002. Oxygen isotope composition of carbonates, silicates, and oxides in selected carbonatites: Constraints on crystallization temperatures of carbonatite magmas. *Chemical Geology* 193, 43-57.

Huntington, K., Eiler, J., Affek, H., Guo, W., Bonifacie, M., Yeung, L., Thiagarajan, N., Passey, B., Tripati, A., Daëron, M., 2009. Methods and limitations of 'clumped' CO_2 isotope (Δ_{47}) analysis by gas-source isotope ratio mass spectrometry. *Journal of Mass Spectrometry* 44, 1318-1329.

Ihinger, P.D., 1991. *An experimental study of the interaction of water with granitic melt*. California Institute of Technology.

Jaffrés, J.B.D., Shields, G.A., Wallmann, K., 2007. The oxygen isotope evolution of seawater: A critical review of a long-standing controversy and an improved geological water cycle model for the past 3.4 billion years. *Earth-Science Reviews* 83, 83-122.

Kapustin, Y.L., 1986. The origin of early calcitic carbonatites. *International Geology Review* 28, 1031-1044.

Khan, M., Raza, H.A., 1986. The role of geothermal gradients in hydrocarbon exploration in Pakistan. *Journal of Petroleum Geology* 9, 245-258.

Koch, P.L., Tuross, N., Fogel, M.L., 1997. The effects of sample treatment and diagenesis on the isotopic integrity of carbonate in biogenic hydroxylapatite. *Journal of Archaeological Science* 24, 417-430.

Kohn, M.J., Cerling, T.E., 2002. *Stable isotope compositions of biological apatite*, in: Kohn, M.J., Rakovan, J.M., Huges, J.M. (Eds.), *Phosphates—Geochemical, Geobiological, and Materials Importance*. Mineralogical Society of America, Washington, DC, pp. 455-488.

Kronenberg, A.K., Yund, R.A., Giletti, B.J., 1984. Carbon and oxygen diffusion in calcite: Effects of Mn content and pH_2O. *Physics and Chemistry of Minerals* 11, 101-112.

Labotka, T., Cole, D., Riciputi, L., 2000. Diffusion of C and O in calcite at 100 MPa. *American Mineralogist* 85, 488-494.

Labotka, T.C., Cole, D.R., Riciputi, L.R., Fayek, M., 2004. Diffusion of C and O in calcite from 0.1 to 200 MPa. *American Mineralogist* 89, 799-806.

Longinelli, A., Wierzbowski, H., Di Matteo, A., 2003. $\delta^{18}O(PO_4^{3-})$ and $\delta^{18}O(CO_3^{2-})$ from belemnite guards from Eastern Europe: Implications for palaeoceanographic reconstructions and for the preservation of pristine isotopic values. *Earth and Planetary Science Letters* 209, 337-350.

McClellan, G.H., 1980. Mineralogy of carbonate fluorapatites. *Journal of the Geological Society* 137, 675-681.

McCrea, J.M., 1950. On the isotopic chemistry of carbonates and a paleotemperature Scale. *Journal of Chemical Physics* 18, 849-857.

Mitchell, R.H., 2005. Carbonatites and carbonatites and carbonatites. *The Canadian Mineralogist* 43, 2049-2068.

Nadeau, S.L., Epstein, S., Stolper, E., 1999. Hydrogen and carbon abundances and isotopic ratios in apatite from alkaline intrusive complexes, with a focus on carbonatites. *Geochimica Et Cosmochimica Acta* 63, 1837-1851.

Passey, B., Henkes, G., 2012. Carbonate clumped isotope bond reordering and geospeedometry. *Earth and Planetary Science Letters* 351-352, 223-236.

Passey, B.H., Levin, N.E., Cerling, T.E., Brown, F.H., Eiler, J.M., 2010. High-temperature environments of human evolution in East Africa based on bond ordering in paleosol carbonates. *Proceedings of the National Academy of Sciences* 107, 11245.

Quade, J., Eiler, J., Daeron, M., Achyuthan, H., 2012. The clumped isotope geothermometer in soil and paleosol carbonate. *Geochimica et Cosmochimica Acta*.

Schauble, E.A., Ghosh, P., Eiler, J.M., 2006. Preferential formation of ^{13}C-^{18}O bonds in carbonate minerals, estimated using first-principles lattice dynamics. *Geochimica et Cosmochimica Acta* 70, 2510-2529.

Shemesh, A., Kolodny, Y., Luz, B., 1988. Isotope geochemistry of oxygen and carbon in phosphate and carbonate of phosphorite francolite. *Geochimica et Cosmochimica Acta* 52, 2565-2572.

Silverman, S.R., Fuyat, R.K., Weiser, J.D., 1952. Quantitative determination of calcite associated with carbonate-bearing apatites. *American Mineralogist* 37, 211-222.

Taylor, H.P., Frechen, J., Degens, E.T., 1967. Oxygen and carbon isotope studies of carbonatites from the Laacher See district, West Germany and the Alnö district, Sweden. *Geochimica Et Cosmochimica Acta* 31, 407-430.

Tichomirowa, M., Grosche, G., Götze, J., Belyatsky, B., Savva, E., Keller, J., Todt, W., 2006. The mineral isotope composition of two Precambrian carbonatite complexes from the Kola Alkaline Province — Alteration versus primary magmatic signatures. *Lithos* 91, 229-249.

Urey, H.C., 1947. The thermodynamic properties of isotopic substances. *Journal of the Chemical Society*, 562-581.

Wang, Z., Schauble, E.A., Eiler, J.M., 2004. Equilibrium thermodynamics of multiply substituted isotopologues of molecular gases. *Geochimica et Cosmochimica Acta* 68, 4779-4797.

Wyllie, P., Tuttle, O., 1960. The system CaO-CO_2-H_2O and the origin of carbonatites. *Journal of Petrology* 1, 1-46.

Zachos, J., Pagani, M., Sloan, L., Thomas, E., Billups, K., 2001. Trends, rhythms, and aberrations in global climate 65 Ma to present. *Science* 292, 686-693.

Zazzo, A., Lécuyer, C., Mariotti, A., 2004. Experimentally-controlled carbon and oxygen isotope exchange between bioapatites and water under inorganic and microbially-mediated conditions. *Geochimica et Cosmochimica Acta* 68, 1-12.

Zhabin, A., 1971. Primary textural-structural features of carbonatites and their metamorphic evolution. *International Geology Review* 13, 1087-1096.

Zhang, Y., 2008. *Geochemical Kinetics*. Princeton University Press.

Zhang, Y., Stolper, E.M., Ihinger, P., 1995. Kinetics of the reaction H20+ 0= 20H in rhyolitic and albitic glasses: Preliminary results. *American Mineralogist* 80, 593-612.

Chapter IV

Constraints on the formation and diagenesis of phosphorites through time using clumped isotopes

DA Stolper[a], Y Kolodny[b], and JM Eiler[a]

[a]*Division of Geological and Planetary Sciences, California Institute of Technology, Pasadena, CA 91107, USA*
[b]*Department of Geology, Institute of Earth Sciences, The Hebrew University of Jerusalem, Jerusalem, Israel*

Abstract: The isotopic composition of apatites from sedimentary phosphorite deposits has been used previously to reconstruct ancient conditions of the surface of the earth. However, whether or not these minerals retain their original isotopic composition or are modified during burial and lithification is not fully know. To better understand how apatites in phosphorites form and are diagenetically modified, we present new isotopic measurements of $\delta^{18}O$ values and clumped isotope (Δ_{47}) temperatures of carbonate groups in apatites from phosphorites from the past 265 million years. We compare these measurements to previously measured $\delta^{18}O$ values of phosphate groups from the same apatites. These results indicate that the isotopic composition of many of the apatites do not reflect reasonable near-surface formation temperatures but instead diagenetic conditions. To better understand these isotopic measurements, we construct a simple kinetic model to quantify the amount of diagenesis each sample has experienced. This model captures the basic features of the dataset and indicates that clumped isotope temperatures provide additional, quantitative constraints on both the formational environment of the apatites and subsequent diagenetic modification.

1. Introduction

Paleoclimate and paleotemperature reconstructions are critical goals of earth science. Although many tools exist for these reconstructions, the original and still most prevalent technique is based on oxygen isotope analyses of carbonate-bearing minerals such as calcite and aragonite. Oxygen isotope abundances in a mineral (or any phase or species) are quantified using δ (Footnote 1) notation (Epstein et al., 1953; McCrea, 1950). $\delta^{18}O$ values of carbonate minerals yield meaningful formation temperatures only if three conditions are met: (i) The mineral must form in isotopic equilibrium with (ii) co-genetic waters (or another phase) of known isotopic composition and (iii) retain that isotopic signature up until measured in the laboratory. The formation of carbonate minerals in isotopic equilibrium is a complex issue (DePaolo, 2011) and can depend on the pH of the solution (Zeebe, 1999), the precipitation rate of the mineral (Dietzel et al., 2009), and can also depend, if the mineral is biological in origin, on the specific organism precipitating the carbonate. Additionally, knowledge of the isotopic composition of water as well as the isotopic integrity of carbonate-bearing minerals over geological time is an old, persistent, controversial, and unresolved issue in earth science (Came et al., 2007; Degens and Epstein, 1962; Finnegan et al., 2011; Jaffrés et al., 2007; Kasting et al., 2006; Killingley, 1983; Land, 1995; Lécuyer and Allemand, 1999; Muehlenbachs, 1986; Schrag et al., 1992, 1995; Trotter et al., 2008; Veizer et al., 1999; Veizer et al., 1997; Veizer et al., 1986).

---

[1] $\delta=(R_{sample}/R_{standard}-1)*1000$ where $R=[^{13}C]/[^{12}C]$ for carbon isotopes and $[^{18}O]/[^{16}O]$ or $[^{17}O]/[^{16}O]$ for oxygen isotopes. For carbon isotopes samples are referenced to VPDB. For oxgyen isotopes samples are referenced to VSMOW. We assume that ^{17}R and ^{18}R are related following a mass law of 0.5164 (Affek and Eiler, 2006).

In response to these potential issues with carbonate minerals, Urey et al. (1951) suggested that the oxygen isotope composition of sedimentary apatite minerals could be measured to complement and test calcite and aragonite based temperature reconstructions. Today these measurements are made on PO_4^{3-} groups chemically liberated from apatite. In fact, apatites are sometimes preferred over carbonate minerals because PO_4^{3-} groups have been argued to be more resistant to post-depositional isotopic exchange than CO_3^{2-} groups in calcite and aragonite (Kolodny et al., 1983; Longinelli et al., 2003; Shemesh et al., 1983). Kolodny et al. (1983) hypothesized that PO_4^{3-} groups are essentially isotopically inert post mineral formation in unmetamorphosed systems. Additionally, apatites, unlike calcite and aragonite, contain both structural PO_4^{3-} and CO_3^{2-} groups, both of which can be measured separately for $\delta^{18}O$ values (Kolodny and Kaplan, 1970), which are denoted as $\delta^{18}O_{PO4}$ and $\delta^{18}O_{CO3}$ respectively. When combined, these measurements allow for the calculation of formation temperatures independent of the isotopic composition of the formation water (Shemesh et al., 1983), thus overcoming a significant hurdle in the interpretation of $\delta^{18}O$ values of minerals in the past.

Apatites from brachiopod shells (e.g., Lécuyer et al., 1998; Lécuyer et al., 1996; Wenzel et al., 2000), conodonts (e.g., Luz et al., 1984b; Sun et al., 2012; Trotter et al., 2008; Wenzel et al., 2000), teeth and bones (e.g., Ayliffe et al., 1994; Eagle et al., 2011; Kohn and Cerling, 2002; Kolodny and Luz, 1991; Kolodny et al., 1983; Longinelli, 1984; Luz et al., 1984a; Sharp et al., 2000), and authigenic phosphorite deposits (Ayliffe et al., 1992; Hiatt and Budd, 2001; Longinelli and Nuti, 1968; Shemesh et al., 1983; Shemesh et al., 1988) have all been used for paleotemperature reconstructions and thus apatites represent a key mineral for paleothermometry. However, it is now recognized that apatite

PO_4^{3-} oxygen is not impervious to exchange as previously assumed (Ayliffe et al., 1994; Kolodny et al., 1996; McArthur and Herczeg, 1990; Sharp et al., 2000; Shemesh et al., 1988; Wenzel et al., 2000; Zazzo et al., 2004), and that, for example, microbially mediated reactions can accelerate phosphate oxygen isotope exchange (Blake et al., 1997; Zazzo et al., 2004). Thus a critical question for all studies of apatites that use oxygen isotopes as a constraint is whether the measured $\delta^{18}O$ values reflects formation temperatures or some other aspect of the sample's geological and diagenetic history.

In order to contribute to our understanding of how and under what conditions sedimentary apatites form and are modified during burial and lithification, we have made 'clumped isotope' measurements of carbonate groups in phosphorite apatites from the past 265 million years with known $\delta^{18}O_{PO4}$ values (Shemesh et al., 1988). Clumped isotopes quantify the portion of the multiply substituted carbonate groups in a mineral that generates mass-47 CO_2 molecules ($^{13}C^{16}O^{18}O$, $^{12}C^{17}O^{18}O$, $^{13}C^{17}O_2$) after digestion with phosphoric acid (Ghosh et al., 2006). At equilibrium, these clumped isotopologues are enriched compared to a random distribution of isotopes, with the size of the enrichment a function of temperature (Eiler, 2007; Eiler, 2011; Eiler, 2013; Schauble et al., 2006; Wang et al., 2004). At lower temperatures, there is a larger enrichment of clumped isotopologues as compared to higher temperatures. Clumped isotope abundances are quantified with the symbol Δ_{47} (footnote 2), which has a known relationship to mineral formation temperature (Ghosh et al., 2006; Zaarur et al., 2013). Importantly, Δ_{47} values only yield mineral formation temperatures when the carbonate groups are precipitated in equilibrium.

[2] $\Delta_{47}=([^{47}R][^{47}R^*]-1) \times 1000$ where $^{47}R=[^{13}C^{16}O^{18}O+^{12}C^{17}O^{18}O+^{13}C^{17}O_2]/[^{12}C^{16}O_2]$ and * denotes the random distribution.

Our motivations for this study are: (i) Initial studies of $\delta^{18}O_{PO4}$ values in phosphorite apatites indicated that they are robust markers of past earth conditions and highly resistant to isotopic modification post formation (Shemesh et al., 1983). However, (ii) additional studies of phosphorite apatites with combined measurements of $\delta^{18}O_{PO4}$ and $\delta^{18}O_{CO3}$ values indicated that oxygen isotopes in both the CO_3^{2-} and PO_4^{3-} groups could be diagenetically altered in ancient samples (McArthur and Herczeg, 1990; Shemesh et al., 1988). (iii) A striking feature of these results is that a strong correlation between $\delta^{18}O_{PO4}$ and $\delta^{18}O_{CO3}$ exists across all samples ranging in age from modern to 1.1 billion years ago and within the same formation (Kastner et al., 1990; Shemesh et al., 1988). However the slope of this correlation, $\delta^{18}O_{PO4}$~0.6 $\delta^{18}O_{CO3}$ (Shemesh et al., 1988), is flatter than expected for precipitation of minerals in isotopic equilibrium with formation waters. This relationship has been suggested to represent either imperfect knowledge of oxygen isotope fractionation factors for apatite paleothermometry, sedimentary diagenesis, or disequilibrium precipitation (Kastner et al., 1990; Kolodny and Luz, 1991; Lecuyer et al., 1999; Shemesh et al., 1988). Regardless, this relationship indicates the presence of an unknown, but uniform set of processes in phosphorite apatite formation and modification throughout earth history. (iv) Clumped isotope based temperatures are independent of a mineral's oxygen isotope composition or the fluids in which it equilibrated. Consequently, clumped isotope measurements can provide an additional constraint in unraveling a sample's formational conditions and geological history.

2. Methods

Phosphorite samples measured in this study are listed in Table 1 and are the same as those used in Shemesh et al. (1983) and Shemesh et al. (1988), except for NBS 120C. All $\delta^{18}O_{PO4}$ values are from Shemesh et al. (1988) and were measured on $BiPO_4$ except NBS 120C, which was analyzed as Ag_3PO_4 (Lécuyer et al., 2013; Pucéat et al., 2010). Measurements of samples analyzed as Ag_3PO_4 are offset in $\delta^{18}O$ from those analyzed as $BiPO_4$ and thus not directly comparable (Pucéat et al., 2010). We converted NBS 120C to the $BiPO_4$ reference frame by assuming a $\delta^{18}O$ value of 20‰ for NBS 120B when measured using the $BiPO_4$ method (Lécuyer et al., 2013; Pucéat et al., 2010) and an offset of 0.3‰ between NBS 120B and 120C (calibrated using a Ag_3PO_4 method) resulting in a $\delta^{18}O$ value of 20.3‰ for NBS 120C in the $BiPO_4$ reference frame.

All samples measured were crushed prior to delivery to the Caltech laboratories where this study was conducted. We first treated each sample with 3% H_2O_2 at room temperature for 4 hours to remove any organic contaminants and then washed each sample three times in deionized (DI) water. Samples were subsequently treated with acetic acid (0.1 M, pH = 4.5) for 48 hours to remove residual carbonate, washed three times in deionized water, then dried overnight in a 70°C oven. This procedure follows those described in Eagle et al. (2010).

Measurements of $\delta^{13}C$ and $\delta^{18}O$ (Table 1) and Δ_{47} (Table 2) values of apatite carbonate groups were made on two separate mass spectrometers at Caltech designed to measure masses 44-49 (Eiler and Schauble, 2004). Samples were digested in a 90 °C stirred acid bath with 104% phosphoric acid on one of two nearly identical automated extraction lines as described in Passey et al. (2010) and Eagle et al. (2010). Δ_{47} values are

reported in both the 'Ghosh' reference frame and 'absolute' reference frame (Dennis et al., 2011) generated using gases isotopically equilibrated with water at 25°C and/or gases heated in quartz glass tubes at 1000 °C (except for NBS 120C which was only measured in the Ghosh reference frame; see below). An acid digestion fractionation factor of 0.081 ‰ was used to convert Ghosh reference frame measurements to the 25°C acid digestion reference frame currently in use (Passey et al., 2010) and an acid digestion fractionation factor 0.092 ‰ for the absolute reference frame conversion (Henkes et al., 2013). Temperatures are calculated in the Ghosh reference frame using the equation of Ghosh et al. (2006) and in the absolute reference frame using Equation 7 given in Zaarur et al. (2013).

Sample precision and accuracy were checked by running two standards, a Carrara marble in-house standard and travertine in-house standard (TV01), in every analytical session. Average Δ_{47}, $\delta^{18}O$ and $\delta^{13}C$ values and precisions for these standards are given in Table 1. Isotope values for standards were found to be both accurate and precise (Table 3).

All phosphorite samples were run at least four times across at least three analytical sessions except for NBS 120C, which was run in a single session. Phosphorite samples were screened for isobaric interferences near mass 47 by measuring Δ_{48} values where $\Delta_{48} = ({}^{48}R/{}^{48}R^{*}-1) \times 1000$ as defined and described in Huntington et al. (2009). All Δ_{48} values are less than 0.6‰ (Table 2). For comparison, the Carrara marble standard has an average Δ_{48} value of 0.4‰ and the TV01 standard has an average Δ_{48} value of 0.6‰. Phosphorite samples have similar, but slightly elevated (i.e., worse) external precisions as compared to the carbonate standards (Tables 3 and 4). The increase in external precision

could be due to heterogeneities in the sample, a result of a poorer performance of the acid digestion reaction for large phosphate samples, or perhaps the greater potential for contamination in these large samples.

All NBS 120C samples were run in the same analytical session before our lab began running 25°C equilibrated gases in order to report samples in the absolute reference frame. We calculated the absolute reference frame values for these samples following the procedures for a 'secondary' absolute reference frame, as described in Dennis et al. (2011). Specifically, we generated a relationship between the two reference frames through a comparison of standards and gases with known absolute and Ghosh reference frame Δ_{47} values. Additionally, samples ASP 3 and ASP 4 each yielded one measurement that was statistically distinct from all other measurements. These single measurements are not included in the final average.

For all calculations and figures, we used temperatures derived from the Ghosh reference frame as opposed to the absolute reference frame. This was done because the reported absolute reference frame Δ_{47} value depends on a choice for the acid digestion fractionation factor to convert 90°C-derived data to the 25°C reference frame. The accepted value for this correction is currently unresolved (Wacker et al., 2013) — we note, though, that our calculated absolute and Ghosh reference frame temperatures differ, on average, by 2.5 °C, with the absolute reference frame temperature always being lower. Because the errors in the reported temperatures are in all cases larger than the differences between the two reference frames (at 2 standard errors; s.e.), and are small in comparison to the temperature variations we interpret here, the choice in reference frame is not significant for this study.

Cleaning experiments were performed to ensure calcite could be quantitatively removed without modifying a sample's $\delta^{18}O_{CO3}$, $\delta^{13}C_{CO3}$ (the $\delta^{13}C$ value of the CO_3^{2-} group substituted in apatite), and Δ_{47} values. A phosphorite standard from Florida, obtained from the Caltech mineralogical collection, was used for these experiments. This standard was reacted with either deionized water, acetic acid (0.1 M, pH = 4.5), or triammonium citrate (TCA; 0.5 M, pH = 0.5). Additionally, for some experiments, a spike of Carrara marble was added to the phosphate standard such that the spike was 5% by weight of the sample. These spiked samples were additionally reacted in acetic acid and TCA for 4 hours, 24 hours, or 48 hours respectively. These samples were not pretreated with H_2O_2 first.

Finally two samples (ASP 6 and ASP 12) investigated gave high CO_2 yields compared to other samples despite acid washing. Though there is nothing specifically wrong with these samples (they follow the same trends as other samples) they are not included in our discussion because it seems possible to us that they were contaminated by a carbonate-bearing phase that was not removed with the acetic acid (e.g., dolomite).

3. Acid washing experiments

A challenge of making clumped isotope measurements on carbonate groups in apatite is the amount of sample needed for each analysis: ~100 mg of apatite compared to 8 mg for calcite. Thus, a critical concern for all measurements is contamination of samples by small amounts (e.g., weight percent) of exogenous carbonate minerals such as calcite. To deal with this, previous studies have used weak acids such as acetic acid or triammonium citrate (TCA) to dissolve calcite and aragonite, but leave apatite undisturbed isotopically

(Eagle et al., 2010; Koch et al., 1997; Kolodny and Kaplan, 1970; Shemesh et al., 1988; Silverman et al., 1952). Although these acids have been used to clean samples for $\delta^{18}O$ and $\delta^{13}C$ measurements of apatites, their effects on Δ_{47} values are not fully constrained — Stolper and Eiler (Accepted, Chapter 3) and Eagle et al. (2010) showed that acetic acid does not appear to change Δ_{47} values of carbonate groups in igneous apatites or fossil material. However, how acid washes affect Δ_{47} values when contaminants are actually present before washing is not known; i.e., the samples used in the experiments of Stolper and Eiler (Accepted, Chapter 3) and Eagle et al. (2010) were not actually known to contain contaminants. To conclusively test this, we measured the effect of acid washes using TCA and acetic acid vs. deionized water for a phosphorite sample from the Caltech mineralogical collection with and without additions (i.e., spikes) of calcite (see methods above).

We present the results of these acid-washing experiments in Figure 1 and Table 5. First we discuss the results in samples that were not spiked with calcite. Interestingly and unexpectedly, washing samples in deionized water has an effect within 4 hours on both the measured $\delta^{18}O$ and Δ_{47} values. Within 4 hours of washing in deionized water, samples plateau to constant (within error) $\delta^{18}O$, $\delta^{13}C$, and Δ_{47} values (Figure 1). We do not know what contaminant is being removed in the water, but we hypothesize it causes an interference at mass 46, raising the sample's $\delta^{18}O$ value and thus lowering the Δ_{47} value. Water washing vs. acid washing in TCA or acetic acid appears to yield indistinguishable isotopic values (within analytical error) after 4 hours of treatment indicating that once this contaminant is solubilized, acid washing is not different from soaking samples in water.

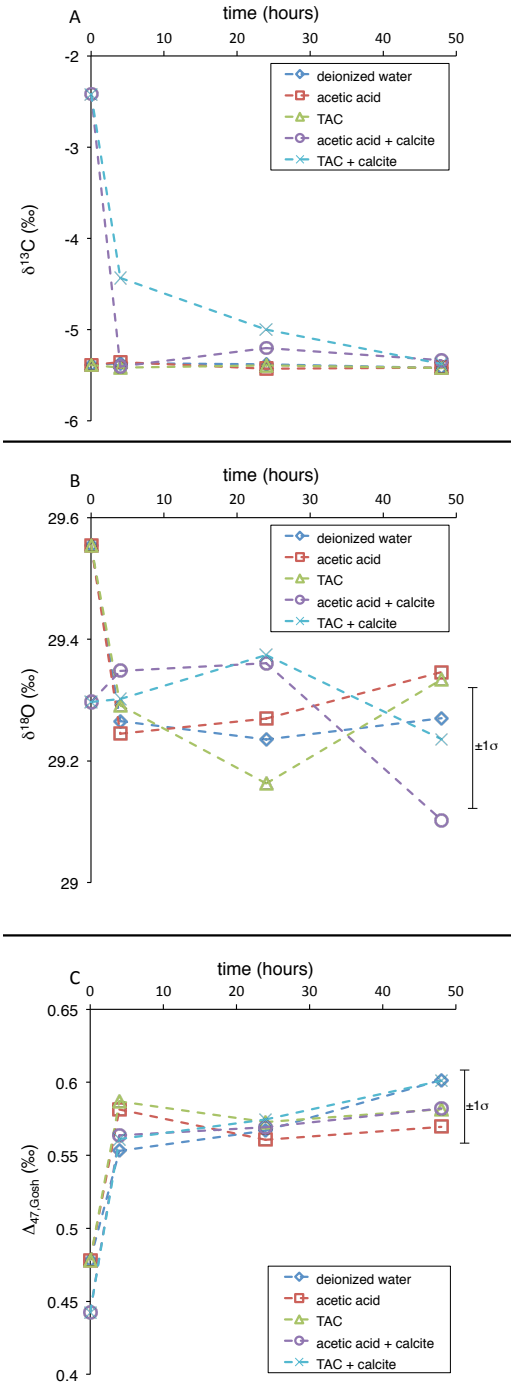

Figure 1. Apatite acid cleaning experiments. A) Effect of different acid washes on $\delta^{13}C$ values of CO_3^{2-} groups liberated from a phosphorite standard. All samples converge to the same value, within error, by 48 hours. Error bars of the measurement are smaller than the symbols. B) Effect of different acid washes on $\delta^{18}O$ values of CO_3^{2-} groups liberated from a phosphorite standard. All samples converge to the same value, within error, by 48 hours. Given error bars are ±1 standard error. C) Effect of different acid washes on Δ_{47} values of CO_3^{2-} groups liberated from a phosphorite standard. All samples converge to the same value, within error, by 48 hours. Given error bars are ±1 standard error. '+ calcite' denotes addition of a Carrara marble spike to the experiment such that the spike was 5% by weight of the sample.

Next we discuss the results of samples spiked with Carrara marble calcite. Addition of Carrara marble to the samples without subsequent acid washing causes a change in $\delta^{13}C$ and Δ_{47} values as would be expected, but the effect of adding marble 'contaminant' produces no obvious change in the $\delta^{18}O$ value of the unwashed mixture. This is simply because the $\delta^{18}O$ value of the calcite we added is closely similar to the value we would measure in unwashed phosphorite alone (i.e., the true value of the carbonate ion groups in the phosphorite, plus the small effect of the contaminant that is removed by washing). Regardless, based on the measurements of $\delta^{13}C$ and Δ_{47} (where the contrast between spike and phosphorite are obvious), acetic acid removes the calcite spike within 4 hours, while TCA removes it within 48 hours (Figure 1). Based on these experiments, we chose to use a 48-hour acetic acid wash for all samples. Additionally, this experiment shows the importance of rinsing all apatite samples with deionized water before making isotopic measurements.

4. Phosphorite data

4.1 Comparison of measurements to those in Shemesh et al. (1988) and first order observations

Data for all phosphorite samples are given in Tables 1 and 2, including Δ_{47}, $\delta^{13}C_{CO3}$, and $\delta^{18}O_{CO3}$ values measured in this study, and $\delta^{18}O_{PO4}$ values previously measured and given in Shemesh et al. (1988). Shemesh et al. (1988) also provides $\delta^{13}C_{CO3}$ and $\delta^{18}O_{CO3}$ values for the samples measured here. We compared our measurements of $\delta^{13}C_{CO3}$ and $\delta^{18}O_{CO3}$ values to those given in their study (Figure 2). Measurements of both $\delta^{13}C_{CO3}$ and $\delta^{18}O_{CO3}$ define trends that are statistically

indistinguishable from 1:1 lines passing through the origins of the respective plots: The best-fit linear regression slope and intercept for the $\delta^{13}C_{CO3}$ comparison are 1.05 ± 0.06 (1 standard deviation, σ) and 0.0 ± 0.4 (1σ) respectively. For the $\delta^{18}O_{CO3}$ comparison, the best-fit linear regression slope and intercept are 0.94 ± 0.08 (1σ) and 0.8 ± 2.0 (1σ). Consequently, we conclude that the datasets and measurements from the two labs are directly comparable and thus, specifically, that our $\delta^{18}O_{CO3}$ values can be directly compared to the $\delta^{18}O_{PO4}$ values measured in Shemesh et al. (1988) (i.e., if these data reflect some analytical artifact, it is the same in both studies). We note, though, that there is scatter beyond the stated error for each point around the 1:1 line for both measurements (Figure 1). This scatter may be due to different methodologies used — Shemesh et al. (1988) digested apatites to release CO_2 at 25°C in McCrea style reactors (McCrea, 1950) while we used a common acid bath held at 90°C. If there are differences in the way some samples react at these two temperatures this could introduce the observed scatter. Additionally, the samples may simply be heterogeneous in isotopic composition, causing different aliquots to have subtly different isotopic values.

$\delta^{13}C$ values of carbonate groups in the measured apatites tend to be isotopically depleted (i.e., negative) compared to marine carbonates, ranging in value from -0.5 to -9.5‰. These ranges are similar to those observed in apatite-bound carbonate groups in other phosphorites (Baioumy et al., 2007; Birch et al., 1983; Jarvis, 1992; Kastner et al., 1990; McArthur et al., 1986; McArthur et al., 1980; Sadaqah et al., 2007; Shemesh et al., 1983; Shemesh et al., 1988). The generation of low $\delta^{13}C$ in the carbonate groups of phosphates is generally explained through the incorporation of dissolved carbonate ions from shallow sedimentary pore waters, which have been enriched in low-$\delta^{13}C$ carbonate

through respiration of buried organic matter (e.g., McArthur et al., 1986), which is isotopically light (generally <-10‰ in $\delta^{13}C$).

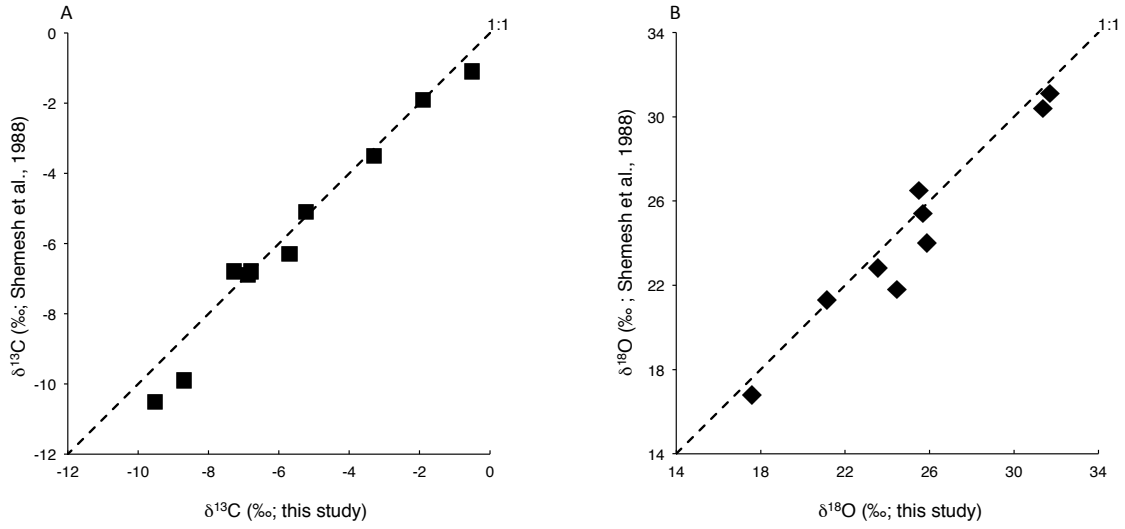

Figure 2. Comparison of bulk isotopic measurements of CO_3^{2-} groups in examined phosphorite samples measured in this study to those measured by Shemesh et al. (1988). Plotted lines are 1:1 lines that pass through the origin. A) Comparison of $\delta^{13}C_{CO3}$ measurements. B) Comparison of $\delta^{18}O_{CO3}$ measurements. Error bars are smaller than the symbols.

$\delta^{18}O_{PO4}$ values for our sample suite (taken from Shemesh et al., 1988) range from 15.8 to 23.4‰. For comparison, in modern (i.e., ~<100,000 year old) phosphorites, $\delta^{18}O_{PO4}$ values range from 21.7 to 24.8‰ (Shemesh et al., 1983; Shemesh et al., 1988). The $\delta^{18}O_{CO3}$ values we measured for these samples range from 17.6 to 35‰ while modern phosphorites tend to range from 30.5 to 33.6 ‰. Thus many of the samples exhibit oxygen isotope values outside of the range observed in recent phosphorites, with most samples examined more isotopically depleted than generally encountered today.

4.2 Results and initial discussion of isotope measurements in the context of thermodynamic equilibrium

We note two important correlations in the data: (1) $\delta^{18}O_{CO3}$ and $\delta^{18}O_{PO4}$ values are linearly correlated with the slope of best-fit line equal to 0.46 ± 0.05 (1σ) (Figure 3a).

This is similar to, but statistically distinct at the 2σ level from the previously observed slope of 0.57 (Shemesh et al., 1988). This difference is possibly related to the additional samples examined by Shemesh et al. (1988) that were not measured here, including various Cenozoic samples with elevated (>23‰) $\delta^{18}O_{PO4}$ values. And (2), 1000 x $\ln(\alpha_{CO3\text{-}PO4})$ values are linearly correlated with the measured clumped isotope temperatures, expressed as 1000/T (Figure 3b) where $\alpha_{a\text{-}b} = (1000 + \delta_A)/(1000 + \delta_B)$, with a slope of 25.0 ± 6.1 (1σ) and intercept of -74.2 ± 25.1 (1σ).

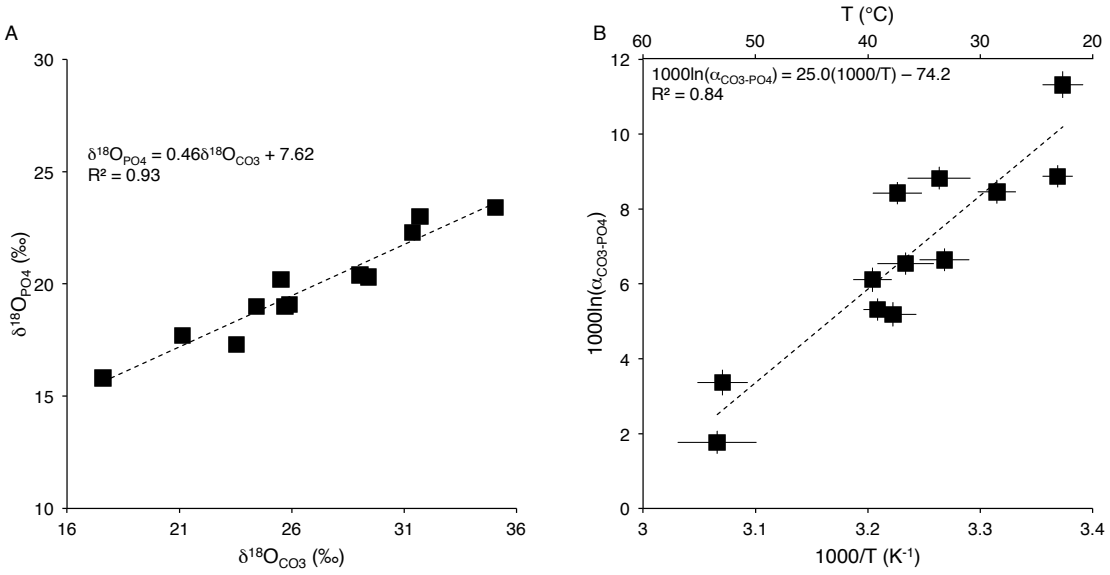

Figure 3. A) Relationship between $\delta^{18}O_{PO4}$ values given in Shemesh et al. (1988) vs. $\delta^{18}O_{CO3}$ values measured in this study. B) Relationship between 1000 x $\ln(\alpha_{CO3\text{-}PO4})$ vs. 1000/T where T, in Kelvin, is the derived clumped isotope temperature. $\alpha_{CO3\text{-}PO4}$ values are calculated as $(1000 + \delta^{18}O_{CO3})/(1000 + \delta^{18}O_{PO4})$. Error bars of data are ±1 standard error.

We first examined whether these trends are consistent with the formation of apatites in oxygen isotope equilibrium (either internally or with some other phase such as water) for both the PO_4^{3-} and CO_3^{2-} groups. We tested this using experimentally derived oxygen isotope fractionation factors (the α above) between carbonate and water and phosphate and water. Multiple phosphate-water fractionation factors have been proposed

(Karhu and Epstein, 1986; Kolodny et al., 1983; Lécuyer et al., 2013; Lécuyer et al., 1996; Pucéat et al., 2010; Shemesh et al., 1988). As all but one of the samples measured here was made using the $BiPO_4$ method (Kolodny et al., 1983), we only consider calibrations created using this method.

After examining all relevant previous calibrations, we chose two equilibrium phosphate-water oxygen isotope fractionation calibrations for this test: the low temperature calibration (<25°C) of Kolodny et al. (1983) and the high temperature (<510°C) calibration of Shemesh et al. (1988). We did not include the calibration of Longinelli and Nuti (1973) as it is identical within error to that of Kolodny et al. (1983). Additionally, we did not include the calibration of Karhu and Epstein (1986) as the high temperature datum from this study is included in the Shemesh et al. (1988) calibration. We note that some caution should be taken when using the Shemesh et al. (1988) calibration for two reasons: First, one of the 'high' temperature data points was taken from Karhu and Epstein (1986) and this sample has an estimated (350°C) as opposed to known formation temperature. Second, the other high temperature (510°C) data point used to calibrate the phosphate-water oxygen isotope fractionation factor vs. temperature from the Shemesh et al. (1988) study implies the presence of a crossover in the calibration (Stern et al., 1968). Specifically, all low temperature (e.g., from the surface of the earth) phosphates precipitated in water have $\delta^{18}O$ values more positive than the fluid. However, the highest temperature (510°C), experimentally derived phosphate has a calculated $\delta^{18}O$ value lower than a fluid in equilibrium with the mineral would have. The presence of this crossover makes use of a linear 1/T or $1/T^2$ form for the temperature dependence of the fractionation factor potentially incorrect as the line may not be linear

between the high temperature and low temperature points used for the calibration (Stern et al., 1968). Regardless, we include this calibration as it is found in the literature.

We compared these phosphate-water calibrations to two separate carbonate-water fractionation factors (four comparisons total). We used the Kim and O'Neil (1997) calibration for carbonate groups in calcite equilibrated with water. Even though carbonate groups in apatite are distinct from those in calcite, calcite-based fractionation factors have been used in the past to interpret the meaning of carbonate oxygen isotopes in phosphates (e.g., McArthur and Herczeg, 1990; Shemesh et al., 1983; Shemesh et al., 1988). We also used the Lécuyer et al. (2010) calibration for carbonate groups substituted into apatite equilibrated with water.

We compared our results to the four different lines that can be produced from the calibrations described above in Figure 4. In Figure 4a, for the calculated relationships between $\delta^{18}O_{PO4}$ and $\delta^{18}O_{CO3}$ in apatite, we assumed mineral formation in waters with a $\delta^{18}O$ = -1.2 ‰, which is the estimated average isotopic composition of ocean without continental ice sheets (Miller et al., 1987). The isotopic composition of the water controls the vertical position of the lines in Figure 4a — increasing the $\delta^{18}O$ of the water in equilibrium with the minerals moves the position of the lines up and vice versa. Importantly, the $\delta^{18}O$ of water has no effect on the slopes of the lines. In Figure 4b, 1000 x $\ln(\alpha_{CO3\text{-}PO4})$ vs. 1000/T for the models is compared to the measured clumped isotope temperatures. Unlike in Figure 4a, this space (Figure 4b) is entirely independent of the isotopic composition of the water chosen.

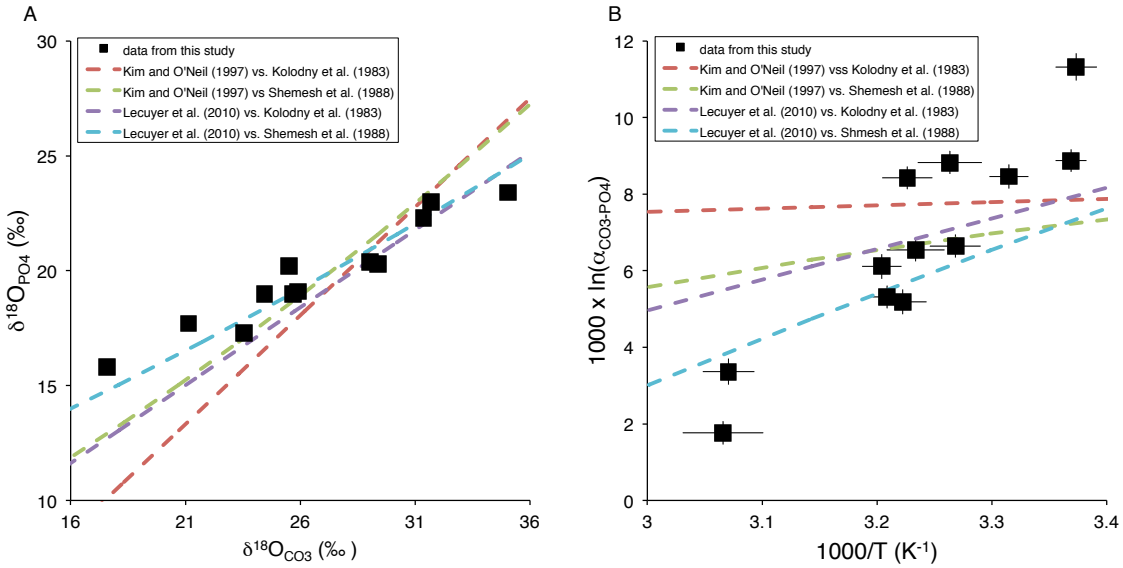

Figure 4. A) Comparison of various theoretical lines for equilibrium between oxygen isotopes of PO_4^{3-} and CO_3^{2-} vs. the measured data. For the theoretical calculations, samples are assumed to have equilibrated with water with a $\delta^{18}O$ value equal to -1.2‰: see text for details. B) Comparison of theoretical lines for 1000 x $\ln(\alpha_{CO3\text{-}PO4})$ vs. 1000/T where T, in Kelvin, is the derived clumped isotope temperature vs. the measured values. $\alpha_{CO3\text{-}PO4}$ values are calculated as $(1000 + \delta^{18}O_{CO3})/(1000 + \delta^{18}O_{PO4})$. Theoretical lines for carbonate-water fractionation factors for $\delta^{18}O_{CO3}$ values are given in Kim and O'Neil (1997) and Lécuyer et al. (2010). Theoretical lines for PO_4-water fractionation factors for $\delta^{18}O_{PO4}$ values are given in Kolodny et al. (1983) and Shemesh et al. (1988). Error bars of data are ±1 standard error.

In Figure 4a, most of the lines, most noticeably the line based on the combination of the Lécuyer et al. (2010) and Shemesh et al. (1988) calibrations, have slopes generally consistent with the trend of the data. Thus it is possible that the $\delta^{18}O_{PO4}$ values and $\delta^{18}O_{CO3}$ values represent the generation and subsequent preservation of apatites in oxygen isotope equilibrium with seawater or diagenetic fluids. Closer inspection, however, demonstrates that this goodness of fit is at least partially fortuitous. Specifically, one sample examined here, ASP 22, has a well-constrained formational and burial history. This sample was dredged from the sea-floor (and thus experienced limited burial diagenesis) in waters with a temperature of ~12 °C and estimated age of <10,000 years (Shemesh et al., 1983). However, the calculated temperature based on the $\delta^{18}O_{PO4}$ and

$\delta^{18}O_{CO3}$ values and the Lécuyer et al. (2010) vs. Shemesh et al. (1988) fractionation factors is -8°C ± 3 (1σ). This temperature is below the modern freezing point of seawater, -2 °C (though it should be noted that these temperatures are within 2σ error), and significantly below the current environmental temperature. Unless the Namibian Shelf was unexpectedly near the freezing point of water in the past 10,000 years (which is unlikely considering it is the tropics), this example indicates that despite the visual goodness of fit of the Lécuyer et al. (2010) vs. Shemesh et al. (1988) line in Figure 4a, at least some samples have $\delta^{18}O_{PO4}$ and $\delta^{18}O_{CO3}$ values that are not consistent with the attainment or preservation of isotopic equilibrium between these groups. The clumped isotope temperatures vs. 1000 x $\ln(\alpha_{CO3\text{-}PO4})$ clearly indicate that the clumped isotope based temperatures of many samples do not correspond to the calculated formation temperatures based on the four estimates we considered for the temperature-dependent fractionation between $\delta^{18}O_{PO4}$ and $\delta^{18}O_{CO3}$ (Figure 4b).

The deviation of the samples from the expected equilibrium values in Figure 4 could have been caused by either: (1) The calibrated mineral-water fractionation factors for either phosphate and/or carbonate groups in apatites are incorrect. Divergence among the four estimates we consider makes it clear they cannot all be correct, and it is possible none of the lines are correct. It may even be possible that the measured clumped isotope compositions capture the correct temperature dependence of the fractionation factors, though this is difficult to evaluate. Or (2), the clumped isotope temperature and oxygen isotope composition of the $PO4^{3-}$ or $CO3^{2-}$ groups (and thus the clumped isotope compositions of carbonate groups) in the apatites do not reflect equilibrium conditions. Instead they could represent post-depositional modification during diagenesis. We

quantitatively test this second hypothesis below with a simple kinetic framework in the next section.

5. A kinetic interpretative framework

5.1 The model

Clumped isotopes are often interpreted in the context of equilibrium processes — i.e., the temperature calculated from the Δ_{47} value of a sample is commonly interpreted to represent a temperature of precipitation or diagenetic or metamorphic recrystallization or thermally activated, internal re-equilibration. This is only true if the mineral formed in isotopic equilibrium during precipitation, or reached a sufficiently high temperature to re-equilibrate through atomic diffusion. Multiple processes can modify a sample's Δ_{47} value post precipitation. For example, the assumption of equilibrium formation fails when samples experience sufficiently high temperatures such that C-O bonds begin to break and atoms diffuse within the crystal lattice (Passey and Henkes, 2012; Stolper and Eiler, Accepted, Chapter 3). In such a case, if a sample cools rapidly before a new equilibrium distribution of isotopes is obtained in the mineral lattice, the clumped isotope temperature will partially reflect both the original formation temperature and the exposure to elevated temperatures.

Alternatively, partial recrystallization of a sample will mix diagenetic components, formed at potentially different temperatures and isotopic compositions with the originally formed material. In such a scenario, all mineral components, diagenetic and original, could have formed in isotopic equilibrium with seawater/pore waters, but the calculated clumped isotope temperature would have no meaning as a physical

temperature. Instead the inferred Δ_{47}-based temperature would represent a mixture of the temperatures of formation of the components, and possibly not equal the weighted average of those formation temperatures due to potential non-linearities when mixing Δ_{47} values (Eiler and Schauble, 2004),.

An additional and important point to consider is that during dissolution and reprecipitation of apatites in sediments, CO_3^{2-} and PO_4^{3-} groups could exchange O with pore water at different rates. The slope observed in Figure 3a is flatter than some of the equilibrium lines (Figure 4a). This 'flatness' was originally attributed to slower oxygen isotope exchange rates of PO_4^{3-} groups vs. CO_3^{2-} groups (Shemesh et al., 1983; Shemesh et al., 1988). Such a difference would cause CO_3^{2-} groups to approach new equilibrium oxygen isotope values faster than $PO4^{3-}$ groups and thus generate the flatter slope observed in Figure 3a than equilibrium would dictate (Figure 4a). This idea has independent support from the observations that $PO4^{3-}$ groups have been experimentally demonstrated to exchange oxygen with water more slowly than CO_3^{2-} groups in the absence of biology (Lecuyer et al., 1999; Zazzo et al., 2004). At earth surface conditions and in waters of normal pH, oxygen isotope exchange of phosphate on laboratory timescales generally requires catalysis by microbial activity (Blake et al., 1997; Zazzo et al., 2004).

We quantitatively explored the consequences that different rates of oxygen isotope exchange between CO_3^{2-} and PO_4^{3-} groups could have in regard to our data using the kinetic framework of Criss et al. (1987) and Gregory et al. (1989). We used this framework specifically to explore the geometric trajectories that different rates of diagenesis for CO_3^{2-} and PO_4^{3-} groups could cause in both the $\delta^{18}O_{CO3}$ vs. $\delta^{18}O_{PO4}$ and

1000 x ln($\alpha_{CO3\text{-}PO4}$) vs. 1000/T spaces of Figure 4 where T is the clumped-isotope derived temperature. In order to use these models, a few assumptions about how the apatites are diagenetically modified must be made. We assumed that dissolution-reprecipitation for bulk oxygen isotope exchange reactions follow kinetic rate laws in a water buffered systems such that

$$F_{PO4}=(F_{CO3})^{k_{PO4}/k_{CO3}} \text{ (Criss et al., 1987; Gregory et al., 1989),} \quad (1)$$

where $F = ({}^{18}R_{measured}-{}^{18}R_{initial})/({}^{18}R_{equillibrium}-{}^{18}R_{initial})$ and k_i are kinetic rate constants — the full derivation and assumptions about the kinetics for this framework can be found in Gregory et al. (1989). As a note, these equations assume that the concentration of ^{18}O in a sample relative to all other oxygen isotopes can be approximated by the ratio of ^{18}O to ^{16}O (^{18}R). This fails when the concentrations of ^{18}O and ^{16}O are similar (and thus ^{18}R values are significantly different from 0), but is an acceptable assumption for samples with oxygen isotopic abundances observed on the earth. F can take on values from 1 to 0 where 1 indicates no reaction has taken place while 0 is complete reaction. Though written in terms of chemical kinetics, the value of F estimated for any one isotopic component of the system by these calculations is essentially equivalent to the value for that component predicted for physical mixtures of two compositionally distinct end members. For example, if F = 0.5 for the progress of phosphate group oxygen isotope exchange, then half of phosphate-associated oxygen is new material (with a $\delta^{18}O$ corresponding to the value for phosphate at a given temperature in equilibrium with a source water) and half of the phosphate associated oxygen is inherited from the original material. We note that the F is specific to a component and, for example, that the F for phosphate-associated oxygen need not be the same at a given time point as the F for

carbonate-associated oxygen. This difference in reaction rates is critical to the success of this model to fit the data, as explained below.

In order to describe the clumped isotope kinetics we make the following assumptions: (1) We assume that the kinetics of the clumped isotopologue composition of the carbonate minerals can be described and modeled using Δ_{47} values. This assumption holds if there is a constant offset between the carbonate's clumped isotopologue composition (dominated by the abundance of the mass 63 isotopologue, $^{13}C^{16}O_2{}^{18}O$) and its Δ_{47} value — this has been observed to be the case experimentally (Ghosh et al., 2006; Guo et al., 2009). We note, though, that theoretical calculations indicate that Δ_{47} values could be non-linear functions of a sample's carbonate clumped isotope composition (Guo et al., 2009).

(2) We assume that changes in abundances of mass 47 isotopologues ($^{13}C^{16}O^{18}O$, $^{12}C^{17}O^{18}O$, $^{13}C^{17}O_2$) vs. mass 44 isotopologue ($^{12}C^{16}O_2$) of the CO_2 derived from the carbonate groups obey the following kinetic form as described in Criss et al. (1987) and Gregory et al. (1989):

$$\frac{{}^{47}R_t - {}^{47}R_i}{{}^{47}R_e - {}^{47}R_i} = e^{-k_{47}t}, \tag{2}$$

and thus

$$F_{47} = \left(F_{CO3}\right)^{k_{47}/k_{CO3}}, \tag{3}$$

where $F_{47} = ({}^{47}R_{measured} - {}^{47}R_{initial})/({}^{47}R_{equillibrium} - {}^{47}R_{initial})$, 't' is time after starting diagenesis, 'i' is the initial composition, 'e' is the equilibrium composition, and k_{47} is the rate constant. Because, Δ_{47} values depend not only and ^{47}R values, but also on bulk isotopic composition, the full equation describing the change in Δ_{47} with time is:

$$\Delta_{47} = \left(\frac{\left[\left({}^{47}R_e - {}^{47}R_i \right) \times \left(F_{CO3} \right)^{k_{47}/k_{CO3}} \right] + {}^{47}R_i}{2^{13}R + {}^{13}R\left({}^{17}R \right)^2 + 2^{17}R^{18}R} - 1 \right) \times 1000 \quad (4)$$

where the denominator is equivalent to $^{47}R^*$ (Affek and Eiler, 2006). We presume in these models that the $\delta^{13}C$ value of the carbonates does not change during diagenesis — this assumption is supported by the results of models that indicate $\delta^{13}C$ values of apatite change more slowly during diagenesis than oxygen isotopes (Wang and Cerling, 1994).

In order to explore the consequences of this model, we have constructed two geologically plausible diagenetic paths in which diagenesis occurs either at hotter or colder temperatures than apatite formation temperatures. Our assumptions for these calculations are:

(1) We use the fractionation factors of Kolodny et al. (1983) and Lécuyer et al. (2010) to calculate the equilibrium $\delta^{18}O_{PO4}$ and $\delta^{18}O_{CO3}$ values of apatite formed at a given temperature in water of a given $\delta^{18}O$ value. We do not use the Shemesh et al. (1988) calibration due to its dependence on high temperature (>300 °C) points that are either poorly constrained or imply a crossover (see above). We use the Lécuyer et al. (2010) over the Kim and O'Neil (1997) calibration because the Lécuyer et al. (2010) calibration was experimentally generated with carbonate groups in apatites as opposed to calcites. We additionally attempted to take in account the statistical errors of these calibrations in our analysis. This is challenging because the phosphate-water fractionation line from Kolodny et al. (1983) has no stated error estimates. However, the line from Lécuyer et al. (2010) does give error estimates for both the slope and intercept of the dependence of 1000 x $\ln(\alpha_{PO4\text{-}H2O})$. The error of the slope is negligible for our interpretations (±0.53, 1σ), but the intercept is significant (±1.81‰ 1σ in $\delta^{18}O_{CO3}$ for a

given $\delta^{18}O_{H2O}$). The upper and lower 1σ error bounds are included in the analysis below, but we recognize that this is likely an underestimate of the true error involved. Additionally, this error analysis does not take into account the fact that there exists no recognized apatite $\delta^{18}O_{CO3}$ standard for the intercalibration of different labs. Such a standard is necessary for the accurate comparison of $\delta^{18}O$ values measured in one lab to a calibration created using $\delta^{18}O$ values generated in another.

(2) We assume that all samples initially formed in oxygen and clumped isotope equilibrium at 20 °C in water with $\delta^{18}O$ value of 0‰ (the current average value of seawater today).

(3) We must assume a ratio for k_{PO4}/k_{CO3}. For this modeling exercise, we have taken a value of $k_{PO4}/k_{CO3} = 0.5$, though values ranging from 0.4 to 0.6 provide reasonable fits to the data as well. This value could vary across environments depending on, for example, inorganic dissolution and reprecipitation rates, availability of organisms to enzymatically catalyze oxygen exchange in PO_4^{3-} groups, and temperature. For simplicity and in the absence of better constraints, we have chosen a constant value that provides a good visual fit to the data.

(4) We must also assume a ratio for k_{47}/k_{CO3}. One study indicates that this exchange is slower for Δ_{47} values vs. $\delta^{18}O$ values for CO_2 gas equilibrating with liquid water by factors ranging from 0.8 to 0.9 (Affek, 2013). This analysis, though, does not differentiate between actual exchange rate differences of the various CO_2 isotopologues vs. changes in Δ_{47} due to shifts in the sample's $\delta^{18}O$ value (which also affects Δ_{47} when the system is out of equilibrium). Such large kinetic isotope effects (100-200‰), between the clumped isotopologues and single substituted isotopologues, are likely overestimates

considering that a diffusive fractionation in the gas phase (which provides a reasonable first order estimate for the general size of kinetic isotope effects) for mass 47 isotopologues vs. 46 isotopologues (which control the $\delta^{18}O$ value of a sample) referenced to the 44 isotopologue differ by ~10‰. Additionally, these rate constant ratios will likely differ as a function of temperature. Given the uncertainties in this value, we performed our calculations with a fixed k_{47}/k_{CO3} equal to 1 — small variations in this number (±.01) only change the modeled trajectories subtly. From a physical standpoint, the assumption that $k_{47}/k_{CO3} = 1$ can be interpreted to indicate that exchange between the mineral and carbonate ions in solution is not rate-limited by exchange reactions between carbonate ions and water, but instead by dissolution and reprecipitation rates. In other words, carbonate ions in solution are assumed to always be in both oxygen isotope and clumped isotope equilibrium.

(5) We created models for two different diagenetic pathways in water-buffered systems. The first pathway has diagenesis occurring at 80°C (i.e., hotter than initial formation temperatures) in pore waters with a $\delta^{18}O = -4‰$. Such environments commonly occur at depths of ~1-3 km below seafloor in oceanic sediments with geotherms ranging from 20-40 °C/km and decreases in pore water $\delta^{18}O$ of ~2-15 ‰/km (Lawrence and Gieskes, 1981) for the first kilometer of depth into the oceanic floor. Such isotopically light waters (i.e., low in $\delta^{18}O$ compared to modern seawater) could also result from infiltration of meteoric waters, which are generally more negative in $\delta^{18}O$ values than marine waters (Bowen, 2010; Craig, 1961; Epstein and Mayeda, 1953), into sediments. The second pathway is modeled to occur at 10 °C (i.e. colder than the initial formation temperature) in waters that are isotopically identical to the formation waters ($\delta^{18}O = 0‰$).

Such a scenario could be envisioned to occur where sinking fish or organic debris from surface waters are deposited in colder deeper waters on the continental slope.

5.2 Comparison of the model to the data

We provide the calculated model trajectories for this kinetic diagenetic framework in Figure 5. Before comparing the model with the measured data, it is important to recognize that such a simple model, in which all samples are presumed to have formed under the same conditions and can only be diagenetically modified in two different ways, is clearly an oversimplification. The purpose of this exercise is not to attempt to reconstruct the original temperatures and complete diagenetic history of each individual sample, but to better understand if the proposed kinetic framework captures the overall structure observed in figure 3.

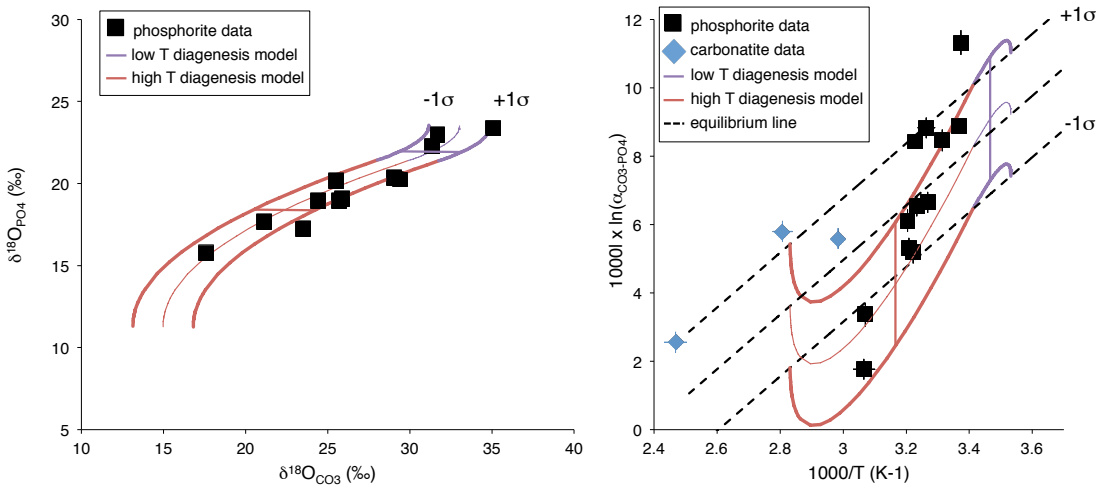

Figure 5. Comparison of data to modeled trajectories during diagenesis. The model is described and developed in the text (section 5). All samples are assumed to have precipitated in isotopic equilibrium at 20°C in waters with a $\delta^{18}O$ value of 0‰. Diagenesis at higher temperatures is assumed to occur at 80°C in waters with a $\delta^{18}O$ value of -4‰. Diagenesis at cooler temperatures is assumed to occur at 10°C in waters with a $\delta^{18}O$ value of 0‰. A) Comparison of bulk $\delta^{18}O_{CO3}$ and $\delta^{18}O_{PO4}$ values vs. the model. B) Comparison of 1000 x $\ln(\alpha_{CO3\text{-}PO4})$ vs. 1000/T where T, in Kelvin, is the derived clumped isotope temperature vs. the model. Carbonatite data come from Stolper and Eiler (Accepted, Chapter 3). 1σ error ranges given for the model are derived from the error given for the published PO_4-H_2O oxygen isotope fractionation factor in Lécuyer et al. (2010). See text for details. Error bars for data are ±1 standard error.

A few key insights can be taken away from this exercise: (1) As seen in Figure 5, this diagenetic model is able to capture the overall structure of the measured data for both the bulk isotopes and clumped isotopes. Generally, most samples are best fit by diagenesis at temperatures higher than original formation temperatures. This indicates that the combination of $\delta^{18}O_{PO4}$, $\delta^{18}O_{CO3}$, and especially temperatures based on Δ_{47} values, provide a more complete understanding of both the formation and subsequent modification of these samples. However, and not unexpectedly, it is also clear that this simple model is not sufficient to fully explain every data point — for example, many of the samples fall in different fields for the degree of diagenesis in the two figures, especially near the assumed starting composition. This disagreement could be eliminated by either relaxing our requirement that each sample was allowed to form and be modified in waters with differing temperature and $\delta^{18}O$ values than chosen here, or allowing for more complex, continuous diagenetic histories in which samples were first partially modified in cooler waters and then warmer waters than in the formational environment.

(2) The comparison of the diagenetic framework to the data also provides a potentially interesting insight into the creation of phosphorites (and perhaps other carbonates) with $\delta^{18}O$ values that are several per mil lower in $\delta^{18}O$ than commonly observed in modern day marine phosphates. Such low values are often assumed to be the result of either meteoric diagenesis or reequillibration with pore waters at elevated temperatures as compared to precipitation temperatures (Degens and Epstein, 1962; Killingley, 1983; Land, 1995), though not without alternative explanations including change in the oxygen isotopic composition of seawater through time (Jaffrés et al., 2007; Kasting et al., 2006; Veizer et al., 1999; Veizer et al., 1997). The correlation between

higher clumped isotope temperatures and lower $\delta^{18}O$ values for the data indicates that diagenesis must have occurred at elevated temperatures and not solely in waters with relatively low $\delta^{18}O$ values and thus elevated temperatures are an essential aspect of phosphorite diagenesis.

(3) The success of the model supports the view that PO_4^{3-} groups are more resistant to exchange in natural materials than CO_3^{2-} groups (Longinelli et al., 2003; Shemesh et al., 1983; Shemesh et al., 1988). However, it is also clear from this data that in the case of phosphorites, apatites are open to significant amounts of oxygen isotope exchange for both carbonate and phosphate groups. Importantly, the arrays observed in Figure 5 could potentially be used as a robust test of digenesis in other samples — if samples fall on disequilibrium arrays in both the $\delta^{18}O_{CO3}$-$\delta^{18}O_{PO4}$ space (figure 5a) and clumped isotope temperature space (Figure 5b) degrees of diagenesis could be estimated and, potentially, original temperatures inferred.

5.3 Do apatites ever fully reequilibrate their oxygen isotopes during diagenesis?

An interesting observation of the model is that for the high temperature diagenesis path no samples return to the equilibrium lines in Figures 5a and b. Instead, all samples observed remain below ~80% re-equilibration. We can compare the phosphorite samples to apatites from igneous carbonatite intrusions that formed at higher temperatures. Interestingly, these igneous samples fall on or near the expected range of equilibrium lines (within the $\pm 1\sigma$ error bounds) for both their difference in $\delta^{18}O$ between PO_4^{3-} and CO_3^{2-} groups as well as clumped isotope temperature (Figure 5b; we do not include them in 5a as this is space depends on the isotopic composition of formation waters which is not relevant for igneous apatites). These igneous apatites formed at temperatures above

~600 °C or so, but preserve lower clumped isotope temperatures due to internal exchange during cooling (Stolper and Eiler, Accepted, Chapter 3). This analysis indicates that during cooling, when these exchange reactions ceased, the clumped isotope and bulk oxygen isotope compositions of the PO_4^{3-} and CO_3^{2-} groups 'closed' at the same temperature. This demonstrates that internal oxygen isotope equilibrium within CO_3^{2-} groups and between CO_3^{2-} and PO_4^{3-} groups can be established at different temperatures than formation temperatures for some apatites.

A question then is why do phosphorites, even those hundreds of millions of years old, not fully reequillibrate? Importantly, the model of Criss et al. (1987) and Gregory et al. (1989) implicitly assumes that all oxygen bearing groups are capable of exchanging at all times—i.e. the physical geometry of the system is ignored for simplicity. However, in nature, this might not necessarily be the case. For example water may be incapable of penetrating and exchanging oxygen with all atoms in an apatite grain due to lack of pores/channels to the interior of the original mineral or, for example armoring of original grains with diagenetic rims or cements. Indeed the presence of apatite cores surrounded and armored with phosphate rims is commonly observed in phosphorite deposits (Figure 6; Braithwaite, 1980; Cook, 1972; Glenn and Arthur, 1988). If correct, this model indicates that the temperatures derived from clumped isotopes, even those heavily modified by diagenesis, do not represent a diagenetic recrystallization temperature, but are instead mixtures of originally deposited apatites with higher (or lower) temperature diagenetic products. If this phenomenon occurs elsewhere, e.g., in calcites or dolomites, it may have implications for the meaning of clumped isotope-based reconstructions of diagenetic recrystallization temperatures and fluid compositions.

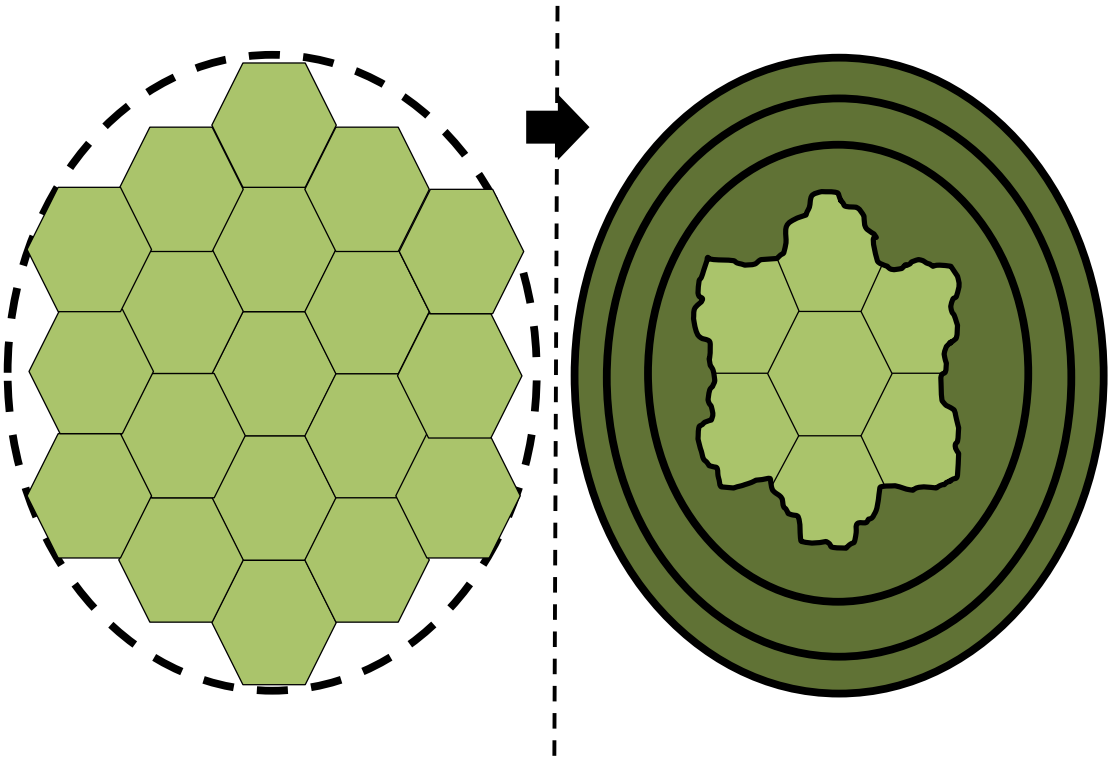

Figure 6. Cartoon representation of the diagenesis of an apatite grain. A) Starting collection of apatite minerals. B) Dissolution and reprecipitation of these minerals armors an inner, original core with an outer rim of diagenetic apatite. This outer rim would prevent further diagenesis of the inner core ensuring that the final phosphorite samples will always contain a mixture of diagenetic and original apatite.

6. Conclusions

The use of oxygen isotopes of carbonate groups and phosphate groups in apatites from phosphorites combined with clumped isotope temperatures yield clear linear relationships between $\delta^{18}O_{CO3}$ and $\delta^{18}O_{PO4}$ as well as $1000\ln(\alpha_{CO3\text{-}PO4})$ and 1/T where T is the derived clumped isotope temperature of the carbonate groups. These relationships cannot be fully reconciled with any current equilibrium-based interpretation of the bulk isotopes or clumped temperatures. Instead these data can be interpreted and modeled in a framework that incorporates kinetics during diagenesis in which originally precipitated minerals partially recrystallize in water-buffered systems with fluids at different temperatures and isotopic compositions. This framework indicates that apatites in

phosphorites undergo isotopic exchange in both carbonate groups and phosphate groups well after precipitation, but never fully isotopically equilibrate with ambient pore waters. This is interpreted as a consequence of the geometry of phosphorites in which original apatite cores are armored by diagenetic rims, preventing further diagenesis. This study sheds light on what the oxygen isotopes of phosphorites mean and demonstrates the utility of clumped isotopes in untangling the dynamics of the formation and diagenesis of sedimentary minerals

7. Tables

Table 1: Age and location of all samples measured. Errors (±) are 1 standard error. All isotopic values have units of ‰. $\delta^{18}O$ values are reported relative to VSMOW and $\delta^{13}C$ relative to VPDB.

Sample	Location	Age (ma)	$\delta^{13}C$ (this study)	±	$\delta^{18}O_{CO3}$ (this study)	±	$\delta^{13}C_{CO3}$ (Shemesh et al., 1988)	$\delta^{18}O_{CO3}$ (Shemesh et al., 1988)	$\delta^{18}O_{PO4}$ (Shemesh et al., 1988)
ASP 3	Phosphoria, USA	265	-3.30	0.02	17.59	0.07	-3.5	16.8	15.8
ASP 4	Monterey, Mexico	30	-6.79	0.01	25.89	0.08	-6.8	24	19.1
ASP 9	Rassaif, Israel	75	-8.69	0.01	24.43	0.04	-9.9	21.8	19
ASP 15	G. Rechavam, Israel	75	-7.27	0.04	23.54	0.14	-6.8	22.8	17.3
ASP 22	Off-Shore, Namibia	0.01	-1.90	0.03	35.05	0.21	-1.9	32.7	23.4
ASP 28	Sechura, Peru	14	-5.22	0.01	31.36	0.05	-5.1	30.4	22.3
ASP 46	Quesir, Peru	75	-5.70	0.02	21.13	0.18	-6.3	21.3	17.7
ASP 49	Monterey, Baja	30	-6.88	0.00	25.69	0.05	-6.9	25.4	19
ASP 78	Blake Plateau	26	-0.52	0.02	31.69	0.11	-1.1	31.1	23
ASP 84	Oron, Israel	75	-9.52	0.08	25.50	0.14	-10.5	26.5	20.2
ASP 105	Central Florida, USA	3.4	-5.45	0.01	29.03	0.03	-5.7	28.2	20.4
NBS 120C			-6.29	0.01	29.40	0.03	-	-	20.3
ASP 6*	Arad, Israel	75	-8.34	.01	24.59	0.24	-8.3	22.5	18.6
ASP 12*	Bir Zafra, Egypt	75	-6.90	.01	21.56	0.24	-5.1	21.5	16.2

*Produced larger quantities of CO2 than other experiments and thus excluded from all discussion in case of contamination by exogenous carbonate phases not removed during acid washing.

Table 2: Δ47 and calculated clumped isotope temperatures of all samples measured. Errors (±) are 1 standard error. All isotopic measurements are in units of ‰.

Sample	n	$\Delta_{47,Ghosh}$	±	$\Delta_{47,ARF}$	±	Δ_{48}	±	T_{Ghosh} (°C)	±	T_{ARF} (°C)	±
ASP 3	4	0.536	0.013	0.613	0.010	0.0	0.2	53	4	49	3
ASP 4	6	0.612	0.008	0.685	0.009	0.5	0.2	33	2	29	2
ASP 9	4	0.589	0.005	0.659	0.007	0.3	0.0	39	1	36	2
ASP 15	5	0.588	0.006	0.654	0.012	0.6	0.5	39	2	37	3
ASP 22	7	0.654	0.007	0.724	0.011	0.2	0.1	23	2	20	2
ASP 28	4	0.611	0.011	0.678	0.007	0.5	0.1	33	3	31	2
ASP 46	5	0.538	0.008	0.601	0.011	0.3	0.2	53	2	52	3
ASP 49	6	0.599	0.010	0.665	0.011	0.3	0.1	36	2	34	3
ASP 78	4	0.630	0.007	0.696	0.009	0.5	0.1	29	2	27	2
ASP 84	4	0.595	0.008	0.658	0.010	0.5	0.2	37	2	36	3
ASP 105	5	0.596	0.008	0.663	0.008	0.5	0.1	37	2	35	2
NBS 120C	10	0.652	0.005	0.720	0.005	0.1	0.2	24	1	21	1
ASP 6*	4	0.563	0.014	0.628	0.019	0.3	0.1	46	4	45	5
ASP 12*	2	0.606	0.015	0.677	0.009	0.5	0.3	34	4	32	2

*Produced larger quantities of CO2 than other experiments and thus excluded from all discussion in case of contamination by exogenous carbonate phases not removed during acid washing.

Table 3: Δ_{47} accuracy and precision of standards and phosphorite samples. n is the number of samples measured. Only the average precision of the phosphorites is given as there is no meaningful total average. Errors (±) are 1 standard deviation. All isotopic values have units of ‰.

	n	$\Delta_{47,Ghosh}$	±	Caltech[a]	$\Delta_{47,abs}$	±	Caltech[a]	Dennis et al. (2011)[b]
Carrara Marble	36	0.348	0.015	0.352	0.399	0.017	0.401	0.403
TVO1	31	0.654	0.015	0.657	0.721	0.013	0.724	-
Average Phosphorites	69	-	0.016	-	-	0.021	-	-

[a]Average, long term value at Caltech

[b]This number is derived from Dennis et al. (2011) by taking the average value for the Carrara in-house marbles and increasing the Harvard, Johns Hopkins, and Caltech values by 0.011 ‰ to account for the use of a 90°C clumped isotope acid digestion fractionation of 0.092 ‰ instead of 0.081 ‰ as was used in that study.

Table 4: $\delta^{13}C$ and $\delta^{18}O$ accuracy and precision of standards and phosphorite samples. Only the average precision of the phosphorites is given as there is no meaningful total average. n is the number of samples measured. Errors (±) are 1 standard deviation. All isotopic values have units of ‰. $\delta^{18}O$ values are reported relative to VSMOW and $\delta^{13}C$ relative to VPDB.

	n[a]	$\delta^{18}O$	±	Caltech[a]	$\delta^{13}C$	±	Caltech[a]
Carrara marble	36	28.87	0.07	28.83	2.35	0.02	2.32
TVO1	31	22.05	0.10	22.03	2.55	0.05	2.53
Average Phosphorites	69	-	0.24	-	-	0.05	-

[a]Average, long term value at Caltech

Table 5: Acid washing experiments. Δ_{47} values are given in the Ghosh and absolute (Abs) reference frame. DI signifies deionized water and TAC triammonium citrate. $\delta^{18}O$ values are reported relative to VSMOW and $\delta^{13}C$ relative to VPDB. All isotopic values have units of ‰. '+ calcite' indicates that Carrara marble was added to the apatite sample.

Sample	$\delta^{13}C$	$\delta^{18}O$	$\Delta_{47,Ghosh}$	$\Delta_{47,Abs}$
apatite unwashed starting material	-5.39	29.55	0.478	0.445
4 hours DI	-5.37	29.27	0.553	0.524
24 hours DI	-5.38	29.24	0.567	0.538
48 hours DI	-5.42	29.27	0.602	0.575
4 hours acetic acid	-5.36	29.24	0.581	0.554
24 hours acetic acid	-5.43	29.27	0.561	0.532
48 hours acetic acid	-5.42	29.35	0.569	0.541
4 hours TAC	-5.42	29.29	0.587	0.559
24 hours TAC	-5.39	29.16	0.573	0.544
48 hours TAC	-5.42	29.33	0.582	0.554
+ calcite with unwashed apatite starting material	-2.42	29.30	0.443	0.408
+ calcite 4 hours acetic acid	-5.40	29.35	0.564	0.535
+ calcite 24 hours acetic acid	-5.20	29.36	0.569	0.541
+ calcite 48 hours acetic	-5.33	29.10	0.582	0.554
+ calcite 4 hours TAC	-4.43	29.30	0.561	0.532
+ calcite 24 hours TAC	-5.00	29.37	0.575	0.546
+ calcite 48 hours TAC	-5.38	29.24	0.601	0.574

8. References

Affek, H.P., 2013. Clumped isotopic equilibrium and the rate of isotope exchange between CO_2 and water. *American Journal of Science* 313, 309-325.

Affek, H.P., Eiler, J.M., 2006. Abundance of mass 47 CO_2 in urban air, car exhaust, and human breath. *Geochimica et Cosmochimica Acta* 70, 1-12.

Ayliffe, L., Chivas, A., Leakey, M., 1994. The retention of primary oxygen isotope compositions of fossil elephant skeletal phosphate. *Geochimica et Cosmochimica Acta* 58, 5291-5298.

Ayliffe, L.K., Herbert Veeh, H., Chivas, A.R., 1992. Oxygen isotopes of phosphate and the origin of island apatite deposits. *Earth and Planetary Science Letters* 108, 119-129.

Baioumy, H., Tada, R., Gharaie, M., 2007. Geochemistry of Late Cretaceous phosphorites in Egypt: Implication for their genesis and diagenesis. *Journal of African Earth Sciences* 49, 12-28.

Birch, G., Thomson, J., McArthur, J., Burnett, W., 1983. Pleistocene phosphorites off the west coast of South Africa. *Nature* 302, 601-603.

Blake, R.E., O'Neil, J., Garcia, G., 1997. Oxygen isotope systematics of biologically mediated reactions of phosphate: I. Microbial degradation of organophosphorus compounds. *Geochimica et Cosmochimica Acta* 61, 4411-4422.

Bowen, G.J., 2010. Isoscapes: Spatial pattern in isotopic biogeochemistry. *Annual Review of Earth and Planetary Sciences* 38, 161-187.

Braithwaite, C.J., 1980. The petrology of oolitic phosphorites from Esprit (Aldabra), western Indian Ocean. *Philosophical Transactions of the Royal Society of London. Series B, Biological Sciences*, 511-540.

Came, R.E., Eiler, J.M., Veizer, J., Azmy, K., Brand, U., Weidman, C.R., 2007. Coupling of surface temperatures and atmospheric CO_2 concentrations during the Palaeozoic era. *Nature* 449, 198-201.

Cook, P.J., 1972. Petrology and geochemistry of the phosphate deposits of northwest Queensland, Australia. *Economic Geology* 67, 1193-1213.

Craig, H., 1961. Isotopic variations in meteoric waters. *Science* 133, 1702-1703.

Criss, R., Gregory, R., Taylor Jr, H., 1987. Kinetic theory of oxygen isotopic exchange between minerals and water. *Geochimica et Cosmochimica Acta* 51, 1099-1108.

Degens, E.T., Epstein, S., 1962. Relationship between O^{18}/O^{16} ratios in coexisting carbonates, cherts, and diatomites: geological notes. *AAPG Bulletin* 46, 534-542.

Dennis, K.J., Affek, H.P., Passey, B.H., Schrag, D.P., Eiler, J.M., 2011. Defining an absolute reference frame for 'clumped' isotope studies of CO_2. *Geochimica et Cosmochimica Acta* 75, 7117-7131.

DePaolo, D.J., 2011. Surface kinetic model for isotopic and trace element fractionation during precipitation of calcite from aqueous solutions. *Geochimica et Cosmochimica Acta* 75, 1039-1056.

Dietzel, M., Tang, J., Leis, A., Köhler, S.J., 2009. Oxygen isotopic fractionation during inorganic calcite precipitation—Effects of temperature, precipitation rate and pH. *Chemical Geology* 268, 107-115.

Eagle, R.A., Schauble, E.A., Tripati, A.K., Tütken, T., Hulbert, R.C., Eiler, J.M., 2010. Body temperatures of modern and extinct vertebrates from ^{13}C-^{18}O bond abundances in bioapatite. *Proceedings of the National Academy of Sciences* 107, 10377.

Eagle, R.A., Tütken, T., Martin, T.S., Tripati, A.K., Fricke, H.C., Connely, M., Cifelli, R.L., Eiler, J.M., 2011. Dinosaur body temperatures determined from isotopic (^{13}C-^{18}O) ordering in fossil biominerals. *Science* 333, 443.

Eiler, J.M., 2007. "Clumped-isotope" geochemistry - The study of naturally-occurring, multiply-substituted isotopologues. *Earth and Planetary Science Letters* 262, 309-327.

Eiler, J.M., 2011. Paleoclimate reconstruction using carbonate clumped isotope thermometry. *Quaternary Science Reviews* 30, 3575-3588.

Eiler, J.M., 2013. The isotopic anatomies of molecules and minerals. *Annual Review of Earth and Planetary Sciences* 41, 411-441.

Eiler, J.M., Schauble, E., 2004. $^{18}O^{13}C^{16}O$ in Earth's atmosphere. *Geochimica et Cosmochimica Acta* 68, 4767-4777.

Epstein, S., Buchsbaum, R., Lowenstam, H.A., Urey, H.C., 1953. Revised carbonate-water isotopic temperature scale. *Geological Society of America Bulletin* 64, 1315-1325.

Epstein, S., Mayeda, T., 1953. Variation of O^{18} content of waters from natural sources. *Geochimica et Cosmochimica Acta* 4, 213-224.

Finnegan, S., Bergmann, K., Eiler, J.M., Jones, D.S., Fike, D.A., Eisenman, I., Hughes, N.C., Tripati, A.K., Fischer, W.W., 2011. The magnitude and duration of Late Ordovician-Early Silurian glaciation. *Science* 331, 903.

Ghosh, P., Adkins, J., Affek, H., Balta, B., Guo, W., Schauble, E.A., Schrag, D., Eiler, J.M., 2006. ^{13}C-^{18}O bonds in carbonate minerals: A new kind of paleothermometer. *Geochimica et Cosmochimica Acta* 70, 1439-1456.

Glenn, C.R., Arthur, M.A., 1988. Petrology and major element geochemistry of Peru margin phosphorites and associated diagenetic minerals: Authigenesis in modern organic-rich sediments. *Marine Geology* 80, 231-267.

Gregory, R.T., Criss, R.E., Taylor Jr, H.P., 1989. Oxygen isotope exchange kinetics of mineral pairs in closed and open systems: Applications to problems of hydrothermal alteration of igneous rocks and Precambrian iron formations. *Chemical Geology* 75, 1-42.

Guo, W., Mosenfelder, J.L., Goddard III, W.A., Eiler, J.M., 2009. Isotopic fractionations associated with phosphoric acid digestion of carbonate minerals: Insights from first-principles theoretical modeling and clumped isotope measurements. *Geochimica et Cosmochimica Acta* 73, 7203-7225.

Henkes, G.A., Passey, B.H., Wanamaker, A.D., Grossman, E.L., Ambrose, W.G., Carroll, M.L., 2013. Carbonate clumped isotope compositions of modern marine mollusk and brachiopod shells. *Geochimica et Cosmochimica Acta*.

Hiatt, E.E., Budd, D.A., 2001. Sedimentary phosphate formation in warm shallow waters: new insights into the palaeoceanography of the Permian Phosphoria Sea from analysis of phosphate oxygen isotopes. *Sedimentary Geology* 145, 119-133.

Huntington, K., Eiler, J., Affek, H., Guo, W., Bonifacie, M., Yeung, L., Thiagarajan, N., Passey, B., Tripati, A., Daëron, M., 2009. Methods and limitations of 'clumped' CO_2 isotope (Δ_{47}) analysis by gas-source isotope ratio mass spectrometry. *Journal of Mass Spectrometry* 44, 1318-1329.

Jaffrés, J.B.D., Shields, G.A., Wallmann, K., 2007. The oxygen isotope evolution of seawater: A critical review of a long-standing controversy and an improved

geological water cycle model for the past 3.4 billion years. *Earth-Science Reviews* 83, 83-122.

Jarvis, I., 1992. Sedimentology, geochemistry and origin of phosphatic chalks: the Upper Cretaceous deposits of NW Europe. *Sedimentology* 39, 55-97.

Karhu, J., Epstein, S., 1986. The implication of the oxygen isotope records in coexisting cherts and phosphates. *Geochimica et Cosmochimica Acta* 50, 1745-1756.

Kasting, J.F., Howard, M.T., Wallmann, K., Veizer, J., Shields, G., Jaffrés, J., 2006. Paleoclimates, ocean depth, and the oxygen isotopic composition of seawater. *Earth and Planetary Science Letters* 252, 82-93.

Kastner, M., Garrison, R., Kolodny, Y., Reimers, C., Shemesh, A., 1990. Coupled changes of oxygen isotopes in PO_4^{3-} and CO_3^{2-} in apatite, with emphasis on the Monterey Formation, California. *Phosphate deposits of the World* 3, 312-324.

Killingley, J.S., 1983. Effects of diagenetic recrystallization on $^{18}O/^{16}O$ values of deep-sea sediments. *Nature* 301, 594-597.

Kim, S.T., O'Neil, J.R., 1997. Equilibrium and nonequilibrium oxygen isotope effects in synthetic carbonates. *Geochimica et Cosmochimica Acta* 61, 3461-3475.

Koch, P.L., Tuross, N., Fogel, M.L., 1997. The effects of sample treatment and diagenesis on the isotopic integrity of carbonate in biogenic hydroxylapatite. *Journal of Archaeological Science* 24, 417-430.

Kohn, M.J., Cerling, T.E., 2002. *Stable isotope compositions of biological apatite*, in: Kohn, M.J., Rakovan, J.M., Huges, J.M. (Eds.), *Phosphates—Geochemical, Geobiological, and Materials Importance*. Mineralogical Society of America, Washington, DC, pp. 455-488.

Kolodny, Y., Kaplan, I., 1970. Carbon and oxygen isotopes in apatite CO_2 and co-existing calcite from sedimentary phosphorite. *Journal of Sedimentary Research* 40, 954-959.

Kolodny, Y., Luz, B., 1991. Oxygen isotopes in phosphates of fossil fish—Devonian to Recent. *Stable isotope geochemistry: A tribute to Samuel Epstein* 3, 105-119.

Kolodny, Y., Luz, B., Navon, O., 1983. Oxygen isotope variations in phosphate of biogenic apatites, I. Fish bone apatite—rechecking the rules of the game. *Earth and Planetary Science Letters* 64, 398-404.

Kolodny, Y., Luz, B., Sander, M., Clemens, W., 1996. Dinosaur bones: Fossils or pseudomorphs? The pitfalls of physiology reconstruction from apatitic fossils. *Palaeogeography, Palaeoclimatology, Palaeoecology* 126, 161-171.

Land, L.S., 1995. Comment on "Oxygen and carbon isotopic composition of Ordovician brachiopods: Implications for coeval seawater" by H. Qing and J. Veizer. *Geochimica et Cosmochimica Acta* 59, 2843-2844.

Lawrence, J., Gieskes, J., 1981. Constraints on water transport and alteration in the oceanic crust from the isotopic composition of pore water. *Journal of Geophysical Research: Solid Earth (1978–2012)* 86, 7924-7934.

Lécuyer, C., Allemand, P., 1999. Modelling of the oxygen isotope evolution of seawater: Implications for the climate interpretation of the $\delta^{18}O$ of marine sediments. *Geochimica et Cosmochimica Acta* 63, 351-361.

Lécuyer, C., Amiot, R., Touzeau, A., Trotter, J., 2013. Calibration of the phosphate $\delta^{18}O$ thermometer with carbonate-water oxygen isotope fractionation equations. *Chemical Geology*.

Lécuyer, C., Balter, V., Martineau, F., Fourel, F., Bernard, A., Amiot, R., Gardien, V., Otero, O., Legendre, S., Panczer, G., 2010. Oxygen isotope fractionation between apatite-bound carbonate and water determined from controlled experiments with synthetic apatites precipitated at 10–37° C. *Geochimica et Cosmochimica Acta* 74, 2072-2081.

Lécuyer, C., Grandjean, P., Barrat, J.-A., Nolvak, J., Emig, C., Paris, F., Robardet, M., 1998. $\delta^{18}O$ and REE contents of phosphatic brachiopods: A comparison between modern and lower Paleozoic populations. *Geochimica et Cosmochimica Acta* 62, 2429-2436.

Lécuyer, C., Grandjean, P., Emig, C., 1996. Determination of oxygen isotope fractionation between water and phosphate from living lingulids: Potential application to palaeoenvironmental studies. *Palaeogeography, Palaeoclimatology, Palaeoecology* 126, 101-108.

Lecuyer, C., Grandjean, P., Sheppard, S.M., 1999. Oxygen isotope exchange between dissolved phosphate and water at temperatures ≤ 135 C: Inorganic versus biological fractionations. *Geochimica et Cosmochimica Acta* 63, 855-862.

Longinelli, A., 1984. Oxygen isotopes in mammal bone phosphate: A new tool for paleohydrological and paleoclimatological research? *Geochimica et Cosmochimica Acta* 48, 385-390.

Longinelli, A., Nuti, S., 1968. Oxygen isotopic composition of phosphorites from marine formations. *Earth and Planetary Science Letters* 5, 13-16.

Longinelli, A., Nuti, S., 1973. Revised phosphate-water isotopic temperature scale. *Earth and Planetary Science Letters* 19, 373-376.

Longinelli, A., Wierzbowski, H., Di Matteo, A., 2003. $\delta^{18}O(PO_4^{3-})$ and $\delta^{18}O(CO_3^{2-})$ from belemnite guards from Eastern Europe: Implications for palaeoceanographic reconstructions and for the preservation of pristine isotopic values. *Earth and Planetary Science Letters* 209, 337-350.

Luz, B., Kolodny, Y., Horowitz, M., 1984a. Fractionation of oxygen isotopes between mammalian bone-phosphate and environmental drinking water. *Geochimica et Cosmochimica Acta* 48, 1689-1693.

Luz, B., Kolodny, Y., Kovach, J., 1984b. Oxygen isotope variations in phosphate of biogenic apatites, III. Conodonts. *Earth and Planetary Science Letters* 69, 255-262.

McArthur, J., Benmore, R., Coleman, M., Soldi, C., Yeh, H.-W., O'Brien, G., 1986. Stable isotopic characterisation of francolite formation. *Earth and Planetary Science Letters* 77, 20-34.

McArthur, J., Coleman, M., Bremner, J., 1980. Carbon and oxygen isotopic composition of structural carbonate in sedimentary francolite. *Journal of the Geological Society* 137, 669-673.

McArthur, J., Herczeg, A., 1990. Diagenetic stability of the isotopic composition of phosphate-oxygen: palaeoenvironmental implications. *Geological Society, London, Special Publications* 52, 119-124.

McCrea, J.M., 1950. On the isotopic chemistry of carbonates and a paleotemperature Scale. *Journal of Chemical Physics* 18, 849-857.

Miller, K.G., Fairbanks, R.G., Mountain, G.S., 1987. Tertiary oxygen isotope synthesis, sea level history, and continental margin erosion. *Paleoceanography* 2, 1-19.

Muehlenbachs, K., 1986. Alteration of the oceanic crust and the ^{18}O history of seawater. *Reviews in Mineralogy and Geochemistry* 16, 425-444.

Passey, B., Henkes, G., 2012. Carbonate clumped isotope bond reordering and geospeedometry. *Earth and Planetary Science Letters* 351-352, 223-236.

Passey, B.H., Levin, N.E., Cerling, T.E., Brown, F.H., Eiler, J.M., 2010. High-temperature environments of human evolution in East Africa based on bond ordering in paleosol carbonates. *Proceedings of the National Academy of Sciences* 107, 11245.

Pucéat, E., Joachimski, M.M., Bouilloux, A., Monna, F., Bonin, A., Motreuil, S., Morinière, P., Hénard, S., Mourin, J., Dera, G., 2010. Revised phosphate–water fractionation equation reassessing paleotemperatures derived from biogenic apatite. *Earth and Planetary Science Letters* 298, 135-142.

Sadaqah, R.M., Abed, A.M., Grimm, K.A., Pufahl, P.K., 2007. Oxygen and carbon isotopes in Jordanian phosphorites and associated fossils. *Journal of Asian Earth Sciences* 29, 803-812.

Schauble, E.A., Ghosh, P., Eiler, J.M., 2006. Preferential formation of ^{13}C-^{18}O bonds in carbonate minerals, estimated using first-principles lattice dynamics. *Geochimica et Cosmochimica Acta* 70, 2510-2529.

Schrag, D.P., DePaolo, D.J., Richter, F.M., 1992. Oxygen isotope exchange in a two-layer model of oceanic crust. *Earth and Planetary Science Letters* 111, 305-317.

Schrag, D.P., DePaolo, D.J., Richter, F.M., 1995. Reconstructing past sea surface temperatures: Correcting for diagenesis of bulk marine carbonate. *Geochimica et Cosmochimica Acta* 59, 2265-2278.

Sharp, Z.D., Atudorei, V., Furrer, H., 2000. The effect of diagenesis on oxygen isotope ratios of biogenic phosphates. *American Journal of Science* 300, 222-237.

Shemesh, A., Kolodny, Y., Luz, B., 1983. Oxygen isotope variations in phosphate of biogenic apatites, II. Phosphorite rocks. *Earth and Planetary Science Letters* 64, 405-416.

Shemesh, A., Kolodny, Y., Luz, B., 1988. Isotope geochemistry of oxygen and carbon in phosphate and carbonate of phosphorite francolite. *Geochimica et Cosmochimica Acta* 52, 2565-2572.

Silverman, S.R., Fuyat, R.K., Weiser, J.D., 1952. Quantitative determination of calcite associated with carbonate-bearing Apatites. *American Mineralogist* 37, 211-222.

Stern, M.J., Spindel, W., Monse, E., 1968. Temperature dependences of isotope effects. *The Journal of Chemical Physics* 48, 2908.

Stolper, D.A., Eiler, J.M., Accepted. The kinetics of clumped isotopes in inorganic calcites and apatites in natural and experimental samples. *American Journal of Science*.

Sun, Y., Joachimski, M.M., Wignall, P.B., Yan, C., Chen, Y., Jiang, H., Wang, L., Lai, X., 2012. Lethally hot temperatures during the Early Triassic greenhouse. *Science* 338, 366-370.

Trotter, J.A., Williams, I.S., Barnes, C.R., Lécuyer, C., Nicoll, R.S., 2008. Did cooling oceans trigger Ordovician biodiversification? Evidence from conodont thermometry. *Science* 321, 550-554.

Urey, H.C., Lowenstam, H.A., Epstein, S., McKinney, C.R., 1951. Measurement of paleotemperatures and temperatures of the Upper Cretaceous of England, Denmark,

and the southeastern United States. *Geological Society of America Bulletin* 62, 399-416.

Veizer, J., Ala, D., Azmy, K., Bruckschen, P., Buhl, D., Bruhn, F., Carden, G.A., Diener, A., Ebneth, S., Godderis, Y., 1999. $^{87}Sr/^{86}Sr$, $\delta^{13}C$ and $\delta^{18}O$ evolution of Phanerozoic seawater. *Chemical Geology* 161, 59-88.

Veizer, J., Bruckschen, P., Pawellek, F., Diener, A., Podlaha, O.G., Carden, G.A., Jasper, T., Korte, C., Strauss, H., Azmy, K., 1997. Oxygen isotope evolution of Phanerozoic seawater. *Palaeogeography, Palaeoclimatology, Palaeoecology* 132, 159-172.

Veizer, J., Fritz, P., Jones, B., 1986. Geochemistry of brachiopods: Oxygen and carbon isotopic records of Paleozoic oceans. *Geochimica et Cosmochimica Acta* 50, 1679-1696.

Wacker, U., Fiebig, J., Schoene, B.R., 2013. Clumped isotope analysis of carbonates: Comparison of two different acid digestion techniques. *Rapid Communications in Mass Spectrometry* 27, 1631-1642.

Wang, Y., Cerling, T.E., 1994. A model of fossil tooth and bone diagenesis: Implications for paleodiet reconstruction from stable isotopes. *Palaeogeography, Palaeoclimatology, Palaeoecology* 107, 281-289.

Wang, Z., Schauble, E.A., Eiler, J.M., 2004. Equilibrium thermodynamics of multiply substituted isotopologues of molecular gases. *Geochimica et Cosmochimica Acta* 68, 4779-4797.

Wenzel, B., Lécuyer, C., Joachimski, M.M., 2000. Comparing oxygen isotope records of silurian calcite and phosphate—$\delta^{18}O$ compositions of brachiopods and conodonts. *Geochimica et Cosmochimica Acta* 64, 1859-1872.

Zaarur, S., Affek, H.P., Brandon, M.T., 2013. A revised calibration of the clumped isotope thermometer. *Earth and Planetary Science Letters* 382, 47-57.

Zazzo, A., Lécuyer, C., Mariotti, A., 2004. Experimentally-controlled carbon and oxygen isotope exchange between bioapatites and water under inorganic and microbially-mediated conditions. *Geochimica et Cosmochimica Acta* 68, 1-12.

Zeebe, R.E., 1999. An explanation of the effect of seawater carbonate concentration on foraminiferal oxygen isotopes. *Geochimica et Cosmochimica Acta* 63, 2001-2007.

Chapter V

The development and application of clumped isotopes to the study of methane formation at both high and low temperatures

1. Introduction

Methane is a critical greenhouse gas (Ramaswamy et al., 2001; Wuebbles and Hayhoe, 2002), energy resource (Hamak and Sigler, 1991), and microbial metabolic product and substrate (Ferry, 1998; Hinrichs et al., 1999; Thauer, 1998). In studying methane in the atmosphere, sediments, or natural gas deposits, a critical, first order question is from where the methane was derived. For example, the relative contributions of methane from various sources, e.g., ruminants (like cows) or stray fossil gases, to the atmosphere today and in the past century is an unresolved and debated issue with critical implications for the climate state of the earth in the future (Aydin et al., 2011; Hristov et al., 2014; Kai et al., 2011; Kirschke et al., 2013; Miller et al., 2013; Simpson et al., 2012). Furthermore, many of the mechanisms and details of methane production in nature remain unresolved as discussed below (Burnham, 1998; Lewan et al., 2008; Lewan and Ruble, 2002; Lewan, 1998a; Mango et al., 1994; Seewald, 2003; Seewald et al., 1998; Valentine et al., 2004; Yoshinaga et al., 2014)

The two key sources of methane on the earth today are (1) biological sources of methane (biogenic methane) generated by organisms known as methanogens. Methanogens make methane in a variety of ways including the combination of CO_2 and H_2 (hydrogenotrophic), splitting of acetate (aceticlastic), or cleavage of methyl groups

(methylotrophs) from larger molecules (Thauer, 1998). And (2), the high-temperature breakdown (pyrolysis or 'cracking') of larger organic macromolecules to methane within the earth's crust and is termed 'thermogenic' methane (Hunt, 1996; Tissot and Welte, 1978).

These two sources of methane are often differentiated in two empirical ways. (1) Methanogens produce pure methane while many thermogenic gases contain not only methane, but larger hydrocarbons such as ethane, propane, and butane (Figure 1; Bernard et al., 1976; Claypool and Kvenvolden, 1983; Hunt, 1996; Tissot and Welte, 1978). (2) The isotopic composition of methane (specifically its $\delta^{13}C$ and δD values; see Footnote 1) is also used, sometimes in combination with the relative amounts of methane to larger hydrocarbon gases, to distinguish the source of methane to the system. Broadly speaking, more negative $\delta^{13}C$ and δD values of methane are associated with biogenic sources and more positive $\delta^{13}C$ and δD values are associated with thermogenic sources (Figures 1 and 2; Bernard et al., 1976; Schoell, 1980, 1983; Whiticar, 1999; Whiticar et al., 1986).

These isotopic and compositional parameters are extremely useful for fingerprinting the sources of methane to a system, but there are examples in which these parameters fail (e.g., Martini et al., 1996) because they are non-unique (Figure 2). An additional parameter that distinguishes biogenic and thermogenic gases from each other is their formation temperatures. Specifically, biogenic gases in nature are generally thought to form below about 80°C (Valentine, 2011; Wilhelms et al., 2001), though methanogens are known to grow up to 122°C in laboratory manipulations (Takai et al.,

[1] $\delta = (R/R_{std}-1) \times 1000$ where $^{13}R = [^{13}C]/[^{12}C]$, $^{D}R = [D]/[H]$, and 'std' denotes the standard to which all measurements are referenced. For this paper all carbon measurements are referenced to VPDB and all hydrogen measurements to VSMOW

2008). Methane produced from thermal processes is thought to be produced in significant quantities only above ~150 °C (Burnham, 1989; Price and Schoell, 1995; Quigley and Mackenzie, 1988), though methane is also produced in smaller quantities along with liquid hydrocarbons in the oil window (~60-150°C; Burnham, 1989; Hunt, 1996; Price and Schoell, 1995; Quigley and Mackenzie, 1988; Seewald, 2003). Thus the formation temperatures of methane should strongly delineate the sources of methane to a given system and give insight into the location and conditions of methane formation. In principle, the determination of the formation temperature and source of methane in nature should be straightforward as methanogens only live and thus produce methane near the earth's surface at relatively low temperatures (e.g., a few kilometers below the earth's surface depending on the local geotherm; Valentine, 2011), while thermogenic methane should only be found at greater depths. However, because methane is generally a gas (except when bound in clathrates) in natural environments, it is often mobile in the subsurface (England et al., 1987; Hunt, 1996; Tissot and Welte, 1978). Consequently, thermogenic gases may rise in sedimentary columns and mix with other thermogenic and biogenic gases. For example, some sedimentary gases in the Gulf of Mexico have been estimated to be ~50% biogenic and 50% thermogenic based on isotopic constraints (Chung et al., 1988). The tendency of gases to move in the subsurface makes it challenging to recognize in all cases whether or not gases are biogenic or thermogenic, even when using typical isotopic and molecular constraints (Martini et al., 1996). Furthermore, identifying the original formational environment of a migrated gas is challenging (Price and Schoell, 1995).

In the next two chapters, I describe the development of a new technique based on the measurement of clumped isotopes of methane that may help resolve many of the issues associated with the original formational location of methane and yield insights into the chemical and physical processes of methane generation. In this chapter, additional background on both biogenic and thermogenic methane not covered in Chapters 6 and 7 is provided. In the next section, as it plays an important role in the final chapter of the thesis (Chapter 7), current models on how organic matter matures to oils and gas are described. I do not provide such a review for biogenic methane because the final chapter is less focused on this type of methane. A brief description of methane clumped isotopes is then given, which is described in detail in Chapter 6. Finally, the current understanding of what processes set the isotopic composition of both thermogenic and biogenic methane is reviewed and I comment on whether there are reasons, before making any measurements, to think that the clumped isotope composition of methane should be set by kinetic or equilibrium processes.

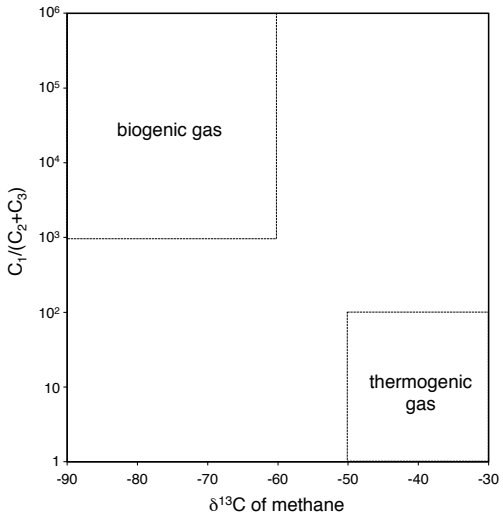

Figure 1. "Bernard Plot" modified from Bernard et al. (1976) and Hunt (1996). Areas within the rectangles delineate fields consistent with methane formed from methanogens (biogenic gas) or from thermally induced breakdown of larger organic molecules into methane (thermogenic gas). C_1 is methane; C_2 is ethane; and C_3 is propane.

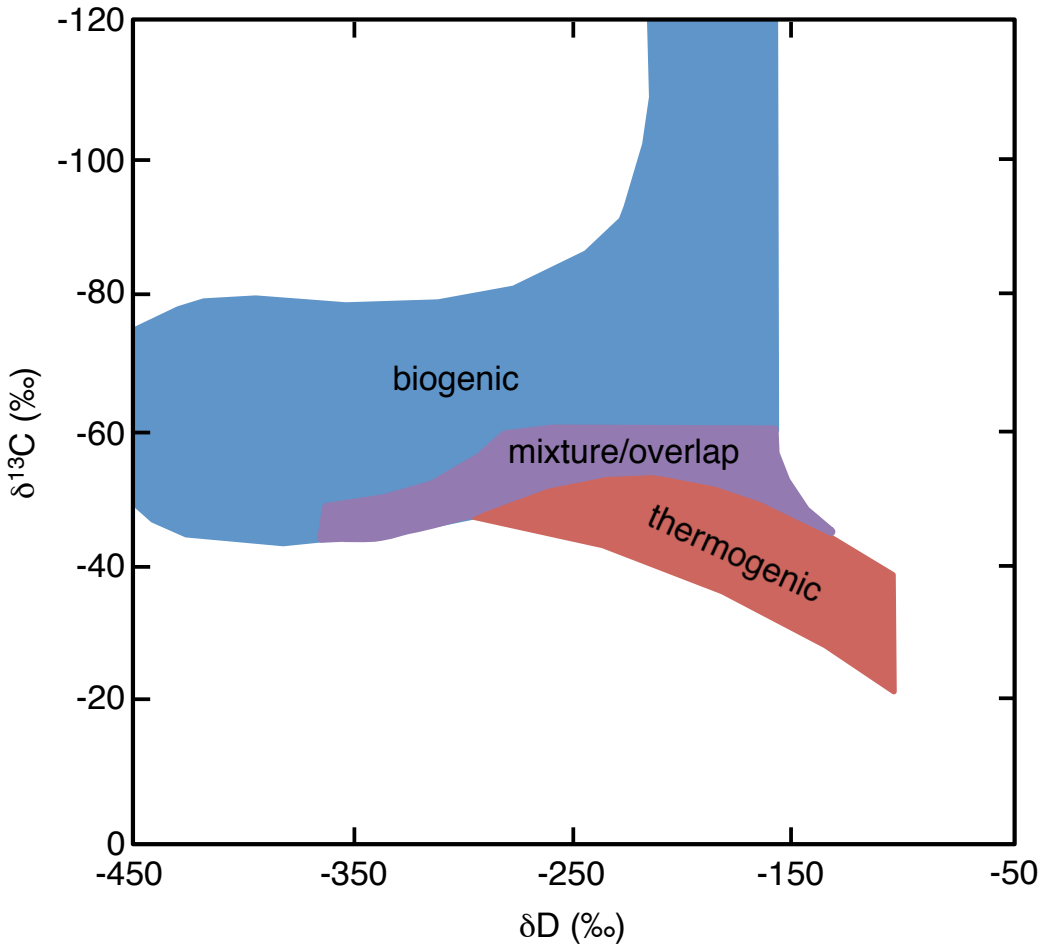

Figure 2. Areas delineating common isotopic ranges of methane derived from methanogens (biogenic) or from thermally induced reactions (thermogenic). Samples in the mixed/overlap zone are either a physical mixture of biogenic and thermogenic gases or gases that formed with this isotopic composition and thus whose origin cannot be ascertained solely using isotopic compositions. Modified from Whiticar (1999).

2. Formation of thermogenic methane

Here I briefly review the basic chemistry, and constraints on that chemistry, involved in the thermal degradation of organic matter to smaller organic molecules like methane. Specifically, thermogenic methane is derived from the cleavage of methyl groups from larger organic molecules. These cleavage reactions occur only at elevated

temperatures (>~60°C) compared to the original formation temperature of the organic matter (Burnham, 1989; Hunt, 1996; Price and Schoell, 1995; Quigley and Mackenzie, 1988; Seewald, 2003). Although methane is ubiquitous in the earth's crust, most quantitative knowledge regarding its formational mechanisms and formation temperature ranges are derived from experimental studies of the 'maturation' of organic matter to oils and gases (Seewald, 2003). In these experiments, organic matter is heated at temperatures well above those observed in nature (Lewan and Ruble, 2002; Lewan, 1998a), and the products, as a function of heating time and temperature, quantified. Though quite straightforward in practice, this sort of approach is only useful if the extrapolation of the high-temperature, laboratory-derived kinetic parameters is applicable to conditions found in the earth. The results of models derived from these experiments will play an important role in providing a basis for comparing clumped-isotope-derived temperatures of thermogenic gases in Chapter 7 to independent estimates of methane formation temperatures. Thus I review some of the basic concepts of and complexities associated with these experiments here.

There are two broad types of experimental procedures used for laboratory organic matter maturation: open system and closed system experiments. In open-system experiments, reactants are constantly purged (generally with an inert gas like helium) such that any products that are formed are instantaneously removed and quantified (Hunt, 1996). A common form of this type of experimental apparatus is termed "Rock-Eval" (Espitalié et al., 1977). In such experiments, samples are usually heated from room temperature a few to tens of degrees Celsius per minute to a final temperature of ~600 °C (Lafargue et al., 1998). Generally, the kinetics derived from these sorts of experiments

when extrapolated to geologically relevant time-temperature histories predict that oils in nature are stable up to ~150-160°C (Burnham, 1989; Lewan and Ruble, 2002) and are completely decomposed to gas by ~180-190°C (Burnham, 1989). The kinetic frameworks used to model these experiments often assume that there exists a distribution of different types of bonds in the sample. The temperature dependence of breaking these bonds is then assumed to follow an Arrhenius law with a range of different activation energies (Burnham et al., 1987; Pepper and Dodd, 1995; Quigley and Mackenzie, 1988; Tissot and Welte, 1978; Waples, 2000).

Such experiments, and the kinetics derived from them have been criticized on multiple grounds. These include such arguments as: the rapid heating rates and temperatures reached in such experiments are far faster and hotter than those experienced in nature (Lewan and Ruble, 2002), the kinetic framework used to describe the reactions lacks a theoretical basis (Hunt, 1996; Lewan and Ruble, 2002; Lewan, 1998a), the derived kinetics depend on the heating rate used for the experiment (Lewan, 1998a), and the immediate removal of products prevents these products from participating in later reactions (Lewan, 1998b). Additionally, oils have been observed in nature to exist up to at least ~190 °C (Vandenbroucke et al., 1999), at which point many of these models predict complete degradation of oils to gas (Burnham, 1989; Vandenbroucke et al., 1999; Waples, 2000).

In contrast to open-system experiments, closed-system pyrolysis experiments do not allow products to exit the experimental apparatus. Two flavors of close-system pyrolysis experiments exist: those that include water (hydrous pyrolysis; e.g., Lewan, 1997; Lewan et al., 1985; Lewan et al., 1979), and those that do not (anhydrous pyrolysis;

e.g., Behar et al., 1992; Behar et al., 1997). Generally, these experiments are conducted at a single (isothermal temperature) for different amounts of time and fit with either a distribution of activation energies (e.g., Seewald et al., 1998) as in the open-system experiments or with a single activation energy (e.g., Lewan and Ruble, 2002). It has been shown that the presence of water in these experiments fundamentally alters the types of reactions present and rates of those reactions as compared to experiments without water — specifically hydrous pyrolysis experiments produce an oil-like product while experiments without water do not (Lewan et al., 1979), yields of gases and larger pyrolysis products (e.g., oils and bitumen) in the presence of water are greater (up to two times higher yields in the presence of water; Lewan, 1997), and the presence of water slows the aromatization of residual kerogen (Michels et al., 1995). Additionally, water has a strong effect on the generation kinetics of oils (Lewan and Ruble, 2002) and the stability of oils — generally increasing the stability to higher temperatures than if water is not present (Lewan, 1997; Michels et al., 1995; Tsuzuki et al., 1999). Additionally, water also affects the kinetics of hydrocarbon gas generation such that these gases form at higher temperatures than would be predicted from experiments without water (Seewald et al., 1998). However, there are criticisms of hydrous pyrolysis experiments. For example, it has been questioned whether the properties of water, such as its polarity or dielectric constant, at 300°C or above (the usual temperature range of hydrous pyrolysis experiments; Lewan, 1997), are sufficiently different from the properties of water at colder temperatures in natural sedimentary systems for the experiments to be relevant to natural organic matter maturation processes (Hill et al., 2007).

There are other factors that are also debated, beyond whether the experiment is opened or closed and if water is included or excluded. These include, most prominently, whether the 'mineralogical' or 'elemental' environment matters for the maturation of organic matter to oil and gases. For example, it has been proposed that transition metals (like nickel) play a critical role in catalyzing the cleavage of C-C bonds in nature (Mango et al., 1994). Although this has been demonstrated to be plausible experimentally (Mango and Hightower, 1997), it is not clear whether it is an important process in nature (Lewan et al., 2008; McNeil and BeMent, 1996; Price and Schoell, 1995).

Each model discussed above is consistent with the experimental conditions under which it was constrained. However, the relevance of the experiments used to constrain the models for understanding natural processes is not clear. Testing these models is difficult because it requires independent knowledge of the thermal history of oils and gases, and/or their source and reservoir rocks. Because formulating accurate, independently known thermal histories for sedimentary basins (where most thermogenic methane is formed) without using other organic parameters is challenging (McKenzie, 1981), it is still unclear which of these models, if any, is 'correct' in the context of natural systems.

3. A brief introduction to methane clumped isotopes

In order to contribute to our understanding of where, how, and at what temperatures methane forms in nature, the second part of the thesis will describe the creation and application of a new technique to measure the clumped isotopologues of methane. In the first chapter in this section (Chapter 6), the methodology and calibration

for the technique is described. In the second chapter (Chapter 7), the technique is applied to natural samples.

Measurements of methane clumped isotopologues could be a useful way to increase our understanding of how and where methane forms because methane clumped isotopologue abundances can always be interpreted in the context of equilibrium thermodynamics. For example, for the following reaction,

$$^{13}CH_3D + {}^{12}CH_4 \leftrightarrow {}^{13}CH_4 + {}^{12}CH_3D\,, \qquad (1)$$

the left side, which has the clumped isotopologue $^{13}CH_3D$, is favored at isotopic equilibrium compared to the right side. This manifests itself as an excess of $^{13}CH_3D$ compared to that expected for a random distribution of isotopes at all finite temperatures. The size of this excess is a unique function of temperature such that there is a larger excess at lower temperatures than higher. Thus, if the abundance of $^{13}CH_3D$ or other clumped isotopologues can be constrained, methane formation temperatures can be calculated.

In order for methane clumped isotopes to serve as a useful geothermometer, the following is required: (1) Clumped isotopologues of methane must be measureable at sufficient precisions and accuracy to be useful and (2) methane needs to form in isotopic equilibrium in nature. Chapter 6 demonstrates that (1) is possible and Chapter 7 indicates that in nature and experiments (2) occurs. Before exploring in detail the methods by which we measure methane clumped isotopes and results from natural samples, I first review how the isotopic composition of both biogenic and thermogenic methane is set, as well as speculate on possible mechanisms that would allow for methane to form in or reach internal isotopic equilibrium.

4. Internal isotopic equilibrium?

4.1 Biogenic methane

In general, the carbon isotopic composition ($\delta^{13}C$ value) of methane generated by methanogens is thought to be controlled by kinetic isotope effects during methane formation and the $\delta^{13}C$ value of the initial substrate (Valentine et al., 2004; Whiticar, 1999; Whiticar et al., 1986). However, the processes that set the hydrogen isotopic composition (δD value) of biogenic methane are not as well understood. For methanogens that use H_2 and CO_2 to generate methane, the ultimate source of hydrogen in the methane is not H_2, but instead H_2O (Daniels et al., 1980; Schoell, 1980; Valentine et al., 2004). Whether or not the expressed hydrogen isotope effect is a kinetic or equilibrium isotope effect or a mixture of the two is also not known (Valentine et al., 2004; Whiticar, 1999). For aceticlastic or methylotrophic methanogenesis, it is sometimes assumed that three fourths of the hydrogen is derived from the pre-existing methyl group and one fourth of the hydrogen from water (Whiticar et al., 1986). However, other studies have indicated that the methyl group of acetate is capable of exchanging hydrogen with water (Waldron et al., 1999) perhaps within the metabolism of methanogens (de Graaf et al., 1996).

It is important to note that the presence of kinetic isotope effects in methane formation for setting $\delta^{13}C$ values does not necessitate that the clumped isotope compositions will also reflect kinetic isotope effects. For example, if methane, during formation, is capable of exchanging hydrogen with its natural environment (e.g., with water or protons) faster than the net rate of methane formation, the clumped isotope

composition could reflect internal equilibrium while the $\delta^{13}C$ could, at the same time, reflect kinetic isotope effects.

There are a few reasons to hypothesize that biogenic methane could, in certain natural systems, form in internal isotopic equilibrium. (1) It has been proposed that in nature the energy barriers (activation energies) of the forward and backward reactions between the metabolic intermediates of biogenic methane are similar (Valentine et al., 2004). In such a case, these intermediates would react forward towards methane at a similar rate as the reaction backward to CO_2. During these forward and backward reactions, hydrogen is added and removed from the carbon atom. Consequently, this exchange of hydrogen could, in principle, allow the C-H bonds in methane to internally equilibrate. This contrasts to pure cultures of methanogens grown in laboratory settings where H_2 partial pressures are often orders of magnitude higher than in nature (Burke Jr, 1993), and the backward reactions are thought to proceed at much slower rates as compared to the forward reactions to methane (Valentine et al., 2004). In this scenario, there would be little exchange of the methyl-bound hydrogen and the clumped isotope signature of the methane could instead reflect kinetic isotope effects. This would predict that natural biogenic methane will be close to internal isotopic equilibrium, but that methane generated from pure cultures of methanogens in the laboratory will not.

(2) The final step of methanogenesis is catalyzed by methyl coenzyme M reductase (MCR) in which a methyl group is hydrogenated to form methane. This enzyme is sometimes described as being non-reversible (Valentine et al., 2004), which would indicate that once it adds a hydrogen atom to methane, the enzyme will not interact with the methane again. However, anaerobic methane-oxidizing archaea, which are

hypothesized to do reverse methanogenesis (i.e., enzymes similar to those of methanogens in reverse for energy conservation), contain the gene for MCR (Hallam et al., 2003; Hallam et al., 2004), which instead suggests that MCR can both add and remove hydrogen from methane. This is further supported by the recent experimental demonstration that MCR from methanogens catalyzes the addition of hydrogen to methyl groups and the removal of hydrogen from methane (Scheller et al., 2010). Thus, MCR could potentially allow biogenic methane to form in internal equilibrium or even re-equilibrate methane such that the methane changes its internal isotopic distribution to reflect the environmental temperature in which the methanogens are present. Additionally it has recently been argued that anaerobic methanotrophs at the interface between sulfate-replete and methane-replete conditions in sediments can actually partially equilibrate the carbon isotopes of methane with CO_2 (Yoshinaga et al., 2014). This equilibration requires the removal and replacement of all hydrogen atoms on the methane and thus could also partially (or wholly) internally equilibrate the isotopologues of methane. Consequently, it is plausible that biogenic methane could be in internal isotopic equilibrium in nature but perhaps not in experimentally grown pure cultures of methanogens.

4.2 Thermogenic methane

The isotopic composition of thermogenic methane is generally thought to be set by kinetic isotope effects (Chung et al., 1988; Clayton, 1991; Ni et al., 2011; Sackett, 1978; Tang et al., 2000). The carbon isotopic composition ($\delta^{13}C$ value) of methane is believed to be controlled by the $\delta^{13}C$ value of the source organic carbon, the type of bond being broken (e.g., a sulfur-carbon vs. a carbon-carbon bond; Tang et al., 2000), the temperature of the reaction (Cramer et al., 1998; Ni et al., 2011; Tang et al., 2000; Xiao,

2001), and/or the amount of organic matter already converted to gas (Clayton, 1991; Rooney et al., 1995).

The source of the hydrogen in methane and what controls the methane's hydrogen isotopic composition (δD value) is less clear. During cleavage of a methyl group from organic matter, a methyl radical is liberated and must then bond a hydrogen atom from its local environment to become methane. Early studies posited that the isotopic fractionation of hydrogen in methane was dominated by the carbon-carbon cleavage event and thus that the hydrogen isotope effect was a secondary isotope effect (Sackett, 1978; Schimmelmann et al., 2006). The source and isotopic composition of the hydrogen atom that is added to the methyl group was not considered important in setting the δD value (and thus size of the fractionation) during methane formation. However, how to quantify the isotopic composition of this final 'capping' hydrogen for methane, and any isotope effect associated with its addition, is not known (Ni et al., 2011).

Additionally, water has been demonstrated to influence the δD values of methane sources such as kerogen, bitumen, and oils. For example, hydrous pyrolysis experiments with deuterated water clearly indicate extensive incorporation of deuterium into reacted organic matter (Hoering, 1984; Lewan, 1997; Schimmelmann et al., 2001; Schimmelmann et al., 1999). Additionally, changes in δD values of organic matter in nature have been suggested to be influenced in part by isotope exchange reactions with sedimentary pore water (Schimmelmann et al., 2006).

It is unlikely that the carbon isotopes of thermogenic methane equilibrate with other organic molecules or CO_2 in nature (except perhaps in hydrothermal settings) given that this would require the formation of carbon-carbon bonds. We note, though, that the

framework of Helgeson et al. (2009), where hydrocarbons are hypothesized to be in metastable equilibrium with each other and with CO_2, may imply that, if this framework is correct, carbon bonds would be breaking and forming between organic molecules. In such a case, the organic molecules could achieve isotopic equilibrium both within and between organic species. Setting this aside, it is also possible for methane to be in internal isotopic equilibrium and still express a kinetic carbon isotope fractionation if hydrogen can be exchanged between methane (or the methyl radical) and hydrogen in its environment faster than the net rate of methane production.

One mechanism that could allow methane precursors to be pre-equilibrated before methane generation is through free radical migration in the backbone of the hydrocarbon precursors. In this situation, as free radicals move from carbon to carbon, hydrogen atoms are added and removed to and from the organic molecule. This processes is how deuterium and hydrogen from water are thought to be added to organic matter (Hoering, 1984). If enough of these hydrogen exchange reactions proceed before C-C bond cleavage, the methyl groups could be in internal isotopic equilibrium before methane formation even occurs.

However, on methane formation, when the carbon isotope fractionation is expressed, hydrogen addition to the methyl radical would have to allow for this internal equilibrium to be maintained or created. Possibilities that could allow this to occur include catalytically induced exchange reactions of methane or methyl groups during formation on minerals such as clays, which have been experimentally demonstrated to catalyze hydrogen exchange in larger organic molecules (Alexander et al., 1982; Alexander et al., 1984), organic surfaces, or transition metals (Mango and Hightower,

1997; Mango et al., 1994), which are known to equilibrate the hydrogen isotopes of methane and H_2 in laboratory experiments in days at temperatures around 200°C (Horibe and Craig, 1995).

5. Prospects

It is clear from this review that knowledge of methane formation temperatures would add new constraints in understanding the sources of methane to a given environment and the metabolic and chemical reactions involved in methane formation. However, without having yet discussed the actual methane clumped isotope measurements, it is unclear, from the start, what the clumped isotope composition of natural methane will mean. There are reasons to believe it could relate to equilibrium isotope effects and thus provide quantitative constraints on methane formation temperatures, but this is something that must be established. The next two chapters are devoted to demonstrating that measurements of clumped isotopologues are possible and then discovering what the values reflect in nature.

6. References

Alexander, R., Kagi, R.I., Larcher, A.V., 1982. Clay catalysis of aromatic hydrogen-exchange reactions. *Geochimica et Cosmochimica Acta* 46, 219-222.

Alexander, R., Kagi, R.I., Larcher, A.V., 1984. Clay catalysis of alkyl hydrogen exchange reactions—reaction mechanisms. *Organic Geochemistry* 6, 755-760.

Aydin, M., Verhulst, K.R., Saltzman, E.S., Battle, M.O., Montzka, S.A., Blake, D.R., Tang, Q., Prather, M.J., 2011. Recent decreases in fossil-fuel emissions of ethane and methane derived from firn air. *Nature* 476, 198-201.

Behar, F., Kressmann, S., Rudkiewicz, J., Vandenbroucke, M., 1992. Experimental simulation in a confined system and kinetic modelling of kerogen and oil cracking. *Organic Geochemistry* 19, 173-189.

Behar, F., Vandenbroucke, M., Tang, Y., Marquis, F., Espitalie, J., 1997. Thermal cracking of kerogen in open and closed systems: Determination of kinetic parameters and stoichiometric coefficients for oil and gas generation. *Organic Geochemistry* 26, 321-339.

Bernard, B.B., Brooks, J.M., Sackett, W.M., 1976. Natural gas seepage in the Gulf of Mexico. *Earth and Planetary Science Letters* 31, 48-54.

Burke Jr, R.A., 1993. Possible influence of hydrogen concentration on microbial methane stable hydrogen isotopic composition. *Chemosphere* 26, 55-67.

Burnham, A., 1989. *A simple kinetic model of petroleum formation and cracking*. Lawrence Livermore National Lab, report UCID 21665.

Burnham, A.K., 1998. Comment on" Experiments on the role of water in petroleum formation" by MD Lewan. *Geochimica et Cosmochimica Acta* 62, 2207-2210.

Burnham, A.K., Braun, R.L., Gregg, H.R., Samoun, A.M., 1987. Comparison of methods for measuring kerogen pyrolysis rates and fitting kinetic parameters. *Energy & Fuels* 1, 452-458.

Chung, H., Gormly, J., Squires, R., 1988. Origin of gaseous hydrocarbons in subsurface environments: Theoretical considerations of carbon isotope distribution. *Chemical Geology* 71, 97-104.

Claypool, G.E., Kvenvolden, K.A., 1983. Methane and other hydrocarbon gases in marine sediment. *Annual Review of Earth and Planetary Sciences* 11, 299.

Clayton, C., 1991. Carbon isotope fractionation during natural gas generation from kerogen. *Marine and Petroleum Geology* 8, 232-240.

Cramer, B., Krooss, B.M., Littke, R., 1998. Modelling isotope fractionation during primary cracking of natural gas: A reaction kinetic approach. *Chemical Geology* 149, 235-250.

Daniels, L., Fulton, G., Spencer, R., Orme-Johnson, W., 1980. Origin of hydrogen in methane produced by *Methanobacterium thermoautotrophicum*. *Journal of Bacteriology* 141, 694-698.

de Graaf, W., Wellsbury, P., Parkes, R.J., Cappenberg, T.E., 1996. Comparison of acetate turnover in methanogenic and sulfate-reducing sediments by radiolabeling and stable isotope labeling and by use of specific inhibitors: Evidence for isotopic exchange. *Applied and Environmental Microbiology* 62, 772-777.

England, W., Mackenzie, A., Mann, D., Quigley, T., 1987. The movement and entrapment of petroleum fluids in the subsurface. *Journal of the Geological Society* 144, 327-347.

Espitalié, J., Laporte, J.L., Madec, M., Marquis, F., Leplat, P., Paulet, J., Boutefeu, A., 1977. Méthode rapide de caractérisation des roches mètres, de leur potentiel pétrolier et de leur degré d'évolution. *Oil & Gas Science and Technology* 32, 23-42.

Ferry, J.G., 1998. Enzymology of one-carbon metabolism in methanogenic pathways. *Microbiology Reviews* 23, 13-38.

Hallam, S.J., Girguis, P.R., Preston, C.M., Richardson, P.M., DeLong, E.F., 2003. Identification of methyl coenzyme M reductase A (mcrA) genes associated with methane-oxidizing archaea. *Applied and Environmental Microbiology* 69, 5483-5491.

Hallam, S.J., Putnam, N., Preston, C.M., Detter, J.C., Rokhsar, D., Richardson, P.M., DeLong, E.F., 2004. Reverse methanogenesis: Testing the hypothesis with environmental genomics. *Science* 305, 1457-1462.

Hamak, J.E., Sigler, S., 1991. *Analyses of natural gases, 1986-90*. Information Circular No. 9301. Bureau of Mines, US Dept. Interior, Pittsburgh, PA.

Helgeson, H.C., Richard, L., McKenzie, W.F., Norton, D.L., Schmitt, A., 2009. A chemical and thermodynamic model of oil generation in hydrocarbon source rocks. *Geochimica et Cosmochimica Acta* 73, 594-695.

Hill, R.J., Zhang, E., Katz, B.J., Tang, Y., 2007. Modeling of gas generation from the Barnett shale, Fort Worth basin, Texas. *AAPG bulletin* 91, 501-521.

Hinrichs, K.-U., Hayes, J.M., Sylva, S.P., Brewer, P.G., DeLong, E.F., 1999. Methane-consuming archaebacteria in marine sediments. *Nature* 398, 802-805.

Hoering, T., 1984. Thermal reactions of kerogen with added water, heavy water and pure organic substances. *Organic Geochemistry* 5, 267-278.

Horibe, Y., Craig, H., 1995. D/H fractionation in the system methane-hydrogen-water. *Geochimica et Cosmochimica Acta* 59, 5209-5217.

Hristov, A.N., Johnson, K.A., Kebreab, E., 2014. Livestock methane emissions in the United States. *Proceedings of the National Academy of Sciences of the United States of America*.

Hunt, J.M., 1996. *Petroleum Geochemistry and Geology*. W. H. Freeman and Company, New York.

Kai, F.M., Tyler, S.C., Randerson, J.T., Blake, D.R., 2011. Reduced methane growth rate explained by decreased Northern Hemisphere microbial sources. *Nature* 476, 194-197.

Kirschke, S., Bousquet, P., Ciais, P., Saunois, M., Canadell, J.G., Dlugokencky, E.J., Bergamaschi, P., Bergmann, D., Blake, D.R., Bruhwiler, L., 2013. Three decades of global methane sources and sinks. *Nature Geoscience* 6, 813-823.

Lafargue, E., Marquis, F., Pillot, D., 1998. Rock-Eval 6 applications in hydrocarbon exploration, production, and soil contamination studies. *Oil & Gas Science and Technology - Revue de l'Institut Français du Pétrole* 53, 421-437.

Lewan, M., 1997. Experiments on the role of water in petroleum formation. *Geochimica et Cosmochimica Acta* 61, 3691-3723.

Lewan, M., Kotarba, M., Więcław, D., Piestrzyński, A., 2008. Evaluating transition-metal catalysis in gas generation from the Permian Kupferschiefer by hydrous pyrolysis. *Geochimica et Cosmochimica Acta* 72, 4069-4093.

Lewan, M., Ruble, T., 2002. Comparison of petroleum generation kinetics by isothermal hydrous and nonisothermal open-system pyrolysis. *Organic Geochemistry* 33, 1457-1475.

Lewan, M., Spiro, B., Illich, H., Raiswell, R., Mackenzie, A., Durand, B., Manning, D., Comet, P., Berner, R., De Leeuw, J., 1985. Evaluation of petroleum generation by hydrous pyrolysis experimentation [and discussion]. *Philosophical Transactions of the Royal Society of London. Series A, Mathematical and Physical Sciences* 315, 123-134.

Lewan, M., Winters, J., McDonald, J., 1979. Generation of oil-like pyrolyzates from organic-rich shales. *Science* 203, 897-899.

Lewan, M.D., 1998a. Reply to the comment by AK Burnham on" Experiments on the role of water in petroleum formation". *Geochimica et Cosmochimica Acta* 62, 2211-2216.

Lewan, M.D., 1998b. Sulphur-radical control on petroleum formation rates. *Nature* 391, 164-166.

Mango, F.D., Hightower, J., 1997. The catalytic decomposition of petroleum into natural gas. *Geochimica et Cosmochimica Acta* 61, 5347-5350.

Mango, F.D., Hightower, J., James, A.T., 1994. Role of transition-metal catalysis in the formation of natural gas. *Nature* 368, 536-538.

Martini, A.M., Budai, J.M., Walter, L.M., Schoell, M., 1996. Microbial generation of economic accumulations of methane within a shallow organic-rich shale. *Nature* 383, 155-158.

McKenzie, D., 1981. The variation of temperature with time and hydrocarbon maturation in sedimentary basins formed by extension. *Earth and Planetary Science Letters* 55, 87-98.

McNeil, R., BeMent, W., 1996. Thermal stability of hydrocarbons: Laboratory criteria and field examples. *Energy & Fuels* 10, 60-67.

Michels, R., Landis, P., Philp, R., Torkelson, B., 1995. Influence of pressure and the presence of water on the evolution of the residual kerogen during confined, hydrous, and high-pressure hydrous pyrolysis of Woodford Shale. *Energy & Fuels* 9, 204-215.

Miller, S.M., Wofsy, S.C., Michalak, A.M., Kort, E.A., Andrews, A.E., Biraud, S.C., Dlugokencky, E.J., Eluszkiewicz, J., Fischer, M.L., Janssens-Maenhout, G., 2013. Anthropogenic emissions of methane in the United States. *Proceedings of the National Academy of Sciences* 110, 20018-20022.

Ni, Y., Ma, Q., Ellis, G.S., Dai, J., Katz, B., Zhang, S., Tang, Y., 2011. Fundamental studies on kinetic isotope effect (KIE) of hydrogen isotope fractionation in natural gas systems. *Geochimica et Cosmochimica Acta* 75, 2696-2707.

Pepper, A.S., Dodd, T.A., 1995. Simple kinetic models of petroleum formation. Part II: Oil-gas cracking. *Marine and Petroleum Geology* 12, 321-340.

Price, L.C., Schoell, M., 1995. Constraints on the origins of hydrocarbon gas from compositions of gases at their site of origin. *Nature* 378, 368-371.

Quigley, T., Mackenzie, A., 1988. The temperatures of oil and gas formation in the sub-surface. *Nature* 333, 549-552.

Ramaswamy, V., Boucher, O., Haigh, J., Hauglustine, D., Haywood, J., Myhre, G., Nakajima, T., Shi, G., Solomon, S., 2001. Radiative forcing of climate. *Climate Change*, 349-416.

Rooney, M.A., Claypool, G.E., Moses Chung, H., 1995. Modeling thermogenic gas generation using carbon isotope ratios of natural gas hydrocarbons. *Chemical Geology* 126, 219-232.

Sackett, W.M., 1978. Carbon and hydrogen isotope effects during the thermocatalytic production of hydrocarbons in laboratory simulation experiments. *Geochimica et Cosmochimica Acta* 42, 571-580.

Scheller, S., Goenrich, M., Boecher, R., Thauer, R.K., Jaun, B., 2010. The key nickel enzyme of methanogenesis catalyses the anaerobic oxidation of methane. *Nature* 465, 606-608.

Schimmelmann, A., Boudou, J.-P., Lewan, M.D., Wintsch, R.P., 2001. Experimental controls on D/H and $^{13}C/^{12}C$ ratios of kerogen, bitumen and oil during hydrous pyrolysis. *Organic Geochemistry* 32, 1009-1018.

Schimmelmann, A., Lewan, M.D., Wintsch, R.P., 1999. D/H isotope ratios of kerogen, bitumen, oil, and water in hydrous pyrolysis of source rocks containing kerogen types I, II, IIS, and III. *Geochimica et Cosmochimica Acta* 63, 3751-3766.

Schimmelmann, A., Sessions, A.L., Mastalerz, M., 2006. Hydrogen isotopic (D/H) composition of organic matter during diagenesis and thermal maturation. *Annu. Rev. Earth Planet. Sci.* 34, 501-533.

Schoell, M., 1980. The hydrogen and carbon isotopic composition of methane from natural gases of various origins. *Geochimica et Cosmochimica Acta* 44, 649-661.

Schoell, M., 1983. Genetic characterization of natural gases. *AAPG Bulletin* 67, 2225-2238.

Seewald, J.S., 2003. Organic–inorganic interactions in petroleum-producing sedimentary basins. *Nature* 426, 327-333.

Seewald, J.S., Benitez-Nelson, B.C., Whelan, J.K., 1998. Laboratory and theoretical constraints on the generation and composition of natural gas. *Geochimica et Cosmochimica Acta* 62, 1599-1617.

Simpson, I.J., Andersen, M.P.S., Meinardi, S., Bruhwiler, L., Blake, N.J., Helmig, D., Rowland, F.S., Blake, D.R., 2012. Long-term decline of global atmospheric ethane concentrations and implications for methane. *Nature* 488, 490-494.

Takai, K., Nakamura, K., Toki, T., Tsunogai, U., Miyazaki, M., Miyazaki, J., Hirayama, H., Nakagawa, S., Nunoura, T., Horikoshi, K., 2008. Cell proliferation at 122 C and isotopically heavy CH4 production by a hyperthermophilic methanogen under high-pressure cultivation. *Proceedings of the National Academy of Sciences* 105, 10949-10954.

Tang, Y., Perry, J., Jenden, P., Schoell, M., 2000. Mathematical modeling of stable carbon isotope ratios in natural gases. *Geochimica et Cosmochimica Acta* 64, 2673-2687.

Thauer, R.K., 1998. Biochemistry of methanogenesis: A tribute to Marjory Stephenson. *Microbiology* 144, 2377-2406.

Tissot, B.P., Welte, D.H., 1978. *Petroleum formation and occurrence: A new approach to oil and gas exploration*. Springer-Verlag, Berlin.

Tsuzuki, N., Takeda, N., Suzuki, M., Yokoi, K., 1999. The kinetic modeling of oil cracking by hydrothermal pyrolysis experiments. *International Journal of Coal Geology* 39, 227-250.

Valentine, D.L., 2011. Emerging topics in marine methane biogeochemistry. *Annu. Rev. Mar. Sci.* 3, 147-171.

Valentine, D.L., Chidthaisong, A., Rice, A., Reeburgh, W.S., Tyler, S.C., 2004. Carbon and hydrogen isotope fractionation by moderately thermophilic methanogens. *Geochimica et Cosmochimica Acta* 68, 1571-1590.

Vandenbroucke, M., Behar, F., Rudkiewicz, J., 1999. Kinetic modelling of petroleum formation and cracking: Implications from the high pressure/high temperature Elgin Field (UK, North Sea). *Organic Geochemistry* 30, 1105-1125.

Waldron, S., Lansdown, J., Scott, E., Fallick, A., Hall, A., 1999. The global influence of the hydrogen iostope composition of water on that of bacteriogenic methane from shallow freshwater environments. *Geochimica et Cosmochimica Acta* 63, 2237-2245.

Waples, D.W., 2000. The kinetics of in-reservoir oil destruction and gas formation: Constraints from experimental and empirical data, and from thermodynamics. *Organic Geochemistry* 31, 553-575.

Whiticar, M.J., 1999. Carbon and hydrogen isotope systematics of bacterial formation and oxidation of methane. *Chemical Geology* 161, 291-314.

Whiticar, M.J., Faber, E., Schoell, M., 1986. Biogenic methane formation in marine and freshwater environments: CO_2 reduction vs acetate fermentation—Isotope evidence. *Geochimica et Cosmochimica Acta* 50, 693-709.

Wilhelms, A., Larter, S., Head, I., Farrimond, P., Di-Primio, R., Zwach, C., 2001. Biodegradation of oil in uplifted basins prevented by deep-burial sterilization. *Nature* 411, 1034-1037.

Wuebbles, D.J., Hayhoe, K., 2002. Atmospheric methane and global change. *Earth-Science Reviews* 57, 177-210.

Xiao, Y., 2001. Modeling the kinetics and mechanisms of petroleum and natural gas generation: A first principles approach. *Reviews in Mineralogy and Geochemistry* 42, 383-436.

Yoshinaga, M.Y., Holler, T., Goldhammer, T., Wegener, G., Pohlman, J.W., Brunner, B., Kuypers, M.M., Hinrichs, K.-U., Elvert, M., 2014. Carbon isotope equilibration during sulphate-limited anaerobic oxidation of methane. *Nature Geoscience*.

Chapter VI

Combined ^{13}C-D and D-D clumping in methane: methods and preliminary results

DA Stolper[a], AL Sessions[a], AA Ferreira[b], EV Santos Neto[b], A Schimmelmann[c], SS Shusta[d], DL Valentine[d], and JM Eiler[a]

[a]*Division of Geological and Planetary Sciences, California Institute of Technology, Pasadena, CA 91125, USA*
[b]*Químico de Petróleo, CENPES, Petrobras, Brazil*
[c]*Department of Geological Sciences, Indiana University, Bloomington, IN 47405, USA*
[d]*Department of Earth Science and Marine Science Institute, University of California, Santa Barbara, CA 93106, USA*

Published in *Geochimica et Cosmochimica Acta* (2014)

Abstract: The stable isotopic composition of methane (e.g., δD and $\delta^{13}C$ values) is often used as a tracer for its sources and sinks. Conventional δD and $\delta^{13}C$ measurements represent the average isotope ratios of all ten isotopologues of methane, though they are effectively controlled by the relative abundances of the three most abundant species: $^{12}CH_4$, $^{13}CH_4$, and $^{12}CH_3D$. The precise relative abundances of the other seven isotopologues remains largely unexplored because these species contain multiple rare isotopes and are thus rare themselves. These multiply substituted (or 'clumped') isotopologues each have their own distinctive chemical and physical properties, which could provide additional constraints on the geochemistry of methane. This work focuses on quantifying the abundances of two rare isotopologues, $^{13}CH_3D$ and $^{12}CH_2D_2$, of methane in order to assess their utility as a window into methane's geochemistry. Specifically, we seek to assess whether clumped isotope distributions might be useful to quantify the temperature at which methane formed and/or equilibrated. To this end, we report the first highly precise combined measurements of the relative abundances of $^{13}CH_3D$ and $^{12}CH_2D_2$ at natural abundances (i.e., unlabeled) via the high-resolution magnetic-sector mass spectrometry of intact methane. We calibrate the use of these measurements as a geothermometer using both theory and experiment, and apply this geothermometer to representative natural samples. The method yields accurate average (i.e., bulk) isotopic ratios based on comparison with conventional techniques. We demonstrate the accuracy and precision of measurements of $^{13}CH_3D$ and $^{12}CH_2D_2$ through analyses of methane driven to high temperature (>200°C) equilibrium in the laboratory. Application of this thermometer to natural samples yields apparent temperatures consistent with their known formation environments and appears to distinguish between biogenic and thermogenic methane.

1. Introduction

Understanding the processes that control the generation, abundance, and fate of methane (CH_4) across the atmosphere, oceans, and shallow crust is critical for both our economic and environmental future. For example, methane is a key constituent of natural gases used for energy (Hamak and Sigler, 1991), a naturally and anthropogenically emitted greenhouse gas (Wuebbles and Hayhoe, 2002), and an important chemical component of geothermal systems (Welhan, 1988). Additionally it is hypothesized to play a role in controlling past climate states (Kennett et al., 2003) and is an important carbon source and product of microbial metabolisms (Valentine, 2011). The stable isotopic building blocks of methane molecules, ^{12}C, ^{13}C, H (^{1}H), and D (^{2}H), as well as radioactive T (^{3}H) and ^{14}C, serve as quantitative tracers of various processes involving methane in the environment. Different formation, transport, and removal processes of methane often impart distinctive isotopic fractionations. As a result, the stable isotopes of methane can be used to reconstruct and quantify those processes. As an example, methane formed from methanogenic organisms sometimes has a distinct isotopic signature as compared to methane formed from the higher temperature, abiotic breakdown of organic matter (Whiticar, 1999). Studies of the stable isotopes of methane have contributed to a better understanding of its biogeochemical cycling in many environments including air (Stevens and Rust, 1982), ice (Craig et al., 1988), gas deposits (Schoell, 1980), and sediment (Whiticar et al., 1986).

The stable isotopic composition of methane is typically quantified through the isotopic ratios $^{13}C/^{12}C$ and D/H, which are reported through $\delta^{13}C$ and δD values (see

footnote 1). These ratios quantify the mean composition of all isotopologues of methane. Though ten different isotopologues of methane contribute to these ratios (Table 1), their precise relative contributions are not directly measured using conventional mass spectrometry. Instead, all isotopologues are converted to a common molecular form (CO_2 or H_2), which destroys all information about how isotopes are partitioned (ordered) amongst the ten isotopologues.

Molecules containing more than one rare isotope are referred to as 'multiply substituted isotopologues' or, equivalently, 'clumped isotopologues' (Eiler, 2007, 2013). Clumped isotopologues are of interest as their chemical and physical properties are distinct from singly substituted (one rare isotope) and unsubstituted (no rare isotopes) isotopologues, which control the average isotopic distributions. For example, at equilibrium, there is, usually, an excess of clumped isotopologues compared to a random distribution of isotopes among all isotopologues. The magnitude of this excess is a function of temperature. Consequently, a measurement that constrains the abundances of unsubstituted, singly substituted, and at least one clumped isotopologue can serve as a geothermometer (Wang et al., 2004). Additionally, non-equilibrium, i.e., kinetic processes often distinctively fractionate clumped isotopologues. Accordingly, measurements of clumped isotopologue abundances can quantify and give insight into kinetic processes (Daëron et al., 2011). Clumped isotopologues have been studied previously in atmospheric CO_2 (Affek and Eiler, 2006; Affek et al., 2007; Eiler and Schauble, 2004), CO_2 released from carbonate bearing minerals via digestion in

[1] $\delta = (R/R_{std}-1)*1000$ where $^{13}R = [^{13}C]/[^{12}C]$, $^{D}R = [D]/[H]$, and 'std' denotes the standard to which all measurements are referenced. For this paper all carbon measurements are referenced to VPDB and all hydrogen measurements to VSMOW.

phosphoric acid (Eiler, 2007, 2011; Ghosh et al., 2006) and in atmospheric O_2 (Yeung et al., 2012). However, sufficiently precise studies of clumped isotopologues of hydrocarbons at natural abundances have not previously been realized because of the inherent difficulty in distinguishing ^{13}C from D substitutions.

Studies of isotopic clumping in methane could have a variety of geochemical and geobiological applications. For example, if methane forms in internal isotopic equilibrium, excesses of clumped isotopologues would yield formation temperatures that allow for unambiguous designations of high-temperature thermogenic vs. low-temperature biogenic sources, which is not always possible using just the stable isotopes of methane (Valentine et al., 2004). Abiogenic sources of methane, such as methane produced via serpentinization or in hydrothermal systems (Etiope and Lollar, 2013) could also yield potentially distinctive temperatures (Fig. 1). If, instead, methane does not form in or preserve internal isotopic equilibrium due to kinetic fractionations associated with transport or irreversible reactions, its distribution of clumped isotopologues could serve as a fingerprint for these processes, much as ^{14}C is used to distinguish fossil from recent sources of methane where $\delta^{13}C$ and δD alone are insufficient (Wahlen et al., 1989). Kinetic isotope effects associated with atmospheric photochemical oxidation of methane are likely to be particularly important applications of this kind. The atmospheric lifetimes of multiply substituted isotopologues are predicted to be longer than their singly and unsubstituted counterparts, such that methane in air may develop an excess in the abundance of $^{13}CH_3D$, $^{12}CH_2D_2$, and other clumped species relative to a random distribution of isotopologues. Although quantitative estimates for this enrichment have only been made for $^{13}CHD_3$ and $^{12}CD_4$ (Kaye and Jackman, 1990), all seven multiply

substituted isotopologues could exhibit distinctive photochemical signatures. Thus abundances of clumped isotopologues of methane in modern or fossil air could reflect changes in atmospheric sink processes (e.g., $OH^{\bullet}$ concentrations). Clearly, some processes could reflect both equilibrium and kinetic processes. Additionally, in some cases, equilibrium and kinetic effects could result in similar clumped isotopic compositions. At present, because so little is understood about multiply substituted isotopologues of methane in nature, we do not attempt to address these possible complexities. Rather, we focus here on the equilibrium effects that will be the basis of any methane clumped isotope thermometer and that will serve as a reference frame for recognizing and interpreting non-equilibrium isotope effects.

Critical to any of these possible applications is the ability to measure the relative abundances of clumped isotopologues of methane precisely and accurately. A few attempts have been made to measure clumped isotopologues of methane in natural materials. Mroz et al. (1989) used a quadrupole mass spectrometer to measure the abundance of mass-20 methane isotopologues ($^{13}CHD_3$ and $^{12}CD_4$) in the troposphere. They found that tropospheric mass-20 methane is ~500 fold (~500,000‰) enriched compared to a random distribution of isotopes, which is two orders of magnitude larger than model predictions (Kaye and Jackman, 1990). Mroz et al. (1989) attributed this extreme enrichment to atmospheric loss processes, but this result has not been tested or reproduced using different samples and techniques — it could be correct, but it also might reflect release of $^{12}CD_4$ in atmospheric circulation experiments or an analytical error. Additionally, two published attempts have been made to measure $^{13}CH_3D$ abundances through infrared spectroscopy (Ma et al., 2008; Tsuji et al., 2012). Only Tsuji

et al. (2012) measured methane with a natural abundance of isotopes. Their precision is ~20‰ (1σ), which is several times (~2.5x) larger than the expected range for equilibrium processes between 0 and 1000°C (see below). If errors improve or, as suggested by Mroz et al. (1989), signals are large, then spectroscopy might become an attractive method to measure clumped isotopes of methane (Ono et al., 2013).

We present here a new mass spectrometric technique to directly measure the stable isotopologues of methane through the introduction of methane gas directly to the ion source of an isotope-ratio mass spectrometer (IRMS) instead of first converting it to H_2 or CO_2, as is commonly done. This paper describes the methodology, accuracy, precision, and experimental reproducibility, including all stages of sample preparation and handling, of our technique, calibrates the relevant clumped isotope thermometer isotope exchange reaction theoretically and experimentally, and reports preliminary measurements of experimentally produced and natural methane. Preliminary reports of this work were presented by Stolper et al. (2012, 2013).

2. Theory and nomenclature of multiply substituted (clumped) isotopologues

A detailed review of the theory and nomenclature of clumped isotope geochemistry is presented in Eiler (2007, 2011, 2013) and Wang et al. (2004). We briefly review the critical concepts of this material here. Generally, most stable isotopic studies assume that isotopes are distributed randomly amongst all isotopologues. For example, this assumption requires the abundance of $^{12}CH_3D$ as a fraction of all methane molecules to equal $4[^{12}C][H]^3[D]$, where $[^{12}C]$ is the fractional abundance of ^{12}C among all carbon atoms, [D] is the fractional abundance of D among all hydrogen atoms, and the prefactor

of 4 is needed to account for the 4 symmetrically equivalent configurations of D in this isotopologue. Although this assumption is at the foundation of nearly all gas-source isotopic measurements of H, C, N, O, and S (excluding SF_6), it is not precisely true except at infinite temperature (Urey and Rittenberg, 1933), or perhaps through unknown non-equilibrium processes that can randomize isotopic distributions. Instead, for systems at equilibrium, isotopes are generally distributed such that isotopologues with two or more heavy (usually rare) isotopes have a higher concentration compared to a random distribution of isotopes amongst all isotopologues (Wang et al., 2004). For example, for the reaction:

$$^{13}CH_3D + {}^{12}CH_4 \leftrightarrow {}^{13}CH_4 + {}^{12}CH_3D \quad (1)$$

the left side of the equation, which contains the clumped species $^{13}CH_3D$, is thermodynamically favored over the right side at finite temperatures. This preference largely occurs due to subtle differences in vibrational energies between isotopologues, which make the left side of the reaction ($^{13}CH_3D$ + $^{12}CH_4$) lower in total zero point energy than the right ($^{13}CH_4$ + $^{12}CH_3D$). The temperature dependence of such reactions arises due to entropic contributions to the total energy, which increasingly favor disorder at higher temperatures. Disorder is maximized when all isotopes are randomly distributed amongst all isotopologues. For equilibrated systems, this maximization occurs at infinite temperature. For a given average isotopic composition ($\delta^{13}C$ and δD), this results in $^{13}CH_3D$ being more abundant at equilibrium at low temperatures and less abundant at high temperatures.

Measurements of stable isotope compositions are generally reported relative to a reference frame based on the known or assumed composition of a reference material such

as VSMOW for oxygen isotopes. For clumped isotope geochemistry, measurements are reported as deviations from a random state in which the isotopes are randomly distributed amongst all isotopologues. We report the enrichment or depletion of multiply substituted species compared to the random state using the symbol Δ_i, where 'i' indicates the reaction or reactions of interest. For the case of equation (1), we write:

$$\Delta_{13CH3D} = \left[\left(\frac{^{13CH3D}R}{^{13CH3D}R^*} - 1 \right) - \left(\frac{^{13CH4}R}{^{13CH4}R^*} - 1 \right) - \left(\frac{^{12CH3D}R}{^{12CH3D}R^*} - 1 \right) \right] * 1000 \quad \text{(Wang et al., 2004).} \qquad (2)$$

In equation (2), $^{i}R = [i]/[^{12}CH_4]$ where brackets denote fractional concentrations and the * denotes the random state. Note that at natural isotopic abundances, Δ_{13CH3D} is overwhelmingly dominated by the first term; i.e., the fractional concentrations of $^{13}CH_4$ and $^{12}CH_3D$ generally do not deviate significantly from their abundances at a random isotopic distribution. For example, if the concentration of $^{13}CH_3D$ is 10‰ enriched over its abundance at a random isotopic distribution, there are 70 pbb 'extra' $^{13}CH_3D$ molecules in the system. These extra molecules dominantly come at the expense of $^{13}CH_4$ and $^{12}CH_3D$ molecules and translate into deficits of 0.01‰ for the concentrations of $^{13}CH_4$ and 0.1‰ for $^{12}CH_3D$ compared to a random isotopic distribution. These depletions are over two orders of magnitude smaller than the enrichment in the concentration of $^{13}CH_3D$ and thus can be ignored for processes with Δ_{13CH3D} values less than ~±10‰, which is the expected range for most equilibrium processes. Consequently, positive values of Δ_{13CH3D} occur when there is more $^{13}CH_3D$ relative to $^{12}CH_4$ in the sample as compared to a random isotopic distribution and negative values when there is less $^{13}CH_3D$ relative to $^{12}CH_4$ as compared to a random isotopic distribution. Δ_{13CH3D} is

related to the equilibrium constant for equation (1), $K_{13CH3D,}$ through the following equation:

$$\Delta_{13CH3D} \cong -1000 \ln\left(\frac{K_{13CH3D}}{K^{*}_{13CH3D}}\right) \quad \text{(Wang et al., 2004).} \tag{3}$$

As explained below, the measurement of isotopic clumping in methane that we present here combines the ion currents of $^{13}CH_3D$ and $^{12}CH_2D_2$, which are the only two mass-18 doubly substituted species. For this reason, we introduce an additional nomenclature:

$$\Delta_{18} = \left(\frac{^{18}R}{^{18}R^{*}} - 1\right) * 1000\,, \tag{4}$$

where ^{18}R = ($[^{13}CH_3D]$ + $[^{12}CH_2D_2]$)/$[^{12}CH_4]$. Equation (4) is exactly analogous to clumped isotope nomenclature for measurements of CO_2 at mass 47, which include all three of the multiply substituted species at mass 47 and assumes the unsubstituted and singly substituted species are randomly distributed. A second homogeneous exchange reaction in addition to equation (1) influences the Δ_{18} value defined in (4):

$$^{12}CH_2D_2 + {}^{12}CH_4 \leftrightarrow 2\,{}^{12}CH_3D\,. \tag{5}$$

Figure 1 presents model predictions of the combined equilibrium constants for equations (1) and (5) using the theory of Bigeleisen and Mayer (1947) and Urey (1947), with vibrational frequencies calculated by Bottinga (1969). The total range of values for equilibrated systems from 0 to 1000 K is ~7‰ with a temperature sensitivity at 25°C of ~30°C/‰. We consider a reasonable target for the precision of initial measurements to be ±10°C at 25°C, which translates into an uncertainty in Δ_{18} (or, almost equivalently, Δ_{13CH3D}) of ±0.3‰. This level of precision would allow for the differentiation of most thermogenic gases from biogenic or low-temperature abiogenic gases if they form in and preserve isotopic equilibrium.

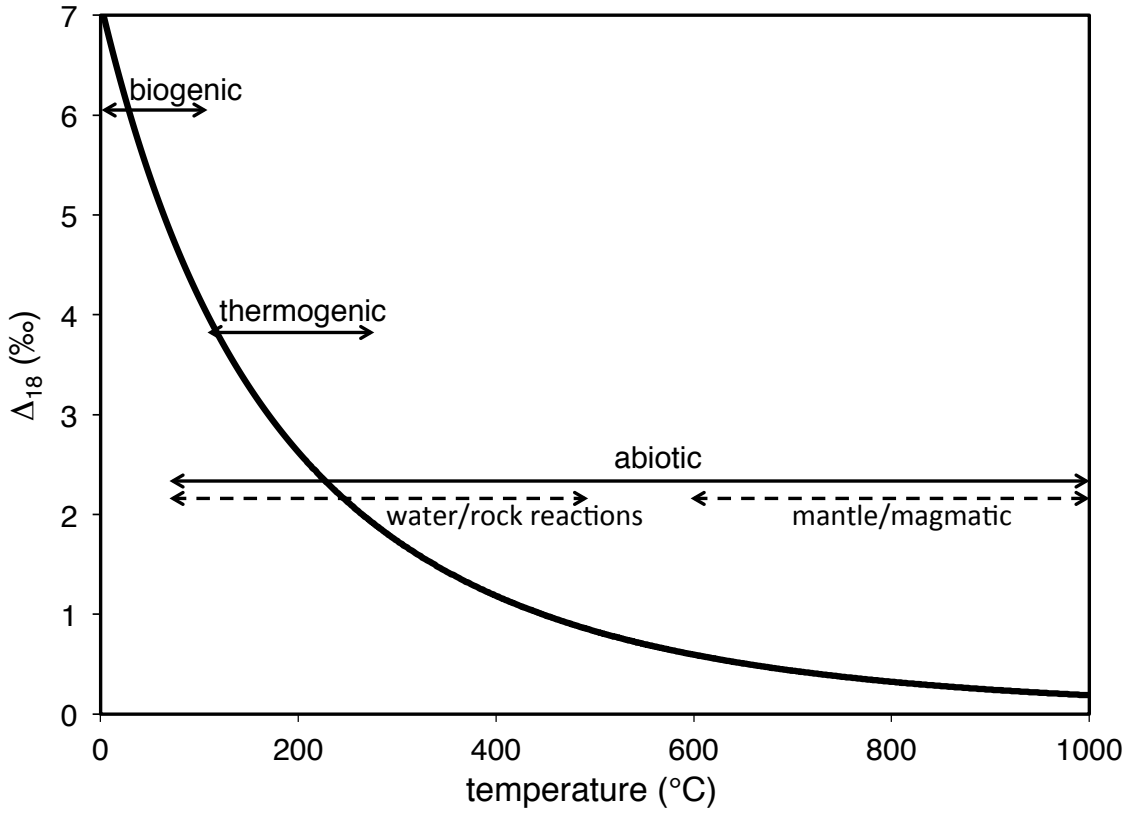

Figure 1. Theoretical calculation of the equilibrium temperature dependence of Δ_{18}. This calculation combines the reactions in equations (1) and (5) using the statistical mechanical theory of Bigeleisen and Mayer (1947) and Urey (1947) and the vibrational frequencies of Bottinga (1969). For reference, the temperatures at which various methane forming processes occur are shown. Biogenic reactions form methane via microbial metabolisms. Thermogenic reactions form methane via pyrolysis of organic matter. Abiotic reactions are highly diverse but can be separated into two distinct groups. The first are reactions mediated in the mantle or in magmatic systems at high (~>600°C) temperatures. The second group are lower temperature abiotic reactions which occur between ~50-500°C and are generally mediated by interactions between water and rock. They include, among others, Fischer-Tropsch reactions, metamorphic reactions with graphite bearing rocks, and uncatalyzed CO_2 reduction. A full review of abiotic reactions can be found in Etiope and Lollar (2013).

The fact that we combine signals from $^{13}CH_3D$ and $^{12}CH_2D_2$ leads to potential ambiguities in the interpretation of Δ_{18} values. At equilibrium, this combination has no meaningful effect as both Δ_{13CH3D} and $\Delta_{12CH2D2}$ are temperature dependent, and thus Δ_{18} values are a well-defined function of temperature (Fig. 1). However, in methane that has been subjected to kinetic fractionations or mixing without re-equilibration, this approach obscures any information that might be recorded by distinctive differences between

Δ_{13CH3D} and $\Delta_{12CH2D2}$. Except in extraordinary circumstances, Δ_{18} values will closely approximate Δ_{13CH3D} values because $^{12}CH_2D_2$ is ~50 times less abundant than $^{13}CH_3D$ at natural isotopic abundances (Table 1). Thus, if $\Delta_{12CH2D2}$ changes by 1‰ without any change in Δ_{13CH3D}, Δ_{18} will change by 0.02‰, which is ~10% of our analytical uncertainty. In order for Δ_{18} to be measurably influenced by differential fractionations of $^{12}CH_2D_2$ vs. $^{13}CH_3D$, $\Delta_{12CH2D2}$ must change by at least ~10-15‰ more than expected based on the Δ_{13CH3D} value. Processes that might lead to such effects include photochemical enrichments or depletions of $^{12}CH_2D_2$ or mixtures of end members that differ in δD by ~200‰ or more. In these cases, interpretations of Δ_{18} measurements would be aided if accompanied by an additional constraint, such as a measurement of $^{13}CH_3D$ alone, such that the abundance of $^{12}CH_2D_2$ could be calculated by difference. This measurement is possible with the instrument we use and methods broadly similar to those we present; however, a full exploration of this alternative approach is beyond the scope of this paper.

3. Stable isotope measurements

Conventional mass spectrometric analyses of the average (bulk) isotopic composition of methane first convert methane to either CO_2 for carbon isotopes (Craig, 1953) or H_2 for hydrogen isotopes (Bigeleisen et al., 1952). This conversion is necessary because most modern gas-source IRMS can only mass resolve species that differ by one or more amu (mass resolutions typically ~200), and thus cannot distinguish between $^{13}CH_4^+$ and $^{12}CH_3D^+$ or interfering isobars like $^{17}O^+$ or $^{16}OH^+$, which are produced mostly from fragmentation of H_2O. These interfering isobars are always present in the

background of mass spectrometers. Similar issues with isobaric interferences would be encountered in any attempt to measure the clumped isotopologues of methane at mass 18, $^{13}CH_3D^+$ and $^{12}CH_2D_2^+$, using a conventional, low-resolution (mass resolution of ~200) gas-source IRMS. $H_2{}^{16}O^+$ is the most problematic as its abundance in any IRMS is generally ~5-fold larger than that of $^{13}CH_3D^+$ and $^{12}CH_2D_2^+$. The conventional response to these challenges — conversion of methane to other gases having simpler mass spectra — cannot be applied to the measurement of clumped isotopologues because the proportional distribution of ^{13}C and D among the various isotopologues of CH_4 is destroyed on conversion along with the original molecules.

Our approach to this problem is the direct mass spectrometric analysis of methane using a high-resolution multi-collector mass spectrometer. Our measurements make use of a new instrument, the Thermo Scientific IRMS-253 Ultra (or 'Ultra') housed in the Division of Geological and Planetary Sciences at Caltech. The design and capabilities of this instrument are described in Eiler et al. (2013). Significantly, for the purposes of the work presented here, the Ultra routinely achieves mass resolving powers between 20,000 to 25,000, which is sufficient to separate methane isotopologues from each other and from contaminating isobars like H_2O^+, OH^+, NH_3^+, etc. We use this instrument to examine the species $^{12}CH_4^+$, $^{13}CH_4^+$, $^{12}CH_3D^+$, $^{13}CH_3D^+$, and $^{12}CH_2D_2^+$. We have found that the most precise and rapid analyses are made when some isotopologues are collected along with isobaric hydrogen adducts (H-adducts) such as $^{12}CH_3D^+$ with $^{12}CH_5^+$ and fragments such as $^{13}CH_3^+$ and $^{12}CH_2D^+$. These isobars are then corrected for during data processing rather than attempting to mass resolve them. Importantly, as previously discussed, we measure $^{13}CH_3D^+$ and $^{12}CH_2D_2^+$ together. However, we demonstrate below

that the direct analysis of $^{13}CH_3D^+$ without $^{13}CH_5^+$, $^{12}CH_2D_2^+$, and $^{12}CH_4D^+$ can be made with a precision of ±0.43‰ similar to the internal precision of our measurements of Δ_{18} (±0.27-0.29‰) and thus that the $^{12}CH_2D_2$ abundance could be calculated by difference between the two measurements. We do not develop this alternative approach in any further detail here, preferring to leave it for future studies that focus on photochemical fractionations of methane, as opposed to the smaller equilibrium thermodynamic effects that motivate this study. We first describe how measurements are made at mass 17 to derive bulk $\delta^{13}C$ and δD values and then discuss measurements at mass 18. The species present in our measurements of masses 16, 17, and 18 and their relative abundances are given in Tables A1 and A2.

3.1 Mass 17

The mass spectrum of methane at mass 17 as measured in the Ultra visibly contains (as read on a Faraday cup through a 10^{12} Ω amplifier), in order from lower to higher mass, $^{16}OH^+$ (produced from the fragmentation of $H_2{}^{16}O$), $^{14}NH_3^+$, $^{13}CH_4^+$, $^{12}CH_3D^+$, and $^{12}CH_5^+$ (produced by the addition of an H to $^{12}CH_4^+$, which we term an H-adduct; Fig. 2a). Additionally, $^{17}O^+$, $^{15}NH_2^+$, and fragments of heavier methane isotopologues (e.g., $^{13}CH_2D^+$) must also be present, but at a level we cannot detect on a Faraday cup read through a 10^{12} Ω amplifier. $^{14}NH_3^+$ is not a contaminant from our samples, but is instead present in the instrument background at all times. $^{16}OH^+$ is fully separated from all methane ions, despite our use of relatively wide collectors (1.3 mm) to permit flat-topped peaks. $^{14}NH_3^+$ is formally mass resolved from methane ions, but overlaps the collector aperture for much of the peak width of the methane isotopologues,

resulting in a shoulder on the high-mass side of the major composite peak that is fully resolved from $^{14}NH_3^+$ (Fig. 2a). As explained below, we measure on this high-mass

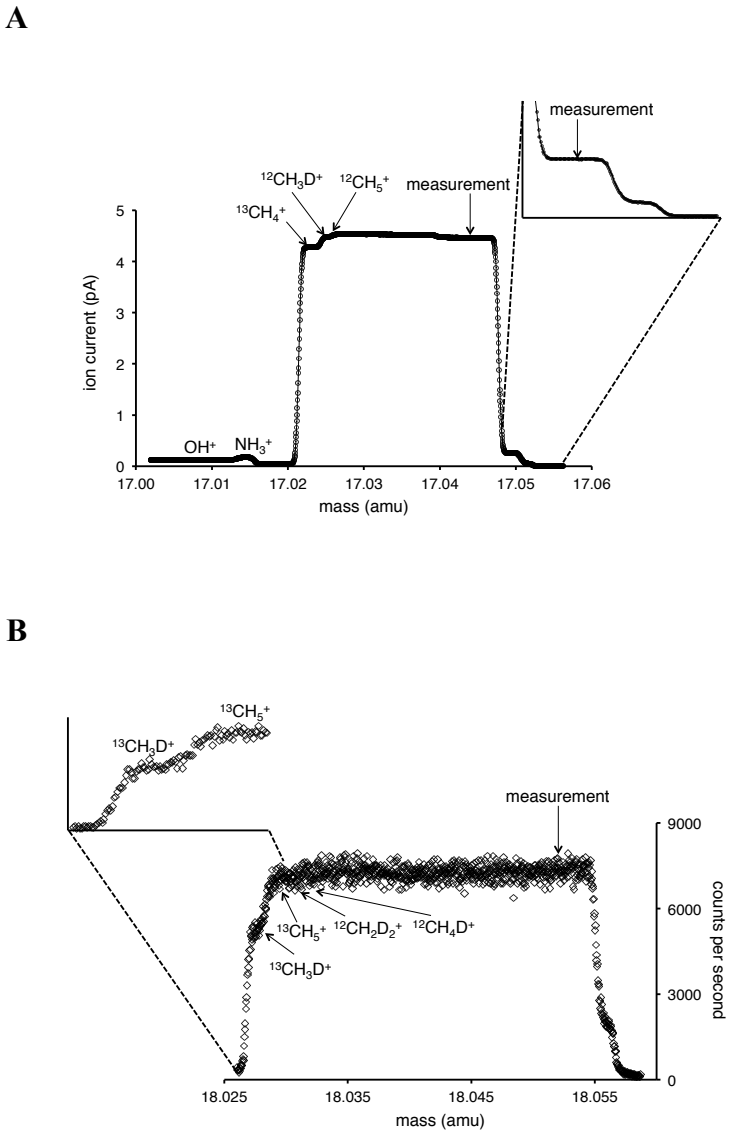

Figure 2: A) Mass spectrum at mass 17. The full spectrum was measured at medium resolution (16,000-17,000 mass resolving power) on a Faraday cup read through a 10^{12} Ω resistor while using the instrument's 16 μm entrance slit. The partial mass spectrum in the smaller inset was measured at high resolution (20,000-22,000 mass resolving power) on a Faraday cup read through 10^{12} Ω resistor using the instrument's 5 μm entrance slit. Measurements and adduct lines are made where indicated. B) High-resolution (~20,000 mass resolving power) scan of mass 18 registered on a secondary electron multiplier. $H_2{}^{16}O^+$ is baseline resolved but not shown due to its higher intensity (100,000 counts per second). Measurements are made where indicated at medium resolution (16,000-17,000 mass resolving power) to increase sensitivity to about 20,000 counts per second. The $^{13}CH_3D^+$ shoulder is shown to demonstrate that it can be resolved from $^{13}CH_5^+$ at the highest resolution setting of the instrument.

shoulder of the methane peak (>17.045 amu). Consequently the only species contributing to the measured mass-17 ion current are $^{13}CH_4^+$, $^{12}CH_3D^+$, $^{12}CH_5^+$, and the fragments, $^{13}CH_2D^+$ and $^{12}CHD_2^+$. Because both fragments are present at low abundances (<0.05% of the signal for both measurements described below) and likely contribute roughly equally to both the sample and the standard gases, we can safely ignore them. Their presence may need to be treated explicitly in the study of gases that exhibit photochemical or other fractionations of many thousands of per mil through additional corrections.

The conceptually simplest approach to determining the $\delta^{13}C$ and δD values for a sample would be to measure the ion-current ratios for $^{13}CH_4^+/^{12}CH_4^+$ and $^{12}CH_3D^+/^{12}CH_4^+$ separately and with no isobaric inferences on either species. However, as is apparent in Fig. 2, this approach is not possible without employing a much narrower collector width because $^{12}CH_3D^+$ is situated between $^{13}CH_4^+$ and $^{12}CH_5^+$ and $^{13}CH_4^+$ is between $^{14}NH_3^+$ and $^{12}CH_3D^+$. Any collector narrow enough to permit resolution of all of these species would likely fail to achieve flat peak tops and thus stable ion currents. For this reason, we opted to retain the wide collectors used to make the scan in Fig. 2 and to constrain the relative abundances of the species of interest through corrections applied to measurements that combine two or more species.

Our approach is to constrain the $\delta^{13}C$ and δD values of a sample by measuring the ratios, $(^{13}CH_4^+ + {}^{12}CH_3D^+ + {}^{12}CH_5^+)/(^{12}CH_4^+ + {}^{13}CH_3^+ + {}^{12}CH_2D^+)$ and $(^{12}CH_3D^+ + {}^{12}CH_5^+)/(^{12}CH_4^+ + {}^{13}CH_3^+ + {}^{12}CH_2D^+)$. The mass-16 measurement includes ~1% contributions from the fragments $^{13}CH_3^+$ and $^{12}CH_2D^+$, which we correct for during data processing (Appendix A). We remove the H-adduct contribution from both the sample

and standard using the independently calibrated dependence of the $^{12}CH_5^+/(^{12}CH_4^+ + ^{13}CH_3^+ + ^{12}CH_2D^+)$ ratio on the intensity of the mass-16 ion beam, and then solve for the $^{13}CH_4^+/^{12}CH_4^+$ and $^{12}CH_3D^+/^{12}CH_4^+$ ratios (Appendix A). We chose not to make any measurements that include $^{14}NH_3^+$ as a background species because it can drift in intensity over the course of a measurement making it difficult to accurately subtract from both the sample and standard measurements. We assume these ratios fully constrain $\delta^{13}C$ and δD; i.e., excesses or deficits in the amount of D and ^{13}C contained in the clumped isotopologues compared to a random distribution of isotopes are too small to change the fractional abundances of $^{13}CH_4$ and $^{12}CH_3D$ measurably beyond their random isotopic distributions. This approach may need to be re-evaluated in cases where samples have large enrichments in multiply substituted species (e.g., >±10‰).

Our approach to correct for the presence of $^{12}CH_5^+$ in our measurements is analogous to that used in conventional δD measurements of hydrogen gas where H_3^+ (the H-adduct of H_2^+) contributions must be subtracted from the mass-3 ion current to recover the true HD signal (Friedman, 1953). We assume, as is similarly done for hydrogen isotope measurements of H_2, that $^{12}CH_5^+$ forms via the ion-neutral reaction:

$$^{12}CH_4 + {}^{12}CH_4^+ \rightarrow {}^{12}CH_3 + {}^{12}CH_5^+. \quad (6)$$

We will assume that this reaction includes both second and third order reactions. Generally, for H_3^+ formation, this equation is assumed to only include a second order reaction. However, we have experimentally verified, as will be developed below, that a third order reaction is needed to describe the formation of $^{12}CH_5^+$ as a function of $^{12}CH_4$ pressure in the source. This combined third and second order dependence is written as

$$^{12}CH_5^+ = k_1\left(^{12}CH_4\right)^3 + k_2\left(^{12}CH_4\right)^2 \quad (7)$$

where k_1 and k_2 are constants. The current registered by a Faraday cup at mass 17 ($i_{17,total}$) is made up of two or three distinct contributors depending on the measurement being made, i_{13CH4} and/or i_{12CH3D} and i_{12CH5} and is given by

$$i_{17,total} = i_{12CH3D} + i_{12CH5} \tag{8a}$$

and

$$i_{17,total} = i_{13CH4} + i_{12CH3D} + i_{12CH5}. \tag{8b}$$

Rewriting equation (7) in terms of ion currents gives $i_{12CH5} = k_1(i_{16})^3 + k_2(i_{16})^2$, where i_{16} is the total current at mass 16. This is not strictly correct as our measurement of i_{16} includes $^{12}CH_4^+$, which makes up 99% of the signal, and the fragments, $^{13}CH_3^+$ + $^{12}CH_2D^+$, which together make up 1% percent of the signal. The correction needed to account for the presence of $^{13}CH_3^+$ and $^{12}CH_2D^+$ at mass 16 is presented in Appendix A. However, it is a small correction, changing Δ_{18} by <0.02‰ compared to not making the correction. Taking the approximation that i_{16} is proportional to CH_4^+, we substitute equation (6) into (8) giving

$$i_{17,total} = i_{12CH3D} + k_1\left(i_{16}\right)^3 + k_2\left(i_{16}\right)^2 \tag{9a}$$

and

$$i_{17,total} = i_{13CH4} + i_{12CH3D} + k_1\left(i_{16}\right)^3 + k_2\left(i_{16}\right)^2. \tag{9b}$$

Division of equation (9) by i_{16} gives:

$$\frac{i_{17,total}}{i_{16}} = \frac{i_{12CH3D}}{i_{16}} + k_1\left(i_{16}\right)^2 + k_2\left(i_{16}\right) \tag{10a}$$

and

$$\frac{i_{17,total}}{i_{16}} = \frac{i_{13CH4} + i_{12CH3D}}{i_{16}} + k_1\left(i_{16}\right)^2 + k_2\left(i_{16}\right). \tag{10b}$$

Equations (10a) and (10b) are equations for a line (called an 'adduct line') where i_{12CH3D}/i_{16} and $(i_{13CH4+12CH3D})/i_{16}$ are both the intercepts, and importantly, the ratios of interest. The constants, k_1 and k_2, define the curvature of the line. We use the constants to remove the adduct contribution from all measured ratios at a given current of mass 16.

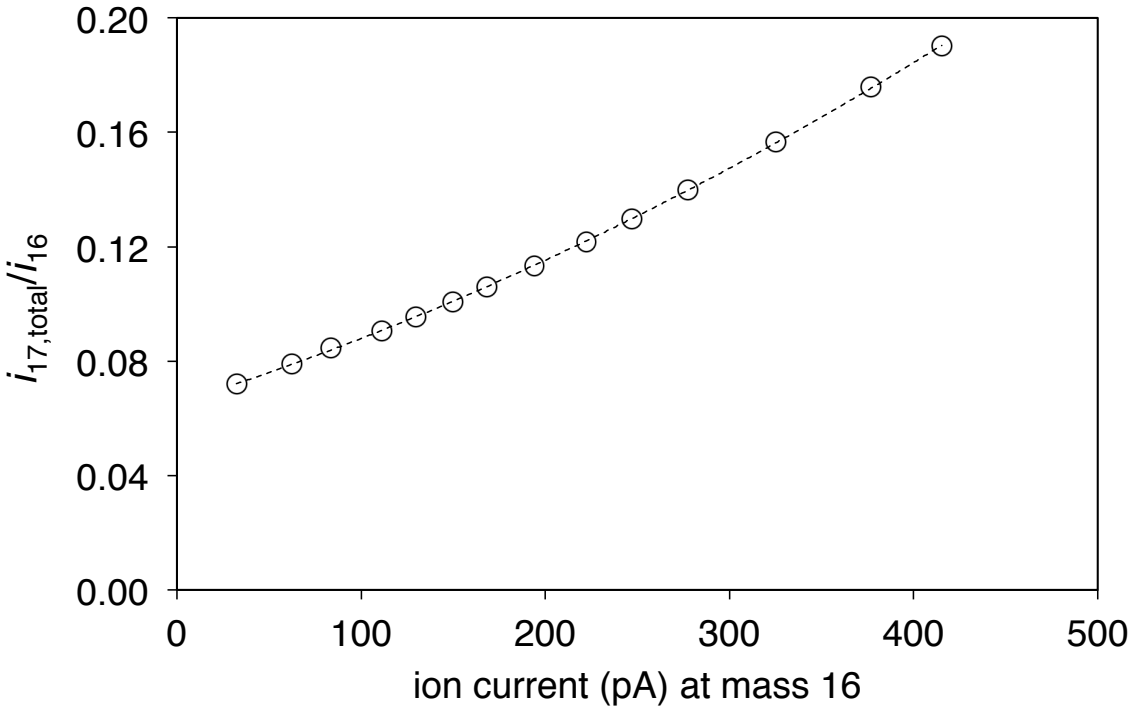

Figure 3. Demonstration of the dependence of the mass-17/mass-16 ion-current ratio ($i_{17,total}/i_{16}$) on the mass-16 ion current. In this example, i_{16} includes $^{12}CH_4^+ + {}^{13}CH_3^+ + {}^{12}CH_2D^+$ and $i_{17,total}$ includes $^{12}CH_3D^+ + {}^{12}CH_5^+$. The line describing the dependence of $i_{17,total}/i_{16}$ on i_{16} is known as an adduct line. The formula for the adduct line is found by fitting the data with a quadratic function. The fitted parameters are used to remove the contribution of $^{12}CH_5^+$ from all measurements. Similar lines are also generated for measurements at mass 17 of $^{13}CH_4^+ + {}^{12}CH_3D^+ + {}^{12}CH_5^+$ in order to remove the contribution of $^{12}CH_5^+$ to the measured ion current and at mass 18 of $^{13}CH_3D^+ + {}^{12}CH_2D_2^+ + {}^{13}CH_5^+ + {}^{12}CH_4D^+$ in order to remove the contributions of $^{13}CH_5^+ + {}^{12}CH_4D^+$ to the measured ion current (Fig. A1).

We determine the value of k_1 and k_2 daily by measuring the $i_{17,total}/i_{16}$ ratio as a function of i_{16} (Fig. 3) — this is done for two separate cases, one in which the ion current for mass 17 includes $^{13}CH_3D^+$, $^{12}CH_3D^+$, and $^{12}CH_5^+$ and one that includes only $^{12}CH_3D^+$ and $^{12}CH_5^+$. We vary i_{16} by manipulating the pressure of gas being delivered to the source via expansion and contraction of the bellows reservoir. A quadratic fit of these data yields the

values of k_1 and k_2, which are then used to correct all subsequent measurements for $^{12}CH_5^+$ contributions.

As discussed above, adduct lines for H_3^+ contributions are generally treated as linear as opposed to quadratic (Sessions et al., 2001) and, thus, the reaction in equation (7) for hydrogen isotope measurements of H_2 is considered to be second order. However, the relationship between $i_{17,total}/i_{16}$ shown in Fig. 3 is demonstrably curved rather than linear, which is why we have assumed that equation (7) includes both a third order and second order reaction pathway. We note, though, that the presence of curvature in adduct lines is also found in hydrogen isotope measurements of H_2 (Friedman, 1953) and thus could be included in those measurements as well. Though we do not know precisely what causes the curvature in the adduct line, some physical causes include: (1) $^{12}CH_5^+$ forms via the combined third and second order reactions as presented in equation (7). (2) $^{12}CH_5^+$ abundances in the source are affected by pressure dependent reactions with $^{12}CH_4$ that form larger hydrocarbons in the source such as $C_2H_5^+$ (Munson and Field, 1966). And (3) the abundance of $^{12}CH_4^+$ is lower via increased fragmentation of $^{12}CH_4$ and $^{12}CH_4^+$ at lower source pressures (Friedman, 1953). Regardless, for our purposes, the critical observation is that $^{12}CH_5^+$ has a defined and stable dependence on $^{12}CH_4$ pressures in the source and thus can be modeled and removed from the measurement. We now proceed to show that this relationship yields accurate δD and $\delta^{13}C$ measurements when compared to conventional mass spectrometric techniques.

To establish the accuracy of our measurements, we compared the δD and $\delta^{13}C$ values of samples measured using both the Ultra and established combustion/reduction techniques. We compared four methane gases with differing δD values and thirteen

samples with differing $\delta^{13}C$ values (Fig. 4; Tables 2 and 3). Conventional, offline δD measurements were made at Indiana University through combustion of CH_4 to CO_2 and H_2O followed by reduction of H_2O to H_2 with uranium following Schimmelmann et al. (1999). Adherence to the principle of equal treatment of sample and standard and the use of two-point calibrations along isotopic axes anchored to VPDB and VSMOW was achieved by using the primary international standards, NBS 19, L-SVEC, VSMOW and SLAP (the latter two waters had been reduced to H_2 with uranium at 800°C).

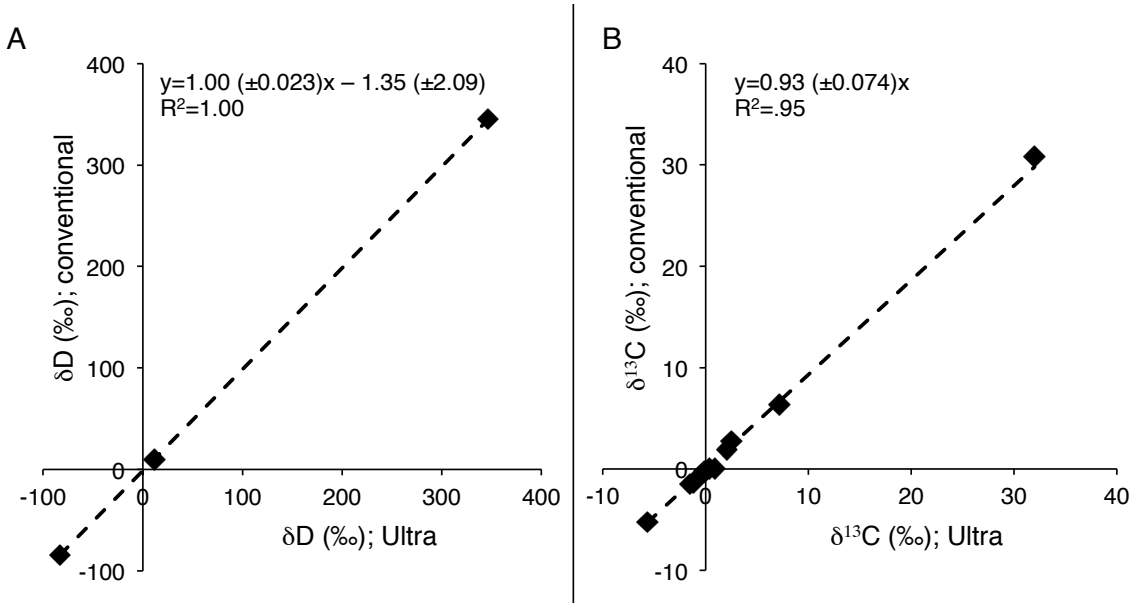

Figure 4 Comparison of bulk isotopic measurements made on the Ultra and through conventional techniques for δD (Fig. 4a) and $\delta^{13}C$ measurements (Fig. 4b). Conventional δD measurements were made through conversion of CH_4 to H_2 while conventional $\delta^{13}C$ measurements were made through conversion of CH_4 to CO_2. For 4b no intercept is given as the fit was forced through the origin — see text for details.

One methane sample is used as the internal standard for the Ultra, leaving only three independent comparisons between the two techniques. All samples are shown on the VSMOW scale. In order to establish our accuracy, we linearly regressed δD values of samples measured using the offline uranium-reduction method (y-axis; Fig. 4a) against our measured δD values from the Ultra from the same samples (x-axis). These

regressions are weighted regressions and incorporate the error in the conventional measurements, which vary from sample to sample. The slope of the line is 1.00 ± 0.023 (1 standard deviation, σ) and the intercept is -1.35 ± 2.09 (1σ); the best fit line is thus indistinguishable within 1 standard deviation from a line with a slope of 1 that passes through the origin.

Conventional $\delta^{13}C$ values were measured at Petrobras's research laboratories, the Power Environmental Energy Research Institute (PEERI), or at Indiana University. At Petrobras and PEERI, measurements were made by introducing a sample to a gas chromatograph coupled to an online combustion furnace with helium as the carrier gas, combusted to CO_2 and measured in continuous flow mode on a mass spectrometer. At Indiana University, samples were processed as above and the CO_2 measured in dual-inlet mode on a mass spectrometer. Two of these three labs (PEERI and Indiana University) analyzed our internal reference standard, letting us evaluate the ability of our approach to recover differences in $\delta^{13}C$ based on direct comparisons to common standards; in these cases, we report the measured difference between a given sample and this standard. Our internal standard was not analyzed by Petrobras's lab, raising the possibility that their measurements do not conform to a common reference frame with the others. To account for this, we compare our $\delta^{13}C$ values to those measured at Petrobras through comparison to the sample closest to the average $\delta^{13}C$ value of those samples. In other words, we treat this sample as the internal standard for this data set (only). This treatment is needed to compare the data, but implicitly requires that the standard is identical for both techniques. Thus, in our regression, we must enforce an intercept of zero. Regressing the values generated with conventional techniques (Fig. 4b; y-axis) against those derived on the

Ultra (Fig. 4b; x-axis) with an intercept of zero results in a line with a slope of 0.93 ± 0.074 (1σ). This slope is statistically indistinguishable from a 1:1 line. This regression is again a weighted regression and includes the errors from the conventional measurement, which vary depending on the technique. Overall, the bulk isotopic ratios measured by Ultra and conventional techniques are within error of each other and we conclude that the Ultra is capable of making measurements that are on the same isotopic scale as conventional $\delta^{13}C$ and δD measurements of methane.

3.2 Mass 18

The mass-18 mass spectrum (measured on an electron multiplier) visibly contains $H_2{}^{16}O^+$, $^{13}CH_3D^+$, and $^{13}CH_5^+$ (Fig. 2b; note we do not display $H_2{}^{16}O^+$ due to its large size, ~100,000 counts per second at high resolution). Additionally, though not visible at the plotted scale, $^{12}CH_2D_2^+$ and $^{12}CH_4D^+$ are present and are significant factors in the interpretation of our measurements. $H^{17}O^+$, $D^{16}O^+$, $^{15}NH_3^+$, $^{14}NH_4^+$ and fragments of heavier methane isotopologues such as, $^{13}CHD_2^+$ must also be present but are either fully mass resolved or sufficiently low in abundance (e.g., $^{13}CHD_2^+$<0.01%) as to be negligible factors. Ions derived from isotopologues of water and ammonia are fully resolved from methane ions at the medium-resolution setting of the instrument (mass resolving power of 16,000-17,000; 16 μm entrance slit). Thus our measurement of the mass-18 ion current includes signals from the $^{13}CHD_2^+$ fragment, which we ignore, the isotopologues of interest, $^{13}CH_3D^+$ and $^{12}CH_2D_2^+$, and the H-adducts, $^{13}CH_5^+$ and $^{12}CH_4D^+$.

$^{13}CH_3D^+$ can be mass-resolved from $^{13}CH_5^+$ and $^{12}CH_2D_2^+$ at the highest-resolution setting of the instrument (mass resolving power of 20,000 using a 5 μm entrance slit) as demonstrated in Fig. 2b. We have performed measurements of the

$^{13}CH_3D^+/(^{13}CH_4^+ + ^{12}CH_3D^+ + ^{12}CH_5^+)$ ratio, which is a direct constraint on $^{13}CH_3D$ abundance when accompanied by the measurements of mass-17 species described above, with an internal precision as good as ±0.43‰ (1σ) and similar to the counting statistics limit for that measurement of 0.35‰. However, there are several advantages to measuring at the high-mass side of the peak in Fig. 2b (near mass 18.053), where the ion currents of $^{13}CH_3D^+$ and $^{12}CH_2D_2^+$ are combined along with the adducts, $^{12}CH_4D^+$ and $^{13}CH_5^+$. First, this approach minimizes potential contributions from $^{15}NH_3^+$ or $^{14}NH_4^+$ that are not clearly visible in Fig. 2b but must be present, based on observations at mass 17 (Fig. 2a). Second, it minimizes potential contributions from the 'tailing' of the water peak. And third, it can be made at the medium-resolution setting of the Ultra, which provides a threefold increase in transmission as compared to the high-resolution setting and thus allows for shorter integration times. For these reasons, we include in the mass-18 ion current $^{13}CH_3D^+$, $^{13}CH_5^+$, $^{12}CH_2D_2^+$, and $^{12}CH_4D^+$. We correct for the contributions from adducts at mass 18 in a manner similar to that for mass-17 species. The details of this correction are provided in Appendix B.

We make measurements of mass-18 methane isotopologues using a secondary electron multiplier with typical signal intensities of ~20,000 counts per second. A dead time of 40 nanoseconds is applied to this amplifier. Consequently, a precision of ±0.3‰ for Δ_{18} measurements requires integration times of ~1200 seconds for both the sample and standard such that their counting statistics errors, added in quadrature, sum to 0.3‰.

4. Analytical procedures

We outline here how each measurement is made on a daily basis. This material is presented in greater detail than is common in published reports of isotopic measurements because this is a new method. All measurements are made in reference to our laboratory's standard 'working' reference gas reference ('wg') taken from a high purity (>99.999%) gas cylinder purchased from Air Liquide America. The reference gas's δD and $\delta^{13}C$ values were calibrated at Indiana University as described above. The procedures outlined below are also provided in a schematic flow chart (Fig. A3) in the appendix.

4.1 Measurement of $^{12}CH_3D^+/(^{12}CH_4^+ + ^{13}CH_3^+ + ^{12}CH_2D^+)$

The Ultra's detector array is first configured to measure the ratio, $(^{12}CH_3D^+ + ^{12}CH_5^+)/(^{12}CH_4^+ + ^{13}CH_3^+ + ^{12}CH_2D^+)$, which is a key constraint on the δD value of the sample. We quantify this measurement, after removing the contribution of $^{12}CH_5^+$ to the measured signal using an adduct line (see above), with δ and R notations similar to δD and ^{D}R. Specifically, the ratio, $^{12}CH_3D^+/(^{12}CH_4^+ + ^{13}CH_3^+ + ^{12}CH_2D^+)$ in the sample vs. in the standard working reference gas ('wg'), is expressed via the symbol δ^{12CH3D} where $\delta^{12CH3D} = [^{12CH3D}R_{sample}/^{12CH3D}R_{wg}-1]*1000$ and $^{12CH3D}R = ^{12}CH_3D^+/(^{12}CH_4^+ + ^{13}CH_3^+ + ^{12}CH_2D^+)$. The denominator of $^{12CH3D}R$ is the mass-16 signal and is dominated by $^{12}CH_4^+$ (99%) but also contains contributions from the fragments, $^{13}CH_3^+$ and $^{12}CH_2D^+$. Because $^{12CH3D}R$ includes contributions from both $^{12}CH_3D^+$ and $^{13}CH_4^+$ (via the fragment $^{13}CH_3^+$), we need a second, independent measurement of $^{13}CH_4$ vs. $^{12}CH_4$ to fully constrain the $^{12}CH_3D/^{12}CH_4$ abundance and thus calculate the δD value. This additional measurement is described in section 4.2. However, to first order, a sample's δD value and precision are controlled by its δ^{12CH3D} value and precision. We correct for the methane fragments,

$^{13}CH_3^+$ and $^{12}CH_2D^+$, in the denominator of $^{12CH3D}R$ during data processing (see Appendix A).

Mass-16 species are collected in a Faraday cup registered through a feedback electrometer employing a nominal 10^{10} Ω feedback resistor (hereafter 10^{10} amplifier) on one of the Ultra's moveable collector trolleys. The sum of $^{12}CH_3D^+$ + $^{12}CH_5^+$ at mass ~17.05 is collected in a Faraday cup registered through 10^{12} amplifier on the central, fixed collector position. The mass spectrometer is set to high resolution (~20,000-25,000 mass resolving power) by using a 5 μm entrance slit in order to generate a flat shoulder in the mass spectrum at ~17.05 amu (Fig. 2). At the beginning of an analytical session, typically once per day, the H-adduct correction is calibrated using the working reference gas on this feature with, generally, 6 points that span ~0.7 to 1.9 V on mass 16 (Fig. A1). The intercept of this calibration measured for the working reference gas is the '$^{12CH3D}R_{wg,int}$' value referred to below. We will show that variations in $^{12CH3D}R_{wg,int}$ values control small (~1%, relative) compressions or expansions of the scale of measured δ^{12CH3D} values within and between analytical sessions. $^{12CH3D}R_{wg,int}$ is the primary variable we examine when we calibrate a uniform reference frame for reporting absolute δ^{12CH3D} values and, thus, absolute δD values.

Measurements are organized into 'blocks' referred to as acquisitions. We start each acquisition by manually balancing the sample and standard bellows such that the ion current at mass 16 for both is 1.3 V, which corresponds to ~100 mV at mass 17. Next, the background signal for each mass is measured manually off-peak at ~16.3 and 17.3 amu with the standard gas flowing into the source. The sample and standard gases are then measured in 10 cycles composed of 15 s integration times and 15 s idle times. Finally,

background signals are measured again as before, averaged with the initial background, and subtracted from the measured voltages. We usually perform 7 acquisitions at which point the standard error of all of the acquisitions approaches 0.10-0.12%. Measurement uncertainty approaches and follows the combined Johnson noise (John and Adkins, 2010) and counting statistics limit (Merritt and Hayes, 1994; Fig. A2a).

4.2 Measurement of ($^{13}CH_4^+$ + $^{12}CH_3D^+$)/($^{12}CH_4^+$ + $^{13}CH_3^+$ + $12CH_2D^+$) and ($^{13}CH_3D^+$ + $^{12}CH_2D_2^+$)/($^{12}CH_4^+$ + $^{13}CH_3^+$ + $^{12}CH_2D^+$)

After measuring the $^{12}CH_3D^+/(^{12}CH_4^+ + ^{13}CH_3^+ + ^{12}CH_2D^+)$ ratio, we replace the high-resolution entrance slit with the 16 μm medium-resolution entrance slit, achieving ~16,000-17,000 mass resolving power, and make a measurement that simultaneously collects ions at mass 16 (as above), the sum of $^{13}CH_4^+ + ^{12}CH_3D^+ + ^{12}CH_5^+$ at mass 17 (near ~17.045 amu in Fig. 2a), and the sum of $^{13}CH_3D^+ + ^{12}CH_2D_2^+ + ^{13}CH_5^+ + ^{12}CH_4D^+$ at mass 18 (near ~18.053 amu in Fig. 2b). The measurements are again quantified using δ and R values. For this mass-17 measurement, we first subtract the contribution of $^{12}CH_5^+$ from the measured signal using an adduct line (see above). We then quantify ratio of $(^{13}CH4^+ + ^{12}CH_3D^+)/(^{12}CH_4^+ + ^{13}CH_3^+ + ^{12}CH_2D^+)$ for the sample vs. the standard working reference gas with the symbol $\delta^{12CH3D+13CH4}$, where $\delta^{12CH3D+13CH4} = (^{12CH3D+13CH4}R_{sample}/^{12CH3D+13CH4}R_{wg}-1)*1000$ and $^{12CH3D+13CH4}R = (^{13}CH4^+ + ^{12}CH_3D^+)/(^{12}CH_4^+ + ^{13}CH_3^+ + 12CH_2D^+)$. This ratio is dominated by the abundance of $^{13}CH4^+$ and provides the first order control on the $\delta^{13}C$ value and precision of a sample — however the δ^{12CH3D} is required to actually calculate the $\delta^{13}C$ value (see below and Appendix A). The presence of the fragments in the measurement of mass 16 is corrected for during data processing (Appendix A).

We quantify and represent the mass-18 measurements similarly. First the contribution of the adducts $^{13}CH_5^+$ and $^{12}CH_4D^+$, to the mass-18 signal are subtracted using an adduct line (Appendix B). We then quantify the ratio of ($^{13}CH_3D^+$ + $^{12}CH_2D_2^+$)/($^{12}CH_4^+$ + $^{13}CH_3^+$ + $^{12}CH_2D^+$) in the sample vs. in the standard working reference gas with the symbol δ^{18}, where δ^{18} = ([$^{18}R_{sample}$/$^{18}R_{wg}$-1]*1000 and ^{18}R = [$^{13}CH_3D^+$ + $^{12}CH_2D_2^+$]/[$^{12}CH_4^+$ + $^{13}CH_3^+$ + 12CH_2D^+]). The precision of a δ^{18} measurement controls the ultimate precision of a sample's Δ_{18} value.

Masses 16 and 17 are collected in the same Faraday cups registered through the same amplifiers as above. Mass 18 is measured on a secondary electron multiplier on a moveable collector trolley. The H-adduct corrections are calibrated on the working reference gas with 6 points from ~3-7 V on mass 16 before the measurements are made. The intercept of this adduct line calibration for the mass-18 measurements is the '$^{18}R_{wg,int}$' value referred to below. We will show that variations in $^{18}R_{wg,int}$ values control small (~1%, relative) compressions or expansions of the scale of measured δ^{18} values within and between analytical sessions. $^{18}R_{wg,int}$ is the primary variable we examine when we calibrate a uniform reference frame for reporting absolute δ^{18} values.

Measurements are again organized into acquisition blocks. First the source pressures are balanced using the bellows as above such that the signal at mass 16 for both the sample and standard registers 4 V, which results in mass-17 signals of ~4.5 V and mass-18 signals of ~20,000 counts per second (cps). Background signals are manually measured at ~16.3, 17.3, and 18.3 amu with the standard gas flowing to take into account the presence of scattered ions, which range from ~300-700 cps at mass 18. We measure the background of the standard gas before and after each acquisition to determine an

average and subtract that number from both the sample and standard measurements. Acquisition parameters are the same as above. We measure until the internal precision of δ^{18} approaches 0.25‰ (~15 acquisitions). Measurement errors for $\delta^{12CH3D+13CH4}$ approach 0.005‰. Both the $\delta^{12CH3D+13CH4}$ and δ^{18} measurements follow counting statistics (Fig. A2b,c).

With measured values for δ^{12CH3D}, $\delta^{12CH3D+13CH4}$, and δ^{18} the values and precisions for δD, $\delta^{13}C$, and Δ_{18} measurements can be calculated for a sample. The equations required for these calculations are provided in Appendix A. Generally, the internal precision achieved for δD measurements is 0.10-0.12‰, for $\delta^{13}C$ is 0.005‰, and for Δ_{18} is 0.27-0.29‰. Additionally, unless otherwise noted, all Δ_{18} values are reported relative to a reference frame in which the Δ_{18} value of our laboratory's working reference gas is assumed to be zero; i.e., $\Delta_{18,wg} = 0$ where 'wg' refers to the laboratory's working reference gas. In section 7 of this paper we develop a universal reference frame based on the analyses of gases equilibrated at known temperatures, demonstrating that a $\Delta_{18,wg}$ value of 0 corresponds to a Δ_{18} value relative to random isotopic distribution of +2.981‰.

5. Sample manipulation

Dual-inlet stable isotopic measurements generally require relatively pure (>99%) samples. As methane is never (to the authors' knowledge) the direct analyte for mass-spectrometric stable isotopic measurements, samples are generally purified from contaminants only after being converted to either CO_2 or H_2. We, however, require pure methane samples. To that end, we developed techniques for its concentration, purification

and storage without isotopic fractionation. If methane must be separated from other components of a natural gas sample, such as other hydrocarbons or H_2, methane is first frozen into a helium-cooled cryostat (CTI-Cryogenics and Janis Research Co.) set to 20 K. Residual gas is pumped away and the cold trap closed. The cold trap is warmed to 40 K, allowed to equilibrate for 2 minutes, and then the sample is exposed to vacuum for 2-3 minutes. Methane has a low vapor pressure at 40 K (~1 mPa) and thus little is lost. The cold trap is again closed and then warmed to 45 K, allowed to equilibrate for 2 minutes, and finally the sample is exposed to vacuum for 2-4 minutes. Methane has a larger vapor pressure at 45 K (25 mPa), but trial experiments demonstrate that pumping for 4 minutes at this temperature causes a negligible isotopic fractionation (see below). The cold trap is then warmed to 70 K, allowed to equilibrate for 2 minutes and then the sample is released from the trap (leaving more condensable compounds behind), condensed onto molecular sieves in a Pyrex® break seal (see below), and sealed with a natural gas torch. Gases removed at 20 K include helium and hydrogen. Oxygen and nitrogen are removed at 40 and 45 K. Ethane and larger hydrocarbons are retained at 70 K. Purified methane samples are stored in Pyrex® break-seals. To condense methane into the break-seals, type 5A molecular sieves (1/16 inch; EM) are used. Sieves are preheated under vacuum using a natural gas torch until baseline pressures are reached (typically <10 mPa). Samples are then condensed onto the sieve by cooling the break-seals in liquid nitrogen. Samples are released from the sieves by heating tubes for ~2 hours using a heat gun set to 150°C. Samples are then introduced into the bellows of the mass spectrometer with the sieve being continually heated. After the break-seal tube is cracked and gas has expanded into

the bellows, the bellows are cycled from 100% to 30% open 25 times to ensure the methane is well mixed (Yeung et al., 2012).

We conducted a series of tests to ensure that our sample handling does not affect the measurements. Samples were measured directly from a bottle of pure gas (i.e., without vacuum line manipulation or condensation into a break seal), frozen onto a sieve and released into the mass spectrometer's bellows without heating above room temperature, frozen onto a sieve and released with heating (i.e., our normal break-seal procedure), frozen into the 20 K trap and pumped for 2 minutes at both 20 and 40 K, then 4 minutes at 45 K, and then transferred to the mass spectrometer using our usual break-seal procedure as described above. The results of these experiments are presented in Table 4. Use of the sieve and heating of the sample during its release from the sieve does subtly shift the measured $\delta^{13}C$ value by 0.1‰ and δD value by 0.5‰. Importantly for our purposes, though, no significant shift is observed in $\Delta_{18,wg}$ values (within 0.05‰; Table 4). We repeated this comparison of gas directly from a bottle vs. that released from a sieve and found offsets of 0.04‰ in δD (identical within error), 0.08‰ in $\delta^{13}C$, and 0.18‰ in Δ_{18} (identical within error). Consequently, it appears the Δ_{18} values are not disturbed within error through use of the sieve, and any fractionations of bulk isotopic compositions are subtle. We conclude that storage and retrieval of samples on and from molecular sieves preserves the Δ_{18} signature with minor changes to the bulk isotopes.

Freezing samples into the helium-cooled cryostat, pumping, then freezing onto a molecular sieve and releasing with heating does not change the bulk isotopic or $\Delta_{18,wg}$ values within the 1σ error of the measurements as compared to not pumping but still freezing onto a sieve and releasing with heating. Failure to heat samples while releasing

from the molecular sieves changes $\delta^{13}C$ by -1.4‰, δD by -1.2‰ and $\Delta_{18,wg}$ by 0.49‰, demonstrating the need to heat gases to fully release them with minimal fractionation. This may reflect a sorption isotope effect associated with the retention of a fraction of methane on the molecular sieve at room temperature.

6. Experimental reproducibility

The internal precision associated with mass spectrometric acquisitions (described above) determines the minimum possible error of a measurement. However, experimental uncertainties associated with analyses of unknown samples may be larger due to random or systematic errors during purification, gas handling, changes in accuracy in the mass spectrometric standardization scheme, or other unknown factors. This is a particular concern for clumped isotope analyses of methane because we seek to achieve errors in Δ_{18} of <0.3‰ — which is better than the analytical uncertainties in conventional measurements of δD of methane and other organic compounds that have typical external precisions of ~1.8‰, 1σ (Dai et al., 2012). Consequently, we must establish our external reproducibility both within a single analytical session and over the course of multiple, separate sessions in order to fully document the real precision of our measurements. Note that the complexities we explore in this section are second order phenomena; our measurements of $\delta^{13}C$ and δD are accurate to within the precision of conventional techniques without the corrections discussed here.

We demonstrate below that the key factors that control our reproducibility both within and between analytical sessions are small variations in the $^{12CH3D}R_{wg,int}$ and $^{18}R_{wg,int}$ values — the intercepts of the adduct lines generated each day (see above). We

show that measurements made days or even many months apart can be mutually standardized to within very narrow limits by normalizing the measurements based on differences in their respective R_{wg} values. We explain this procedure by first demonstrating experimental reproducibility within a single measurement session (generally 1-3 weeks), and then apply the same concept to the problem of external reproducibility between sessions months apart.

6.1 Intrasession reproducibility

Within a single analytical session (~1-3 weeks), we notice that on replicate analysis, a sample's measured δ^{12CH3D} value and δ^{18} value are linear functions of the intercepts of the adduct lines, $^{12CH3D}R_{wg,int}$ and $^{18}R_{wg,int}$, used to correct those samples for H-adducts (Fig. 5). Importantly, the slopes of the lines in Fig. 5 imply that measured δ^{12CH3D} and δ^{18} values decrease in direct proportion to increases in the $R_{wg,int}$ value; i.e., if $R_{wg,int}$ increases by 1% relative, the δ value decreases by 1% relative. This relationship is seen in samples with compositions varying by over 150‰ in δD and 29‰ in $\delta^{13}C$.

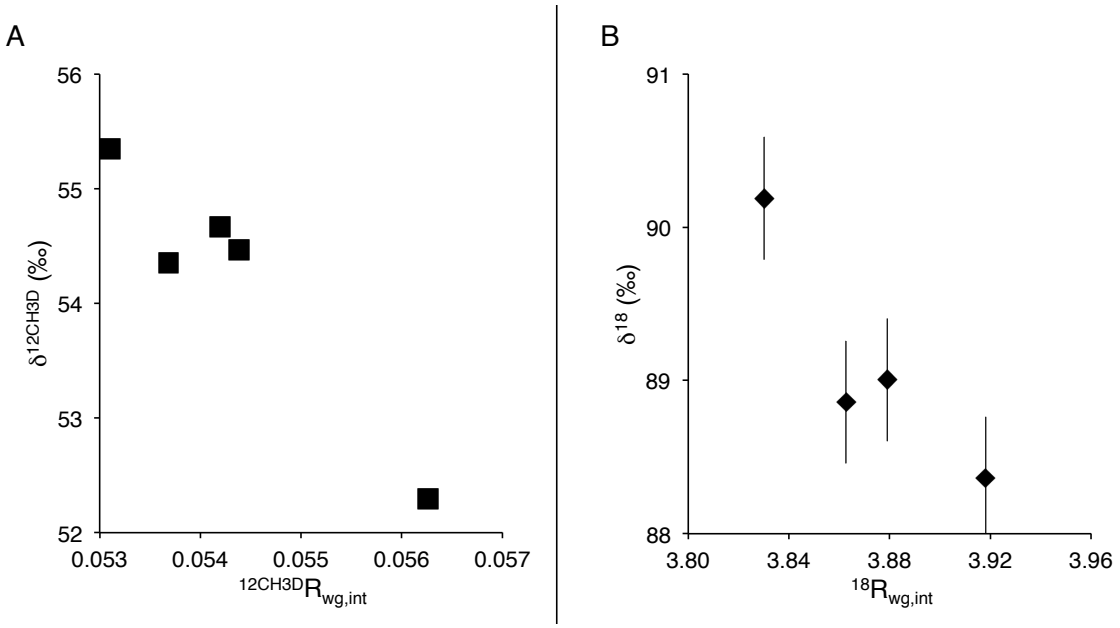

Figure 5. Dependence of the δ value of a sample on the $R_{wg,int}$ value of the adduct line (the intercept) generated for each individual measurement using the working reference gas. In both 5a and b, all measurements have been made on aliquots of the same sample over multiple days. The linear dependence of the measured δ on the $R_{wg,int}$ is likely created due to slight inaccuracies in the adduct lines used to remove the contribution of $^{12}CH_5^+$ from the measurement of δ^{12CH3D} and $^{13}CH_5^+$ and $^{12}CH_4D^+$ from the measurement of δ^{18}. Correction to a constant $^{12CH3D}R_{wg}$ and $^{18}R_{wg}$ for each measurement in an analytical session (generally 1-3 weeks) can be made such that the internal and external precisions of the measurements overlap and these dependencies disappear. See text for a full explanation. A) Dependence of δ^{12CH3D} on $^{12CH3D}R_{wg,int}$. B) Dependence δ^{18} on $^{18}R_{wg,int}$.

1

Regardless, we correct for this artifact by normalizing the data generated in each session to a constant value for $^{12CH3D}R_{wg}$. We perform this normalization by multiplying the δ^{12CH3D} for each sample cycle of each acquisition by the average $^{12CH3D}R_{wg}$ for that cycle and then dividing by a constant assumed value of $^{12CH3D}R_{wg}$ that is used in all measurements in that analytical session. This procedure reduces the external precision of replicate analyses made in the same session to near the level of internal precision of each sample analysis. For the example in Fig. 5a, before correction, the standard deviation of the five δ^{12CH3D} measurements is 1.14‰. This is an unacceptably high standard deviation because, no matter how precise a δ^{18} value can be achieved, the external precision for a δD will be ~1.14‰. Consequently, the external precision for Δ_{18} will be at least 1.14‰,

which translates into a precision of ~±40°C at 25°C. Application of the correction outlined above reduces the standard deviation of δ^{12CH3D} to 0.18‰. In this example, the constant $^{12CH3D}R_{wg}$ used for the correction is the average $^{12CH3D}R_{wg,int}$ from all adduct lines measured up to February 2013 analytical session. With the exclusion of 1 measurement, the standard deviation of the four remaining samples is 0.08‰. This case is representative; generally external precisions for a single session for δ^{12CH3D} range from 0.07 to 0.18‰ — similar, but sometimes slightly larger than the internal precision of 0.1-0.12‰. No analogous correction is needed for measurements of $\delta^{12CH3D+13CH4}$, which has internal precisions, generally, of 0.005-0.006% and an external precision of ~0.020‰ — i.e., any increase in error due to this artifact is not important to the overall precision of Δ_{18}. A clear question is what is the correct $^{12CH3D}R_{wg}$ value that samples in an analytical session should be corrected to and does that value vary across analytical sessions. We address this question in more rigorous terms in the next section related to intersession reproducibility.

We interpret the correlation between δ^{18} and $^{18}R_{wg,int}$ in a single analytical session of a sample measured multiple times (Fig. 5b) to be caused for the same reasons given for the relationship between δ^{12CH3D} and $^{12CH3D}R$ above. Again, the errors of the slopes and intercepts for a given day generally overlap in error with the average values for the whole session. For the example in Fig. 5b, internal precisions of the δ^{18} measurements range from 0.3 to 0.4‰ with an average internal precision of 0.37‰ (we had not yet decreased our internal errors to 0.25‰ when the measurements represented in Fig. 5b were made). However, the standard deviation of the measurements, 0.77‰, is larger than the internal precision. If, however, we correct, as above, each cycle within an acquisition to a

constant $^{18}R_{wg}$ value and correct all samples using the sample $^{18}R_{wg}$ (in this case the average $^{18}R_{wg,int}$ for all adduct lines from that measurement session), the standard deviation of the δ^{18} values contracts from 0.77 to 0.33‰, similar to the average internal precision of 0.37‰ for these samples. Again, as before, it is not obvious what value to use for $^{18}R_{wg}$ when making this correction; we establish this in the next section.

6.2 Intersession reproducibility

The corrections described above work well for short timescales (weeks) for both δ^{12CH3D} and δ^{18}. However over many month time scales, during which there are filament changes, source bakes and venting of the mass spectrometer, external precision degrades when correcting all samples from different analytical sessions with the same $^{12CH3D}R_{wg}$ and $^{18}R_{wg}$ values. For δ^{12CH3D} measurements, differences up to ~1‰ between sessions are seen for samples ~200‰ different in δ^{12CH3D} than the working reference gas, with smaller differences for samples that are more similar to the standard in bulk composition. For δ^{18} measurements, deviations up to 1‰ are seen between sessions for δ^{18} values ~100‰ different from the working reference gas, with smaller deviations if samples are more similar to the standard in δ^{18}.

We examined whether these intersession variations are caused by changes in the instrumental mass bias, i.e., changes in the measured $^{12CH3D}R_{wg}$ value that arise from differences in fractionation in the ion source, detector efficiency, or other time-varying instrument properties. If so, it should be possible to correct for such artifacts by adopting a reference frame in which we assume a constant difference in δ value between two or more standards, which can be analyzed in each session and serve as a basis for 'stretching' or 'compressing' measured data to a constant long-term reference frame. Our

approach here draws on a common practice in conventional δD measurements (Hagemann et al., 1970), as well as many other measurements that attempt to observe relative differences between samples with high long-term precision. Here, we perform such a correction by adopting an assumed value for the difference in δ values between two standards (our working reference gas and a second reference material), and then test the success of our scheme by examining a third known material, which is analyzed and corrected as if it were an unknown sample.

For example, in a session run in September 2012, the average δ^{12CH3D} of a standard, 'standard 1,' was 227.97 ± 0.07‰ (n = 3, 1σ) and in February 2013 was 226.92 ± 0.12‰ (n = 1,1σ). 'Standard 2' had a δ^{12CH3D} of 56.41 ± 0.18‰ (n = 5,1σ) in September 2012, and 56.12 ± 0.11‰ (n = 3, 1σ) in February 2013, where n is the number of measurements. During the February session, we analyzed a variety of gases having independently known δD values. We varied the $^{12CH3D}R_{wg}$ value to which all measurements are corrected for this session to find the value that best fits all measured δD values to those already established by conventional analyses standardized to the VSMOW-SLAP scale. This yielded a value for $^{12CH3D}R_{wg}$ that is indistinguishable from the average measured intercept value of all adduct lines over all sessions up to that point, i.e., our average value for $^{12CH3D}R_{wg,int}$ yields a 'scale' for δD values that is indistinguishable from the VSMOW-SLAP scale.

Next, we rescaled our September 2012 data to the February 2013 session. To do this, we chose an $^{12CH3D}R_{wg}$ value for the September 2012 session that forces the average δ^{12CH3D} value for standard 1 data to be 226.92‰ (again, relative to our working reference gas). Importantly, this $^{12CH3D}R_{wg}$ value was chosen only by using standard 1. After

applying this $^{12CH3D}R_{wg}$ value to the measurement of standard 2 in September 2012, the average δ^{12CH3D} value for standard 2 becomes 56.15‰, indistinguishable from the value for February 2013 (56.12‰). Thus, even subtle inter-session variations in our δD scale can be removed through this procedure. We have tested this approach over the course of 1 year on standard 2 using standard 1 for the normalizations. Doing so yields a long-term external precision for δD of 0.11‰ (1σ) on 10 total measurements.

One implication of the success of this calibration of long-term accuracy is that the methods we present can be used to establish the δD values of methane samples with external precisions approximately an order of magnitude smaller than previous δD measurements of methane within a reference frame that asserts some axiomatic values of two or more methane standards. This could be useful for the study of hydrogen isotope variations in methane sources that are complex mixtures of sources but vary little in δD (e.g., the atmosphere). Generally, we find it best to anchor this long-term calibration of the accuracy of δD using standards with large absolute values of δ^{12CH3D} (100-200‰ greater than the working reference gas intralab standard) as they are more sensitive to scale compressions. This is the same reason that VSMOW and SLAP are used to calibrate scale compressions of conventional δD measurements.

We use a similar approach as above to correct for session-to-session variations in δ^{18} values of samples. However, unlike for δD measurements, there are no available gases with known δ^{18} values making it difficult to assign correct δ^{18} values to our standards as was done for the δ^{12CH3D} measurements above. Our solution to this problem is patterned after that taken to calibrate previously established clumped isotope measurements of CO_2 and O_2, which report data relative to a ‘stochastic reference frame’

(i.e., a state in which all isotopes are distributed randomly among all isotopologues). The accepted method for establishing this reference frame is to equilibrate gases at known temperatures and then assume that they have taken on the theoretically predicted equilibrium constants for reactions such as equations (1) and (5) at those temperatures. When these standards are equilibrated at very high temperatures, this is sometimes referred to as the 'heated gas reference frame' (Eiler and Schauble, 2004; Yeung et al., 2012). Note that an explicit assumption of these calibration methods is that statistical thermodynamic methods for calculating equilibrium constants for reactions such as equations (1) and (5) are accurate. Although we cannot externally establish whether these models are correct, this assumption has allowed multiple labs to share the same reference frame for clumped isotope measurements of CO_2 and thus have comparable measurements (Dennis et al., 2011).

One feature of such reference frames is that they can be experimentally generated by heating or otherwise equilibrating gases over a range of bulk isotopic compositions. This capacity has been crucial for permitting clumped isotope measurements of CO_2 and O_2 to match, or interpolate between the bulk compositions of samples and standards, to recognize and correct for any composition-dependent analytical artifacts, and to allow different labs and mass spectrometers to be mutually calibrated. We adopt a similar strategy to establishing the reference frame for clumped isotope analyses of methane. In particular, we analyze a set of gases that vary in $\delta^{13}C$ and, particularly, δD that have been equilibrated to a uniform temperature and thus should have a constant value of Δ_{18}.

In the February 2013 session we ran gases that were heated with catalysts at 500°C; we show below that this procedure internally equilibrates methane. We measured

samples with δ^{18} values varying by over 500‰ and all yielded $\Delta_{18,wg}$ values within error of each other when corrected to the average $^{18}R_{wg,int}$ value from the daily adduct line intercepts for that analytical session. Thus, as for the δD values measured in that session, the average $^{18}R_{wg,int}$ value measured in the February 2013 session for all adduct lines appears to yield an accurate scale for δ^{18} values of samples over a considerable range of values. Consequently, we consider the February 2013 session to be accurate in δ^{18} values and we correct our measurements using standards measured in the February 2013 session.

For example, in September 2012, standard 1 has a δ^{18} value of 226.38 ± 0.30‰ (n = 3, 1σ) while standard 2 is 89.99 ± 0.33‰ (n = 4, 1σ). In February 2013, standard 1 had a δ^{18} of 230.87 ± 0.28‰ (n = 1, 1σ) and standard 2 had a δ^{18} of 91.96 ± 0.02‰ (n = 2, 1σ). When we re-normalize these two sessions based on the difference in $^{18}R_{wg}$ values between their respective mass-18 adduct lines (such that the standard 1 δ^{18} average for September increases from 226.38‰ to the February 2013 value of 230.87‰), the standard 2 average value from September 2012 rises to 91.77‰, which is within 1σ of the February 2013 average of 91.96‰. We have used this correction scheme over 5 measurement sessions. Measurements of standard 2 have an external precision for Δ_{18} of 0.23‰ (10 measurements). Additionally, gases heated to 500°C have an external precision for Δ_{18} of 0.20‰ (10 measurements) over those same sessions. These data demonstrate that our external precision is equal to or better than our nominal internal precision of 0.27-0.29‰. Additionally, standard 2 and 500°C heated gases differ in their $\Delta_{18,wg}$ values by ~4 ‰. Thus, the heating of samples previously frozen onto molecular sieves at 150°C before introduction into the mass spectrometer does not cause significant internal re-equilibration of isotopes within methane.

It thus appears, that the schemes we describe for correcting for adducts and establishing accurate reference frames yield long-term external reproducibilities equal to or smaller than our internal precisions for the various measurements. Nevertheless, the complexity of this issue suggests that, as for most high-precision measurements, it is best to composition-match samples and standards as closely as possible to minimize all analytical artifacts.

7. Calibration of a methane clumped isotope thermometer

There are no previously demonstrated methods to internally equilibrate the isotopes of methane, which is needed to ensure accuracy and calibrate a clumped isotope thermometer. CO_2 can be equilibrated at high temperatures through heating in quartz glass at 1000°C for 2 hours (Eiler and Schauble, 2004). However, heating of CH_4 at 1000°C results in decomposition to H_2 and C with 50% loss of methane within 4 hours (Sackett, 1995). Additionally, even at these temperatures, it is not known if the sample will equilibrate its hydrogen and carbon isotopes either internally or with the graphite and hydrogen generated. Therefore, in order to generate samples with known clumped isotope compositions, we exposed methane gas to nickel catalysts at temperatures between 200-500°C. A similar method was used by Horibe and Craig (1995) to equilibrate the hydrogen isotopes of H_2 and CH_4 and by Horita (2001) to equilibrate the carbon isotopes of CO_2 and CH_4. We performed two experiments to examine whether these established procedures drive methane to an internal equilibrium. First we performed a bracketing experiment in which samples with varying bulk isotopic and starting Δ_{18} values were all heated to 500°C to ensure samples all converge to the same Δ_{18} value at the same

temperature. Second, we performed a series of heating experiments from 200-500°C to see whether Δ_{18} values have the same temperature dependence as predicted by theory.

For all heating experiments, we condensed samples in Pyrex® tubes on 5A molecular sieves along with a nickel catalyst (65 wt. % nickel dispersed on a silica/alumina support; 190 m^2/g; Sigma Aldrich). Samples were heated for the given time periods (Table 5) in a box furnace, directly adjacent to a calibrated thermocouple in the furnace. Additionally, the catalyst was packed at the tip of the tube and held in place with glass wool to minimize the importance of any thermal gradients that exist in the box furnace. We quenched samples in ~1 minute to room temperature with a flow of air from a fan. Samples were then recovered, purified and analyzed following the procedures above. Sample purification is necessary as methane always forms H_2 due to catalytic decomposition. We observe this H_2 as a measurable residual vapor pressure in the vacuum line at 20 K. Generally, ~1/2 of the starting methane converts to H_2 over the course of our heating experiments at 500°C, with less at lower temperatures.

To perform a bracketing experiment, we first created samples of methane that differed markedly in Δ_{18} from both our intralaboratory reference gas and expected equilibrium compositions by mixing aliquots of our intralaboratory reference gas with small amounts of synthetically enriched methane comprised of 99% $^{12}CH_3D$ (Sigma Aldrich). This spike caused δD values to increase and Δ_{18} values to decrease relative to the references gas but changed the $\delta^{13}C$ by <1‰ (Table 5 and Fig. 6). Mixing alters Δ_{18} values due to the curvature of the random reference frame ($^{18}R^*$) as a function of isotopic composition — full explanations of this effect can be found in Eiler and Schauble (2004)

and Eiler (2007, 2013). Mixtures were exposed to nickel catalysts at 500°C for 3-4 days, following the procedure outlined above.

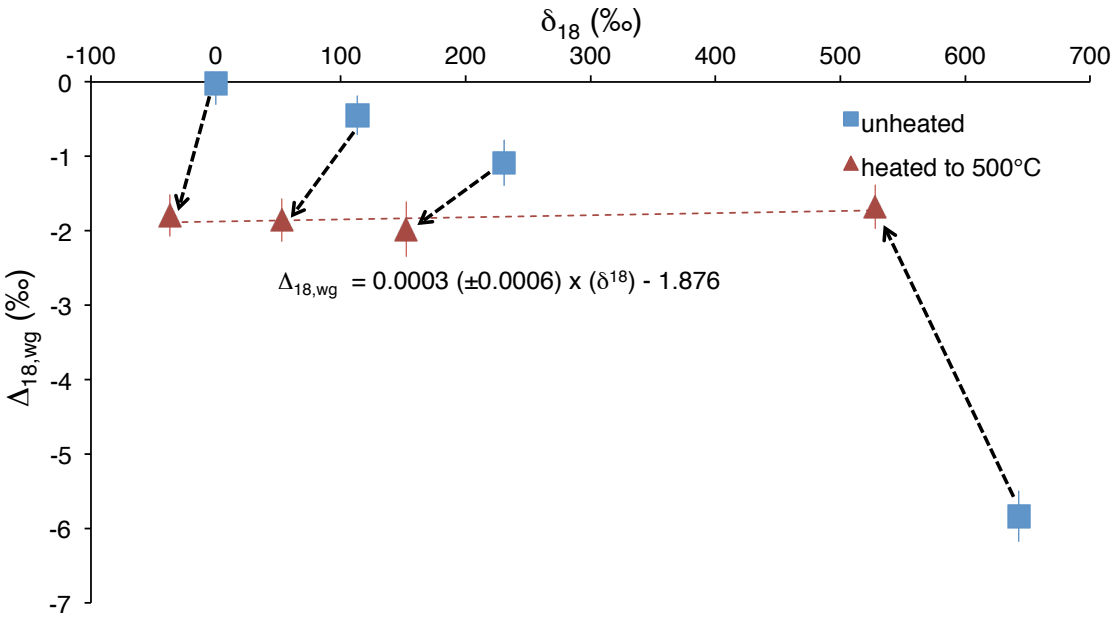

Figure 6. Bracketed heating experiments at 500°C. Samples of methane with varying Δ_{18} and bulk isotopic compositions were heated at 500°C in the presence of a nickel catalyst. The bulk isotopic composition is tracked through δ^{18} values and all samples are referenced such that the working reference gas is defined to have a $\Delta_{18,wg} = 0$. For these samples, the changes in δ^{18} are controlled dominantly by changes in the concentration of D in each sample. All heated samples converge to the same value $\Delta_{18,wg}$ value (~-2‰), within error. Additionally, there is no statistical dependence on the bulk isotopic compositions (tracked through δ^{18}) and $\Delta_{18,wg}$ values.

The isotopic compositions of gases before and after heating are presented in Table 5 and Fig. 6. The horizontal axis of Fig. 6 tracks the overall bulk composition of the gas with higher δ^{18} values signifying an increase in δD and/or $\delta^{13}C$. For these experiments, δ^{18} mostly tracks the increase in δD from the addition of the labeled $^{12}CH_3D$ to the experiments. Note that after heating the residual methane is lower in both δD and $\delta^{13}C$ values compared to their starting compositions. These changes are surprising because any kinetic isotope effects associated with methane decomposition and the exchange equilibrium between methane and generated H_2 should serve to enrich the residual

methane in heavy stable isotopes. Though we do not know precisely the reason for the lowering of δD and $\delta^{13}C$ values of methane over the course of the experiments, a potential cause could be interactions between methane in the gas phase and that sorbed on the nickel catalyst or partially dehydrogenated methyl groups (e.g., Ni-CH_3, Ni-CH_2, etc.). If these species were to be enriched in D and ^{13}C at equilibrium, then the bulk methane would be depleted. Exchange with water vapor or other unknown species contained on the glass wall could also result in isotopic changes. Regardless, as long as internal equilibrium is reached, the precise cause of the depletion in bulk composition is unimportant.

The data presented in Table 5 and Fig. 6 demonstrate two key aspects of the measurements: (1) heating of samples with different starting Δ_{18} values — both above and below the measured final value — generate the same final $\Delta_{18,wg}$ value; and (2) for samples heated to the same temperature, there appears to be no dependence of Δ_{18} on bulk isotopic composition, as reflected by the slope of the δ^{18} vs. Δ_{18} line in Fig. 6, which is 0.0003 ± 0.0006 (1σ) and thus indistinguishable from zero. Thus, for samples equilibrated to the same clumped composition, our measurement of Δ_{18} of methane is, within the error of the measurement, independent of differences in bulk isotopic composition (i.e., $\delta^{13}C$ and δD values). This is distinct from measurements of Δ_{47} of CO_2, which typically have slopes of 0.01 to 0.02 in analogous dimensions (Huntington et al., 2009) and Δ_{36} measurements of O_2 which have slopes of ~-0.06. This difference may reflect the fact that our measurements make use of a background correction that takes into account scattered or secondary ions, whereas conventional clumped isotope measurements of CO_2 do not (although clumped O_2 measurements do attempt to take this

into account); scattered secondary ions have been suggested as the cause of the dependence of uncorrected Δ_{47} values on bulk isotope compositions for measurements of clumped isotopes in CO_2 (Bernasconi et al., 2013; He et al., 2012).

A potential issue with the experiments above is that the results are dependent on the $^{12CH3D}R_{wg}$ and $^{18}R_{wg}$ values used to normalize the data. If different numbers were chosen, then the line in Fig. 6 could have a slope. However, the $^{12CH3D}R_{wg}$ value used to correct the measurements was chosen independent of the clumped isotope measurements in Fig. 6 — instead it is used only to correct our measurements so that they adhere to the VSMOW-SLAP scale. The $^{18}R_{wg}$ value used to correct the measurements in Fig. 6 is the average value of the intercept for all mass-18 vs. 16 adduct lines made during that analytical session ($^{18}R_{wg,int}$). This demonstrates that our choice in value for $^{18}R_{wg}$ to correct all samples is the session average for that value and independent of the results of the heating experiments. Consequently, we suggest that we are justified in our choices of $^{12CH3D}R_{wg}$ and $^{18}R_{wg}$ used for the corrections independent of the bracketing experiment in Fig. 6. This experiment has been repeated three additional times, all in different sessions, though over smaller isotopic ranges in δ^{18} of 80‰. Measurements of samples with an average δ^{18} value of -11.8 ± 2.3‰ (n = 3; 1σ) have Δ_{18} values of -2.10 ± 0.22‰ (1σ). Measurements of samples with an average δ^{18} value of 69.4 ± 8.4‰ (n = 3; 1σ) have Δ_{18} values of -2.06 ± 0.25‰ (1σ) and thus have Δ_{18} values that are indistinguishable statistically from the heated gases with lower δ^{18} values. Thus, use of the correction scheme outlined above not only causes standards to give reproducible values across months of time, but also allows for a stable, external, and experimentally derived heated gas reference frame.

We also internally equilibrated methane at temperatures varying from 200 to 500°C in order to experimentally calibrate the methane clumped isotope thermometer. These data were generated in two separate sets of experiments. One set of experiments was evaluated before we fully understood the importance of 2-hour long heating during extraction of methane from molecular sieves. The second set of experiments included this heating step. We corrected the samples that were not heated during removal from the molecular sieves by subtracting 0.49% from the $\Delta_{18,wg}$ values of measurements — i.e., the measured offset between samples heated during recovery from molecular sieve and those recovered without heating (see above). Though exclusion of these data does not significantly change our calibration, we include all data here, both for completeness and because it illustrates the apparent consistency of the fractionation on the molecular sieve.

Table 6 presents the compiled results of heating experiments between 200 and 500°C (along with the heating durations). The samples show a clear trend of decreasing Δ_{18} with increasing temperature, as expected from theory (Fig. 1). In order to directly compare the experimental data to the theoretical model, we must account for the fact that our working reference gas standard (i.e., intralaboratory reference gas) is highly unlikely to have a Δ_{18} value of zero; i.e., our measurements, as presented so far, reflect differences between gases equilibrated at known temperatures and this gas. When the average measured Δ_{18} value at each temperature is compared to the expected theoretical value (Fig. 7a), the data define a linear trend with a slope of 1 and an x intercept of 2.981 ± 0.015‰ (1σ). This line is found through a weighted regression of the measured $\Delta_{18,wg}$ values (incorporating their error) against the theoretical Δ_{18} values with the requirement that the slope equal 1. Assuming that the there are no intrinsic errors in the theoretical

line, this implies that the intralaboratory reference gas has a 'true' Δ_{18} value of +2.981‰ relative to a random isotopic distribution.

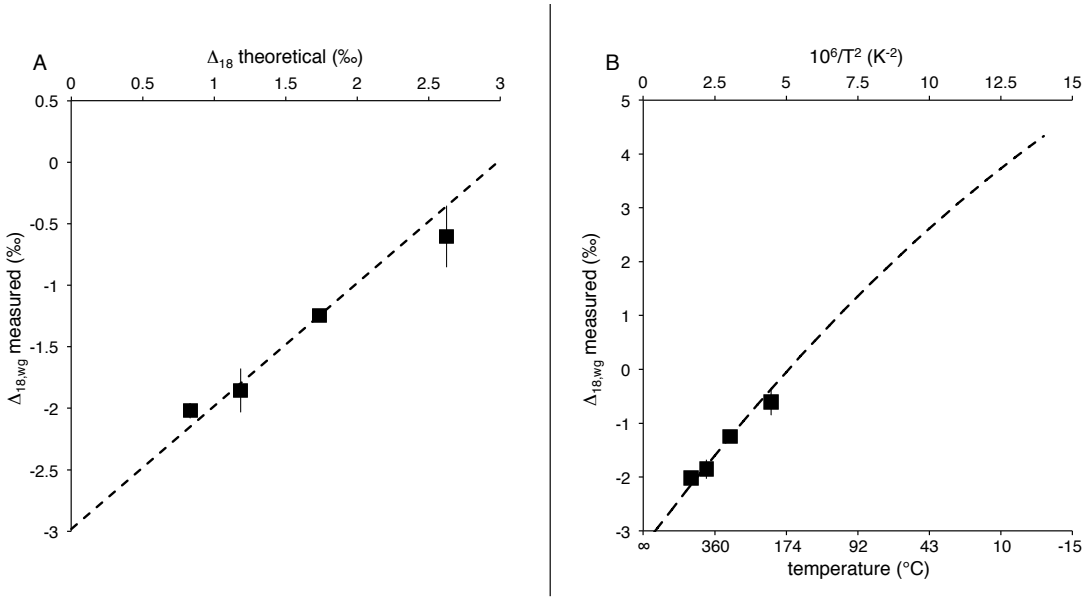

Figure 7. Heating experiments from 200-500°C. Samples were heated with a nickel catalyst for varying amounts of time (Table 5). Each point represents an average of experiments if multiple samples were measured. A) Comparison of measured values vs. theoretically expected values for equilibrium. A 1:1 line has been fit through the data. Data are offset from the origin as all samples are measured relative to a working reference gas, which has a real, but unknown Δ_{18} value. If this line is used to find that value, the standard has a Δ_{18} value of ~2.981‰, or 170°C. B) Experimentally derived $\Delta_{18,wg}$ vs. temperature calibration. 2.981‰ has been subtracted from the theoretical line to account for the difference between the theoretical and working gas reference frames.

A question is whether or not the plot of measured vs. expected Δ_{18} values (Fig. 7a) defines a line of exactly slope 1 or follows some other slope, which might be evidence for either an analytical artifact such as fragmentation/recombination reactions in the ion source that tend to diminish differences in Δ_{18} between samples (Dennis et al., 2011; Huntington et al., 2009) or inaccuracies in the modeled dependence of Δ_{18} on temperature (Fig. 1). However, a weighted least squares regression of the data results in a slope of 0.86 ± 0.09 (1σ), which could indicate a scale 'compression' of Δ_{18} values as previously observed for clumped isotope measurements of CO_2 (Dennis et al., 2011), O_2

(Yeung et al., 2012) and position-specific measurements of N_2O (Yoshida and Toyoda, 2000), but is statistically indistinguishable from a slope of 1 at the 95% confidence level. These mass spectrometric artifacts generally have amplitudes of about 10%, relative (Dennis et al., 2011). Inaccuracies in the statistical mechanical calculation can be examined through more advanced treatments of the calculation using, for example, anharmonic corrections. Regardless, our data are statistically consistent with the hypothesis that measured values are directly proportional to predicted values, but do not disprove the possibility of some form of 'compression' of the scale due to ion source reactions. This issue might be resolved by measurements of methane samples equilibrated at much lower temperatures (e.g., 25°C), where expected Δ_{18} values are larger (as was done to establish an absolute scale for Δ_{47} measurements of CO_2; Dennis et al., 2011), by deeper exploration of the effects of instrument components and methods on measured differences in Δ_{18} values, and/or by more advanced statistical mechanical calculations of the equilibrium constants for equations (1) and (5).

In the absence of any statistically significant evidence for scale compression or other artifacts, we assume here that our measurements follow the same functional form as the theoretically predicted dependence of Δ_{18} on temperature (i.e., we assume our measurements are 1:1 with the theoretical values), with a constant offset equal to the Δ_{18} value of our intralaboratory standard, which we take to be +2.981‰. This set of assumptions lets us create a $\Delta_{18,wg}$ vs. temperature (in Kelvin) calibration where the dependent variable is $10^6/T^2$ (Fig. 7b), which results in the following equation:

$$\Delta_{18,wg} = -0.0117\left(\frac{10^6}{T^2}\right)^2 + 0.708\left(\frac{10^6}{T^2}\right) - 3.318\,. \qquad (11)$$

Alternatively, one could simply add +2.981 ‰ to Δ_{18} values measured vs. our working reference gas and compare the resulting value to the theoretically predicted relationship in Fig. 1.

8. Initial analyses of natural methane

A critical question for clumped isotope measurements of methane is whether or not Δ_{18} values reflect formational temperatures and thus equilibrium processes or if they are entirely controlled by kinetics. Additionally, once a gas forms (in isotopic equilibrium or not), it is not known if the sample will preserve its formational Δ_{18} during transport and storage. The working reference gas used in our laboratory is a commercially supplied sample that we believe to be a natural thermogenic gas based on its $\delta^{13}C$ and δD values (-42.88 and -175.5‰), which fall in the thermogenic gas field of Whiticar (1999). When the composition of this gas is compared with gases equilibrated in the laboratory, its apparent clumped isotope temperature is 170 ± 1 ˚C — roughly in the middle of the range generally inferred for formation of thermogenic methane (Killops and Killops, 2005). This could be a coincidence but suggests natural gases may record their temperatures of formation and preserve that record through extraction, storage, and handling in the laboratory.

Much of the methane produced on earth and released to the atmosphere is generated by methanogens at temperatures from 0-100°C. It is of interest to establish if this other end member process produces methane distinct in Δ_{18} from thermogenic gases and indicative of low temperatures. If so, one could apply methane clumped isotope thermometry to recognize biogenic methane and perhaps even characterize the specific

environments in which it is formed. We performed a preliminary test of this possibility by measuring a gas of known biological origin (Fig. 8).

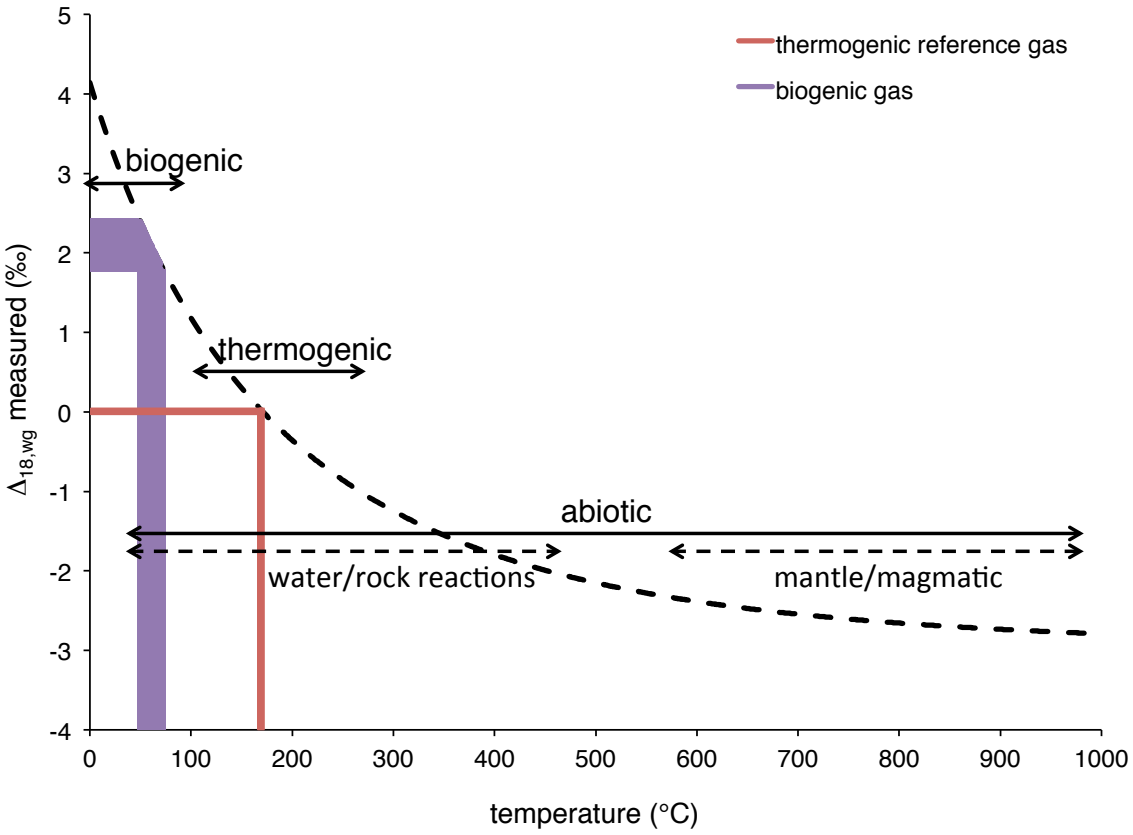

Figure 8: Samples measured compared to their calculated $\Delta_{18,wg}$-based temperatures. Ranges include 1 standard error of the measurement. As seen, the thermogenic reference gas gives a high but reasonable temperature of 170 °C while the biogenic sample from a methanogen grown at 65°C yields a temperature of 63°C.

This sample was produced by a pure culture of *Methanothermobacter marburgensis,* grown in an H_2/CO_2 (80:20) atmosphere following Boone et al. (1989) at 65°C until only methane remained. Samples were purified on the vacuum extraction line as explained above and corrected using standards run at the time for both δ^{12CH3D} and δ^{18} as explained above. Additionally, this sample was run before we routinely heated molecular sieves during release of methane, and so a correction for the isotope effect associated with partial retention of methane was applied (i.e., we subtracted 0.49‰ from

the measured Δ_{18} value, as explained above). This gives a $\Delta_{18,wg}$ value of 2.05 ± 0.29‰, or 5.03 ± 0.29 relative to a stochastic reference frame. Based on the temperature calibration above, this yields a temperature of 63 ± 11 °C (1σ), within error of its known growth temperature of 65°C. This result, interpreted in the most straightforward manner, indicates that this methanogen generates methane with a clumped isotopic composition that is within error of the equilibrium value for this growth temperature. This result may have implications for our understanding of methane's biogeochemistry and opens the possibility of identifying the source of methane in a given environment as a function of formation temperature, such as methane from psychrophiles vs. thermophiles vs. thermogenic sources. Furthermore, this technique may help to elucidate biochemical mechanisms in biogenic methane formation. For example, it is currently unknown whether methanogens that use acetate or methyl groups from larger organic molecules will form methane that is similar or distinct in clumped isotopic compositions from methanogens that metabolize H_2 and CO_2 — these questions represent clear targets for future studies.

We present data for only two natural methane samples here, and more detailed studies are clearly required to develop confident interpretations of the clumped isotope compositions of natural methane. Additionally, an experimental calibration of this thermometer needs to be extended to lower temperatures, perhaps using specialized catalysts to promote equilibration in the range 0-100°C. Nevertheless, these initial results suggest that the clumped isotope composition of natural methane can reflect its temperature of formation, can be preserved through later storage, extraction and

processing, and distinguishes between high-temperature and low-temperature natural sources by amounts that are a large multiple (~10x) of analytical precision.

9. Conclusions

We have presented a method to measure the combined ratio of $^{13}CH_3D^+$ and $^{12}CH_2D_2^+$ to $^{12}CH_4^+$, relative to its random distribution, through mass spectrometry. We have documented the accuracy of this technique through comparison to established methods for the determination of δD and $\delta^{13}C$ values and through measurements of gases that have been driven to equilibrium with respect to the abundances of their multiply substituted isotopologues by heating in the presence of a catalyst. We have additionally generated a calibration of the equilibrium-based thermometer between 200 and 500°C. Our working reference gas, which appears to be of thermogenic origin, gives a geologically reasonable temperature (170°C), while a biogenic gas gives a lower temperatures appropriate to its growth conditions (63°C). This suggests that methane may form through mechanisms in nature where its isotopes are internally equilibrated. If so, then clumped isotopes of methane may prove useful for understanding the physics and chemistry of methane formation, for characterizing the sources of natural methane, and perhaps for identifying the location where it formed.

10. Tables

Table 1: Relative abundances and masses of the isotopologues of methane.

Cardinal mass	Isotopologue	Proportional relative abundance of CH_4*	Exact mass (amu)
16	$^{12}CH_4$	$9.88*10^{-1}$	16.031
17	$^{13}CH_4$	$1.11*10^{-2}$	17.035
	$^{12}CH_3D$	$6.16*10^{-4}$	17.038
18	$^{13}CH_3D$	$6.92*10^{-6}$	18.041
	$^{12}CH_2D_2$	$1.44*10^{-7}$	18.044
19	$^{13}CH_2D_2$	$1.62*10^{-9}$	19.047
	$^{12}CHD_3$	$1.49*10^{-11}$	19.050
20	$^{13}CHD_3$	$1.68*10^{-13}$	20.053
	$^{12}CD_4$	$5.82*10^{-16}$	20.056
21	$^{13}CD_4$	$6.54*10^{-18}$	21.060

*Assumes that isotopes are randomly distributed throughout all isotopologues and that $\delta^{13}C$ = 0‰ and δD = 0‰ (relative to VPDB and VSMOW respectively).

Table 2: Comparison of $\delta^{13}C$ and δD values between independent techniques and measurements on the Ultra for samples where both the δD and $\delta^{13}C$ values were measured. All offline measurements were made at Indiana University through sealed-tube combustion of methane to CO_2 and H_2O followed by reduction of H_2O to H_2 with uranium on a vacuum line.

δD* offline (‰)	± (‰)†	δD* Ultra (‰)	± (‰)†	$\delta^{13}C$* offline (‰)	± (‰)†	$\delta^{13}C$* Ultra (‰)	± (‰)†
-84.5	0.2	-83.4	0.12	-43.15	0.01	-42.997	0.005
9.7	0.6	11.7	0.12	-42.86	0.02	-42.569	0.005
345.2	1.4	346.6	0.12	-42.82	0.04	-42.093	0.007

*On the VSMOW scale for δD and VPDB scale for $\delta^{13}C$.

†1σ error.

Table 3: Comparison of independent $\delta^{13}C$ measurements from established techniques and measurements on the Ultra.

$\delta^{13}C$* external (‰)	± (‰)†	$\delta^{13}C$ * Ultra (‰)	± (‰)†
-5.22[A]	0.35	-5.79	0.006
-1.49[A]	0.35	-1.54	0.005
-1.37[A]	0.35	-1.26	0.005
-0.33[A]	0.35	-0.11	0.006
-0.28[B]	0.01	-0.11	0.005
-0.18[A]	0.35	-0.10	0.005
0.02[B]	0.02	0.35	0.005
0.06[B]	0.04	0.88	0.007
1.90[A]	0.35	2.06	0.005
2.77[A]	0.35	2.49	0.006
6.34[A]	0.35	7.12	0.005
30.81[C]	0.35	31.99	0.005

*The reference standard is the sample measured with the closest $\delta^{13}C$ to the average of the entire suite for samples supplied by Petrobras and for the others is referenced relative to our working reference gas.

†1σ error.

'A' indicates measurements made at Petrobras, 'B' PEERI, and 'C' Indiana University.

Table 4: Experiments involving sample handling. The sample marked 'bottle' is a sample stored as a gas and expanded into the mass spectrometer. 'Sieve' denotes a sample that was first frozen onto a molecular sieve and stored in a break seal. 'Preheated' represents a sample that was heated with a heat gun prior to introduction to the mass spectrometer. Finally 'pumped on' is a sample that was exposed to vacuum at a variety of temperatures before being frozen onto a sieve. See text for full details. All samples were taken from the same reservoir before manipulation.

Sample	$\delta^{13}C$ (‰)	± (‰)	δD (‰)	± (‰)	Δ_{18} (‰)	± (‰)
Bottle	-42.867	0.005	-175.692	0.111	-0.380	0.269
Sieve, preheated	-42.799	0.005	-175.214	0.125	-0.421	0.284
Sieve, pumped on and preheated	-42.778	0.005	-175.277	0.121	-0.217	0.267
Sieve, not preheated	-44.233	0.005	-174.494	0.117	0.111	0.261

Table 5: Bracketing experiment where samples were heated in the presence of a nickel catalyst at 500°C. 'Unheated' marks a sample from a larger reservoir that was not heated. 'Heated' denotes a sample from a larger reservoir (same reservoir as the 'unheated' sample) that was heated.

Sample	$\delta^{13}C$ (‰)	± (‰)	δD (‰)	± (‰)	Δ_{18} (‰)	± (‰)
#1 unheated	-42.857	0.006	-175.528	0.110	-0.021	0.286
#1 heated	-48.083	0.005	-199.778	0.110	-1.794	0.281
#2 unheated	-42.997	0.005	-83.431	0.118	-0.450	0.262
#2 heated	-47.493	0.005	-127.165	0.099	-1.855	0.290
#3 unheated	-42.569	0.005	11.673	0.122	-1.088	0.308
#3 heated	-46.711	0.007	-46.647	0.150	-1.979	0.370
#4 unheated	-42.093	0.007	346.611	0.123	-5.838	0.341
#4 heated	-44.476	0.005	252.659	0.116	-1.678	0.299

Table 6: Heating Experiment. Samples were heated for the given amounts of time in the presence of a nickel catalyst.

Temperature (°C)	Time (days)	Δ_{18} (‰)	± (‰)
200*	1	-0.603	0.258
300	3.8	-1.242	0.270
300*	0.9	-1.254	0.296
400	3.8	-2.033	0.272
400*	0.2	-1.676	0.244
500	4	-2.079	0.283
500	3.9	-1.979	0.370
500	3	-1.794	0.281
500†	3	-1.678	0.299
500	2.9	-1.855	0.290
500	2	-2.364	0.222
500	2	-1.7669	0.242
500	2	-1.941	0.248
500	2	-2.225	0.271
500	2	-2.002	0.256
500	2	-2.188	0.242

*Denotes correction by subtracting 0.49‰ to account for sieve fractionation artifact.

†Not used in calibration as this sample is ~500 ‰ different in δ^{18} from typical samples. As such if there are unknown scale compressions or analytical artifacts over such ranges, this sample would be the most susceptible.

11. Appendix

Appendix A: Calculation of $\delta^{13}C$, δD, and Δ_{18}

Finding the $\delta^{13}C$, δD, and Δ_{18} values from measurements of mass-17/16 and mass-18/16 ion-current ratios must be done through iteration due to the inclusion of fragments at mass 16. Measurements of mass 16 include measurable quantities of $^{13}CH_3^+$ and $^{12}CH_2D^+$. These fragments must be accounted for as they are approximately 1% of the mass-16 signal, with $^{13}CH_3^+$ representing 95% of the fragments. A measurement can be made without the fragments (as the resolution is sufficient to resolve them out), but we find it methodologically easier to correct for the fragments at the end of the measurement.

We correct for the fragments by first measuring a 'fragmentation' rate. This is the amount of fragment produced for a given amount of $^{12}CH_4$ in the source. We do this by measuring the ion-current ratio of mass-15/16 via peak hopping. Mass 15 includes $^{12}CH_3^+$ and mass 16 $^{12}CH_4^+$ only. These fragmentation measurements are made at the same source pressure as the actual isotope ratio measurements. Generally, the mass-15/16 ion-current ratio is ~0.8, with a range seen over a year of measurements of about ±0.02. We assume that this fragmentation rate (F) is independent of isotopologues and is identical for $^{12}CH_4$, $^{13}CH_4$, and $^{12}CH_3D$. We can then generate a non-linear system of equations to describe our bulk isotopic measurements where:

$$^{12CH3D}R=\frac{[^{12}CH_3D]}{[^{12}CH_4]+F\left([^{13}CH_4]+0.75[^{12}CH_3D]\right)} \tag{A1a}$$

and

$$^{12CH3D+13CH4}R=\frac{[^{12}CH_3D]+[^{13}CH_4]}{[^{12}CH_4]+F\left([^{13}CH_4]+0.75[^{12}CH_3D]\right)}, \tag{A1b}$$

where F is the fragmentation rate (usually ~0.8). If we assume that the isotopes are randomly distributed we can write these as:

$$^{12CH3D}R=\frac{4[^{12}C][H]^3[D]}{[^{12}C][H]^4+F\left([^{13}C][H]^4+3[^{12}C][H]^3[D]\right)} \quad \text{(A2a)}$$

and

$$^{12CH3D+13CH4}R=\frac{4[^{12}C][H]^3[D]+[^{13}C][H]^4}{[^{12}C][H]^4]+F\left([^{13}C][H]^4+3[^{12}C][H]^3[D]\right)}. \quad \text{(A2b)}$$

These can be written as

$$^{12CH3D}R=\frac{4^{D}R}{1+F\left(^{13}R+3^{D}R\right)} \quad \text{(A3a)}$$

and

$$^{12CH3D+13CH4}R=\frac{4^{D}R+^{13}R}{1+F\left(^{13}R+3^{D}R\right)}. \quad \text{(A3b)}$$

These equations are solved iteratively in Matlab™ to find the ^{13}R and ^{D}R values of the sample. As a note, we have implicitly removed the standard (which is in the denominator of all original measurements) through multiplication of its known isotopologue concentrations for a random distribution.

To calculate Δ_{18}, we first assume that our working reference gas is randomly distributed. This is necessary as the ^{18}R value of the standard was not a priori known. We make this calculation through the following equation:

$$\Delta_{18,wg}=\left(\frac{^{18}R_{sample}}{^{18}R_{standard}}*\frac{^{18}R^{*}_{standard}}{^{18}R^{*}_{sample}}-1\right)1000 \quad \text{(A4)}$$

or, if expanded

$$\Delta_{18,wg} = \left(\frac{{}^{18}R_{sample}}{{}^{18}R_{standard}} \text{ x } \left(\frac{\dfrac{6({}^{D}R_{standard})^2 + 4({}^{D}R_{standard})({}^{13}R_{standard})}{1 + F\left({}^{13}R_{standard} + 3\,{}^{D}R_{standard}\right)}}{\dfrac{6({}^{D}R_{sample})^2 + 4({}^{D}R_{sample})({}^{13}R_{sample})}{1 + F\left({}^{13}R_{sample} + 3\,{}^{D}R_{sample}\right)}} \right) - 1 \right) \text{ x } 1000\,. \qquad \text{(A5)}$$

Implicit in doing this is that the standard is defined to have a Δ_{18} of zero. Hence all Δ_{18} measurements are made in what is known as the 'working gas reference frame.'

Appendix B: Adduct line for mass 18

We assume that the adducts at mass 18 form through the following reactions:

$${}^{12}CH_4 + {}^{13}CH_4^+ \longrightarrow {}^{12}CH_3 + {}^{13}CH_5^+ \qquad \text{(B1a)}$$

and

$${}^{12}CH_4 + {}^{12}CH_3D^+ \longrightarrow {}^{12}CH_3 + {}^{12}CH_4D^+\,. \qquad \text{(B1b)}$$

We assume the following kinetics for adduct formation based on these equations:

$${}^{13}CH_5^+ = k_{13,1}({}^{12}CH_4)({}^{13}CH_4)^2 + k_{13,2}({}^{12}CH_4)({}^{13}CH_4) \qquad \text{(B2a)}$$

and

$${}^{12}CH_4D^+ = k_{D,1}({}^{12}CH_4)({}^{12}CH_3D)^2 + k_{D,2}({}^{12}CH_4)({}^{12}CH_3D)\,. \qquad \text{(B2b)}$$

In these equations, the k terms are constants. We can relate the amount of current we measure, $i_{18,total}$ to the current containing ${}^{13}CH_3D^+$ and ${}^{12}CH_2D_2{}^+$, $i_{18,istopes}$ and the current from the adducts, $i_{18,addcuts}$ via the following relation:

$$i_{18,total} = i_{18,isotopes} + i_{18,adduct}\,. \qquad \text{(B3)}$$

Substitution of (B2a) and (B2b) into (B3) and the assumption that the fragments at mass 16 can be corrected for later and that the rate constants are identical gives

$$i_{18,total} = i_{18,isotopes} + k_1\left(i_{16}\right)\left(i_{17}\right)^2 + k_2\left(i_{16}\right)\left(i_{17}\right), \qquad \text{(B4)}$$

where $i_{17} = i_{13CH4} + i_{12CH3D}$. Division of (4) by i_{16} gives

$$\frac{i_{18,\text{total}}}{i_{16}} = \frac{i_{18,\text{isotopes}}}{i_{16}} + \mathrm{k}_1\left(i_{17}\right)^2 + \mathrm{k}_2\left(i_{17}\right), \tag{B5}$$

which is the equation of line in which the curvature is defined by k_1 and k_2 and the intercept, which is the measurement of interest, is $i_{18,isotopes}/i_{16}$. i_{17} does not include the adduct at mass 17 ($^{12}CH_5^+$). Thus to find i_{17} we generate, adducts lines at both mass 17 and mass 18 where the mass-17 adduct line includes $^{13}CH_4^+$, $^{12}CH_3D^+$, and $^{12}CH_5^+$. This line is used to both correct the mass 17-measurement for bulk isotope calculations and to have an adductless current for mass 17 that can be used to make the mass-18 adduct line. An example mass-18 adduct line is give in Fig. A1. As in the case of the mass-17 adduct line, the mass-18 adduct line is best fit with a quadratic line. The assumption that the rate constants for reactions involving $^{13}CH_4$ and $^{12}CH_3D$ are the same is likely incorrect. However, as the adduct is dominantly $^{13}CH_5$ (>98%), the error from not knowing the precise value for the $^{12}CH_4D$ rate constant is diminished. However, at large δD differences, this could be an issue. We demonstrate this not to be the case in the bracketing experiment described in the text where Δ_{18} is not a function of δD.

Appendix Tables:

Table A1: Species present in the mass-17 to mass-16 measurement (δ^{12CH3D}) used to constrain the $^{12}CH_3D/^{12}CH_4$ ratio. This measurement is made at the high-resolution setting of the instrument (20,000-25,000 mass resolving power). In bold are the major methane peaks at a given mass. Abundances are given relative to the major methane peak at the given mass. Species $<1*10^{-4}$ of the major methane peak are not shown.

Species (Mass 16)	Mass (amu)	Relative abundance	notes	Species (Mass 17)	Mass (amu)	Relative abundance	notes
^{16}O	15.995	$1.48*10^{-4}$	resolved	^{17}O	16.999	$2.98*10^{-4}$	resolved
$^{13}CH_3$	16.027	$8.99*10^{-3}$	corrected	^{16}OH	17.003	1.68	resolved
$^{12}CH_2D$	16.030	$4.98*10^{-4}$	corrected	$^{15}NH_2$	17.016	$3.9*10^{-4}$	resolved
$^{12}CH_4$	**16.031**	**1**	**measured**	$^{14}NH_3$	17.027	0.133	resolved
				$^{13}CH_2D$	17.033	$8.99*10^{-3}$	resolved
				$^{13}CH_4$	17.035	18.036	resolved
				$^{12}CHD_2$	17.036	$1.87*10^{-4}$	ignored
				$^{12}CH_3D$	**17.038**	**1**	**measured**
				$^{12}CH_5$	17.039	0.333	corrected

Table A2: Species present in the mass-17 to mass-16 measurement ($\delta^{12CH3D+13CH4}$) used to constrain the ($^{12}CH_3D$ + $^{13}CH_4$)/$^{12}CH_4$ ratio and in the mass-18 to mass-16 measurement (δ^{18}) used to constrain the ($^{13}CH_3D$ + $^{12}CH_2D_2$)/$^{12}CH_4$ ratio. The mass-16 species are identical to those given in Table A1 and are not shown. This measurement is made at the medium-resolution setting of the instrument (16,000-17,000 mass resolving power). In bold are the major methane peaks at a given mass. Abundances are given relative to the major methane peak at the given mass. Species $<1*10^{-4}$ of the major methane peak are not shown.

Species (Mass 17)	Mass (amu)	Relative abundance	notes	Species (Mass 18)	Mass (amu)	Relative abundance	notes
^{16}OH	17.003	0.03	resolved	^{18}O	17.999	0.018	resolved
$^{14}NH_3$	17.027	$2.39*10^{-3}$	resolved	^{17}OH	18.007	0.022	resolved
$^{13}CH_2D$	17.033	$4.98*10^{-4}$	ignored	$H_2{}^{16}O$	18.011	14.815	resolved
$^{13}CH_4$	**17.035**	**1**	**measured**	$^{15}NH_3$	18.024	0.017	resolved
$^{12}CH_3D$	17.038	0.055	measured	$^{14}NH_4$	18.034	5.77*10-4	resolved
$^{12}CH_5$	17.039	$5.98*10^{-3}$	corrected	$^{13}CD_2H$	18.039	1.87*10-4	ignored
				$^{13}CH_3D$	**18.041**	**1**	**measured**
				$^{13}CH_5$	18.042	0.407	corrected
				$^{12}CH_2D_2$	18.044	0.021	measured
				$^{12}CH_4D$	18.045	0.023	corrected

Appendix Figures

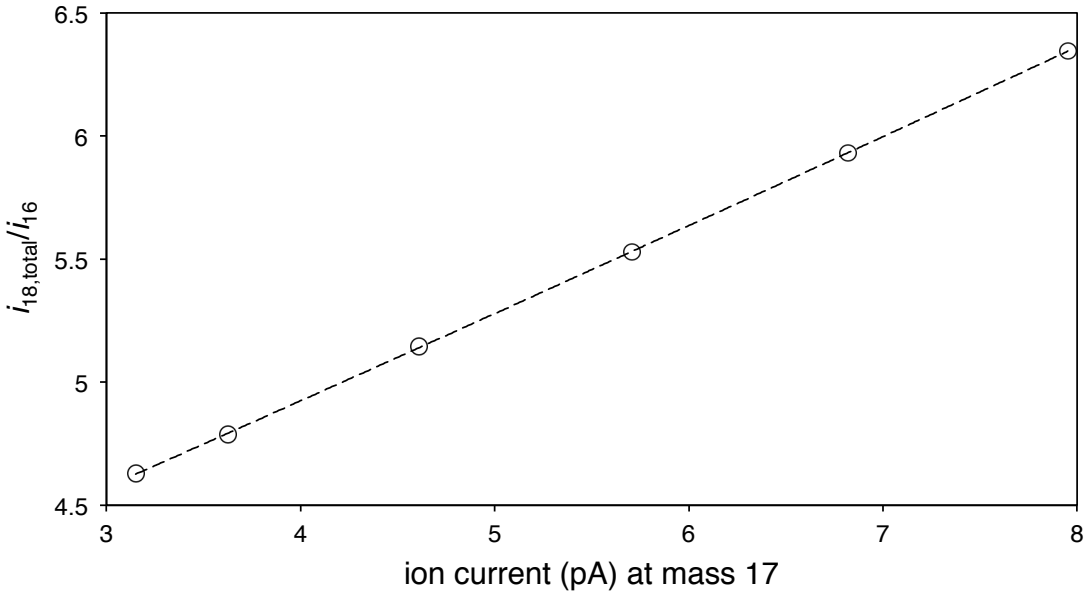

Figure A1. Demonstration of the dependence of the mass-18/mass-16 ion-current ratio ($i_{18,total}/i_{17}$) on the mass-17 ion current (i_{17}). In this example, i_{16} includes $^{12}CH_4^+$ + $^{13}CH_3^+$ + $^{12}CH_2D^+$, i_{17} includes $^{13}CH_4^+$ + $^{12}CH_3D^+$, and i_{18} $^{13}CH_3D^+$ + $^{12}CH_2D_2^+$ + $^{13}CH_5^+$ + $^{12}CH_4D^+$. The line describing the dependence of $i_{18,total}/i_{16}$ on i_{17} is known as an adduct line. The formula for the adduct line is found by fitting the data with a quadratic function. The fitted parameters are used to remove the contribution of $^{13}CH_5^+$ + $^{12}CH_4D^+$ from all measurements.

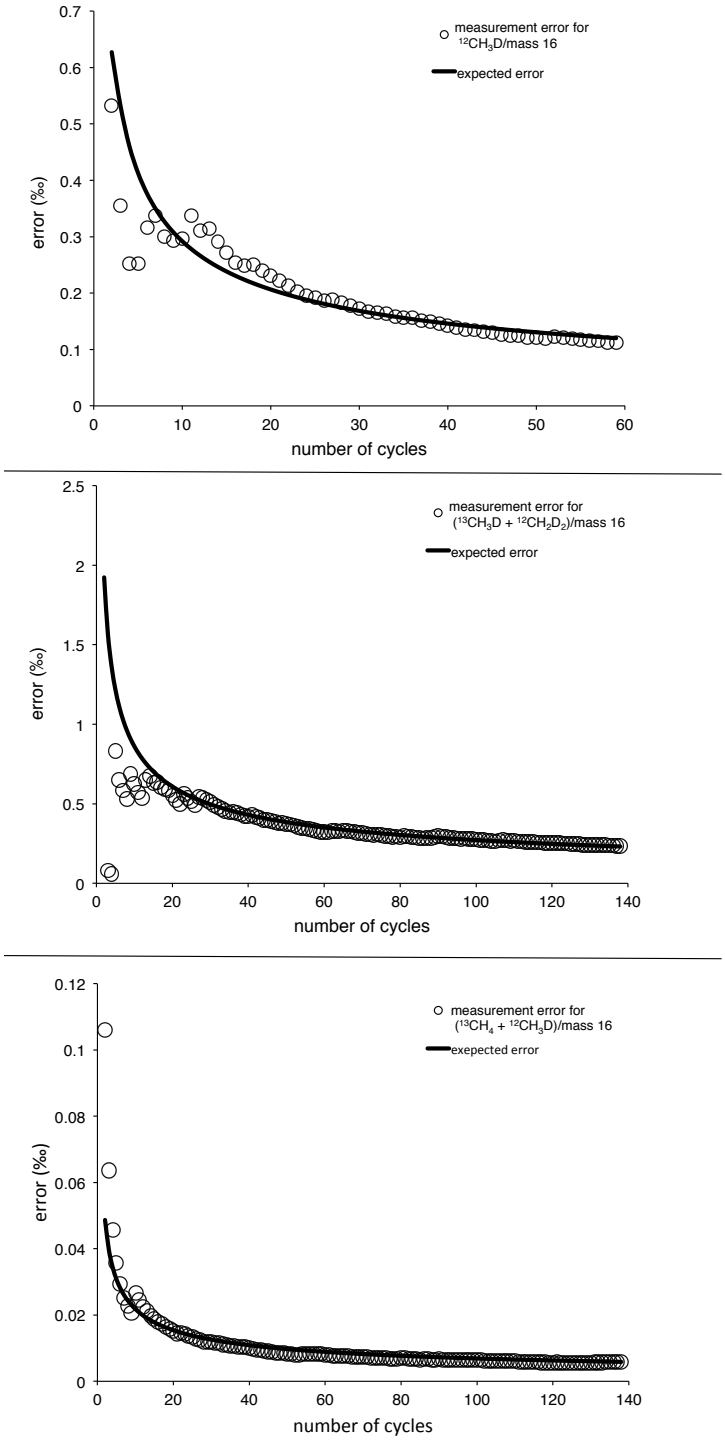

Figure A2. Demonstration that all measurements follow their theoretical statistical limits in precision. A) Measurement of δ^{12CH3D} where mass 17 includes $^{12}CH_3D^+$. Measurements are shown after the H-adducts have been removed. Samples approach the combined Johnson noise and counting statistics limit of 0.1-0.12‰ at the end of the measurement. B) Measurement of $\delta^{12CH3D+13CH4}$ where mass 17 includes $^{12}CH_3D^+$ and $^{13}CH_4^+$. Measurements have been corrected for the presence of H-adducts and approach the theoretical counting statistics limit of 0.005‰ at the end of the measurement. C) Measurement of δ^{18}, which at mass 18 includes $^{13}CH_3D^+$ and $^{12}CH_2D_2^+$. H-adducts have been corrected for and samples approach the counting statistics limit of 0.25‰ at the end of the measurement.

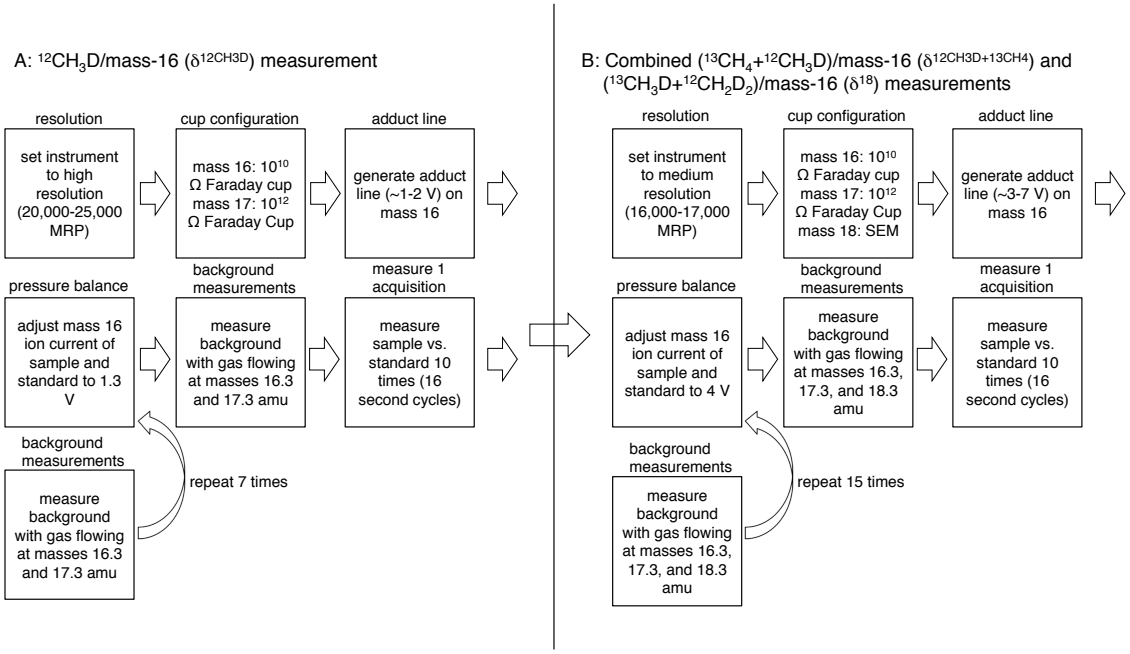

Figure A3. Flow chart representation of the analytical procedures involved in making a measurement. Abbreviations: mass resolving power (MRP); secondary electron multiplier (SEM). A) Measurement of δ^{12CH3D}. B) Simultaneous measurement of $\delta^{12CH3D+13CH4}$ and δ^{18}.

12. References

Affek, H.P., Eiler, J.M., 2006. Abundance of mass 47 CO_2 in urban air, car exhaust, and human breath. *Geochimica et Cosmochimica Acta* 70, 1-12.

Affek, H.P., Xu, X.M., Eiler, J.M., 2007. Seasonal and diurnal variations of $^{13}C^{18}O^{16}O$ in air: Initial observations from Pasadena, CA. *Geochimica et Cosmochimica Acta* 71, 5033-5043.

Bernasconi, S.M., Hu, B., Wacker, U., Fiebig, J., Breitenbach, S.F., Rutz, T., 2013. Background effects on Faraday collectors in gas-source mass spectrometry and implications for clumped isotope measurements. *Rapid Communications in Mass Spectrometry* 27, 603-612.

Bigeleisen, J., Mayer, M.G., 1947. Calculation of equilibrium constants for isotopic exchange reactions. *The Journal of Chemical Physics* 15, 261.

Bigeleisen, J., Perlman, M., Prosser, H., 1952. Conversion of hydrogenic materials to hydrogen for isotopic analysis. *Analytical Chemistry* 24, 1356-1357.

Boone, D.R., Johnson, R.L., Liu, Y., 1989. Diffusion of the interspecies electron carriers H_2 and formate in methanogenic ecosystems and its implications in the measurement of K_m for H_2 or formate uptake. *Applied and Environmental Microbiology* 55, 1735-1741.

Bottinga, Y., 1969. Calculated fractionation factors for carbon and hydrogen isotope exchange in the system calcite-carbon dioxide-graphite-methane-hydrogen-water vapor. *Geochimica et Cosmochimica Acta* 33, 49-64.

Craig, H., 1953. The geochemistry of the stable carbon isotopes. *Geochimica et Cosmochimica Acta* 3, 53-92.

Craig, H., Chou, C., Welhan, J., Stevens, C., Engelkemeir, A., 1988. The isotopic composition of methane in polar ice cores. *Science* 242, 1535.

Daëron, M., Guo, W., Eiler, J., Genty, D., Blamart, D., Boch, R., Drysdale, R., Maire, R., Wainer, K., Zanchetta, G., 2011. $^{13}C^{18}O$ clumping in speleothems: Observations from natural caves and precipitation experiments. *Geochimica et Cosmochimica Acta* 75, 3303-3317.

Dai, J., Xia, X., Li, Z., Coleman, D.D., Dias, R.F., Gao, L., Li, J., Deev, A., Li, J., Dessort, D., 2012. Inter-laboratory calibration of natural gas round robins for δ^2H and $\delta^{13}C$ using off-line and on-line techniques. *Chemical Geology* 310, 49-55.

Dennis, K.J., Affek, H.P., Passey, B.H., Schrag, D.P., Eiler, J.M., 2011. Defining an absolute reference frame for 'clumped' isotope studies of CO_2. *Geochimica et Cosmochimica Acta* 75, 7117-7131.

Eiler, J.M., 2007. "Clumped-isotope" geochemistry - The study of naturally-occurring, multiply-substituted isotopologues. *Earth and Planetary Science Letters* 262, 309-327.

Eiler, J.M., 2011. Paleoclimate reconstruction using carbonate clumped isotope thermometry. *Quaternary Science Reviews* 30, 3575-3588.

Eiler, J.M., 2013. The isotopic anatomies of molecules and minerals. *Annual Review of Earth and Planetary Sciences* 41, 411-441.

Eiler, J.M., Clog, M., Magyar, P., Piasecki, A., Sessions, A., Stolper, D., Deerberg, M., Schlueter, H.-J., Schwieters, J., 2013. A high-resolution gas-source isotope ratio mass spectrometer. *International Journal of Mass Spectrometry* 335, 45-56.

Eiler, J.M., Schauble, E., 2004. $^{18}O^{13}C^{16}O$ in Earth's atmosphere. *Geochimica et Cosmochimica Acta* 68, 4767-4777.

Etiope, G., Lollar, B.S., 2013. Abiotic methane on Earth. *Reviews of Geophysics* 51, 276-299.

Friedman, I., 1953. Deuterium content of natural waters and other substances. *Geochimica et Cosmochimica Acta* 4, 89-103.

Ghosh, P., Adkins, J., Affek, H., Balta, B., Guo, W., Schauble, E.A., Schrag, D., Eiler, J.M., 2006. ^{13}C-^{18}O bonds in carbonate minerals: A new kind of paleothermometer. *Geochimica et Cosmochimica Acta* 70, 1439-1456.

Hagemann, R., Nief, G., Roth, E., 1970. Absolute isotopic scale for deuterium analysis of natural waters. Absolute D/H ratio for SMOW. *Tellus* 22, 712-715.

Hamak, J.E., Sigler, S., 1991. *Analyses of natural gases, 1986-90*. Information Circular No. 9301. Bureau of Mines, US Dept. Interior, Pittsburgh, PA.

He, B., Olack, G.A., Colman, A.S., 2012. Pressure baseline correction and high-precision CO_2 clumped-isotope (Δ_{47}) measurements in bellows and micro-volume modes. *Rapid Communications in Mass Spectrometry* 26, 2837-2853.

Horibe, Y., Craig, H., 1995. D/H fractionation in the system methane-hydrogen-water. *Geochimica et Cosmochimica Acta* 59, 5209-5217.

Horita, J., 2001. Carbon isotope exchange in the system CO_2-CH_4 at elevated temperatures. *Geochimica et Cosmochimica Acta* 65, 1907-1919.

Huntington, K., Eiler, J., Affek, H., Guo, W., Bonifacie, M., Yeung, L., Thiagarajan, N., Passey, B., Tripati, A., Daëron, M., 2009. Methods and limitations of 'clumped' CO_2

isotope (Δ_{47}) analysis by gas-source isotope ratio mass spectrometry. *Journal of Mass Spectrometry* 44, 1318-1329.

John, S.G., Adkins, J.F., 2010. Analysis of dissolved iron isotopes in seawater. *Marine Chemistry* 119, 65-76.

Kaye, J.A., Jackman, C.H., 1990. Comment on "Detection of multiply deuterated methane in the atmosphere". *Geophysical Research Letters* 17, 659-660.

Kennett, J.P., Cannariato, K.G., Hendy, I.L., Behl, R.J., 2003. *Methane Hydrates in Quaternary Climate Change: The Clathrate Gun Hypothesis*. American Geophysical Union, Washington, D.C.

Killops, S., Killops, V., 2005. *Introduction to Organic Geochemistry*. Blackwell Publishing, Malden, MA.

Ma, Q., Wu, S., Tang, Y., 2008. Formation and abundance of doubly-substituted methane isotopologues ($^{13}CH_3D$) in natural gas systems. *Geochimica et Cosmochimica Acta* 72, 5446-5456.

Merritt, D.A., Hayes, J., 1994. Factors controlling precision and accuracy in isotope-ratio-monitoring mass spectrometry. *Analytical Chemistry* 66, 2336-2347.

Mroz, E.J., Alei, M., Cappis, J.H., Guthals, P.R., Mason, A.S., Rokop, D.J., 1989. Detection of multiply deuterated methane in the atmosphere. *Geophysical Research Letters* 16, 677-678.

Munson, M.S., Field, F.H., 1966. Chemical ionization mass spectrometry. I. General introduction. *Journal of the American Chemical Society* 88, 2621-2630.

Ono, S., Sherwood Lollar, B., Harris, E., McManus, B., Zahniser, M., Nelson, D., 2013. Clumped methane isotopologue ($^{13}CH_3D$) thermometry of geological methane by

tunable mid-infrared laser spectroscopy, Goldschmidt Conference. *Mineralogical Magazine*, Florence, Italy, p. 1992.

Sackett, W.M., 1995. The thermal stability of methane from 600 to 1000°C. *Organic Geochemistry* 23, 403-406.

Schimmelmann, A., Lewan, M.D., Wintsch, R.P., 1999. D/H isotope ratios of kerogen, bitumen, oil, and water in hydrous pyrolysis of source rocks containing kerogen types I, II, IIS, and III. *Geochimica et Cosmochimica Acta* 63, 3751-3766.

Schoell, M., 1980. The hydrogen and carbon isotopic composition of methane from natural gases of various origins. *Geochimica et Cosmochimica Acta* 44, 649-661.

Sessions, A.L., Burgoyne, T.W., Hayes, J.M., 2001. Determination of the H_3 factor in hydrogen isotope ratio monitoring mass spectrometry. *Analytical Chemistry* 73, 200-207.

Stevens, C., Rust, F., 1982. The carbon isotopic composition of atmospheric methane. *Journal of Geophysical Research* 87, 4879-4882.

Stolper, D.A., Sessions, A.L., Eiler, J.M., 2012. Measurement of intact methane isotopologues, including $^{13}CH_3D$, Goldschmidt Conference. *Mineralogical Magazine*, Montreal, Canada, p. 2413.

Stolper, D.A., Shusta, S.S., Valentine, D.L., Sessions, A.L., Ferreira, A., Santos Neto, E.V., Eiler, J.M., 2013. Combined ^{13}C-D and D-D clumping in CH_4: Preliminary results, Goldschmidt Conference. *Mineralogical Magazine*, Florence, Italy, p. 2269.

Tsuji, K., Teshima, H., Sasada, H., Yoshida, N., 2012. Spectroscopic isotope ratio measurement of doubly-substituted methane. *Spectrochimica Acta Part A: Molecular and Biomolecular Spectroscopy* 98, 43-46.

Urey, H.C., 1947. The thermodynamic properties of isotopic substances. *Journal of the Chemical Society*, 562-581.

Urey, H.C., Rittenberg, D., 1933. Some thermodynamic properties of the H^1H^1, H^2H^2 molecules and compounds containing the H^2 atom. *The Journal of Chemical Physics* 1, 137.

Valentine, D.L., 2011. Emerging topics in marine methane biogeochemistry. *Annu. Rev. Mar. Sci.* 3, 147-171.

Valentine, D.L., Chidthaisong, A., Rice, A., Reeburgh, W.S., Tyler, S.C., 2004. Carbon and hydrogen isotope fractionation by moderately thermophilic methanogens. *Geochimica et Cosmochimica Acta* 68, 1571-1590.

Wahlen, M., Tanaka, N., Henry, R., Deck, B., Zeglen, J., Vogel, J., Southon, J., Shemesh, A., Fairbanks, R., Broecker, W., 1989. Carbon-14 in methane sources and in atmospheric methane: The contribution from fossil carbon. *Science* 245, 286-290.

Wang, Z., Schauble, E.A., Eiler, J.M., 2004. Equilibrium thermodynamics of multiply substituted isotopologues of molecular gases. *Geochimica et Cosmochimica Acta* 68, 4779-4797.

Welhan, J.A., 1988. Origins of methane in hydrothermal systems. *Chemical Geology* 71, 183-198.

Whiticar, M.J., 1999. Carbon and hydrogen isotope systematics of bacterial formation and oxidation of methane. *Chemical Geology* 161, 291-314.

Whiticar, M.J., Faber, E., Schoell, M., 1986. Biogenic methane formation in marine and freshwater environments: CO_2 reduction vs acetate fermentation—Isotope evidence. *Geochimica et Cosmochimica Acta* 50, 693-709.

Wuebbles, D.J., Hayhoe, K., 2002. Atmospheric methane and global change. *Earth-Science Reviews* 57, 177-210.

Yeung, L.Y., Young, E.D., Schauble, E.A., 2012. Measurements of $^{18}O^{18}O$ and $^{17}O^{18}O$ in the atmosphere and the role of isotope-exchange reactions. *Journal of Geophysical Research* 117, DOI: 10.1029/2012JD017992.

Yoshida, N., Toyoda, S., 2000. Constraining the atmospheric N_2O budget from intramolecular site preference in N_2O isotopomers. *Nature* 405, 330-334.

Chapter VII

Formation temperatures of methane in natural environments

DA Stolper[a], M Lawson[b], CL Davis[b], AA Ferreira[c], EV Santos Neto[c], GS Ellis[d], MD Lewan[d], AM Martini[e], Y Tang[f], M Schoell[g], AL Sessions[a], JM Eiler[a]

[a]*Division of Geological and Planetary Sciences, California Institute of Technology, Pasadena, CA, USA*
[b]*ExxonMobil Upstream Research Company, Houston, TX, USA*
[c]*Division of Geochemistry, Petrobras Research and Development Center (CENPES), Rio de Janeiro, RJ, Brazil*
[d]*U.S. Geological Survey, Denver Federal Center, Denver, CO, USA*
[e]*Department of Geology, Amherst College, Amherst, MA, USA*
[f]*Power, Environmental, and Energy Research Institute, Covina, CA* USA
[g]*GasConsult International Inc, Berkeley, CA, USA*

Abstract: Formation temperatures of methane from both low (<50°C) and high (>100°C) temperature natural settings have been measured for the first time using a 'clumped isotope' technique. Thermogenic gases yield formation temperatures between 157-221°C, within the nominal gas window. Data for thermogenic gases with well-known thermal histories indicate that methane forms in internal isotopic equilibrium and preserves clumped-isotope formation temperatures through uplift, migration, and extraction. In a system where thermogenic gases have migrated and other proxies for gas generation temperature yield ambiguous results, methane clumped isotope temperatures distinguish among and allow for independent tests of possible gas formation models. Natural biogenic gases yield clumped-isotope temperatures consistent with their known lower formation temperatures (<50°C). These results indicate that methane clumped isotope temperatures can be used to help recognize the location and timing of thermogenic gas formation, to establish the conditions of microbial methanogenesis, and to identify the proportions and end-member properties of mixtures of biogenic and thermogenic gases.

1. Introduction

Knowledge of the environmental conditions, rates, and mechanisms of methane formation is critical for a quantitative understanding of the carbon cycle and for predicting where economically significant amounts of methane form. Conventional models of thermogenic methane formation predict that: (i) gas formation is kinetically controlled by time, temperature, and organic matter composition (Seewald, 2003); (ii) gases co-generated with oil form below ~150-160°C (Clayton, 1991; Hunt, 1996; Quigley and Mackenzie, 1988); and (iii) gases created from the breakdown (cracking) of oil or refractory kerogen form above 150-160°C (Clayton, 1991; Hunt, 1996; Quigley and Mackenzie, 1988). Microbially-produced (biogenic) methane in nature is thought to form below ~80°C (Wilhelms et al., 2001) and results in pure methane gas (Hunt, 1996; Valentine, 2011; Whiticar et al., 1986). We present here the first direct measurements of formation temperatures for thermogenic and biogenic methane in natural, economically significant systems using multiply substituted (clumped) methane isotopologue abundances (Stolper et al., 2014b).

Our current understanding of the chemical kinetics of thermogenic methane formation is dominantly constrained by the extrapolation of kinetic rate constants from laboratory experiments to geologically relevant conditions. These experiments must be performed at rates higher ($>10^6$) than those found in nature, which is achieved by heating samples hundreds of degrees above relevant gas formation temperatures. These experimentally-derived kinetics are sensitive to heating rate (Lewan and Ruble, 2002) and the presence or absence of water (Espitalie et al., 1988; Lewan, 1997; Lewan and Ruble, 2002; Seewald, 2003; Seewald et al., 1998), minerals (Seewald, 2003; Seewald et

al., 1998), and transition metals (Mango and Hightower, 1997). Extrapolations of these differing kinetic parameters to geologically relevant conditions results in divergent predictions for natural methane formation temperatures. The ability to directly measure methane formation temperatures in natural samples would allow these models to be rigorously tested and improved.

An additional difficulty in understanding the histories of thermogenic gases in nature is that they commonly migrate from their source to a reservoir (England et al., 1987; Hunt, 1996; Price and Schoell, 1995; Tissot and Welte, 1978). Although these migrated gases dominate the datasets used to calibrate empirical models for thermogenic methane formation (Hunt, 1996; Price and Schoell, 1995; Schoell, 1983; Tissot and Welte, 1978), the ability to understand their thermal histories, and thus accurately calibrate these models, is hampered by: (i) a lack of independent constraints on the thermal histories of the source *and* reservoir rocks and the timing of gas migration, and (ii) the possibility that a reservoir contains a mixture of gases from different sources.

In order to provide independent constraints on the formation temperatures of methane and to test the predictions of various formation models, we measured the clumped isotope temperatures of methane samples from five natural systems including three thermogenic gas deposits, one biogenic gas deposit, and one deposit comprising a mixture of the two. We complemented these data with measurements of experimentally-produced methane from high-temperature (>350°C) pyrolysis of larger hydrocarbons. For isotopically equilibrated systems, clumped isotopologue abundances are functions of temperature and thus can be used to calculate methane formation temperatures (Eiler,

2007; Stolper et al., 2014b). For example, for the following reaction at finite temperatures and equilibrium,

$$^{13}CH_3D + {}^{12}CH_4 \longleftrightarrow {}^{13}CH_4 + {}^{12}CH_3D\,, \quad (1)$$

the left side is favored resulting in more $^{13}CH_3D$ (the clumped isotopologue) compared to a random isotopic distribution. The excess in $^{13}CH_3D$ decreases with increasing temperature (Eiler, 2007; Stolper et al., 2014b). We quantify the abundance of both $^{13}CH_3D$ and $^{12}CH_2D_2$ relative to a random isotopic distribution via the parameter Δ_{18} (see appendix). As demonstrated by Stolper et al. (2014b), Δ_{18} values yield formation temperatures for internally equilibrated systems both in theory and as shown experimentally (Figure 1A). Importantly, this approach potentially provides a straightforward, quantitative measure of the temperatures of methane formation, independent of the model assumptions of previous methods. However, conventional models assume that methane forms through kinetically-controlled reaction mechanisms (Clayton, 1991; Espitalie et al., 1988; Hunt, 1996; Ni et al., 2011; Seewald, 2003; Tang et al., 2000; Xiao, 2001), so it is not obvious, *a priori*, what Δ_{18} values of natural samples will mean. One previous measurement of a possibly thermogenic methane sample suggested that Δ_{18} values reflect formation temperatures (Stolper et al., 2014b).

2. Results and discussion

We first consider methane generated from larger hydrocarbon molecules at known temperatures in two experiments. We first thermally cracked (pyrolyzed) pure propane to form methane at 600°C (12 hours; see appendix) and, second, generated methane from closed-system hydrous pyrolysis (Lewan, 1997; Lewan and Ruble, 2002; Seewald et al.,

1998) of organic matter at 360°C (72 hours; see appendix). In both cases, Δ_{18} temperatures are within 2σ of the experimental temperature (Figure 1a; Table A1). This supports the suggestion in (Stolper et al., 2014b) that the measured Δ_{18} temperatures of thermogenic methane could represent formation temperatures.

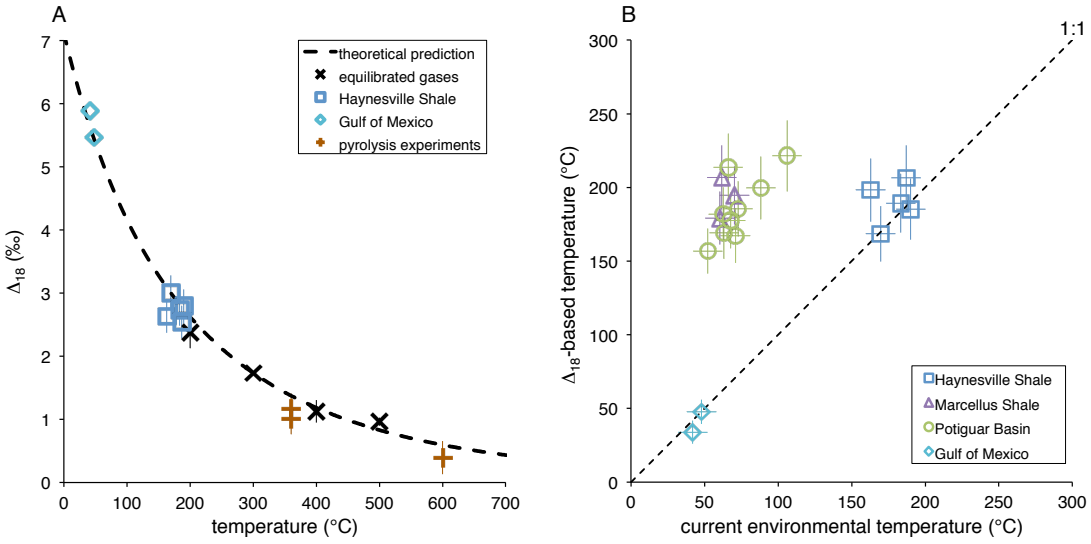

Figure 1: A) Formation or reservoir temperatures vs. measured Δ_{18} values. The dashed line is the expected theoretical dependence of Δ_{18} on temperature for an isotopically equilibrated system (Stolper et al., 2014b). Data for equilibrated gases generated using nickel catalysts come from Stolper et al. (2014b). Temperatures are formation/equilibration temperatures for the pyrolysis and equilibrated samples. Haynesville Shale and Gulf of Mexico temperatures are current reservoir temperatures. B) Current reservoir temperatures vs. Δ_{18} temperatures for all natural samples investigated except the Antrim Shale samples. These are not included as they are a mixture of thermogenic and biogenic gases. The dotted line is a 1:1 line. Well temperature is estimated to be ~ ± 10°C. Error bars are 1σ.

Next, we consider data for thermogenic shale gases from the Haynesville Shale (USA) (Hammes et al., 2011). In shale gas systems, the shale is thought to act as both source and reservoir for generated hydrocarbons (Curtis, 2002), thus gas migration should not be a confounding factor in interpreting measured temperatures. Based on both geological constraints and models (see appendix and below), the Haynesville Shale has undergone minimal uplift (less than ~0.5 km; see appendix) since reaching its maximum

burial temperature, and thus has a relatively simple thermal history. Measured Δ_{18} temperatures for methane range from 169-207°C, overlapping, within uncertainty, current reservoir temperatures (163-190°C; Fig 1A,B; Table A2). The similarity between Δ_{18} temperatures and current/peak burial temperatures suggests that either the Δ_{18} temperatures reflect methane formation temperatures (i.e., methane in the shale dominantly formed near peak burial temperatures) or that the methane formed at some lower temperature and re-equilibrated at the current environmental temperatures after further burial. To distinguish between these two possibilities, we compared our measured Δ_{18} temperatures to independently calculated gas formation temperatures using the hydrocarbon generation kinetics of Burnham (1989; see appendix). This model requires a time-temperature history for each sample, which was constructed using in-house ExxonMobil basin models based on geological constraints for the shales (see appendix; Table A3). These models calculate current well temperatures to be within 5-17°C of maximum burial temperatures (Table A2,3). Modeled average gas formation temperatures from oil and residual kerogen cracking range from 169-175°C (see appendix; Table A3) — earlier formed gases produced with oils are assumed to be lost during original oil expulsion (*appendix*). The modeled temperatures are lower than measured Δ_{18} temperatures (although within uncertainty of our Δ_{18} based temperatures; Table A2). This difference is expected — the Burnham (1989) kinetics treats hydrocarbon gas components (e.g., $C_{1\text{-}5}$ alkanes, where C_n indicates an alkane with 'n' number of carbon atoms) as identical. However, these kinetics are based on experiments that only generate gases enriched in methane like the gases examined here (>96% mole % C_1 vs. total $C_{1\text{-}5}$ hereafter $C_1/\Sigma C_{1\text{-}5}$; Table A2) by the thermal breakdown of $C_{2\text{-}5}$ alkanes

at temperatures above the average C_{2-5} formation temperatures (Ungerer, 1990). Thus average methane formation temperatures, in this model's framework, should be higher than the average ΣC_{1-5} formation temperatures. We conclude that the correspondence between modeled formation temperatures, current environmental temperatures, and Δ_{18} temperatures indicate that Δ_{18} temperatures are indistinguishable from methane formation temperatures.

We next consider shale gases from the Marcellus Shale (Lash and Engelder, 2011), which — in contrast to the Haynesville Shale — experienced significant uplift (>3 km; see appendix) after maximum burial. Here, current well temperatures range from 60-70°C and are much lower than modeled maximum burial temperatures (183-219°C; see appendix; Table A3). This system thus allows us to examine the effects of cooling on methane Δ_{18} temperatures. These samples yield Δ_{18} temperatures from 179-207°C, which overlap those measured for the Haynesville Shale (Figure 1b) and are hotter than the current reservoir temperatures (Figure 1b). Modeled formation temperatures using the Burnham (1989) as above are 171-173°C (Table A3) – the modeled temperatures are again slightly lower than the measured Δ_{18} temperatures, but the two are within analytical uncertainty (Table A2). As for the Haynesville Shale samples, the difference between measured Δ_{18} and modeled temperatures likely reflect the fact that the model averages across formation temperatures of C_{1-5} components whereas we measure only the methane formation temperature. As for the Haynesville Shale samples, we conclude that Δ_{18} temperatures of Marcellus Shale methane are indistinguishable from independent expectations regarding methane formation temperatures.

The final group of thermogenic gases we consider are oil-associated gases from the southwestern sector of the Potiguar Basin (Brazil; Prinzhofer et al., 2010), where gases migrated from their source(s) to shallower, presumably lower temperature reservoirs (Trindade et al., 1992). Measured Δ_{18} temperatures range from 157-221°C and exceed reservoir temperatures (66-106°C). This is consistent with vertical migration of gases from hotter sources to cooler reservoirs (Hunt, 1996). We note that some source rocks in the Potiguar Basin near where samples were collected have experienced sufficient burial temperatures to reach a vitrinite reflectance of 2.7% (Petrobras, unpublished results), within the range observed for the source rocks of the Haynesville and Marcellus shale gases (1.7-3.1%; Table A3) and consistent with the empirical, high-temperature, 'dry gas zone' in which oil is hypothesized to crack to methane (Hunt, 1996) at temperatures above 150-160°C (Clayton, 1991; Hunt, 1996; Quigley and Mackenzie, 1988). Thus the Δ_{18} temperature range of the Potiguar Basin methane (157-221°C) is compatible with the thermal history of at least some source rocks in the region. A positive correlation exists between the Δ_{18} temperatures and $\delta^{13}C^{*}$ values of Potiguar Basin gases (Figure 2; *p*-value = 0.008). This is expected because earlier-generated methane is thought to form at lower temperatures with lower $\delta^{13}C$ values than methane formed later at higher temperatures (Clayton, 1991; Hunt, 1996; Schoell, 1983; Tang et al., 2000). Furthermore, the slope of the $\delta^{13}C$ vs. temperature relationship is 5.3°C/‰ (± 2.2; 1 standard deviation, σ) and is within error of some (but not all; see appendix) theoretical estimates of this slope: 8.8°C/‰ (Ni et al., 2011) and 9.4°C/‰ (Tang et al., 2000).

[*] $\delta = (R/R_{std}-1) \times 1000$ where $^{13}R = [^{13}C]/[^{12}C]$, $^{D}R = [D]/[H]$, and 'std' denotes the standard to which all measurements are referenced. For this paper all carbon measurements are referenced to VPDB and all hydrogen measurements to VSMOW

Further details about these and other models can be found in the appendix. Because the Potiguar Basin gases migrated from source rocks with unknown thermal histories to their current, cooler reservoirs, we cannot directly compare our results with quantitative models of gas formation directly tied to basin thermal models.

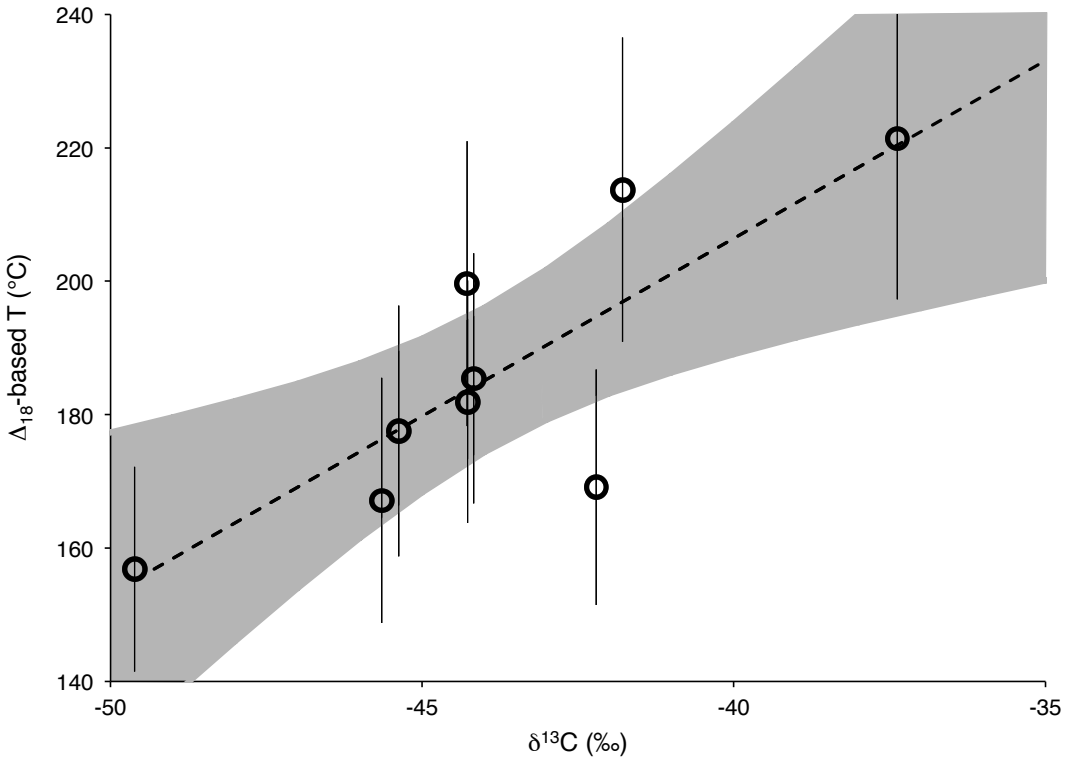

Figure 2: $\delta^{13}C$ values vs. Δ_{18}-based temperatures for methane from the Potiguar Basin. A positive correlation (*p*-value = 0.008) is observed. The gray band is the 95% confidence interval for the linear regression through the data. Error bars are 1σ.

Two key questions are raised by these results: (I) do Δ_{18} values reflect equilibrium- or kinetically-based isotope effects? And (II) if Δ_{18} values reflect equilibrium isotope effects, do the inferred temperatures reflect formation or 'closure' (Dodson, 1973) temperatures? Closure temperatures occur when isotopic exchange continues post formation via temperature-dependent isotope-exchange reactions. As a

sample cools, the rates of these reactions slow, eventually locking in a final Δ_{18} 'closure' temperature. Several observations indicate that measured Δ_{18} temperatures represent average methane formation temperatures and thus internal isotopic equilibration of methane during formation, and that any 'closure' temperature for methane re-equilibration in nature is higher than temperatures reached by the samples examined in this study: (i) Experimentally generated methane yields Δ_{18} values within error of known formation temperatures (Figure 1A). (ii) All Δ_{18} temperatures from natural samples are geologically reasonable methane formation temperatures (Clayton, 1991; Hunt, 1996; Quigley and Mackenzie, 1988; Seewald, 2003; Seewald et al., 1998). (iii) Haynesville Shale Δ_{18} temperatures are within uncertainty of current and modeled maximum burial temperatures (Figure 1A,B). (iv) Haynesville Shale and Marcellus Shale Δ_{18} temperatures are within error of independently modeled gas formation temperatures. (v) Haynesville Shale and Marcellus Shale Δ_{18} temperatures overlap despite the differing thermal histories of each system. This would not be expected if Δ_{18} temperatures reset during cooling of the host rocks (i.e., because the Marcellus shale cooled by >100 ˚C after gas generation). And (vi) Potiguar Basin Δ_{18} temperatures and $\delta^{13}C$ values are positively correlated (Figure 2), with a slope within error of some theoretical predictions. Consequently, we hypothesize and will proceed with the interpretation below that the measured Δ_{18} temperatures for thermogenic methane represent average methane formation temperatures. We note though that we have not, nor could we ever prove this to be true and stress that this remains an operating hypothesis regarding a novel proxy — all of its implications must be tested and informed by future work. One additional issue is that mixing of gases with differing $\delta^{13}C$ and δD can result in non-linear mixing of Δ_{18}

values (and thus temperature (Stolper et al., 2014b)); however, for the thermogenic samples examined here, the $\delta^{13}C$, δD and Δ_{18} values are all sufficiently similar that unknown amounts of mixing between samples would not result in Δ_{18} temperatures different (within the 2σ error of the measurement) from the actual average temperature of the mixtures.

If the interpretation of Δ_{18}-based temperatures as formation temperatures is correct, it has important implications for our understanding of the chemistry of thermogenic methane formation. Specifically, it requires a heretofore unrecognized step that allows C-H bonds to equilibrate during methane formation, but not continue after methane formation. This interpretation is unexpected because $\delta^{13}C$ and δD values of thermogenic methane are almost universally considered to be controlled by kinetic isotope effects associated with cracking reactions rather than equilibrium thermodynamic effects (Clayton, 1991; Ni et al., 2011; Tang et al., 2000; Xiao, 2001). This apparent contradiction can be reconciled if reacting methane precursors (e.g., methyl groups) undergo local hydrogen exchange faster than the rate of net methane generation. Such a mechanism would allow $\delta^{13}C$ values and overall methane production rates to be kinetically controlled while also allowing methane to reach internal isotopic equilibrium. Rapid local hydrogen exchange could be promoted by catalysis on organic macromolecules, mineral surfaces, or transition metals: e.g., Mango et al. (1994), Mango and Hightower (1997), and the Ni-catalyzed equilibration experiments of (Stolper et al., 2014b); though see Lewan et al. (2008) and Price and Schoell (1995) for arguments against the importance of transition metals in hydrocarbon generation. Additionally, such

rapid exchange could also be an intrinsic property of highly reactive methane precursors (e.g., methyl radicals).

Because some natural gas accumulations are thought to be microbial in origin (Martini et al., 1996b; Whiticar et al., 1986), we also tested whether Δ_{18} values distinguish natural thermogenic gases from biogenic gases. We first measured Δ_{18} values from two gases produced from the biodegradation of oil (Gulf of Mexico, USA). Both are suspected of being >80% biogenic gas formed in their current reservoirs. They return Δ_{18} temperatures (34 ± 8 and 48 ± 8°C) within error of their current reservoir temperatures (42 and 48°C respectively; Fig 1A,B; Table A2). We also measured two gases from the Antrim Shale (USA), which has been interpreted as containing a mixture of biogenic gases higher in $C_1/\Sigma C_{1\text{-}5}$ and thermogenic gases lower in $C_1/\Sigma C_{1\text{-}5}$ (Martini et al., 1996b). The sample closer to the biogenic end-member (99.99% $C_1/\Sigma C_{1\text{-}5}$) returns a Δ_{18} temperature of 40°C (± 10; 1σ) while the sample interpreted here to be closer to a thermogenic end-member (88.9% $C_1/\Sigma C_{1\text{-}5}$) returns a higher temperature of 115°C (± 12°C; 1σ). Thus, the studied natural biogenic gases have Δ_{18} temperatures consistent with their expected formation temperatures, both as pure end members and as dominant components of mixtures. As was the case for the thermogenic gases, it is not expected that biogenic gases would display an equilibrium clumped isotope signature because microbial methanogenesis exhibits substantial kinetic isotope effects (Valentine et al., 2004; Whiticar et al., 1986). These reasonable Δ_{18} temperatures suggest that biogenic methane is in internal isotopic equilibrium, which may arise through rapid hydrogen isotope exchange during the metabolism of methanogens (Valentine et al., 2004). We note that preliminary results for methanogens grown in pure culture (Stolper et al.,

2014a) indicate that they can — in some cases — produce methane out of internal equilibrium. Nevertheless, our measurements of natural biogenic methane indicate that natural environments (at least those investigated to-date) permit the attainment of local equilibrium.

The agreement between the Haynesville Shale and Marcellus Shale methane Δ_{18} temperatures and the modeled formation temperatures of Burnham (1989) demonstrates that in at least some cases when the source rocks and their thermal histories are known, existing gas generation models can constrain the formation temperature of methane. The formation temperatures of the Potiguar Basin gases are more difficult to constrain using models of this kind because gas migration has separated them from their source rocks; thus it is not clear precisely where or when they formed in the basin's history. Such migrated gases are common, and have motivated the creation of several approaches to infer gas formation temperatures (or, more qualitatively, rankings of thermal 'maturity') based on molecular and/or isotopic compositions. These approaches range from qualitative fingerprinting tools (Lorant et al., 1998; Prinzhofer and Huc, 1995; Schoell, 1983) to more elaborate models that incorporate temperature-dependent kinetic parameters, thermal histories of the source and reservoir rocks, and sometimes isotopic constraints (Burnham, 1989; Seewald et al., 1998; Tang et al., 2000). The measurements of methane formation temperature provided by clumped isotope thermometry allow us to directly evaluate environmental temperatures of methane formation and thus test these models.

Figure 3 compares representative model-derived gas formation temperatures for Potiguar Basin methane to the measured methane Δ_{18} temperatures; a more detailed

discussion of each model and their assumptions is given in the appendix. All models presented in Figure 3 are consistent with the input parameters measured for the Potiguar Basin gases (e.g., isotopic compositions and/or abundances of C_{1-5} alkanes). However, inferred temperature ranges for many of these models are mutually exclusive. The

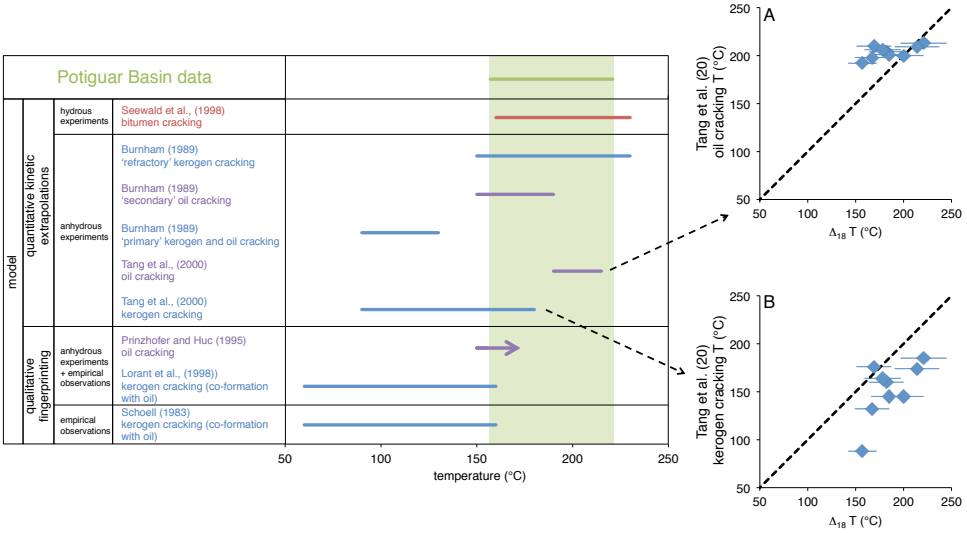

Figure 3: Comparison of various models (described in the appenix) to the observed temperature range for the Potiguar Basin methane (given by the green line). Blue lines indicate gases are generated from kerogen cracking, purple lines from oil cracking, and red lines from bitumen cracking. For the Schoell (1983) and Lorant et al. (1998) models that predict gas formation with oils, we assume oils form from 60-160°C (Clayton, 1991; Hunt, 1996; Quigley and Mackenzie, 1988). For the Prinzhofer and Huc (1995) model, oil cracking is assumed to occur above 150°C (Clayton, 1991; Hunt, 1996; Quigley and Mackenzie, 1988) as indicated by the arrow. In the insets are sample by sample comparisons of Δ_{18} temperatures vs. calculated formation temperatures using the model of Tang et al. (2000) for both oil (inset A) and kerogen cracking (inset B). Dashed lines are 1:1 lines. See the appendix for details. Error bars are 1σ.

measured Δ_{18} temperatures for the Potiguar Basin methane samples provide a basis for assessing the accuracy of such models. For example, the model of Lorant et al. (1998) was used previously by Prinzhofer et al. (2010) to indicate that gases from the southwestern sector of the Potiguar Basin were co-generated with oils within the oil window, below ~160°C (Clayton, 1991; Hunt, 1996; Quigley and Mackenzie, 1988). This conclusion is inconsistent with the observed Δ_{18} temperatures. However, this model is

calibrated using C_2 and C_3 abundances and $\delta^{13}C$ values, but not methane abundances or isotopic composition (see appendix). Thus it is possible that the methane could have a different average formation temperature from the C_{2-5} alkanes. The model of Tang et al. (2000) results in estimated methane formation temperatures that are systematically lower than Δ_{18} temperatures (Figure 3, inset A) when methane is assumed to derive from kerogen cracking. However, if gas is assumed to come from oil cracking, that model predicts temperatures similar to average measured Δ_{18} temperatures (though it still does not reproduce the overall range in temperature observed; Figure 3, inset B).

One way to reconcile these models with the observed Δ_{18} temperatures and other gas properties is by mixing gases produced from kerogen cracking at lower temperatures (e.g., <~150-180°C) with gases generated from oil cracking at higher temperatures (e.g., >~150-160°C). In this scenario, both the models of Tang et al. (2000) and Burnham (1989) are compatible with the Δ_{18} temperatures, but require a very specific set of mixing components to generate the observed temperatures, range in temperatures, range in % $C_1/\Sigma C_{1-5}$ values (Table A2), and correlation of temperature with methane $\delta^{13}C$ values. Alternatively, a few models are consistent with the observed Δ_{18} temperature range without the need for mixing of distinct methane sources. The model of Prinzhofer and Huc (1995) indicates the gases formed in part from cracking of oil above ~160°C (Clayton, 1991; Hunt, 1996; Quigley and Mackenzie, 1988), which is consistent with the range of Δ_{18} temperatures. Unfortunately, this model is not sufficiently quantitative in terms of predicted gas formation temperatures to interrogate further. The Burnham (1989) model for refractory kerogen cracking is also consistent with the observed range in Δ_{18} temperatures; however refractory kerogen is conceptualized in this model to be a

precursor mostly to methane (as opposed to C_{2-5} alkanes), which is inconsistent with the significant quantities of C_{2-5} alkanes in all observed Potiguar Basin gases (<85% $C_1/\Sigma C_{1-5}$; Table A2). Finally, the model of Seewald et al. (1998) is consistent with the entire range of Δ_{18} temperature observed, and predicts formation of gases with similar $C_1/\Sigma C_{1-5}$ (~<90%) to the Potiguar Basin gases. This model is also the only one to include the role of water explicitly in gas formation and may indicate the importance of considering water in gas formation kinetics. Thus, while the addition of Δ_{18} temperatures does not provide a unique interpretation of the origin of the Potiguar Basin gases, it rules out several otherwise plausible-seeming interpretations and places specific constraints on the remaining models.

3. Conclusions

The results of this study indicate that Δ_{18} values constrain methane formation temperatures from natural thermogenic and biogenic gases. Consequently, measurements of Δ_{18} values introduce a new means of understanding petroleum genesis, microbial ecosystems that produce methane, and perhaps methane emissions to the atmosphere. Moreover, the simple observation that thermogenic and biogenic methane appear to form in internal isotopic equilibrium offers a new (and unexpected) constraint on the chemistry of methane formation. I.e., it implies that these reactions generally involve locally reversible hydrogen additions.

A key implication of our results for the Potiguar Basin is that the formation environments for methane extend to higher temperatures (and presumably depths) than many models of petroleum genesis would predict. Although methane is the main product

of the highest levels of thermal maturation of organic-rich source rocks, if it is mixed into lower-maturity petroleum products during later migration and storage, conventional gas-chemistry proxies might not reflect the methane's true origins. Methane clumped isotope thermometry demonstrates the existence of a component of methane in the Potiguar Basin that was generated at higher temperatures than might be (Prinzhofer et al., 2010) predicted from many tools used to interpret gas chemistry (Figure 3). This finding indicates that this basin possesses a previously unsuspected ‘root’ that reached high temperatures at some point in its history, generating high-temperature methane that ascended into shallower reservoirs where it mingled with oils and higher order hydrocarbon gases. Thus, measured methane formation temperatures not only constrain the conditions and mechanisms of methane formation, but also provide a new window into the geological and thermal histories of basins in which it forms.

4. Appendix

Δ_{18} Notation

Δ_{18} values are calculated as

$$\Delta_{18} = (^{18}R/^{18}R^{*}\text{-}1) \times 1000 \quad \text{(A1)}$$

where

$$^{(18}R = ([^{13}CH_3D] + [^{12}CH_2D_2])/[^{12}CH_4], \quad \text{(A2)}$$

brackets denote the relative abundance of the isotopologue as measured by mass spectrometry, and the * denotes the relative abundance for a random internal distribution of isotopes (Stolper et al., 2014b). Δ_{18} values are reported in a reference frame in which Δ_{18} values of 0‰ refer to a gas internally equilibrated at infinite temperature. All samples are compared to (i.e. referenced against) an internal lab standard with a Δ_{18} in this reference frame of 2.981‰, which was calibrated in the study of Stolper et al. (2014b). Δ_{18} values are converted into temperature (in Kelvin) via the equation:

$$\Delta_{18}\text{=-}0.0117\left(\frac{10^6}{T^2}\right)^2 + 0.708\left(\frac{10^6}{T^2}\right) - 0.337 \text{ (Stolper et al., 2014b).} \quad \text{(A3)}$$

A full discussion of the relationship between Δ_{18} and temperature for equilibrated systems both theoretically and empirically is given in Stolper et al. (2014b).

Experimental Methods

Purification and isotopic measurements of methane

All samples from natural systems reported in this study were recovered directly from gas wells in sealed metal containers of varying design and transported to the California Institute of Technology (Caltech). All samples other than those from the

Potiguar Basin were first sent to Isotech Laboratories Inc. (Champaign, IL) and subsampled before then being sent to Caltech. Potiguar Basin samples were subsampled at Petrobras before being sent to Caltech. Methane was purified from sampled gases by cryogenic distillation on a glass vacuum line. Values of δD, $\delta^{13}C$, and Δ_{18} were measured on a prototype Thermo 253 Ultra mass spectrometer (Eiler et al., 2013) housed at Caltech following the methodology outlined in Stolper et al. (2014b). In the methane purification procedure described in Stolper et al. (2014b), N_2 was removed by a single exposure of samples frozen at 45 K to vacuum. We have subsequently found that this is insufficient to fully remove N_2 from many natural gas samples. Repeated (3-5 times) freezing (45 K) and thawing (80 K), with exposure to vacuum in every cycle at 45 K was found to be sufficient to fully remove N_2. After this cleanup procedure, samples always contained <0.2% N_2. This cleanup is necessary because significant N_2 concentrations (>0.5%) can result in mass spectrometric measurement artifacts.

To ensure that this new cleaning protocol did not fractionate gases, we compared Δ_{18} values of pure methane gases (thus containing no N_2) heated with nickel catalysts at 500°C and treated using either the original or new cleaning procedure. The original cleaning procedure resulted in a mean Δ_{18} value of 1.01 ± 0.09‰, (1 standard error; s.e.; n = 6) while the new cleaning procedure yielded a mean Δ_{18} value of 1.00 ± 0.11‰ (1 s.e., n = 10). We thus conclude that repeated freeze-thaw cycling does not introduce any measurement artifacts. We employed this procedure for all samples reported here. We note that the gas derived from the pure methanogen culture grown at 65°C and reported by (Stolper et al., 2014b) had unknown amounts of N_2 gas in it and so likely resulted in measurement artifacts. Remeasurement with the new cleaning procedure has

demonstrated that the sample, as well as methane from other methanogen cultures, yield Δ_{18} values that are not in internal isotopic equilibrium (Stolper et al., 2014a).

Precision and accuracy of isotopic measurements of methane

Internal precision for the Δ_{18} values from a single measurement is generally between 0.24-0.27‰ and is near the limit imposed by counting statistics (Stolper et al., 2014b). We evaluated external precision in two different ways. First, we measured a standard multiple times during every measurement session. It differs in average isotopic composition from the internal reference standard by +46.5‰ in δD and +30.5‰ in $\delta^{13}C$. External precision for 15 measurements over 1 year and 6 different measurement sessions for Δ_{18} is ± 0.19‰ (1 standard deviation; σ). The samples used to calculate this standard deviation include some taken directly from a bottle as well as aliquots frozen onto molecular sieves and stored in Pyrex® tubes sealed with a natural gas torch following Stolper et al. (2014b). To ensure that freezing samples onto molecular sieves and storing them in Pyrex® tubes does not result in an isotopic fractionation, we compared average Δ_{18} values from samples taken directly from the bottle vs. stored in the Pyrex® tubes using molecular sieves. The average Δ_{18} value of samples taken directly from the bottle is 4.71 ± 0.05‰ (1 s.e., n = 8). The average Δ_{18} value of samples frozen onto molecular sieves and stored in Pyrex® tubes is 4.67 ± 0.10 (1 s.e., n = 7). Thus, as concluded in Stolper et al. (2014b), the use of molecular sieves to store gases in Pyrex® tubes does not measurably alter Δ_{18} values.

Second, to check the external reproducibility of Δ_{18} values for gases cleaned on the vacuum line as described above and in Stolper et al. (2014b), we measured gases that were equilibrated at 500°C on nickel catalysts. These heated gases were purified in an

identical way as all samples reported in this study. The standard deviation of replicate measurements of these gases (16 total measurements across 1 year and 7 sessions) yields an external precision in Δ_{18} of ± 0.29‰ (1σ). The error is dominated by a single point, which, if removed, improves the precision to ± 0.23‰ (1σ). We thus conclude that our external precision for Δ_{18} measurements is similar to our internal precision of 0.24-0.27‰.

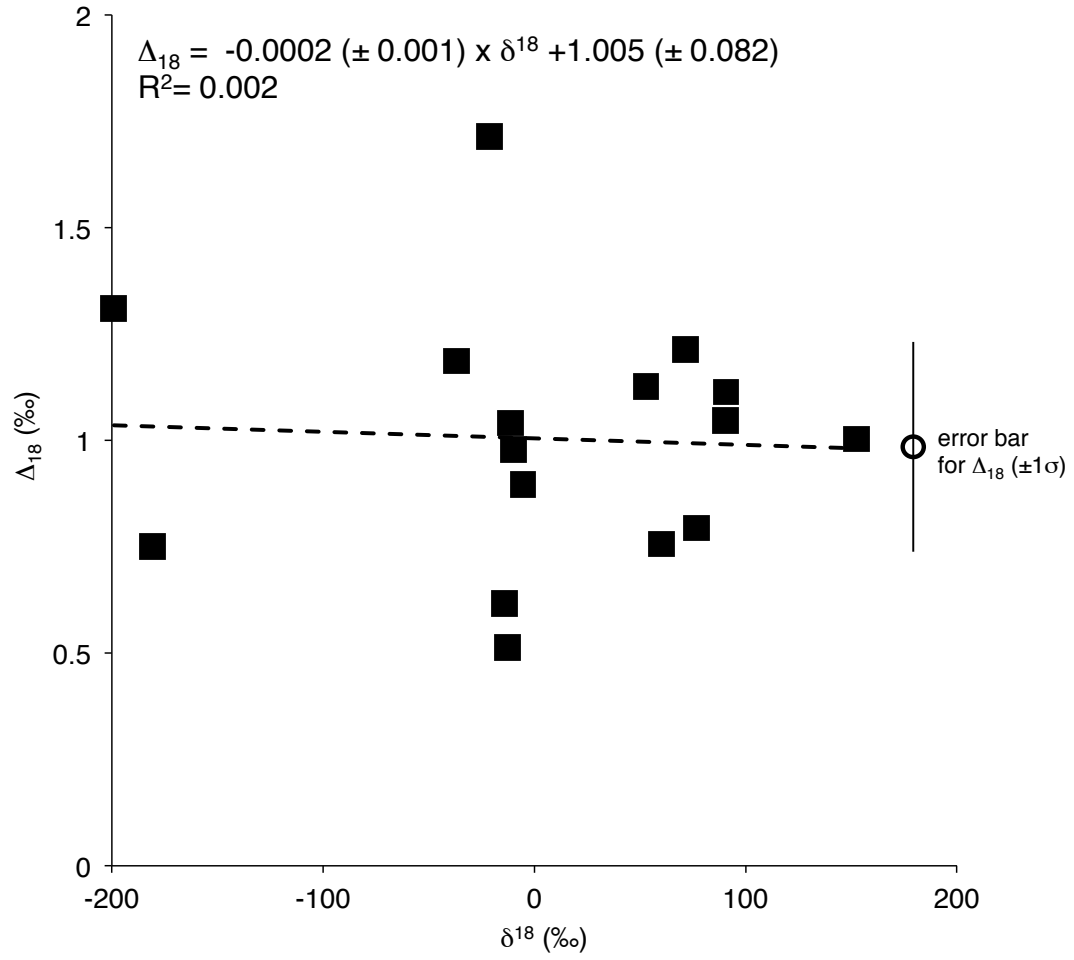

Figure A1. Relationship between average isotopic composition (δ^{18}) and Δ_{18} in methane equilibrated at 500°C over nickel catalysts. The slope of the relationship is −0.0002 ± 0.001 (1σ), and is thus not significantly different from zero.

We also evaluated whether there is any dependence of measured Δ_{18} values on a sample's average isotopic composition. To do so, we measured methane that was equilibrated at 500°C on nickel catalysts with a range of starting δD and $\delta^{13}C$ values. The average isotopic composition at mass 18 is tracked through the parameter δ^{18}, which reflects differences in either the ^{13}C or D abundance of a methane sample vs. a standard:

$$\delta^{18}=(^{18}R_{sample}/^{18}R_{standard}-1) \times 1000. \quad (A4)$$

As seen in Figure A1, the slope that defines the dependence of Δ_{18} on δ^{18} across an ~350‰ range in δ^{18} is -0.0002 ± 0.001 (1σ; Figure A1), and thus indistinguishable, within error, from 0. We thus confirm the findings of Stolper et al. (2014b) that there is no statistically significant dependence of measured Δ_{18} values on a sample's average isotopic composition within the range of δ^{18} values commonly observed in nature.

Generation of methane from cracking experiments

Methane was generated from larger hydrocarbon precursors in two separate experiments. Data for these samples are given in Table A1. In the first experiment (at Caltech), an aliquot of propane was frozen into a Pyrex® tube and flame-sealed. The glass tube was placed in a box furnace at 600°C and heated for 12 hours. During the experiment, the sample developed a black film along the side of the tube, which we believe to be graphite. The tube was removed from the furnace and methane was recovered and cleaned following typical gas separations described in Stolper et al. (2014b) and above.

The second experiment (at the U.S. Geologic Survey in Denver) involved hydrous pyrolysis of an organic-rich black shale from the U. Devonian-L. Mississippian Woodford Shale. The sample was collected from a stream-cut outcrop along Henry

House Creek in southern Oklahoma, USA, located approximately 8 km west of the Woodford outcrop previously sampled by Lewan (1983). The sample was collected from a 9 cm thick bed that appears to be lithologically homogeneous, and is similar in mineralogy to the quartzose claystone lithology described by Lewan (1983). The total organic carbon content is 21.97 weight percent and the kerogen is predominately amorphous type-II. The sample is thermally immature and in the pre-oil generation stage.

The hydrous pyrolysis experiment was conducted in a 1-liter reactor composed of Hastelloy-C276 (Parr Instrument Company, Illinois, USA) generally following the procedure described by Lewan (1997). Specifically, the sample was crushed to gravel size (0.6 to 2.0 cm) with no prior extraction or drying before the experiment. The reactor was loaded with 200.3 g of whole rock and 400.2 g of deionized water and closed. This volume of water was sufficient to submerge the rock in liquid water throughout the experiment. The loaded reactors were then evacuated and purged with 6.9 MPa of helium, which was vented until only 172 kPa of He remained in the reactor headspace. The reactor was heated to a temperature of 360 ± 1.3°C within 75 minutes and maintained at this temperature for 72 hours. The reactor was air cooled to ambient temperature before sampling. The final gas pressure was 1.1 MPa at 21.7°C and gas samples were collected in 50-mL stainless-steel cylinders. Two replicate sample aliquots were collected from the same experiment. Methane was separated from other gases following Stolper et al. (2014b) for both aliquots. We noted a difference in both the $\delta^{13}C$ (0.6‰) and δD (0.5‰) values of the two aliquots, but a statistically insignificant difference in Δ_{18} values (0.14‰) compared to the precision of the measurements (± 0.25‰ for both samples; Table A1). The similar offsets between $\delta^{13}C$ and δD values of

the two aliquots (0.5-0.6‰) may indicate a diffusive fractionation during sample collection from the reactor. Regardless, the Δ_{18} value is insensitive to changes in δD and $\delta^{13}C$ between the two aliquots. Nevertheless, we treat the two aliquots as separate samples in Figure 1 of the main text due to these differences in δD and $\delta^{13}C$.

Isotopic measurements of ethane and propane

The $\delta^{13}C$ values of ethane and propane were also measured and are presented in Table A2 for the Potiguar Basin samples. These were measured at Petrobras's laboratories using a Delta V Advantage mass spectrometer (Thermo Scientific). Hydrocarbon compounds were separated using an Agilent 6890 gas chromatograph (GC) with helium as the carrier gas. Samples were combusted on-line to CO_2 using a GC/C III interface (Thermo Scientific) with the reactor held at 960°C. Sample $\delta^{13}C$ values were calibrated against in-house, secondary standards that were in turn calibrated against the Natural Gas Standard #2 (NGS-2) distributed by the National Institute of Standards and Technology. Precision for these measurements is generally ±0.5‰ (1σ).

C_1-C_5 abundances

The relative abundances of methane (C_1), ethane (C_2), propane (C_3), butane (C_4), and pentane (C_5) were measured at Petrobras's laboratories for the Potiguar Basin gases and at Isotech Laboratories Inc. for all other gases. Hydrocarbon abundances were measured using standard GC techniques. At Isotech, Shimadzu 2014 and 2010 GCs were employed for separations with both thermal conductivity and flame ionization detectors used to quantify gas abundances. At Petrobras, a Hewlett Packard GC was used with both thermal conductivity and flame ionization detectors. Relative precision was typically ± 5% for C_{1-3} hydrocarbon abundance and ± 10% for C_{4-5} hydrocarbon abundance. For

measurements made at Petrobras (i.e., Potiguar Basin samples), the abundance of pentane was not measured, which will cause $C_1/\Sigma C_{1\text{-}5}$ ratios to be overestimated. Given that the relative amounts of C_4 vs. $C_{1\text{-}4}$ are between 2-9%, with an average of 4% for the Potiguar Basin gases, and that C_5 is typically less abundant than C_4, this overestimation will be ~<4% on average.

Well Temperatures

Natural thermogenic gases were recovered from wells with known borehole temperatures, which are reported in Tables A2 and A3. These temperatures were measured following standard industry practice via the introduction of a thermal conductivity sensor directly into the well borehole. However, these temperatures can be biased by thermal disturbances created during drilling, fluid injection, and hydrocarbon extraction (Price et al., 1981). The best way to measure accurate borehole temperatures is to close the borehole for some duration, allowing the system to return to ambient temperatures (Price et al., 1981). In practice, however, active production wells cannot be closed for sufficient lengths of time, and instead a temperature correction is required. Temperatures for the Potiguar Basin and Gulf of Mexico samples were previously corrected by the petroleum engineering departments of the companies supplying the samples. Temperatures for the Haynesville Shale and Marcellus Shale samples were corrected following typical industry practices by increasing all temperatures by 10%. We note that this is clearly an estimate and indicates the challenge of obtaining accurate borehole temperatures. To account for uncertainty in these corrections, we estimated a 1σ error for these borehole temperatures of ± 10°C.

Geology of studied natural gas deposits

Here we provide a brief summary of the geology of the various basins examined in this study. References with more information are provided.

Haynesville Shale: The Haynesville Shale is upper Jurassic in age and is found in eastern Texas and western Louisiana (Hammes et al., 2011). The Haynesville Shale formed during the opening of the Gulf of Mexico in a deep (below storm-wave base) basin surrounded by carbonate banks and shoals (Hammes et al., 2011).

Marcellus Shale: The Marcellus shale is Devonian in age and formed as part of the Catskill delta complex in a foreland basin during the Acadian Orogeny (Ettensohn, 1985). All studied gases come from Pennsylvania, but the shale is also found in New York, Ohio, West Virginia, Virginia, and Maryland.

Potiguar Basin: The Potiguar Basin formed during rifting of South America from Africa in Early Cretaceous time (Matos, 1992). The dominant source rocks for oils and gases in the area are the lacustrine and deltaic Pendêcia formation (shales and sandstones) and lagoonal Alagamar formation (shales and carbonates) (dos Santos Neto and Hayes, 1999).

Antrim Shale: The Antrim Shale, like the Marcellus Shale, is Devonian in age and formed as part of the Catskill delta complex during the Acadian Orogeny (Ettensohn, 1985). It occurs in the Michigan Basin. Large fracture systems occur in the shale that have allowed

meteoric waters from glacial episodes to flow into the shale and introduce methanogens (Martini et al., 1998). Hydrocarbon gases in the basin include thermogenic gases and, based on isotopic arguments, significant proportions of biogenic gases (Martini et al., 1996a).

Estimates of the carbon isotope fractionation between methane and larger hydrocarbons as a function of temperature.

The $\delta^{13}C$ values of Potiguar Basin methane samples are correlated with the measured Δ_{18} temperatures (Figure 2 in the main text of this chapter). This relationship has a slope of 5.3 °C/‰ (± 2.2, 1σ). In the main text of this chapter, we compared this slope to theoretical estimates for the temperature dependence of carbon isotope fractionation from 100-250°C based on methane formation from an ethane precursor using the studies of Ni et al. (2011) and Tang et al. (2000). Here we provide details of those calculations, and similar estimates for this temperature dependence from other studies of which we are aware. All isotope fractionation factors described below are for carbon isotope fractionations between methane and larger precursor hydrocarbon molecules.

From Ni et al. (2011), the fractionation factor between methane (product) and ethane (reactant) via a homolytic cleavage reaction is given by:

$$\ln(\alpha_{CH4\text{-}C2H6}) = -22.854*(1/T) + 0.0211, \quad \text{(A5)}$$

(Figure 2 in Ni et al., 2011) where $\alpha_{CH4\text{-}C2H6}$ is $(1000 + \delta^{13}C_{methane})/(1000 + \delta^{13}C_{ethane})$ and T is temperature in Kelvin. Using this relationship, we calculated 1000 x ($\alpha_{CH4\text{-}C2H6}$-1) for 100, 150, 200, and 250°C, and used these data to calculate the slope, 8.8 °C/‰ (Table A4). 1000 x (α−1) gives an estimate for the fractionation of $^{13}C/^{12}C$ between a source

hydrocarbon molecule and generated methane, regardless of absolute $\delta^{13}C$ values. Thus comparing the dependence of temperature on 1000 x (α–1) for this theoretical data allows for the direct comparison to the data from Potiguar Basin presented in Figure 2 of the main text of this chapter.

Tang et al. (2000) does not provide an equation for the dependence of ln(α) on temperature. Instead, data for α at 300, 400, 500, and 600 K are given for methane formation from ethane, propane, butane, pentane, and hexane via homolytic cleavage. To directly compare these results to those from Ni et al. (2011), we used the data for the isotope fractionation factors between methane and the residual ethane. Fitting ln($\alpha_{CH4\text{-}C2H6}$) vs. 1/T yields the following equation:

$$\ln(\alpha_{CH4\text{-}C2H6}) = -22.155*(1/T) + 0.0226. \quad \text{(A6)}$$

We again calculated 1000 x ($\alpha_{CH4\text{-}C2H6}$-1) at 100, 150, 200, and 250°C, and used these data to calculate the dependence of T (°C) on 1000 x ($\alpha_{CH4\text{-}C2H6}$-1), and thus the dependence of temperature on the $\delta^{13}C$ of methane as above (Table A4). This yields a slope of 9.4 °C/‰.

We are aware of two other theoretical estimates for these fractionation factors from the study of Xiao (2001). In this study, two separate mechanisms for methane formation are considered: homolytic cleavage and β-scission. The fractionation factors ($\alpha_{CH4\text{-}C8H18}$) for methane formation from octane vs. the residual octane as a function of temperature at 0, 100, 200, 300, 400, 500, and 600°C are given in Figure 14 of that study, but not in tables. We estimated the values of these points from the figures and provide them in Table A5. We fit ln(α) vs. 1/T using a quadratic fit for each yielding

$$\ln(\alpha_{CH4\text{-}C8H18}) = -1886*(1/T)^2 - 9.086*(1/T) + 0.0068 \quad \text{(A7)}$$

for homolytic cleavage and

$$\ln(\alpha_{CH4\text{-}C8H18}) = -2205*(1/T)^2 - 5.539*(1/T) - 0.0176 \quad \text{(A8)}$$

for β-scission.

We then calculated 1000 x ($\alpha_{CH4\text{-}C8H18}$-1) at 100, 150, 200, and 250°C (Table A4) and calculated the temperature-dependence of 1000 x ($\alpha_{CH4\text{-}C8H18}$-1) for homolytic cleavage (11.1 °C/‰) and for β-scission (12.8 °C/‰).

It is important to note that the fractionation factors from Ni et al. (2011) and Tang et al. (2000) considered methane formation from ethane, whereas those from Xiao (2001) considered methane formation from octane. It is possible that the use of different reactant molecules results in significantly different fractionation factors. To consider this further, we compared modeled fractionation factors from Tang et al. (2000) for methane formation from ethane vs. hexane. The differences vary from 2‰ to 0‰ at any given temperature, with no obvious dependence on temperature. Because these differences are far smaller than the differences in fractionation factors between the various studies (see below), we consider it reasonable to directly compare fractionation factors for methane formation from ethane and octane.

As discussed in the main text, the data from Ni et al. (2011) and Tang et al. (2000) yield slopes for 1000 x (α−1) versus temperature within error (2σ) of that for Potiguar Basin samples. However, the slopes (°C/‰) derived for both homolytic cleavage and β-scission from Xiao (2001) lie more than 2σ above the Potiguar Basin value. Importantly, the actual fractionation factors from these studies, despite having roughly similar temperature dependencies, differ strongly in absolute value at the various temperatures. For example, at 100°C, the difference between the maximum and minimum predicted

fractionation factors among these studies is 8.8‰ for homolytic cleavage. Moreover, there is a 16.5‰ difference between fractionation factors for homolytic cleavage and β-scission from the study of Xiao (2001) at 100°C. The differences between homolytic cleavage and β-scission are presumably related to the different mechanisms and thus transitions states of these reactions. However, the differences in fractionation factors for homolytic cleavage are not clear. They perhaps arise due to inaccuracies, approximations, or differences in the quantum mechanical models used to estimate these fractionation factors.

The differences between these models for calculated fractionation factors of methane formation from a hydrocarbon precursor are significant and demonstrate the importance of having empirical constraints from samples of known formation temperature. Given these discrepancies, we find it neither surprising nor discouraging that the temperature dependence of some of the modeled fractionation factors (and thus $\delta^{13}C$ of methane) are not within error of the observed trend for T vs. $\delta^{13}C$ for the Potiguar Basin samples.

Models of thermal histories and gas generation for shale gases

Thermal histories were developed for each well in the Marcellus and Haynesville shales using an in-house, unpublished model of ExxonMobil's with the following input parameters: paleo-water depth, basal heating rate (mW/m^2), and current sedimentary column thickness, lithology, and conductive properties of different rock types. Maximum burial temperatures of the models are given in Table A3. Basal heat flows for the Haynesville Shale were estimated to be 70 mW/m^2 for the past 80 million years following

Blackwell and Richards (2004). From 180-80 ma, basal heating rates were higher for the Haynesville Shale, starting at 85 mW/m^2 and then decaying linearly to 80 mW/m^2 by 80 ma following Dutton (1987). Basal heating rates were estimated to be 52 mW/m^2 for the entire depositional history of the Marcellus Shale following Blackwell and Richards (2004). These models all assume a 20 km thick thermal insulator. These models were calibrated using corrected present-day bottom-hole temperatures for each well (in °C) and vitrinite reflectance (R_0) data derived from a combination of measurements in the sampled wells and interpolations between other wells; these data are given in Table A3. The model of Sweeney and Burnham (1990) is used here to calculate the dependence of vitrinite maturation as a function of time and temperature. These thermal histories consider and incorporate data from published external constraints. The thermal histories of the Haynesville Shale samples were modeled as reaching maximum burial 40 million years ago with total erosion less than 500 meters following Dutton (1987) and Torsch (2012). For the Marcellus Shale, maximum burial occurred 270 million years ago following constraints from apatite fission-track thermochronology (Roden and Miller, 1989) and paleomagnetic ages (Levine, 1986). Calculated erosion thicknesses of 3-4 km for the Marcellus Shale are consistent with previous fluid inclusion, vitrinite, and apatite fission-track based estimates (Johnsson, 1986; Levine, 1986; Roden and Miller, 1989).

The thermal histories derived above were then used to calculate the total gas yield per area of source rock as a function of time and temperature. Gas formation temperatures were modeled using gas generation kinetics from Burnham (1989). In this model, C_{1-5} gases are lumped, with no consideration for changes in their relative distribution as a function of formation temperature. To calculate the average formation

temperature, we assumed that gases in the shales were generated *after* oil formation during secondary cracking of oil and cracking of refractory kerogen. This assumption is based on the following observations: (i) The study of Jarvie et al. (2007) indicates that some fraction of oils and co-generated gases are lost from many shale-gas systems, and that a small amount (1%) of oil cracking to gas is sufficient to overcome the strength of the shale and initiate fracturing and hydrocarbon expulsion. Indeed, models of hydrocarbon generation and migration for the Haynesville Shale indicate that initially formed oils and gases did migrate into neighboring strata (Torsch, 2012). Thus, the retained gases in the shale should be derived dominantly from cracking reactions occurring after this initial expulsion of oil and gas. (ii) All gases have >96% $C_1/\Sigma C_{1-5}$. Such methane-rich thermogenic gases are thought to form only after oils have been produced (Clayton, 1991; Price and Schoell, 1995). Regardless, if we included all gases formed during the generation of oils, modeled formation temperatures would drop by only ~10°C, which is not significant. The averaged modeled temperatures presented in the main text of this chapter and Table A3 are weighted average gas formation temperatures. The weight of each temperature is determined by taking the amount of gas calculated at that temperature and dividing by the total amount of gas formed.

Application of published gas classification schemes and models to the Potiguar Basin samples

In the main text, we compared the measured Δ_{18} temperatures for the Potiguar Basin samples to the predicated formation temperatures of multiple gas classification schemes and models. Here we provide additional details, figures, and data to aid in

understanding how we used these models to make statements about modeled formation temperatures for the Potiguar Basin samples. All of the models discussed below either do not distinguish between methane vs. the other C_{2-5} alkanes, or use the abundances or isotopic composition of some of the C_{2-5} alkanes to infer gas formation temperatures. Thus, it is challenging to directly compare the gas formation temperature estimates of these models to measured methane formation temperatures inferred from Δ_{18} temperatures. Additionally, it is possible, as discussed in the main text, that the studied Potiguar Basin gases reflect a mixture of gases with, for example, lower $C_1/\Sigma C_{1-5}$ gases originally formed with oil and higher $C_1/\Sigma C_{1-5}$ gases that migrated into that oil reservoir and formed at a different, likely higher temperature. In this case, the models discussed below and in the main text that are dominantly constrained by C_{2-5} chemical and isotopic compositions would not yield useful information on average methane formation temperatures. In such a scenario, the idea of an 'average gas' temperature may be conceptually misleading. Additional, there is also a concern when examining gases that have migrated and then dissolved in oil that the samples could have experienced chemical fractionation (i.e. changes in $C_1/\Sigma C_{1-5}$ values) during migration, storage, or extraction (Schoell, 1983). Thus any failings of the thermal maturity proxies we consider may be due to complexities of these samples rather than some fundamental error in the tools in question. Nevertheless, these types of ambiguities exists in the interpretation of all migrated gas samples, and so this case illustrates the role clumped isotope thermometry of methane can play in clarifying these challenging issues.

(I) The Schoell (1983) gas classification scheme: This classification scheme uses the $\delta^{13}C$ values of methane and $\Sigma C_{2-4}/\Sigma C_{1-4}$ ratios (i.e., fraction of non-methane

hydrocarbon gases) to identify the source of the gas (Figure A2). All of our samples but one reside in the field indicating gases co-formed with oil, which is thought to occur between ~60-160°C (Hunt, 1996).

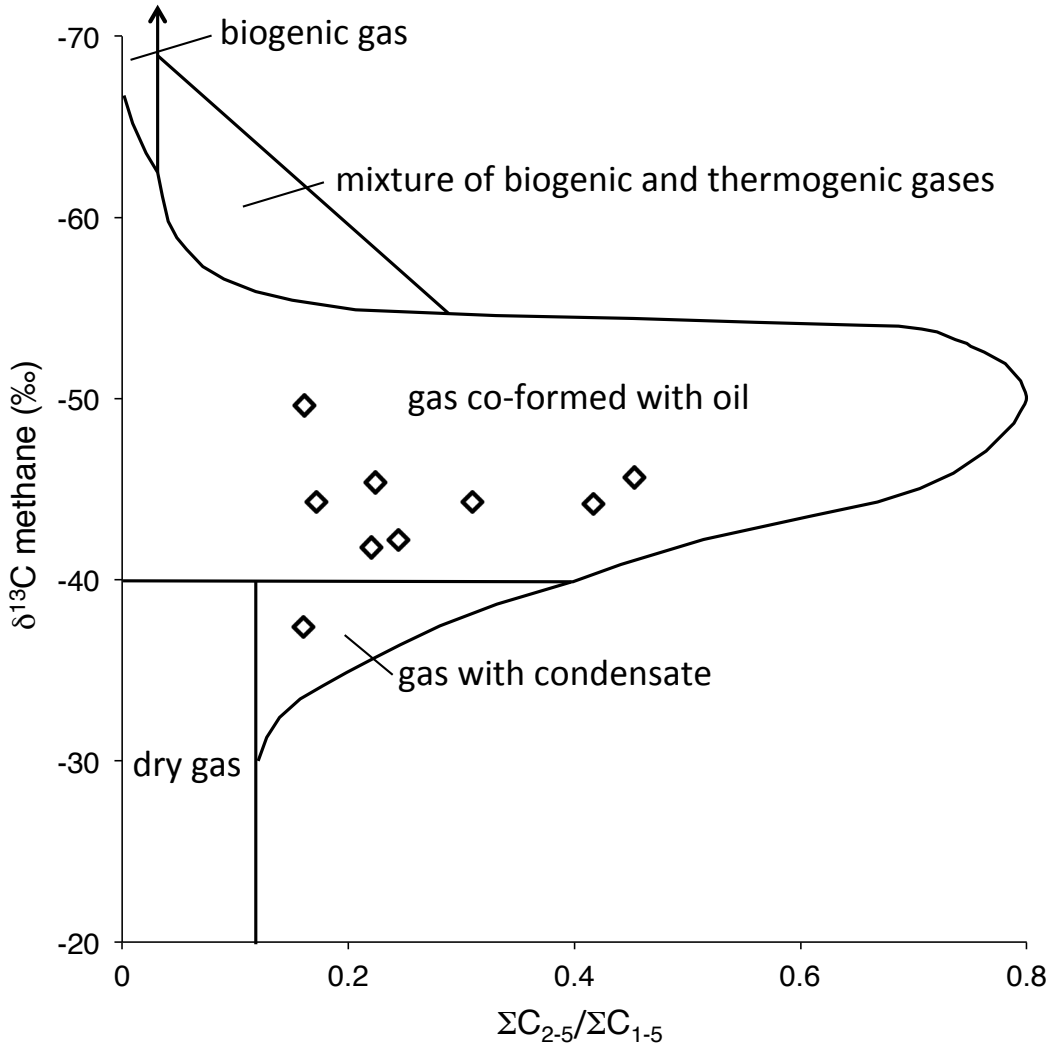

Figure A2. Gas classification scheme of Schoell (1983) based on the $\delta^{13}C$ value of methane and amount of non-methane hydrocarbon gases ($\Sigma C_{2-5}/\Sigma C_{1-5}$). Based on this scheme, all but one of our samples would be classified as having formed at the same time as oil and thus at temperatures <160°C (Hunt, 1996). In contrast, the Δ_{18} values suggest a much higher temperature range (157-221°C).

(II) The Lorant et al. (1998) gas classification scheme: This classification scheme uses the difference in $\delta^{13}C$ values between ethane and propane and the ratio of their abundances (C_2/C_3) to classify the origins of gases (Figure A3). All of our samples sit in the field indicative of primary cracking of kerogen. Prinzhofer et al. (2010) used this same classification scheme to interpret other gas samples from the same southwestern sector of Potiguar Basin and also concluded that the gases were derived from kerogen cracking. Based on this, they further inferred that the gases formed at the same time as oils, and thus at temperatures between 60-160°C (Hunt, 1996).

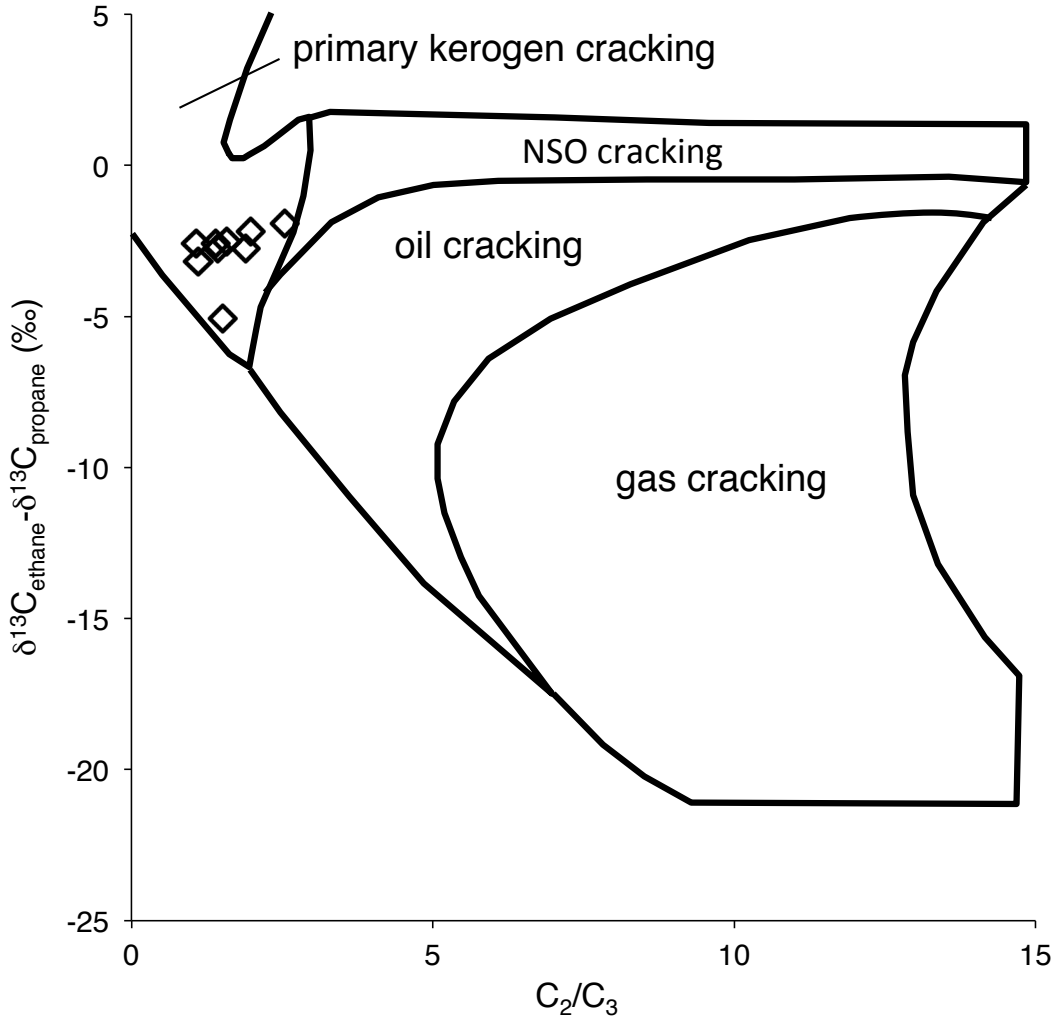

Figure A3. Gas classification scheme of Lorant et al. (1998) based on the difference in $\delta^{13}C$ values of ethane and propane and the molar ratio of ethane:propane (C_2/C_3). The figure is taken from an updated version of the Lorant et al. (1998) classification scheme from the study of Prinzhofer et al. (2010). Based on this scheme, all of our gas samples would be classified as forming from primary cracking of kerogen. Prinzhofer et al. (2010) interpreted other samples from the southwestern sector of the Potiguar Basin that fell in the same space in this plot (primary kerogen cracking) to have co-formed with oils and thus at temperature <160°C (Hunt, 1996). In contrast, the Δ_{18} values suggest a higher formation temperature range (157-221°C). Note that the 'NSO' field refers to gases formed from cracking of polar organic molecules that contain nitrogen, sulfur and oxygen.

(III) The Prinzhofer and Huc (1995) gas classification scheme: This classification scheme uses the difference in $\delta^{13}C$ values between ethane and propane and the logarithm of the ratio of their abundances, $\ln(C_2/C_3)$, to infer gas formation mechanisms (Figure A4). In this scheme, primary cracking of kerogen (i.e. gas formation with oils), causes

large changes in $\delta^{13}C$ differences between ethane and propane, but small changes in their relative abundances. In contrast, gas formation via cracking of oil causes large changes in ethane vs. propane relative abundances, with minor changes in the difference in $\delta^{13}C$ values. The vectors of these processes are given in Figure A4. With one exception, our data are consistent with the gases being formed mainly via oil cracking. Oil cracking occurs at temperatures above 150-160°C (Clayton, 1991; Hunt, 1996; Quigley and Mackenzie, 1988), thus this model would predict gas formation temperatures >160°C.

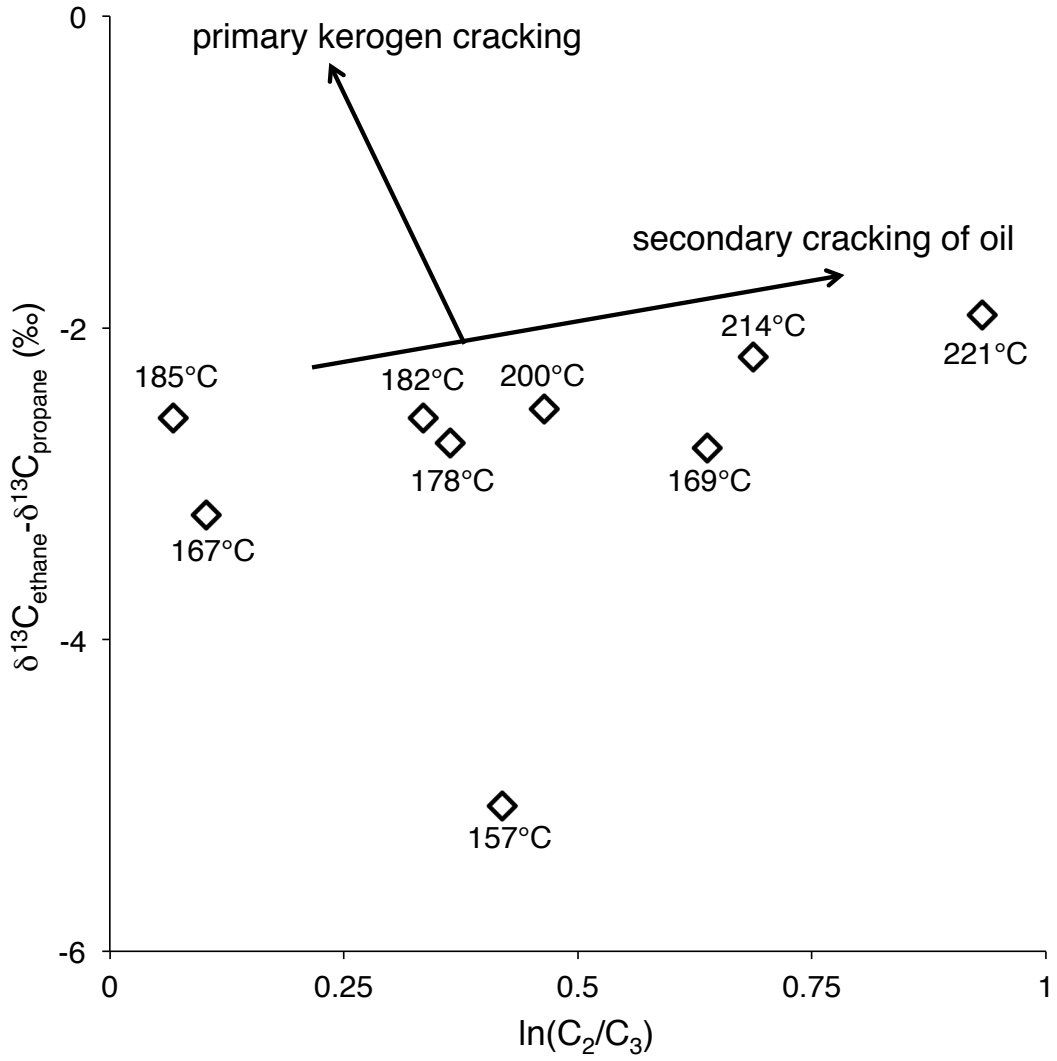

Figure A4. Gas classification scheme of Prinzhofer and Huc (1995) based on the difference in $\delta^{13}C$ values of ethane and propane and the logarithm of the ethane:propane ratio [$\ln(C_2/C_3)$]. Sample arrays following a

sub-vertical trend are attributed to kerogen cracking, whereas those following a sub-horizontal trend are interpreted to derive from oil cracking. Our samples are consistent with the oil-cracking trend. Moreover, samples with the hottest Δ_{18} temperatures generally plot further to the right (higher C_2/C_3 ratio), as would be expected. Oil cracking is thought to occur above ~150-160°C (Clayton, 1991; Hunt, 1996; Quigley and Mackenzie, 1988), and thus this model is consistent with the Δ_{18} temperature range exhibited by the samples (157-221°C).

(IV) The Tang et al. (2000) kinetic model: This model uses kinetic and isotope fractionation data from both anhydrous pyrolysis experiments and from quantitative theoretical calculations. This model assumes kinetics for a default, generic type II kerogen and generic oil given in the GOR software package (GOR, Version 2.3.9). It assumes a 2 °C/million year heating rate and uses the C_{1-3} and $\delta^{13}C$ values to provide a best fit gas generation history from which formation temperatures can be calculated. The model was run in two separate ways for closed-system generation of gases: first with cracking of kerogen and second with cracking of oil. Gases derived from kerogen cracking range in formation temperature from 90-180°C. Gases derived from oil cracking range from 190-215°C (Table S6).

(V) The Burnham (1989) kinetic model: The quantitative model of Burnham (Burnham, 1989) can be used to explicitly calculate formation temperatures based on kinetic data from anhydrous cracking experiments. We used model outputs directly from that study for a type-II kerogen heated at 3.3°C per million years. For such a source rock and heating rate, gases could have formed via cracking of 'primary' kerogen and 'labile' oil from ~90-130°C, via cracking of 'refractory' oil from 150-190°C, or via cracking of 'refractory' kerogen above 150°C. We note that in this model, oil cracking occurs below 150-160°C for the 'labile' fraction, in contrast to the generally assumed stability of oil up to ~150-160°C (Hunt, 1996).

(VI) The Seewald et al. (1998) kinetic model: This model uses kinetic data from hydrothermal pyrolysis experiments, i.e. with water present. We used model outputs directly from that study for an 8°C per million year heating rate. This model predicts that gases with $C_1/\Sigma C_{1\text{-}5}$ <90%, as is the case for all Potiguar Basin samples, form from 160-230°C.

5. Tables

Table A1. Experimentally produced methane details and measured values

experimental T (°C)	duration (hr)	δD (‰)[a]	$\delta^{13}C$[b]	Δ_{18} (‰)	±[c]	Δ_{18}-based T (°C)	±[c]
360	72	-332.6	-44.6	1.16	0.25	407	53
360	72	-333.1	-45.2	1.02	0.25	443	61
600	12	-190.1	-35.5	0.39	0.26	717	147

[a]Referenced to VSMOW, 1σ precisions range from 0.005-0.007 ‰

[b]Referenced to VPDB, 1σ precisions range from 0.10-0.12 ‰

[c]1 standard error

Table A2. Composition and isotope ratios of studied natural gases

sample name	location	δD C_1 (‰)[a]	$\delta^{13}C$ C_1 (‰)[b]	Δ_{18} (‰)	±[c]	Δ_{18} T (°C)	±[c]	$\%CH_4$ (mol%)[d]	well T (°C)	$\delta^{13}C$ C_2 (‰)[e]	$\delta^{13}C$ C_3 (‰)[e]
H1	Haynesville Shale	-144.3	-38.9	2.63	0.26	198	21	96.0	163		
H2	Haynesville Shale	-129.8	-35.2	2.79	0.27	185	21	99.9	190		
H3	Haynesville Shale	-131.9	-36.0	3.01	0.27	169	19	99.7	170		
H4	Haynesville Shale	-132.7	-35.4	2.74	0.26	189	20	99.9	183		
H5	Haynesville Shale	-130.2	-35.4	2.54	0.26	207	22	99.9	187		
M1	Marcellus Shale	-153.5	-35.8	2.87	0.24	179	18	96.9	60		
M2	Marcellus Shale	-155.6	-35.8	2.54	0.26	207	22	97.2	62		
M3	Marcellus Shale	-156.2	-34.2	2.68	0.25	195	20	97.8	70		
P1	Potiguar Basin	-126.7	-37.4	2.38	0.26	221	24	84.0	106	-31.2	-29.3
P2	Potiguar Basin	-200.3	-45.6	3.03	0.27	167	18	54.7	71	-38.0	-34.8
P3	Potiguar Basin	-190.0	-44.3	2.83	0.24	182	18	69.0	63	-34.8	-32.3
P4	Potiguar Basin	-155.6	-42.2	3.00	0.25	169	18	75.6	63	-32.6	-29.8
P5	Potiguar Basin	-200.6	-49.6	3.17	0.24	157	15	83.9	52	-41.7	-36.7
P6	Potiguar Basin	-184.4	-44.2	2.79	0.25	185	19	58.3	73	-36.8	-34.2
P7	Potiguar Basin	-178.4	-44.3	2.62	0.26	200	21	82.9	88	-36.8	-34.3
P8	Potiguar Basin	-169.2	-45.4	2.89	0.26	178	19	77.5	68	-34.3	-31.5
P9	Potiguar Basin	-150.3	-41.8	2.46	0.26	214	23	77.9	66	-32.9	-30.7
GM1	Gulf of Mexico	-173.9	-60.4	5.88	0.26	34	8	-	42		
GM2	Gulf of Mexico	-173.7	-58.0	5.46	0.24	48	8	-	48		
A1[f]	Antrim Shale	-247.5	-50.2	5.68	0.30	40	10	99.99	-		
A2	Antrim Shale	-221.6	-53.2	3.87	0.25	115	13	88.9	-		

[a]Referenced to VSMOW, 1σ internal precisions range from 0.10-0.12‰.

[b]Referenced to VPDB, 1σ internal precisions range from 0.005-0.007‰.

[c]1 standard error.

[d]Represents the ratio of $C_1/(C_1+C_2+C_3+C_4+C_5)$ where $C_\#$ is the mole concentration of all alkanes and all isomers with that number of carbon atoms. Note that C_5 gases were not measured in the Potiguar Basin gases.

[e]Referenced to VPDB, 1σ internal precisions are ~0.5‰.

[f]Sample was measured twice. Δ_{47} error is the standard error of the replicates ($\sigma/\sqrt{2}$). δD standard error or the replicates is ±0.14‰ and $\delta^{13}C$ standard error of the replicates is ±0.05‰.

Table A3. Model inputs and outputs for shale gas thermal histories and gas formation temperatures

sample name	system	well	county	state	well T (°C)	vitrinite reflectance (R_0)	modeled max burial T (°C)	average model gas formation T (°C)
H1	Haynesville Shale	New Horizons E1H	Panola	TX	163	1.7	175	169
H2	Haynesville Shale	Hiltoppers 1H	San Augustine	TX	190	2.5	207	175
H3	Haynesville Shale	Congo 1HB	Shelby	TX	170	1.9	175	168
H4	Haynesville Shale	Barcoo 1	Shelby	TX	183	2.2	187	173
H5	Haynesville Shale	Longhorns 4H	Nacogdoches	TX	187	2.5	202	173
M1	Marcellus Shale	1H Winslow RC	Jefferson	PN	60	2.04	183	173
M2	Marcellus Shale	A K Stear 1H	Indiana	PN	62	2.35	198	171
M3	Marcellus Shale	8558H Nelson	Westmoreland	PN	70	3.1	219	171

Table A4. Modeled ^{13}C fractionations in methane formed from a larger hydrocarbon precursor.

T (°C)	1000*(α-1) Study: homolytic cleavage (Ni et al., 2011)*	1000*(α-1) Study: homolytic cleavage (Tang et al., 2000)*	1000*(α-1) Study: homolyitc cleavage (Xiao, 2001)*	1000*(α-1) Study: β-scission (Xiao, 2001)*
100	-39.4	-35.1	-30.6	-47.1
150	-32.4	-28.6	-24.9	-42.1
200	-26.8	-23.5	-20.6	-38.4
250	-22.3	-19.3	-17.3	-35.6
slope	8.8 °C/‰	9.4 °C/‰	11.1 °C/‰	12.8 °C/‰

*α is calculated as $(1000+\delta^{13}C_{methane})/(1000+\delta^{13}C_{source})$. The source for models (Ni et al., 2011) and (Tang et al., 2000) is ethane while the source for (Xiao, 2001) is octane.

Table A5. Modeled ^{13}C fractionation between methane and octane (Xiao, 2001)

T (°C)	α* (homolytic cleavage)	α *(β-scission)
0	0.95	0.935
100	0.968	0.952
200	0.98	0.962
300	0.986	0.967
400	0.99	0.97
500	0.992	0.972
600	0.993	0.973

*α is calculated as $(1000+\delta^{13}C_{methane})/(1000+\delta^{13}C_{octane})$.

Table S6: Modeled methane formation temperatures for the Potiguar Basin samples calculated using the model of Tang et al. (2000) for both kerogen and oil cracking as compared to measured Δ_{18} temperatures.

sample	Δ_{18} T (°C)	kerogen cracking model T (°C)	oil cracking model T (°C)
P1	221	185	213
P2	167	132	198
P3	182	160	204
P4	169	176	210
P5	157	88	192
P6	185	145	201
P7	200	145	200
P8	178	164	206
P9	214	174	209

6. References

Blackwell, D.D., Richards, M., 2004. *Geothermal Map of North America*. American Association of Petroleum Geologists, pp. 1 sheet, scale 1:6,500,000.

Burnham, A., 1989. *A simple kinetic model of petroleum formation and cracking*. Lawrence Livermore National Lab, report UCID 21665.

Clayton, C., 1991. Carbon isotope fractionation during natural gas generation from kerogen. *Marine and Petroleum Geology* 8, 232-240.

Curtis, J.B., 2002. Fractured shale-gas systems. *AAPG bulletin* 86, 1921-1938.

Dodson, M.H., 1973. Closure temperature in cooling geochronological and petrological systems. *Contributions to Mineralogy and Petrology* 40, 259-274.

dos Santos Neto, E.V., Hayes, J.M., 1999. Use of hydrogen and carbon stable isotopes characterizing oils from the Potiguar Basin (onshore), Northeastern Brazil. *AAPG bulletin* 83, 496-518.

Dutton, S.P., 1987. *Diagenesis and burial history of the lower cretaceous travis peak formation, East Texas*. Bureau of Economic Geology Report of Investigations No. 164.

Eiler, J.M., 2007. "Clumped-isotope" geochemistry—The study of naturally-occurring, multiply-substituted isotopologues. *Earth and Planetary Science Letters* 262, 309-327.

Eiler, J.M., Clog, M., Magyar, P., Piasecki, A., Sessions, A., Stolper, D., Deerberg, M., Schlueter, H.-J., Schwieters, J., 2013. A high-resolution gas-source isotope ratio mass spectrometer. *International Journal of Mass Spectrometry* 335, 45-56.

England, W., Mackenzie, A., Mann, D., Quigley, T., 1987. The movement and entrapment of petroleum fluids in the subsurface. *Journal of the Geological Society* 144, 327-347.

Espitalie, J., Ungerer, P., Irwin, I., Marquis, F., 1988. Primary cracking of kerogens. Experimenting and modeling C_1, C_2–C_5, C_6–C_{15+} classes of hydrocarbons formed. *Organic Geochemistry* 13, 893-899.

Ettensohn, F.R., 1985. The Catskill delta complex and the Acadian orogeny: A model. *The Catskill delta: Geological Society of America Special Paper* 201, 39-49.

GOR, Version 2.3.9. GeoIsochem Corp.

Hammes, U., Hamlin, H.S., Ewing, T.E., 2011. Geologic analysis of the Upper Jurassic Haynesville Shale in east Texas and west Louisiana. *AAPG bulletin* 95, 1643-1666.

Hunt, J.M., 1996. *Petroleum Geochemistry and Geology*. W. H. Freeman and Company, New York.

Jarvie, D.M., Hill, R.J., Ruble, T.E., Pollastro, R.M., 2007. Unconventional shale-gas systems: The Mississippian Barnett Shale of north-central Texas as one model for thermogenic shale-gas assessment. *AAPG bulletin* 91, 475-499.

Johnsson, M.J., 1986. Distribution of maximum burial temperatures across northern Appalachian Basin and implications for Carboniferous sedimentation patterns. *Geology* 14, 384-387.

Lash, G.G., Engelder, T., 2011. Thickness trends and sequence stratigraphy of the Middle Devonian Marcellus Formation, Appalachian Basin: Implications for Acadian foreland basin evolution. *AAPG Bulletin* 95, 61-103.

Levine, J.R., 1986. Deep burial of coal-bearing strata, Anthracite region, Pennsylvania: Sedimentation or tectonics? *Geology* 14, 577-580.

Lewan, M., 1983. Effects of thermal maturation on stable organic carbon isotopes as determined by hydrous pyrolysis of Woodford Shale. *Geochimica et Cosmochimica Acta* 47, 1471-1479.

Lewan, M., 1997. Experiments on the role of water in petroleum formation. *Geochimica et Cosmochimica Acta* 61, 3691-3723.

Lewan, M., Kotarba, M., Więcław, D., Piestrzyński, A., 2008. Evaluating transition-metal catalysis in gas generation from the Permian Kupferschiefer by hydrous pyrolysis. *Geochimica et Cosmochimica Acta* 72, 4069-4093.

Lewan, M., Ruble, T., 2002. Comparison of petroleum generation kinetics by isothermal hydrous and nonisothermal open-system pyrolysis. *Organic Geochemistry* 33, 1457-1475.

Lorant, F., Prinzhofer, A., Behar, F., Huc, A.-Y., 1998. Carbon isotopic and molecular constraints on the formation and the expulsion of thermogenic hydrocarbon gases. *Chemical Geology* 147, 249-264.

Mango, F.D., Hightower, J., 1997. The catalytic decomposition of petroleum into natural gas. *Geochimica et Cosmochimica Acta* 61, 5347-5350.

Mango, F.D., Hightower, J., James, A.T., 1994. Role of transition-metal catalysis in the formation of natural gas. *Nature* 368, 536-538.

Martini, A., Walter, L., Budai, J., Ku, T., Kaiser, C., Schoell, M., 1998. Genetic and temporal relations between formation waters and biogenic methane: Upper Devonian

Antrim Shale, Michigan Basin, USA. *Geochimica et Cosmochimica Acta* 62, 1699-1720.

Martini, A.M., Budai, J.M., Walter, L.M., Schoell, M., 1996a. Microbial generation of economic accumulations of methane within a shallow organic-rich shale.

Martini, A.M., Budai, J.M., Walter, L.M., Schoell, M., 1996b. Microbial generation of economic accumulations of methane within a shallow organic-rich shale. *Nature* 383, 155-158.

Matos, R.M.D., 1992. The northeast Brazilian rift system. *Tectonics* 11, 766-791.

Ni, Y., Ma, Q., Ellis, G.S., Dai, J., Katz, B., Zhang, S., Tang, Y., 2011. Fundamental studies on kinetic isotope effect (KIE) of hydrogen isotope fractionation in natural gas systems. *Geochimica et Cosmochimica Acta* 75, 2696-2707.

Price, L.C., Clayton, J.L., Rumen, L.L., 1981. Organic geochemistry of the 9.6 km Bertha Rogers No. 1. well, Oklahoma. *Organic Geochemistry* 3, 59-77.

Price, L.C., Schoell, M., 1995. Constraints on the origins of hydrocarbon gas from compositions of gases at their site of origin. *Nature* 378, 368-371.

Prinzhofer, A., Santos Neto, E.V., Battani, A., 2010. Coupled use of carbon isotopes and noble gas isotopes in the Potiguar basin (Brazil): Fluids migration and mantle influence. *Marine and Petroleum Geology* 27, 1273-1284.

Prinzhofer, A.A., Huc, A.Y., 1995. Genetic and post-genetic molecular and isotopic fractionations in natural gases. *Chemical Geology* 126, 281-290.

Quigley, T., Mackenzie, A., 1988. The temperatures of oil and gas formation in the sub-surface. *Nature* 333, 549-552.

Roden, M.K., Miller, D.S., 1989. Apatite fission-track thermochronology of the Pennsylvania Appalachian Basin. *Geomorphology* 2, 39-51.

Schoell, M., 1983. Genetic characterization of natural gases. *AAPG Bulletin* 67, 2225-2238.

Seewald, J.S., 2003. Organic–inorganic interactions in petroleum-producing sedimentary basins. *Nature* 426, 327-333.

Seewald, J.S., Benitez-Nelson, B.C., Whelan, J.K., 1998. Laboratory and theoretical constraints on the generation and composition of natural gas. *Geochimica et Cosmochimica Acta* 62, 1599-1617.

Stolper, D.A., Davis, C.L., Eiler, J.M., Ellis, G.S., Ferreira, A.A., Lawson, M., Martini, A.M., Santos Neto, E.V., Schoell, M., Sessions, A.L., Shusta, S.S., Tang, Y., Valentine, D.L., 2014a. Clumped isotopes of methane: applications to both low and high temperature natural systems. *Mineralogical Magazine* 78, 2393.

Stolper, D.A., Shusta, S.S., Valentine, D.L., Sessions, A.L., Ferreira, A., Santos Neto, E.V., Eiler, J.M., 2014b. Combined ^{13}C-D and D-D clumping in methane: methods and preliminary results. *Geochimica Et Cosmochimica Acta* 126, 169-191.

Sweeney, J.J., Burnham, A.K., 1990. Evaluation of a simple model of vitrinite reflectance based on chemical kinetics. *AAPG Bulletin* 74, 1559-1570.

Tang, Y., Perry, J., Jenden, P., Schoell, M., 2000. Mathematical modeling of stable carbon isotope ratios in natural gases. *Geochimica et Cosmochimica Acta* 64, 2673-2687.

Tissot, B.P., Welte, D.H., 1978. *Petroleum formation and occurrence: A new approach to oil and gas exploration*. Springer-Verlag, Berlin.

Torsch, W.C., 2012. *Thermal and pore pressure history of the Haynesville Shale in North Lousiana: A numerical study of hydrocarbon generation, overpressure, and natural hydraulic fractures*, Geology & Geophysics. Lousiana State University.

Trindade, L., Brassell, S.C., Santos Neto, E.V., 1992. Petroleum migration and mixing in the Potiguar Basin, Brazil. *AAPG Bulletin* 76, 1903-1924.

Ungerer, P., 1990. State of the art of research in kinetic modelling of oil formation and expulsion. *Organic Geochemistry* 16, 1-25.

Valentine, D.L., 2011. Emerging topics in marine methane biogeochemistry. *Annu. Rev. Mar. Sci.* 3, 147-171.

Valentine, D.L., Chidthaisong, A., Rice, A., Reeburgh, W.S., Tyler, S.C., 2004. Carbon and hydrogen isotope fractionation by moderately thermophilic methanogens. *Geochimica et Cosmochimica Acta* 68, 1571-1590.

Whiticar, M.J., Faber, E., Schoell, M., 1986. Biogenic methane formation in marine and freshwater environments: CO_2 reduction vs acetate fermentation—Isotope evidence. *Geochimica et Cosmochimica Acta* 50, 693-709.

Wilhelms, A., Larter, S., Head, I., Farrimond, P., Di-Primio, R., Zwach, C., 2001. Biodegradation of oil in uplifted basins prevented by deep-burial sterilization. *Nature* 411, 1034-1037.

Xiao, Y., 2001. Modeling the kinetics and mechanisms of petroleum and natural gas generation: A first principles approach. *Reviews in Mineralogy and Geochemistry* 42, 383-436.